



Technische Universität München
TUM School of Natural Sciences

**Exploring the Proteomic Landscape of Infection:
Chemical Proteomics in the Pursuit of Novel
Antibacterial Targets**

Dissertation

Dietrich Waldemar Mostert

München 2024



Technische Universität München
TUM School of Natural Sciences

**Exploring the Proteomic Landscape of Infection:
Chemical Proteomics in the Pursuit of Novel
Antibacterial Targets**

Dietrich Waldemar Mostert

Vollständiger Abdruck der von der TUM School of Natural Sciences der
Technischen Universität München zur Erlangung eines
Doktors der Naturwissenschaften (Dr. rer. nat.)
genehmigten Dissertation.

Vorsitz: Prof. Dr. rer. nat. Martin Zacharias

Prüfer der Dissertation: 1. Prof. Dr. rer. nat. Stephan A. Sieber
2. apl. Prof. Dr. rer. nat. Wolfgang Eisenreich

Die Dissertation wurde am 25.01.2024 bei der Technischen Universität München eingereicht
und durch die TUM School of Natural Sciences am 07.03.2024 angenommen.

“The advancement of science is slow; it is effected only by virtue of hard work and perseverance. And when a result is attained, should we not in recognition connect it with the efforts of those who have preceded us, who have struggled and suffered in advance?”

- Henri Moissan

Abstract

The rise in antibacterial resistance is one of the most significant threats to public health. This increase has coincided with a decline in the development of novel antibiotics in recent decades. Consequently, there is an urgent, unmet medical need to develop antibacterial drugs with novel molecular targets. Over the past two decades, chemical proteomics has emerged as a powerful tool for identifying the protein targets of potential drugs, making it ideally suited for developing drug candidates with novel mechanisms of action. This thesis comprises three distinct projects, each addressing a different part of antibacterial research, utilising various chemical proteomic approaches to identify new potential drug targets.

In the first project, the focus lies on addressing the necessity for novel Tuberculosis (TB) drugs. Starting with an initial hit compound from an in-house library, the objective was to identify the cellular targets in Mycobacteria. Using affinity-based protein profiling (AfBPP), the mycolic acid transporter MmpL3 was identified as a target of the new compound class. The target was validated by radioactively labelling fatty acids in living cells and analysing the extracted fatty acids by autoradiography. Furthermore, isolation of resistant *M. tuberculosis* (Mtb) strains confirmed MmpL3 as the primary target of the new compound. The lack of a shift in susceptibility in Mtb overexpressing MmpL3 suggested a polypharmacological mode of action. Using a new affinity-based probe, more closely resembling the structure of the hit compound, two epoxide hydrolases (Eph) were identified as additional targets. An in vitro assay using purified EphF confirmed that the novel compound inhibits this enzyme, affirming the dual mode of action of the new compound class. Meanwhile, based on the hit compound's core structure and the information about the identified protein targets, an extensive hit-to-lead optimisation focusing on improving the pharmacokinetic (PK) profile was conducted, resulting in a new lead compound with enhanced antibacterial activity and superior PK properties.

The second project aimed to identify the molecular targets of Chlorotonil, a novel antibacterial natural product isolated from *Sorangium cellulosum*. Thermal proteome profiling (TPP) in *Staphylococcus aureus* identified the essential methionine aminopeptidase (MetAP) as a potential protein target. Subsequent investigations demonstrated that Chlorotonil-derivatives inhibit the MetAP in an in vitro assay. The rapid onset of bacterial cell death upon treatment suggested that inhibition of the MetAP is only a secondary effect. Therefore, the role of the most stabilised hit from the TPP experiment, a potassium efflux channel, was investigated. Significant shifts in susceptibility when supplementing media with potassium confirmed the role of potassium homeostasis in the mode of action (MoA). Full proteome analysis of treated cells further corroborated this, as many dysregulated proteins play a role in this cellular process.

Proteomic profiling of Chlorotoniil-resistant *S. aureus* identified an intriguing resistance mechanism. A mutation in the transcription factor *farR* leads to a strong upregulation of the fatty acid efflux pump FarE. The exported fatty acids interact with Chlorotoniil, causing neutralisation of Chlorotoniil and high-level resistance. While the entire mechanism of action of Chlorotoniil is still under investigation, this study contributes to a better understanding of the complex MoA of Chlorotoniil.

The third project aimed to investigate the nucleotide promiscuity of AMPylators and whether the target scope changes depending on the nucleotide substrate. AMPylation is a crucial post-translational modification (PTM) in cellular homeostasis and during bacterial infection of host cells. The role of other nucleotides has yet to be studied extensively. A novel UMPylation prodrug activity-based probe was used to profile uninfected and *Vibrio parahaemolyticus*-infected human cells. These proteomic studies of labelled protein targets revealed an unexpected promiscuity of human nucleotide transferases with an almost identical target set of AMP- and UMPylated proteins. On the other hand, studies in cells infected by *V. parahaemolyticus* and its effector VopS revealed solely AMPylation of host enzymes, highlighting a hitherto unknown specificity of this transferase for ATP. Gaining a better understanding of the protein targets and the molecular mechanism of PTMs catalysed by bacterial effector proteins could identify novel pathways that antibacterial and anti-virulence drugs could address.

Together, these three projects underscore the utility of chemical proteomic methods in understanding complex bacterial pathways and identifying the mechanism of action of novel antibacterial drugs.

Zusammenfassung

Die Zunahme der Antibiotikaresistenz ist eine der größten Bedrohungen für die öffentliche Gesundheit. Dieser Anstieg fiel in den letzten Jahrzehnten mit einem Einbruch bei der Entwicklung neuer Antibiotika zusammen. Daher besteht ein dringender medizinischer Bedarf an der Entwicklung von antibakteriellen Medikamenten mit neuen molekularen Zielen. In den letzten 20 Jahren hat sich die chemische Proteomik zu einem leistungsfähigen Instrument für die Identifizierung der Proteinziele potenzieller Arzneimittel entwickelt und ist damit ein ideales Instrument für die Entwicklung von Arzneimittelkandidaten mit neuartigen Wirkmechanismen. Diese Arbeit ist eine Kombination aus drei verschiedenen Projekten, die sich jeweils mit einem anderen Teilbereich der antibakteriellen Forschung befassen. In allen Projekten wurden verschiedene chemische proteomische Ansätze verwendet, um neue potenzielle Zielstrukturen für Medikamente zu identifizieren.

Das erste Projekt befasst sich mit dem Bedarf an neuen TB-Medikamenten. Ausgehend von einer ersten Hit-Struktur aus einer internen Bibliothek sollten die zellulären Ziele in Mykobakterien identifiziert werden. Mittels *affinity-based protein profiling* (AfBPP) wurde der Mykolsäuretransporter MmpL3 als Ziel der neuen Wirkstoffklasse identifiziert. Das Ziel wurde durch die radioaktive Markierung von Fettsäuren in lebenden Zellen und die Analyse der extrahierten Fettsäuren durch Autoradiographie validiert. Darüber hinaus bestätigte die Isolierung resistenter *M. tuberculosis* (Mtb) Stämme MmpL3 als primäres Ziel der neuen Verbindung. Das Fehlen einer Änderung der minimalen bakteriziden Konzentration (MIC) von Mtb, die MmpL3 überexprimieren, deutet auf einen polypharmakologischen Wirkmechanismus hin. Mit Hilfe einer neuen affinitätsbasierten Sonde, die der Struktur des neuen Wirkstoffs ähnlicher ist, konnten zwei Epoxidhydrolasen (Eph) als zusätzliche Ziele identifiziert werden. Ein *in vitro* Test mit EphF bestätigte, dass die neue Verbindung dieses Enzym hemmt, was den dualen Wirkmechanismus der neuen Wirkstoffklasse bestätigt. In der Zwischenzeit wurde auf der Grundlage der Kernstruktur der Hit-Substanz und der Informationen über die identifizierten Protein-Targets eine umfassende *Hit-to-Lead*-Optimierung mit Schwerpunkt auf der Verbesserung des pharmakokinetischen (PK) Profils durchgeführt, was zu einer neuen Leitverbindung mit verstärkter antibakterieller Aktivität und verbesserten PK-Eigenschaften führte.

Das zweite Projekt zielte darauf ab, die molekularen Ziele von Chlorotonil, einem neuartigen antibakteriellen Naturstoff, der aus *Sorangium cellulosum* isoliert wurde, zu identifizieren. Mittels *thermal proteome profiling* (TPP) in *Staphylococcus aureus* wurde die essentielle Methionin-Aminopeptidase (MetAP) als potenzielles Proteinziel identifiziert. Es wurde dann

gezeigt, dass die Chlorotonil-Derivate die MetAP in einem in vitro Test hemmen. Das schnelle Einsetzen des bakteriellen Zelltods nach der Behandlung deutet darauf hin, dass die Hemmung der MetAP nur ein sekundärer Effekt ist. Daher wurde die Rolle des am stärksten stabilisierten Treffers aus dem TPP-Experiment, eines Kalium-Efflux-Kanals, untersucht. Erhebliche Änderungen in der MIC, wenn das Medium mit Kalium supplementiert wurde, bestätigten die Rolle der Kalium-Homöostase in der Wirkungsweise (MoA). Eine Proteomanalyse der behandelten Zellen bestätigte dies zusätzlich, da viele dysregulierte Proteine eine Rolle in diesem zellulären Prozess spielen. Weitere Proteomanalysen von Chlorotonil-resistenten *S. aureus* Stämmen identifizierten einen interessanten Resistenzmechanismus. Eine Mutation im Transkriptionsfaktor *farR* führt zu einer starken Hochregulierung der Fettsäure-Effluxpumpe FarE, die Fettsäuren aus den Zellen exportiert, welche Chlorotonil binden und somit neutralisieren. Der vollständige Wirkmechanismus von Chlorotonil wird noch weiter untersucht, diese Studie trägt jedoch schon zu einem besseren Verständnis des komplexen Wirkmechanismus von Chlorotonil bei.

Das dritte Projekt zielte darauf ab, die Nukleotid-Promiskuität von AMPylatoren zu untersuchen und festzustellen, ob sich die Zielproteine je nach Nukleotidsubstrat ändern. Die AMPylierung ist eine wichtige Post-translationale Modifikation (PTM) in der zellulären Homöostase und während der bakteriellen Infektion von Wirtszellen. In diesem Projekt wurde eine neuartige *prodrug* UMPylierungs-Sonde verwendet, um Zielproteine von nicht infizierten und von *Vibrio parahaemolyticus*-infizierten menschlichen Zellen zu identifizieren. Diese proteomischen Untersuchungen zeigen eine unerwartete Promiskuität menschlicher Nukleotid-Transferasen mit einem fast identischen Target-Set von AMP- und UMPylierten Proteinen. Andererseits ergaben Untersuchungen an Zellen, die mit *V. parahaemolyticus* und seinem Effektor VopS infiziert waren, dass Wirtsenzyme ausschließlich AMPyliert wurden, was auf eine bisher unbekannte Spezifität dieser Transferase für ATP hinweist. Ein besseres Verständnis der Zielproteine und des molekularen Mechanismus der PTMs, die von bakteriellen Effektorproteinen katalysiert werden, könnte neue Wege aufzeigen, auf die antibakterielle und antivirulente Medikamente ansetzen könnten.

Zusammengenommen unterstreichen diese drei Projekte die Nützlichkeit chemischer Proteomik-Methoden für das Verständnis komplexer bakterieller Stoffwechselwege und die Identifizierung der Wirkmechanismen neuartiger antibakterieller Medikamente.

Danksagung

Über die letzten Jahre haben mich sehr viele Menschen begleitet und diese Promotion möglich gemacht.

Mein erster Dank geht an meinen Doktorvater Prof. Dr. Stephan A. Sieber, der mich nicht nur an seinem Lehrstuhl aufgenommen hat, sondern auch tagtäglich unterstützt hat. Ich bedanke mich vor allem für die sehr hilfreichen Diskussionen und für die Freiheit beim Forschen. Vielen Dank für das Vertrauen, dass ich auch einfach mal neue Sachen im Labor ausprobieren konnte. Vielen Dank auch dafür, dass man sich immer darauf verlassen konnte, dass du schnellstmöglich Manuskripte durchliest und sehr hilfreich kommentierst.

Ein besonderer Dank geht an meinen engsten internen Kooperationspartner Josef Braun. Ich habe die Zusammenarbeit mit dir sehr genossen und das Original 5. Stock Team hat sich über die Jahre zu einem echten Dream Team entwickelt (auch wenn ich immer noch kein Fan vom mongolischen Kehlkopfgesang geworden bin). Ich wünsche dir für die letzten Züge deiner Promotion und den weiteren Weg nur das Beste. Ein großer Dank geht auch an Laura Eck für das sorgfältige Korrekturlesen. Vielen Dank für die Mühe und die gut durchdachten Anmerkungen. Des Weiteren möchte ich mich bei meinem Kooperationspartner Felix Deschner bedanken. Die Zusammenarbeit mit dir am Chlorotonilprojekt hat super funktioniert und ich habe bei unseren langen Besprechungen viel dazu gelernt. Für die tolle Hilfe bei der Arbeit am UMPylation Projekt möchte ich mich auch bei Pavel Kielkowski bedanken. Hier auch ein besonderer Dank an Andrei Bubeneck von dem ich das Projekt nach seiner Masterarbeit übernommen habe.

Ein großer Dank geht auch an Volker Kirsch, meinen ersten Mentor hier am Lehrstuhl. Vielen Dank für die tolle Betreuung in meinen Praktika und die Hilfe am Anfang meiner Promotion. Dank dir bin ich an diesen Lehrstuhl gekommen und auch durch dich habe ich die Faszination für alles um LC-MS entwickelt. Ich wünsche dir und deiner jungen Familie nur das Beste.

Vielen Dank auch an meine Betreuer der Masterarbeit Franziska Mandl, Christian Fetzer und Mathias Hackl. Danke für die tolle Betreuung und lustige Stimmung im aBACTER Büro. An dieser Stelle auch ein großer Dank an Stephan Hacker für die hilfreichen wissenschaftlichen Diskussionen und die ein oder andere Runde Darts (manchmal auch beides gleichzeitig).

Ebenfalls ein großer Dank an alle meine Praktikanten über die Jahre. Hier vor allem ein riesen Dank an Sara Berndl für die Hilfe bei der Optimierung des neuen Masseworkflows und an Laura Leidel für die riesen Hilfe während des Praktikums und als HiWi bei der Durchführung der Eph-assays.

Schwierige Zeiten gehören bei einer Promotion immer dazu. Mit den richtigen Kollegen lassen sich aber auch diese Zeiten gut meistern. Hierbei geht ein ganz großer Dank an die Kollegen, die mich schon besonders Lang am AK begleiten. Dazu gehören Till Reinhardt, Konstantin Eckel, Angela Weigert Muñoz, Jan-Niklas Dienemann, Alexandra Geißler, Thomas Gronauer, Michael Zollo und Robert Macsics. Vielen Dank für die tolle Zusammenarbeit und auch die ein oder anderen Feierabend Biere.

Natürlich geht auch ein großer Dank an alle Kollegen, die während meiner Zeit am AK den Lehrstuhl verlassen haben und mit denen ich viel schöne Erinnerungen habe: Vadim Korotkov, Markus Lakemeyer, Philipp Le, Tobias Becker, Barbara Eyermann, Anja Fux, Kyu Myung Lee, Ramona Absmeier, Jonas Drechsel, Johannes Wenger, Ines Hübner, Carolin Gleißner, Dora Balogh, Theresa Rauh, Patrick Allihn, Stuart Ruddell und Martin Pfanzelt. Ich bin froh, dass ich mit vielen von euch noch Kontakt habe und freue mich immer wieder euch zu sehen.

Das tolle am AK Sieber ist, dass auch wenn es traurig ist, wenn alte Kollegen gehen, immer wieder neue Kollegen nachkommen, aus denen auch wieder neue Freunde werden: Markus Schwarz, Michaela Fiedler, Dominik Schum, Davide Boldini, Martin Köllen, Max Bottlinger, Yasmine El Harraoui, Franziska von Elsen, Katrin Eisenmenger, Wie Ding, Maximilian Schum, Nina Weidlein und Mary Pandler. Vielen Dank für die lustige Arbeitsatmosphäre und die vielen lustigen Feiern.

Während Doktoranden und Post Docs kommen und gehen, würde vieles am AK nicht funktionieren, wenn da nicht ein Paar Mitarbeiter mit mehr Erfahrung wären. Ein großer Dank geht an Nina Bach, für die ganze Organisation des AKs. Danke auch an Katja Bäuml und Mona Wolff für die tagtägliche Unterstützung im Labor. Ein ganz großer Dank geht auch an das Sekretariat des Lehrstuhls, ohne dem nichts funktionieren würde. Danke Christina Brumer und Barbara Müller für all eure Mühe beim rumschlagen mit der nervenzehrenden Bürokratie an der TUM.

Nun zu denen, ohne die ich es nie bis zu diesem Punkt in meinem Leben geschafft hätte. Vielen Dank Mama für all deine Mühe während meiner Schulzeit und, dass du dafür gesorgt hast, dass ich die bestmögliche schulische Ausbildung bekommen habe und für eine tolle Kindheit. Papa, I want to thank you for your support throughout my school and University life and for always being interested in what I do. I hope you will stay interested once I have moved on to a new job.

Mein größter Dank geht an Laura. Danke dass du über die letzten 11 Jahre immer an meiner Seite warst. Ohne deine aufbauenden Worte an manch so schweren Tagen hätte ich diese Promotion nicht geschafft. Ich danke dir dafür vom ganzen Herzen.

Table of Content

I. INTRODUCTION

1. Antimicrobial Resistance Crisis.....	2
2. <i>Mycobacterium tuberculosis</i>	5
3. Post-Translational Modifications During Bacterial Infection.....	7
4. Proteomics – Finding the Molecular Targets of Novel Drugs.....	9
4.1. Proteomics – Over 20 Years of Technological Advancement.....	9
4.2. Activity/Affinity Based Protein profiling (ABPP, AfBPP).....	15
4.3. Thermal Proteome Profiling (TPP).....	17
5. Aim of this Doctoral Thesis.....	20

II. TAILORED PHENYLUREAS ERADICATE DRUG-RESISTANT *MYCOBACTERIUM TUBERCULOSIS* BY TARGETING THE MYCOLIC ACID CELL WALL ASSEMBLY

1. Introduction.....	22
2. Results and Discussion.....	23
2.1. Screening of an in-house urea library reveals a potent Mtb antibiotic hit molecule.....	23
2.2. Chemical proteomics reveal essential targets in the mycolic acid pathway.....	23
2.3. MmpL3 and two epoxide hydrolases are targets of 227 and derivatives.....	26
2.4. Optimised 227-analogues are more potent, less hydrophobic and exhibit improved pharmacokinetic properties.....	31
2.5. Compound 21 displays improved pharmacokinetic properties.....	34
3. Conclusion.....	36
4. Supplementary Information.....	38
5. Methods.....	44
5.1. Biochemical Methods.....	44

III. ELUCIDATING THE MECHANISM OF ACTION OF CHLOROTONIL

1. Introduction.....	65
2. Results and Discussion.....	66
2.1. Thermal Proteome Profiling in <i>S. aureus</i>	66

2.2.	Full proteome analysis of <i>S. aureus</i> and <i>E. faecium</i> treated with DHG	72
2.3.	Full proteome analysis of Chlorotoniil-resistant <i>S. aureus</i>	74
3.	Conclusion	77
4.	Supplementary Information	79
5.	Methods	82
5.1.	Biochemical Methods	82

IV. PRONUCLEOTIDE PROBES REVEAL A DIVERGING SPECIFICITY FOR AMPYLATION VS. UMPYLATION OF HUMAN AND BACTERIAL NUCLEOTIDE TRANSFERASES

1.	Introduction	91
2.	Results and Discussion	93
2.1.	Design and synthesis of UMPylation pronucleotides	93
2.2.	Labeling in human cells reveals promiscuity of nucleotide transfer	94
2.3.	<i>V. parahaemolyticus</i> effector protein VopS solely AMPylates human proteins	95
3.	Conclusion	98
4.	Supplementary Figures	99
5.	Methods	102
5.1.	Biochemical Methods	102
V.	REFERENCES	108

Introductory Remarks

This doctoral dissertation was accomplished between October 2019 and January 2024 under the supervision of Prof. Dr. Stephan A. Sieber at the Chair of Organic Chemistry II of the Technische Universität München. This dissertation consists of three independent projects. First, an introduction into topics relevant to the different projects will provide the necessary background for the projects. Then, each project is independently reported, including a short project-specific introduction, results, discussion, and all relevant supplementary information.

This dissertation includes parts of the following publications

D. Mostert*, J. Braun*, M. D. Zimmerman, C. A. Engelhart, D. Schnappinger, V. Dartois and S. A. Sieber. Tailored phenylureas eradicate drug-resistant *Mycobacterium tuberculosis* by targeting the mycolic acid cell wall assembly. *Manuscript in preparation*, **2024**

F. Deschner, **D. Mostert**, J. M. Daniel, D. Schneider, A. Andreas, A. Volz, T. Risch, L. Herraiz-Benitez, A. M. Kany, G. Jézéquel, W. Hofer, M. Müsken, M. Bischoff, H. Brötz-Oesterhelt, T. Schneider, S. A. Sieber, J. Herrmann and R. Müller. Mode of action of Chlorotonil. *Manuscript in preparation*, **2024**

D. Mostert, W. A. Bubeneck, T. Rauh, P. Kielkowski, A. Itzen, K. Jung and S. A. Sieber, Pronucleotide probes reveal a diverging specificity for AMPylation vs UMPylation of human and bacterial nucleotide transferases. *Biochemistry*, **2024**, <https://pubs.acs.org/doi/full/10.1021/acs.biochem.3c00568>

Publications not mentioned in this dissertation

Y. Hu*; **D. Mostert***; C. Orgler; O. Andler; H. Zischka; U. Kazmaier; A. Vollmar; S. Braig; S. A. Sieber; S. Zahler. Lagunamide A causes potent antiproliferative and pro-apoptotic effects in cancer cells by modulating EYA3. *Manuscript under review*, **2024**

R. Macsics, M. W. Hackl, C. Fetzer, **D. Mostert**, J. Bende, F. Layer, S. A. Sieber. Comparative Target Analysis of Chlorinated Biphenyl Antimicrobials Highlights MenG as a Molecular Target of Triclocarban. *Appl Environ Microbiol*, **2020**. 86(16), e00933-20. doi: 10.1128/AEM.00933-20.

S. A. Ruddell, **D. Mostert** and S. A. Sieber. Target identification of usnic acid in bacterial and human cells. *Manuscript in preparation*, **2024**

*Authors contributed equally

I. Introduction

1. Antimicrobial Resistance Crisis

Antimicrobial resistance (AMR) occurs when bacteria, fungi, viruses or parasites change over time and no longer respond to medicines. As a result of drug resistance, antibiotics and other antimicrobial medications become ineffective, and infections become difficult or impossible to treat¹. In 2019, AMR was directly responsible for 1.27 million deaths and contributed to nearly 5 million deaths². If no further efforts are undertaken, it is estimated that by 2050, 10 million a year will die due to AMR^{3,4}. Antibiotic-resistant bacteria are especially concerning as there are already multi-drug resistant (MDR) *Pseudomonas* and *Acinetobacter* species resistant to almost all available antibiotics^{5,6}. Since the advent of antibiotics nearly 100 years ago, when Alexander Fleming discovered Penicillin⁷, many antibiotics with different cellular targets have been developed. Most of them target five different cellular targets and processes, and there are resistance mechanisms for all known antibiotics⁸: (1) Cell wall biosynthesis targeting antibiotics such as β -lactams were the first commercially available antibiotics. Resistance against these antibiotics is often conferred through the expression of β -lactamases, enzymes that open the β -lactam ring⁹. (2) Lipopeptides such as daptomycin target the cell membrane, leading to depolarisation. Some bacteria have become resistant to this by thickening and increasing the cell wall's positive charge, reducing the effect of depolarisation^{10,11}. (3) The folate biosynthesis can be inhibited by sulfonamides, which inhibit the dihydropteroate synthase, stopping the folate biosynthesis. Simple mutations in the target protein sequence can confer resistance¹². (4) Nucleic acid biosynthesis is targeted by many antibiotics, such as quinolones. Here, DNA replication is arrested by inhibiting the gyrase and topoisomerase IV, which are involved in DNA supercoiling, strand cutting, and ligation. Mutations of the target enzymes and efflux of quinolones can confer resistance against this class of antibiotics¹³. (5) Aminoglycoside antibiotics such as gentamicin can inhibit protein synthesis by targeting ribosomal proteins. Here, enzymes that modify aminoglycosides, such as acetyl-transferases, can cause resistance¹⁴. Overall, antibiotic resistance can be conferred by many different molecular mechanisms such as drug efflux, target bypass, target site modification, decreased influx, inactivation of the antibiotic or down-regulation of the target¹⁵. These resistance mechanisms can be transferred from one species to another through horizontal gene transfer, or resistance can arise through random mutations. The use of antibiotics then leads to selective pressure, killing of drug-sensitive bacteria, and selecting resistant ones¹⁶. This selective pressure is increased through the overuse of antibiotics and prophylactic use in agriculture¹⁶⁻

¹⁸.

I – 1. Antimicrobial Resistance Crisis

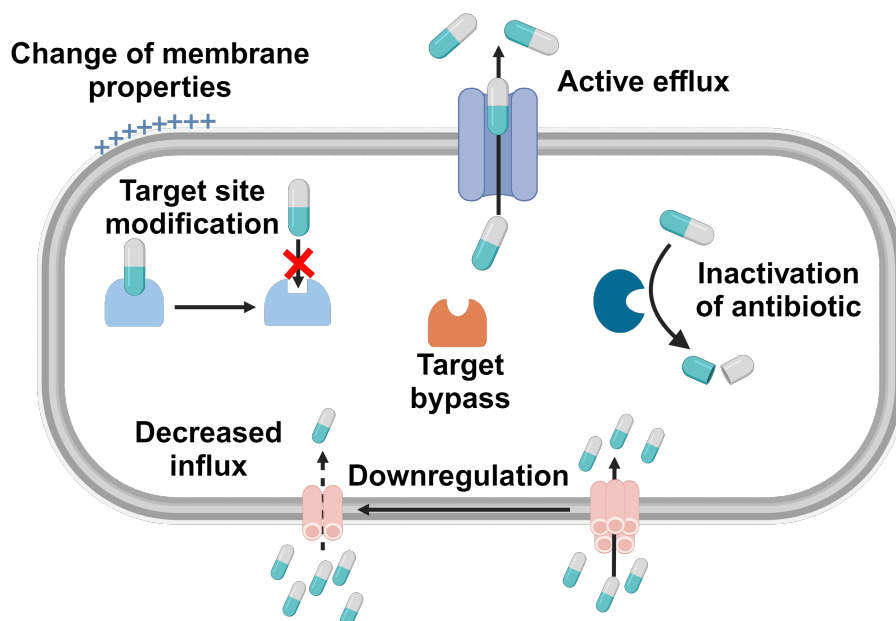


Figure 1. Molecular mechanisms of antibacterial resistance. Bacteria have various resistance mechanisms. Some bacteria actively pump out the antibiotic through ATP-driven drug efflux. Resistance can also be conferred through the expression of drug-inactivating enzymes such as β -lactamases. Drug-influx can be tuned down through *the* down-regulation of porins through which the drug enters the cell. Alternative enzymes can be expressed that bypass the targeted enzyme, or the enzyme itself is mutated so that the drug does not inhibit it anymore. Resistance against membrane-acting antibiotics can be conferred through changes in membrane properties such as a more positive charge at the outer membrane. This figure was created with BioRender.com.

While many high-income countries have started to adapt to a more conservative and targeted use of antibiotics^{5,19}, many low- and middle-income countries (LMICs) still struggle to provide antimicrobial medicines to all of their population. Coupled with a higher infectious disease burden in LMICs, antibiotic use will rise in the future, as it has risen by 39% from 2000-2015 already²⁰. The rise in AMR and the greater need for antibiotics coincide with a slump in the pharmaceutical development of antibiotics. Most large pharmaceutical companies have left the antibiotic field due to economic and regulatory barriers¹⁷. To prolong the efficacy of newer antibiotics, the World Health Organisation (WHO) has released a classification of antibiotics into first- or second-line antibiotics and last-line therapies (“Reserve”)²¹. While restricting the use of newer antibiotics will indeed prolong the time in which resistance to them is minimal, this leads to the economic difficulties faced by the few companies that have brought new antibiotics to market in recent years. The rare use of new antibiotics is at odds with a pay-per-use model²². In 2018, plazomicin, a broad-spectrum aminoglycoside antibiotic active against difficult-to-treat carbapenem-resistant *Enterobacteriaceae* (CRE), was approved by the Food and Drug Administration (FDA). Plazomicin was developed by Achagogen, a small biotechnology company. Difficulties in finding enough patients for a phase III clinical study against CRE meant that it was only approved for complex urinary tract infections (cUTIs). In

I – 1. Antimicrobial Resistance Crisis

the first year, the drug earned less than USD 1 million in sales, forcing the company to file for bankruptcy in 2019²³. This example highlights the inadequacies in antibiotic drug approval and pricing. In the current economic landscape for antibiotic development, the true societal worth of new antibiotics is not considered, even though the cumulative loss of economic output is projected to be up to 100 trillion dollars by 2050 if the AMR crisis continues as it has in the previous years⁴. To address the economic issues of antibiotic development, policymakers are contemplating new programs in which income for new antibiotics is delinked from the volume of drug sales. For example, the UK's National Health Service (NHS) has piloted a scheme in which drugs effective against crucial ESKAPE pathogens are paid for in a subscription model by the NHS. This should incentivise more investment in research and development, as this generates a path to return on investment^{22,24}. Whether these financial commitments are enough remains to be seen. Meanwhile, basic research into novel potential antibiotics with unexploited cellular targets is vital to generate the next generation of clinical candidates.

2. *Mycobacterium tuberculosis*

Tuberculosis (TB) remains a formidable challenge to global health. Its causative agent, *Mycobacterium tuberculosis* (Mtb), has evolved to be perfectly adapted to humans, its primary host²⁵. About a quarter of the world population has a latent *M. tuberculosis* infection²⁶, resulting in 10.6 million people becoming ill with TB and 1.6 million deaths in 2021, the highest number of deaths caused by a single infectious agent, apart from SARS-COV2²⁷. One of the challenges of fighting Mtb is its unique and complex cell wall structure, which effectively prevents the penetration of many small molecules^{28,29}. The cell wall comprises peptidoglycan and arabinogalactan layers, which are, in turn, surrounded by the outer mycomembrane. This outer membrane comprises trehalose dimycolates (TDMs), consisting of a trehalose head group and two mycolic acids. Mycolic acids are very long fatty acids (70-90 carbons), exclusive to mycobacteria³⁰ (Figure 2a). They are the reason for the low fluidity and, therefore, the low penetrability of the mycomembrane^{30,31}. Overall, the mycobacterial cell envelope is rich in a wide variety of lipids, many of which are important for virulence and immune evasion³². Another unique feature of Mycobacteria is their cell division mechanism. Unlike other bacteria, Mycobacteria undergo asymmetric division, leading to the formation of daughter cells and a distinctly slow replication rate³³. Interestingly, growth rates of more pathogenic and virulent mycobacterial species such as Mtb are significantly lower than less virulent, faster-growing species such as *M. smegmatis*. The exact reason for the correlation between virulence and growth rate is still unknown³⁴. Furthermore, Mtb has evolved strategies to survive and persist within human host cells, particularly in macrophages. Macrophages are cells of the innate immune system and are vital for the first-line defence against pathogens³⁵. Mtb enters the macrophage through passive phagocytosis. Once inside the cell, macrophage phagosomes usually fuse with lysosomes for degradation of the content and, therefore, lysis of the pathogen. Mtb can modulate phagosomal maturation and prevent phagolysosome formation^{36,37}. Its ability to modulate this immune response while adapting to other stressors, such as acidification and reactive oxygen species³⁸, allows Mtb to survive and grow inside macrophages³⁶.

I – 2. Mycobacterium tuberculosis

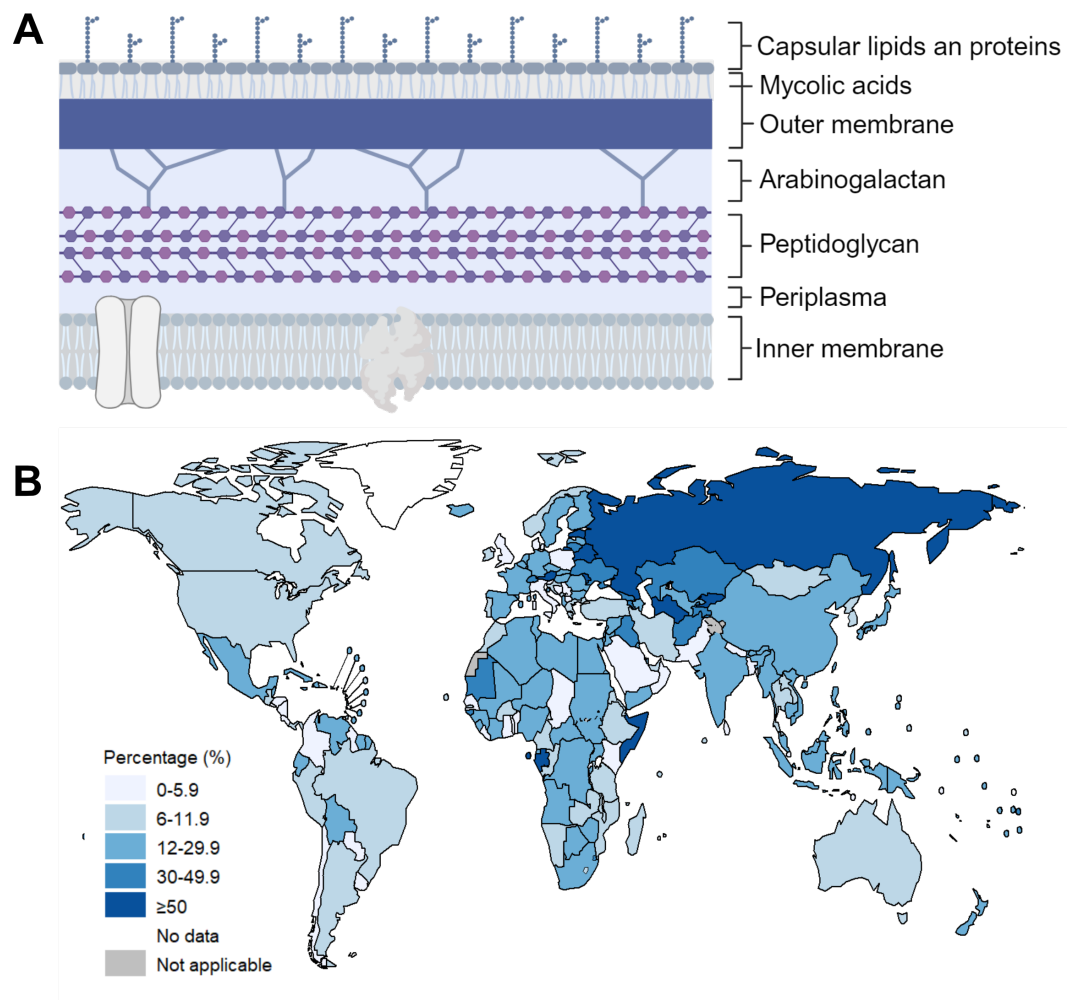


Figure 2. Tuberculosis is hard to treat, and MDR-TB is a big burden on public health in many countries. (A) Schematic representation of the Mycobacterial membranes and cell wall. This figure was created with BioRender.com (B) World map showing the percentage of previously treated TB cases with MDR or rifampicin-resistant (RR) TB in 2021. Figure was adapted from the WHO World TB Report 2022²⁷.

Due to the distinct attributes of *Mtb* compared to other bacteria, treatment relies on only a few drugs, most of which were developed decades ago. These drugs have to be applied in combination for several months with possible severe side effects³⁹. Over the past 20 years, only two new drugs, bedaquiline and delamanid, have been approved against *Mtb*⁴⁰. Meanwhile, more and more infections with multidrug-resistant (MDR TB) and extensively drug-resistant *Mtb* (XDR-*Mtb*) are being reported²⁷. Armed conflicts such as the war in Ukraine and the related displacement of people are likely to increase the incidence of MDR-TB throughout Europe⁴¹. The global burden of TB necessitates novel drugs that can kill the emerging drug-resistant *Mtb* strains. The prevalence of TB in low-income countries also requires that new drugs be low-cost, easy to transport, and store, thereby highlighting small molecule drugs as ideal candidates for new TB drugs.

3. Post-Translational Modifications During Bacterial Infection

The human genome consists of approximately 20,000 protein-coding genes. The number of proteoforms vastly exceeds the number of canonical gene sequences. This protein heterogeneity is partly achieved through post-translational modifications (PTMs)^{42,43}. PTMs can be categorised into reversible modifications with chemical groups, such as phosphorylation, or more complex molecules, such as glycosylation, and irreversible modifications, such as deamidation or proteolytic cleavage⁴⁴. PTMs influence protein stability, conformation, cellular location, activity and protein-protein interactions, enabling rapid responses to all kinds of stimuli. PTMs are integral to almost all cellular processes. Enzymes responsible for PTMs represent around 5% of all proteins in eukaryotic cells, highlighting their importance⁴⁵. For example, the human kinome, proteins that perform phosphorylation, consists of over 500 proteins, many of which are important drug targets^{46–48}.

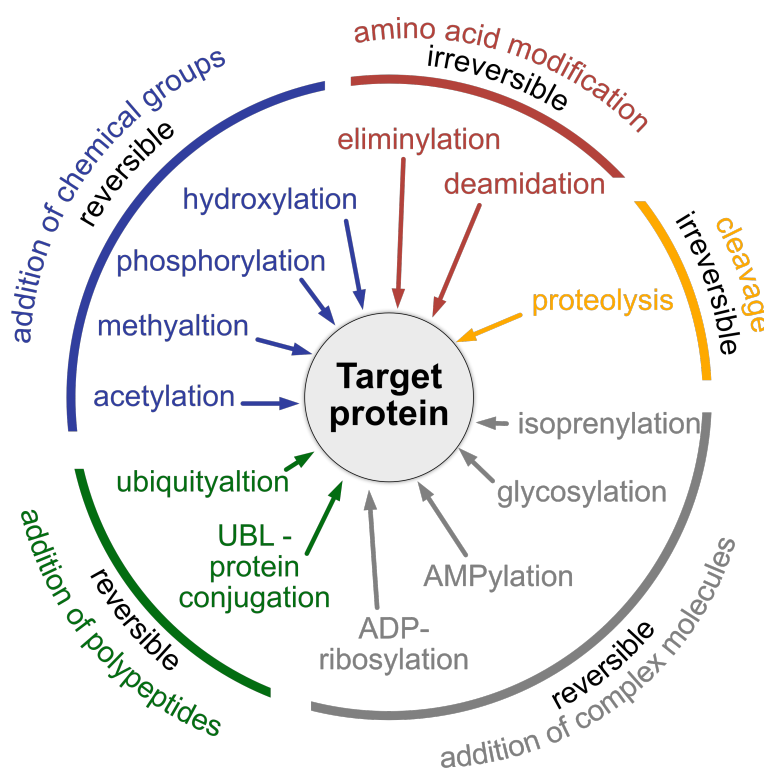


Figure 3. Overview of a selection of important PTMs categorised into different classes. The figure was adapted from Ribet et al.⁴⁹

However, cellular homeostasis is not the only process in which PTMs are crucial. Many bacteria use PTMs as key virulence strategies⁵⁰. These bacteria often use bacterial type III secretion systems to deliver effector proteins into the host cell⁴⁹. Once inside the host cell, bacterial effector proteins catalyse PTMs to modulate cellular processes to their advantage. The first such virulence mechanism to be elucidated was that of the diphtheria toxin from *Corynebacterium diphtheriae*. It catalyses the transfer of an adenosine diphosphate ribose

I – 3. Post-Translational Modifications During Bacterial Infection

moiety from NAD⁺ onto the mammalian Elongation-Factor 2 (EF-2). This ADP-ribosylation inhibits host cell protein synthesis and leads to cell death⁵¹. Some bacteria secrete up to 300 effector proteins into host cells, waging biochemical warfare, in which PTMs play a crucial role^{52–54}. The importance of PTMs during bacterial infections has become more evident over the years, with discoveries of a variety of PTMs catalysed by many different pathogens that modulate the host immune response, promoting further infection⁵². For example, *Yersinia pestis*, the causative agent of the plague, secretes the acetyltransferase YopJ which inhibits the MAPK and NF-κB pathways used in the innate immune response. It does this by using coenzyme A (CoA) to acetylate critical serine and threonine residues in the activation loops of MAPKK6 and IKK, directly competing with phosphorylation and therefore preventing activation^{55,56}. Another example is PtpA from *Mycobacterium tuberculosis*. PtpA is an effector phosphatase, which dephosphorylates two host proteins important for innate immunity upon binding to host Ubiquitin. Furthermore, its binding to Ubiquitin competes with the binding of TAB3 to Ubiquitin, affecting the NF-κB signalling pathway^{57,58}. PtpA is an important regulatory protein in attenuating phagosome-lysosome fusion⁵⁹. Gaining a better understanding of PTMs introduced by bacterial effector proteins during infection could become a novel approach for virulence attenuation. Fighting bacterial virulence instead of killing bacteria is a promising strategy to fight bacterial infections with a much lower risk of bacterial resistance due to reduced selective pressure.

4. Proteomics – Finding the Molecular Targets of Novel Drugs

4.1. Proteomics – Over 20 Years of Technological Advancement

In all three projects of this thesis, various proteomic methods constitute integral parts of the research. Proteomics is the study of all proteins in a living system. It represents the third tier of the omics fields consisting of genomics, transcriptomics, proteomics and metabolomics. Each tier increases in complexity to the previous one. A single protein-encoding gene can give rise to several mRNA isoforms on a transcriptomic level through alternative splicing or the use of different promoters^{60,61}. After translation, proteins can be further modified by PTMs or protein splicing, resulting in a wide variety of proteoforms⁴². Most currently known drugs act by targeting proteins⁶², highlighting the importance of understanding proteomic differences in diverse biological contexts. Therefore, modern mass spectrometry (MS) based proteomics has become a vital tool for drug discovery⁶³. Every MS-based bottom-up proteomic experiment consists of at least three fundamental steps: (1) sample preparation and proteolytic digest, (2) data acquisition (MS), and (3) protein identification and quantification⁶⁴ (Figure 4). All three parts have been improved significantly over the past 20 years to achieve deeper proteome coverage, higher throughput, and more robust quantification⁶⁵.

4.1.1. Proteomic sample preparation

For the sample preparation, the cells of interest need to be lysed to extract cellular proteins. While human cells are easy to lyse merely through using detergents in a buffer, many bacterial cells are hard to lyse. Here, the use of detergents in combination with mechanical disruption, such as sonication or small beads, is often used. For some bacteria, the rigid cell wall or lipopolysaccharide layer can also be enzymatically degraded using Lysozyme or more genus-specific enzymes such as Lysostaphin⁶⁶, making the subsequent lysis with detergents easier. Next, the proteins need to be isolated from other cellular components. For many years, the standard procedure was the simple precipitation of the proteins with organic solvents such as acetone or chloroform and subsequent separation through centrifugation or liquid-liquid extraction. In recent years, other methods such as the acid-based one-pot lysis and protein clean-up method termed SPEED⁶⁷, filter-aided sample preparation (FASP)⁶⁸, in-StageTip digestion (iST)⁶⁹, or single-pot solid-phase-enhanced sample preparation (SP3) have been described^{70,71}. All these methods were developed to improve quantitative protein recovery even at low input amounts, simplify the experimental setup, and, in some cases, make the sample preparation automation compatible with high throughput workflows. Every method has

I – 4. Proteomics – Finding the Molecular Targets of Novel Drugs

benefits and limitations. However, SP3 has been widely adopted due to its applicability with a wide variety of lysis and protein solubilisation components, minimal handling time, reproducibility at low protein input amounts and automation compatibility^{70–72}. In SP3, cell lysates of any origin are precipitated onto magnetic beads using organic solvent. Magnets can then be used to separate bead-bound precipitated proteins from the supernatant. The proteins can be washed several times before adding the proteolytic enzymes for on-bead digest. This results in very clean peptide samples free of detergents or chaotropic salts, allowing the sample to be measured without further peptide clean-up, such as desalting⁷¹. As this method uses magnetic beads, it requires no centrifugation steps, making it adaptable to most liquid handling systems⁷³.

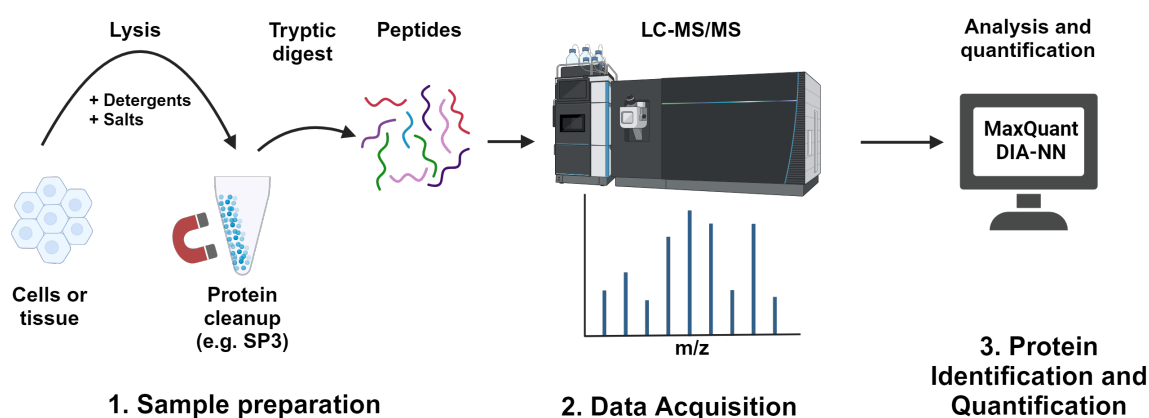


Figure 4. General Proteomics workflow. Cells are lysed, and the proteins are extracted. Clean protein mixture (bound to beads) is digested with a protease to yield a peptide mixture of all proteins from the sample. Peptides are separated through liquid chromatography before being ionised (ESI) and analysed using tandem mass spectrometry. Spectra are analysed and matched with peptides, which are then allocated to proteins for quantification. This figure was created with BioRender.com.

4.1.2. LC-MS/MS measurements and data acquisition

After sample preparation, the complex peptide mixture is analysed by liquid chromatography coupled to tandem mass spectrometry (LC-MS/MS). The peptides are usually separated based on their hydrophobicity using reversed-phase material, such as C18. Nano-flow liquid chromatography has been the most used LC setup for proteomics for 25 years⁷⁴. The low flow rate coupled to electrospray ionisation (ESI) or nano-electrospray ionisation (NSI) leads to efficient peptide ionisation and, hence, high sensitivity^{75–77}. In recent years, micro-flow LC has been used more often when the sample amount is not limited. Micro-flow LC is significantly less sensitive due to lower ionisation efficiency, but the chromatographic performance is increased due to lower peak widths, allowing shorter gradient lengths and increasing throughput⁷⁷. However, the large amount of sample needed per measurement is not feasible

I – 4. Proteomics – Finding the Molecular Targets of Novel Drugs

for many new applications, such as single-cell proteomics and miniaturisation for higher throughput. Therefore, nano-flow LC is still the state-of-the-art method used for most applications. After chromatographic separation and ionisation of the peptides, they are analysed by tandem mass spectrometry. Here, the full-length peptides are first measured in a survey scan (MS1) before being selected, fragmented, and then measured (MS2) to allow peptide identification. For over 20 years, the most used mass spectrometers for proteomics have been Orbitrap instruments^{78,79}. Their high resolution and low cycle time, when combined with linear ion traps, have proven to be ideally suited for the quantitative analysis of complex peptide samples⁸⁰. Introducing hybrid quadrupole, Orbitrap, and linear ion trap (Tribrid) instruments was another leap in performance, as the parallelisation of ion trapping, MS1, and MS2 measurements led to significantly shorter cycle times⁸¹. Recently, the Orbitrap has been coupled with another novel mass analyser termed Asymmetric Track Lossless (Astral), characterised by ultra-fast scan rates and high sensitivity, promising another leap in performance⁸². In recent years, time of flight (TOF) analysers, which used to lack the sensitivity needed for proteomics applications, have improved significantly. The breakthrough was coupling trapped ion mobility spectrometry (TIMS) with quadrupole-TOF technology⁸³. TIMS adds another chromatographic dimension in which co-eluting ionised peptides are separated in the gas phase based on their cross-section relative to their m/z . Ions entering the TIMS analyser are positioned within an electrical field by the drag of the gas flow⁸⁴ and can then be separately released into the quadrupole-TOF mass analyser. One such TIMS scan (50 ms) is much shorter than a typical full MS/MS scan (1-2 s), allowing one survey scan (MS1) followed by multiple TIMS-separated MS2 scans using the parallel accumulation serial fragmentation (PASEF) method⁸³. The accumulation of a given peptide in the TIMS device increases the subsequent signal-to-noise ratio in the TOF analyser, alleviating the issue of low sensitivity of previous TOF generations⁸³.

Since the start of MS-based bottom-up untargeted proteomics, data-dependent acquisition (DDA) has been the standard MS data acquisition method. When an MS instrument is used in DDA mode, all precursor ions are scanned during the survey scan (MS1), which is then followed by the selection of a defined number (TopN) of, or as many precursors as possible within a given cycle time, for fragmentation and MS2 scans, normally in order of decreasing intensity⁸⁵ (Figure 5). This sequential fragmentation and scanning of single precursors results in easy-to-interpret peptide sequences in the MS2 scans. Over time, improvements in MS technologies and data analysis tools have led to improved speed and sensitivity that have enabled the development of a novel acquisition method, previously not applicable to untargeted proteomics, termed data-independent acquisition (DIA). All DIA methods used for bottom-up proteomics are essentially based on Sequential Windowed Acquisition of All Theoretical Fragment Ion Mass Spectra (SWATH-MS)⁸⁶. After the survey scan (MS1), all

I – 4. Proteomics – Finding the Molecular Targets of Novel Drugs

precursor ions within a predefined m/z window are isolated, co-fragmented, and measured in several fixed m/z isolation windows covering all of the relevant m/z range⁸⁶ (Figure 5). This acquisition method results in far more complex MS2 spectra that must be deconvoluted in silico after data acquisition. For this, the obtained spectra are searched against a previously generated spectral library that includes information on peptide-spectrum matches and retention times⁸⁶. The spectral libraries are usually generated through deeply fractionated DDA measurements of the same type of samples⁸⁶. The generation of such libraries is very laborious and uses a lot of instrument time. In recent years, the use of in silico generated libraries using deep neural networks has proven to be a useful tool that does not require extensive measurements for library generation^{87,88}. The stochastic nature of precursor selection in DDA leads to less reproducible peptide identifications and less reliable quantification of low abundant proteins⁸⁵. The fact that all precursor ions are fragmented and measured in DIA methods alleviates the problem of stochastic precursor sampling⁸⁶. Until recently, one of the limitations of DIA has been the availability of high-quality spectral libraries. However, in recent years, the new deep neural network-based DIA analysis tools have proven to acquire deeper proteome coverage while improving quantitative accuracy compared to DDA^{85–87}.

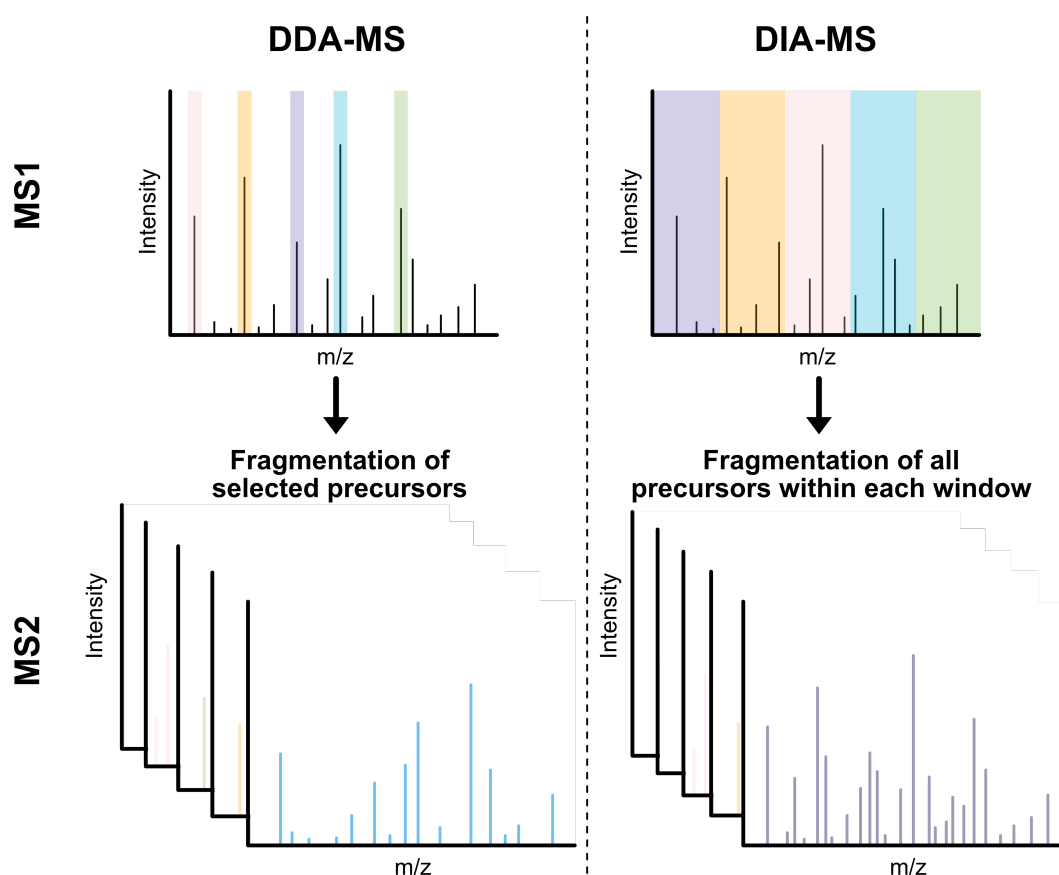


Figure 5. Comparison of data-dependent (DDA) and data-independent acquisition (DIA) for proteomics. Figure was adapted from Krasny et al.⁸⁵.

4.1.3. Protein quantification

After data acquisition and peptide/protein identification, the peptides and proteins must be quantified to identify differences in the proteome of different biological samples. To attain quantitative information, the intensities of peptides between samples are compared. For accurate quantification, several technical approaches include isotopic labels. One of the earliest methods developed was stable isotope labelling in cell culture (SILAC)⁸⁹. In this metabolic labelling method, cells are grown in a medium that contains $^{13}\text{C}_6$ -arginine and $^{13}\text{C}_6$ -lysine, which ensures that at least one labelled amino acid is present in all tryptic peptides⁹⁰. Protein quantification is then based on the ratio of co-eluting labelled (heavy) and light peptides. The advantage of this method is that the differentially treated samples can be combined at the level of intact cells, which excludes quantitative differences based on downstream sample processing and mass spectrometry measurements⁹⁰. The disadvantages of SILAC are the cost and time-intensive generation of fully labelled cell lines and the maximum number of three comparisons (light, $^{13}\text{C}_6$, and $^{15}\text{N}_4$). Additionally, SILAC is mainly limited to immortalised cell lines and is not expandable to many other biological samples. Another quantification method using isotopic labels is the use of isobaric labels, such as tandem mass tags (TMTs)⁹¹. Isobaric mass tags have identical overall mass but vary in the distribution of heavy isotopes. TMT labels consist of three functional groups: an amine-reactive group, a mass normalisation linker, and a reporter ion group. TMT labels are introduced on the peptide level through amine-reactive NHS esters. The differentially labelled peptides can be combined (multiplexing) and measured in a single LC-MS/MS run. The labelled peptides are isobaric, meaning the co-eluting peptides from the differently labelled samples have the same mass on MS1 level. The reporter-ions can then be cleaved off through fragmentation at the same time as the peptide bonds on MS2 level or, when using tribrid mass spectrometers, separately on MS3 level. Quantification on MS3 level alleviates the problem posed by co-fragmenting peptides⁹². TMT labels allow multiplexing of up to 18 samples while delivering highly accurate quantification⁹³. All isotopic labelling strategies, including isobaric labelling and SILAC, introduce additional steps in sample preparation and additional costs but reduce the amount of separate LC-MS/MS measurements. When LC-MS/MS measurement times are not limiting, label-free quantification is often the most used quantification method. Here, the MaxLFQ algorithm is the most commonly used algorithm for label-free protein quantification for both DDA and DIA data^{87,94}. In general, the MaxLFQ algorithm allows the relative quantification of a large number of samples without the use of labels. It is based on the assumption that the overall intensity of protein abundance is stable across different samples. A delayed normalisation, in which intensities are summed up with the normalisation values as free variables and a final global normalisation procedure, together with an innovative way of determining which peptides to use for protein quantification, has cemented the MaxLFQ

I – 4. Proteomics – Finding the Molecular Targets of Novel Drugs

algorithm as the benchmark for accurate label-free protein quantification for over ten years⁹⁴. The advantage of label-free quantification compared to label-based methods is that no additional sample preparation steps are introduced, making sample preparation time and cost-effective. However, the lack of sample-multiplexing leads to increased measurement times of LC-MS instruments.

Taken together, the field of proteomics has taken vast leaps forward over the past 25 years. Every technological aspect of the methodology, including sample preparation, chromatography, mass spectrometry, and software for data analysis, has been improved to a point where proteomics is set to play a vital role in clinical settings^{95,96}. Proteomics has already proven that it is an ideal candidate for discovering and profiling novel biomarkers, a precondition for precision medicine⁹⁵. Proteomic profiling of drug-treated cells (human or pathogens) can also help to identify drug targets, and more precise chemical proteomic tools such as activity-based protein profiling (ABPP) enable drug-target identification in an unbiased manner^{63,66,97}.

4.2. Activity/Affinity-Based Protein profiling (ABPP, AfBPP)

Phenotypic drug discovery approaches have seen a resurgence due to their potential to address the incompletely understood complexity of diseases. In contrast, target-based drug discovery is limited to well-understood concepts and does not necessarily yield active drugs *in vivo*. The challenge of phenotypic approaches is that target deconvolution can be difficult⁹⁸, while the knowledge of the drug target is invaluable for further hit-to-lead optimisation. A leading chemical proteomic approach to identifying the targets of novel drugs in an unbiased manner is activity- or affinity-based protein profiling (ABPP, AfBPP)⁹⁹. Pioneered by Cravatt and Bogoy^{100,101}, the method employs a chemical probe based on the structure of the active hit compound, which is further functionalised to allow subsequent analysis. These approaches operate on the principle that the active compounds bind to their protein targets in a covalent or non-covalent manner. The activity-based probes (ABPs) are equipped with a tag moiety, which allows the visualisation or purification of bound proteins based on the functionality of the applied tag. Classical ABPP utilises ABPs with covalent electrophiles, often called “warheads”, to covalently bind to nucleophilic residues in the active sites of protein targets. Depending on the warhead and molecule used, it is possible to target specific enzymes or whole classes of enzymes, such as kinases, cysteine proteases, or serine hydrolases^{100,102}. Once the targets are covalently attached to the probe, the cells can be lysed and, depending on the functional tag of the ABP, further processed. The most used tag in ABPs is a terminal alkyne moiety due to its small size and chemical inertness. It can be used for copper(I) catalysed azide-alkyne Huisgen cycloaddition, for which Sharpless and Meldal won the Nobel Prize for Chemistry in 2022, together with Carolyn Bertozzi, who further developed biorthogonal click-reactions for biological use¹⁰³. Using click chemistry, the ABP bound to a target protein can be reacted with an affinity tag such as biotin, which allows purification or enrichment of target proteins using streptavidin. The proteomic workflow follows the same procedure as discussed above, with the addition of an enrichment step using streptavidin. After LC-MS/MS analysis, comparing ABP-treated to untreated samples enables the identification of protein targets in an unbiased way^{66,97,104}. Classical ABPP has a distinctive advantage in that, by specifically targeting the active sites of enzymes, it not only identifies the protein targets of new drugs but also offers a comprehensive understanding of disease-specific enzyme dysregulation through warheads designed for entire enzyme classes¹⁰⁰. However, many drugs and bioactive natural products do not bind covalently to their protein targets, and the target site does not always have a nucleophilic group that can react with an ABP. The covalent attachment of ABPs to their targets is essential for processing samples for ABPP. Therefore, ABPs of non-covalent molecules are further functionalised with photo-reactive groups (termed AfBPPs), enabling affinity-based protein profiling (AfBPP)¹⁰⁵. The most commonly used photo-reactive groups for AfBPP are aryl azides and diazirines¹⁰⁶. These groups form highly reactive intermediates upon UV

I – 4. Proteomics – Finding the Molecular Targets of Novel Drugs

irradiation, thereby inserting non-specifically into any non-reactive C-H bond in close proximity (Figure 6). Diazirines are the most widely used photo-reactive group due to their small size, lowering the chance that the AfBP loses its biological activity. Upon UV irradiation, a singlet carbene is formed by the release of molecular nitrogen, which can insert into C-H, O-H, and N-H bonds. A side reaction of diazirines is the formation of the diazoisomer. However, this reaction is significantly slower, and the side product is readily eliminated by reacting with water. Diazirines have been used successfully for AfBPP for many years and are being developed and improved further through functionalisation^{107–109}. Aryl azides are often used to substitute aryl moieties in the molecule of interest, minimising structural perturbation of the molecule of interest. Upon UV irradiation, a reactive and short-lived singlet nitrene is formed through the release of molecular nitrogen, which can insert into C-H bonds in close proximity. The singlet nitrene can also form benzazirines, which can, upon rearrangement, lead to the formation of dihydroazepine, which can react as an electrophile with nucleophiles in proximity¹⁰⁶. The disadvantage of aryl azides compared to diazirines is that they necessitate UV irradiation of lower wavelengths, which can be harmful to biological samples. Using various probes and photo-reactive groups, AfBPP has been a crucial method for the target elucidation of many drugs and natural products¹⁰⁵.

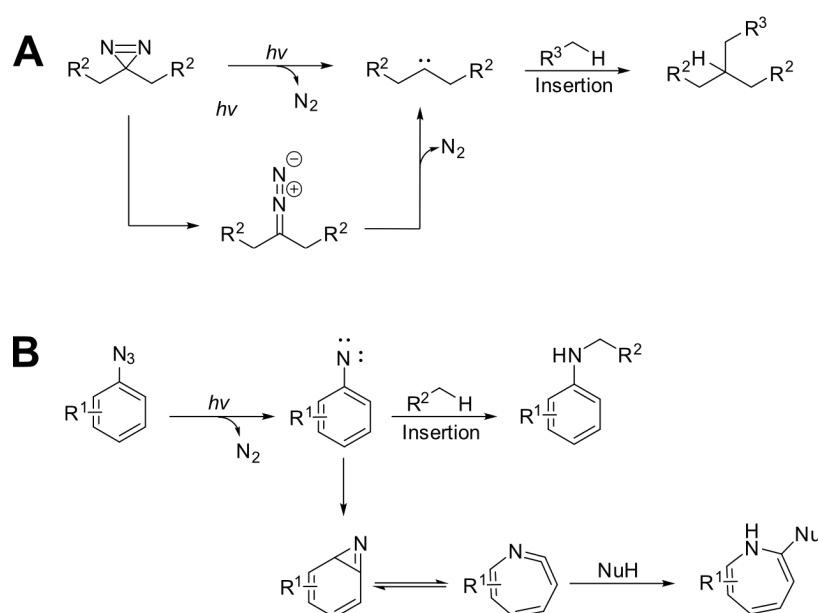


Figure 6. Two commonly applied photocrosslinking moieties for AfBPP and their respective mechanism of action for insertion upon UV irradiation. (A) Diazirines (B) Aryl azides.

4.3. Thermal Proteome Profiling (TPP)

As discussed, ABPP and AfBPP have proven very useful in studying the activity of whole enzyme classes and have successfully been used to identify drug targets. The main drawback of these methods is the need to modify the drugs or natural products to obtain the ABPs. In many cases, any perturbation of the molecular structure of a drug can lead to the loss of its biological activity. In other cases, introducing the chemical moieties needed for an ABP is synthetically not feasible, especially for many natural products with no published total synthesis. In these cases, methods such as thermal proteome profiling (TPP) can be applied in which no ABPs, and therefore no prior derivatisation of the compound, are needed. TPP is based on the thermal shift assay, in which stabilising or destabilising effects of protein-ligand binding are analysed¹¹⁰. The method is based on the fact that proteins are stabilised upon ligand binding, thereby shifting the melting curve towards higher temperatures. This can be analysed by exposing the samples to a temperature gradient and comparing the melting curves of treated and untreated proteins. This concept was developed further to be used in living cells. The cellular thermal shift assay (CETSA) has been used to identify or confirm drug targets in living cells¹¹¹. Cells are treated with a compound of interest and heated, followed by the separation of cell debris and aggregates. Then, the melting curves of specific proteins are analysed using western blotting¹¹¹. The main disadvantage of this method is that only a limited number of potential protein targets can be analysed, and there needs to be a specific antibody for each investigated protein. In 2014, Savitski *et al.* published TPP, in which they showed that they could analyse the melting curves of over 7000 human proteins and thereby identify over 50 targets of a known broad-spectrum kinase inhibitor and identified off-targets of the cancer drugs Vemurafenib and Alectinib which are responsible for known side-effects¹¹². They used state-of-the-art proteomics methods to achieve this. In principle, the method is based on the previously described CETSA protocol. Instead of using western blotting, each sample from each temperature gradient is processed for proteomics LC-MS/MS measurements. The tryptic peptides of each sample are then TMT labelled before combining all temperature points of one experiment. These multiplexed samples are then fractionated offline to lower sample complexity and then analysed by high-resolution mass spectrometry on orbitrap instruments. The melting curves for all identified proteins can be calculated using the TMT reporter ion quantification. Treated and untreated samples can be compared to identify drug targets and other downstream effects¹¹³.

I – 4. Proteomics – Finding the Molecular Targets of Novel Drugs

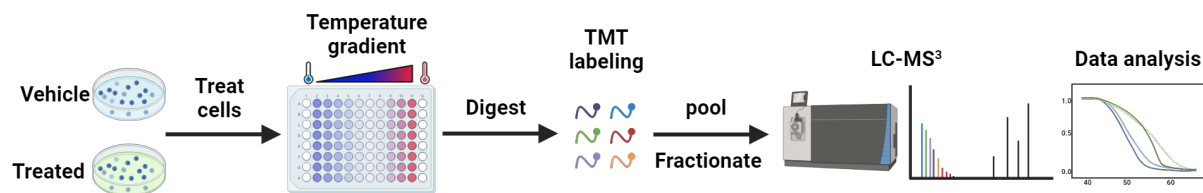


Figure 7. Schematic workflow of a thermal proteome profiling experiment. Cells are treated with compound or vehicle. Subsequently, aliquots of each sample are incubated at ten different temperatures ranging from 37 °C to 67 °C. After isolating the soluble fraction via centrifugation, the proteins are digested and TMT labelled before being fractionated and analysed by mass spectrometry. For more accurate reporter ion quantification, tribrid instruments can be operated in MS3 methods, in which the TMT reporter ions are only cleaved off from the already fragmented peptide ions to avoid co-quantification from co-eluting peptides. For each identified protein, melting curves can then be calculated to analyse the effect of compound on thermal stability of all proteins.

Since its first publication, TPP has been used to identify various drug (off-)targets, showcasing the capability of this relatively new method^{114–116}. Due to the global nature of TPP in living cells, in that it measures the thermal stability of the whole proteome, the breadth of data does not just allow drug target identification but can identify numerous down-stream effects of drugs and other environmental stimuli, which affect proteins such as protein-protein interactions, nucleic acid binding, metabolite binding, and even PTMs^{117–120}. While this large quantity of data can aid in getting a more holistic understanding of a drug's effects on cells, it makes it more difficult to identify direct drug targets amid secondary effects. One way to address this is using 2-dimensional (2-D) TPP, in which the TPP experiment is conducted at various compound concentrations to estimate a drug's affinity to certain proteins¹¹⁷. One of the biggest caveats of TPP is the time-intensive sample preparation, especially when performing 2D-TPP experiments. The continued trend towards more automation of proteomic sample preparation will help allay this problem in the future. A method which already significantly reduces the sample preparation time for thermal shift proteomics is proteome integral solubility alteration (PISA)¹²¹. Here, the temperature points of a sample are pooled and later, the replicates of treated and untreated samples are TMT labelled. In essence, instead of measuring melting curves as in TPP, in PISA, the integral of the melting curves is measured, and any change in the integral through stabilisation or destabilisation leads to a lower or higher intensity of a given protein. This method has been shown to successfully identify drug targets¹²¹, although its sensitivity is lower. The biggest caveat of all thermal shift-based analyses is that ligand binding has to induce a significant thermal shift to identify drug targets, which is not always the case, especially for larger proteins¹¹¹. Overall, TPP is a capable resource in the chemical proteomic toolbox, which complements probe-based methods such as ABPP very well when ABPs are unavailable. Additionally, TPP is not just a method to identify direct drug targets but can give

I – 4. Proteomics – Finding the Molecular Targets of Novel Drugs

a holistic view of pathways that are dysregulated through drug treatment or other stimuli without the need for changes in expression levels to identify these effects.

5. Aim of this Doctoral Thesis

With the backdrop of the growing antibiotic resistance crisis, finding novel antibacterial compounds that address new cellular targets is vital for the future of the antibiotic clinical pipeline. While the pharmaceutical industry is still holding back on this issue due to the aforementioned financial and regulatory issues, publicly funded basic research has to continue to deliver novel candidates for further clinical studies. This thesis is a combination of three different projects, each addressing a different part of antibacterial research. In all projects, various chemical proteomic approaches were used to identify new potential drug targets.

In the first project, the need for novel TB drugs is addressed. From an initial hit compound from an in-house library, the aim was to identify the cellular targets and validate these. Meanwhile, based on the hit compound's core structure and the information about the identified protein targets, the aim was an extensive hit-to-lead optimisation focusing on improving the pharmacokinetic profile.

The second project aimed to identify the molecular targets of Chlorotonil, a novel antibacterial compound isolated from Myxobacteria. The aim was to establish a thermal proteome profiling (TPP) protocol in *S. aureus*. This is the first time TPP is attempted in a pathogenic Gram-positive bacterium. Using TPP and other proteomics and biochemical experiments, the complex mode of action of Chlorotonil was further investigated.

In the third project, the aim was to investigate the nucleotide promiscuity of AMPylators. AMPylation is a crucial PTM in cellular homeostasis and during bacterial infection of host cells. Gaining a better understanding of the protein targets and the molecular mechanism of PTMs catalysed by bacterial effector proteins could identify novel pathways which antibacterial and anti-virulence drugs could address. Here, a novel UMPylation prodrug activity-based probe is used to identify potential differences in nucleotide promiscuity between human AMPylators and the bacterial effector protein VopS.

Together, these three projects highlight the usefulness of chemical proteomic methods in the pursuit of understanding complex bacterial pathways and identifying the mechanism of action of novel antibacterial drugs.

II. Tailored phenylureas eradicate drug-resistant *Mycobacterium tuberculosis* by targeting the mycolic acid cell wall assembly

This Chapter is based on the following publication:

Dietrich Mostert*, Josef Braun*, Matthew D. Zimmerman, Curtis A. Engelhart, Dirk Schnappinger, Véronique Dartois and Stephan A. Sieber. Tailored phenylureas eradicate drug-resistant *Mycobacterium tuberculosis* by targeting the mycolic acid cell wall assembly. *Manuscript in preparation, 2024*

*Authors contributed equally

Contributions:

DM and SAS planned the project and all Experiments. JB synthesised all previously unpublished affinity-based probes and all derivatives in the SAR study. DM Performed all proteomic and validation experiments included in this work. Susceptibility testing in *mmpL3* TetON strains and generation of 227-resistant mutants was performed by CAE. PK studies were performed by MDZ. DM and SAS prepared the manuscript for publication and DM created all figures.

1. Introduction

With rising numbers of multi-resistant superbugs, healthcare professionals desperately call for novel strategies to fight pathogenic bacteria, with particular emphasis on those with already limited treatment options^{27,122,123}. *Mycobacterium tuberculosis* (Mtb) especially poses a significant challenge due to its elaborate and unique cell wall structure, effectively preventing the penetration of small molecules^{28,29}. Front-line antibiotics comprise compounds such as isoniazid (INH) and ethambutol, all addressing cell wall biosynthesis as a hot spot target. For example, INH is a prodrug that forms a radical intermediate readily reacting with NADH upon activation by catalase peroxidase (KatG). The resulting NADH-INH conjugate effectively blocks enoyl-acyl carrier protein reductase (InhA), which is crucial for the biosynthesis of essential cell wall mycolic acids. Mutations in the prodrug activating KatG are one of the major INH resistance mechanisms limiting its application¹²⁴.

Several other targets in the cell wall biosynthesis pathway have been identified as sweet spots to kill the pathogen, including D-Alanyl-D-alanine ligase¹²⁵, polyketide synthase Pks13¹²⁶ and mycobacterial membrane protein large (MmpL3)^{127–135}. MmpL3 is a membrane transporter required for the translocation of trehalose monomycolates (TMM) across the Mtb inner membrane, where the mycolic acid chain is transferred to arabinogalactan via the Ag85 complex to yield trehalose dimycolate (TDM). MmpL3 also transports other lipids needed to strengthen the cell wall and is thus regarded as an essential protein and promising drug target^{130,136}. Several inhibitors of MmpL3 have been identified via high-throughput screens and rational design campaigns^{131,137}. Among those, SQ109, an ethylene diamine derivative, was the most advanced and reached clinical phase 2¹³⁸ (Figure 1A). In addition, carboxamides, benzothiazole amides, pyrrols, benzimidazoles, spiropiperidines, and adamantly ureas (AU1235) have been reported as MmpL3 inhibitors^{130,139–142}. The co-crystal structures of several MmpL3 inhibitors, including SQ109, AU1235, and ICA38, have been obtained, demonstrating a conserved binding pocket in the proton translocating channel¹⁴³(Figure 1A). For most compounds, MmpL3 was confirmed as a target via sequencing of resistant strains with corresponding mutations in the respective binding site^{141,144}. Some of these molecules also address additional targets, such as menaquinone biosynthesis enzymes, dissipation of the proton motive force, and epoxide hydrolases (Eph)^{145,146}. However, limitations of the current MmpL3 compound generations include the decoration by large lipophilic, non-aromatic groups associated with high CLogP values, low solubility and limited pharmacokinetics (PK)¹⁴⁷.

2. Results and Discussion

2.1. Screening of an in-house urea library reveals a potent Mtb antibiotic hit molecule

The diphenyl urea compound **PK150** (Figure S1) was previously shown to rapidly kill *Staphylococcus aureus* by a dual mode of action targeting menaquinone methyltransferase MenG and the signal peptidase SpsB⁶⁶. The compound was also tested against other bacteria and displayed high activity against Mtb with a minimal inhibitory concentration (MIC) of 6.25 μ M. However, the underlying MoA in Mtb remains unknown. Prior to an in-depth target deconvolution, an in-house urea library comprising 450 compounds was screened against *M. smegmatis* (Msm), an easier-to-handle surrogate of Mtb, to search for hits with even better activity. 26 compounds displayed the same or better MIC values than **PK150** (3,1 μ M in Msm) with **275** as the most potent derivative (MIC = 0.8 μ M) (Figure 1A). The top 3 hits plus **PK150** as a reference were selected for a counter screen against Mtb H37Rv, which largely confirmed their potency. **227**, a cyclohexyl substituted phenyl urea, stood out with the best MIC of 1.8 μ M, which is in the same range as front-line antibiotics such as ethambutol.

2.2. Chemical proteomics reveal essential targets in the mycolic acid pathway

Prior to chemical proteomic studies, unspecific effects on the membrane integrity were excluded. No pronounced membrane disruption was observed for the most active compounds (Figure S2). To decipher the cellular targets responsible for the antibiotic effect, three probes closely mimicking **227** were designed and synthesised (synthesis conducted by Josef Braun). In the first case, the aryl ring was substituted with an azide moiety to install a photocrosslinker. The cyclohexyl ring was equipped with an alkyne handle to enrich bound proteins via click chemistry to affinity handles (**227-p1**). In the second probe, a minimal alkyne photocrosslinker was appended to the aryl ring (**227-p2**) and in the third probe, on the cyclohexyl ring (**227-p3**) (Figure 1B). All probes were tested for their anti-mycobacterial activities, and although probes **227-p2** and **-p3** were inactive, **227-p1** retained antibiotic activity albeit with a higher MIC of 25 μ M. In addition, the existing **PK150**-like probe (**150-p**), which exhibited a MIC of 25 μ M was used and an inactive analogue (**150-ip**) was used as control (Figure S1).

II – 2. Results and Discussion

Scheme 1. Synthesis of affinity-based probes based on the structure of **227**.

Affinity-based protein profiling (AfBPP) studies were initiated by **150-p** labelling in living Msm cells. As described in the introduction, live bacteria were incubated with various probe concentrations, followed by lysis, click to rhodamine azide, and SDS-gel analysis via fluorescence scanning^{100,101,148,149}. Several fluorescent bands were visible on the gel with a concentration for a good signal-to-noise ratio of 12.5 μ M (Figure S3A). Mass spectrometry based studies were initiated by treatment of Msm cells with **150-p** and the inactive derivative probe **150-ip**, followed by lysis, click to biotin azide, enrichment on avidin beads, and tryptic digest to release peptides for LC-MS/MS analysis via label free-quantification (LFQ)⁹⁴. Identified proteins were visualised in a volcano plot with significantly enriched targets compared to the inactive probe (p-value < 0.01, fold-change >2 ($\text{Log}_2(1)$)) displayed on the upper right side (Figure 1D, Table S1). Among the proteins solely enriched by the active probe, MmpL3 and the signal peptidase LepB were the only proteins assigned to be essential for mycobacterial growth according to the *Mycobrowser* database¹⁵⁰. Of note, MmpL3 was also significantly enriched when Mtb H37Ra cells were labelled with **150-p** (Figure S3C). AfBPP experiments in *M. smegmatis* were conducted with an older protocol and data-dependent acquisition, which explains why less proteins were found overall. All subsequent AfBPP experiments were conducted using the SP2E¹⁰⁴ workflow coupled to data-independent acquisition, enhancing the proteomic depth.

To gain further insight into the target scope of the hit-compound **227**, the optimised **227-p1** probe, which more closely resembles the hit-compound, was applied in the labelling of intact Mtb H37Ra, with a pre-treatment of the bacteria with a 5-fold excess of parent **227** prior to probe addition, to verify high-confident targets by competition (Figure 1E). Interestingly, two epoxide hydrolases, EphD and EphF, involved in mycolic acid metabolism, were the only competed hits and thus pertained as high-confident targets. MmpL3 could not be enriched with **227-p1** (Figure 1F), which might be due to the different location of the photocrosslinker compared to **150-p** and the introduction of the charged azide which might hinder the probe from getting into the MmpL3 binding pocket. This could also explain the significant drop in activity of the probe compared to **227**. Overall, chemical proteomic studies with two different affinity-based probes suggest that LepB, MmpL3, and two epoxide hydrolases are putative targets which are selected for in-depth validation.

II – 2. Results and Discussion

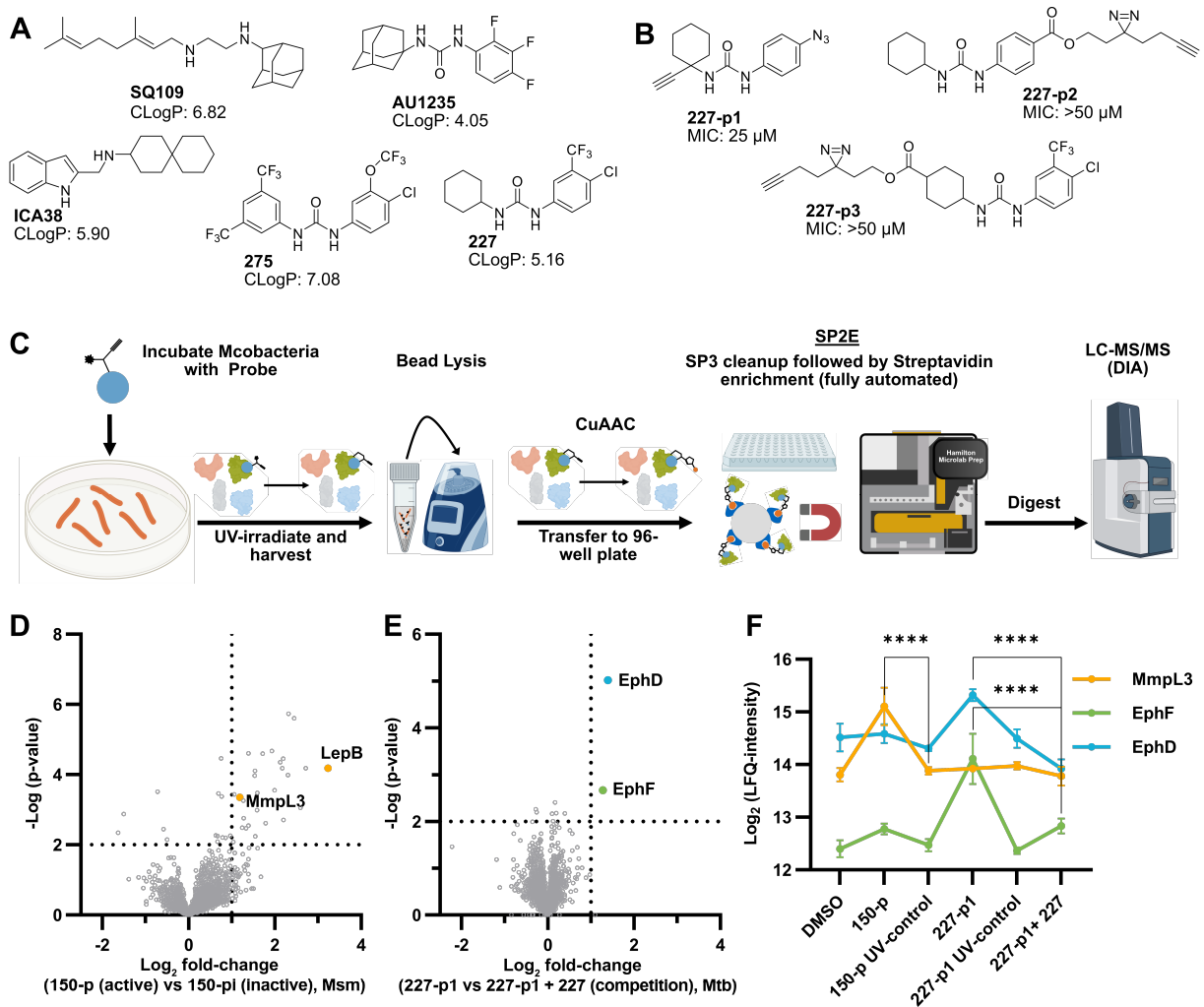


Figure 1. AFBPP to decipher protein targets. (A) Structures of known MmpL3 inhibitors SQ109, AU1235, and ICA38 and the best two hits, **275** and **227**, from a screen against *M. smegmatis* and their respective CLogP-values. (B) Structures of affinity-based probes based on the structure of **227** and their respective MIC against MTB H37Ra. (C) Schematic overview of the AFBPP workflow used in this study. An affinity-based probe is incubated with a Mycobacterial culture followed by UV-irradiation for covalent attachment of the probe to its bound protein. After cell lysis, the protein-bound probe is clicked to a biotin-azide, the proteins are captured on magnetic beads, and the probe-bound proteins are enriched using streptavidin beads. After tryptic digest, the bound proteins can be identified by LC-MS/MS analysis. (D) Volcano-plot of *M. smegmatis* cells treated with 12.5 μ M **150-p** compared to the inactive probe **150-pi**. Both MmpL3 and LepB (both essential) are significantly enriched. Dotted lines indicate significance cut-off at $p < 0.01$ ($n=7$) and a $\text{Log}_2(\text{fold change}) > 1$. (E) Volcano-plot of *M. tuberculosis* cells treated with 5 μ M **227-p1** compared to 5 μ M **227-p1** in competition with 25 μ M **227**. Both EphD and EphF are significantly enriched and out-competed by parent compound **227**. Dotted lines indicate significance cut-off at $p < 0.01$ ($n=4$) and a $\text{Log}_2(\text{fold change}) > 1$. (F) Profile plot of the mean LFQ-values of MmpL3, EphF and EphD across different proteomic samples in Mtb. **150-p** significantly enriches MmpL3 compared to its UV-control ($p < 0.0001$, $n=7$), while **227-p1** significantly enriches EphF and EphD and is out-competed by **227** ($p < 0.0001$, $n=4$), adjusted p-values, two-way ANOVA.

2.3. MmpL3 and two epoxide hydrolases are targets of 227 and derivatives

The signal peptidase LepB is essential for the cleavage of protein signal tags prior to secretion and is needed for survival. Although the corresponding signal peptidase of *S. aureus*, SpsB, was a significant target of **PK150**⁶⁶, the corresponding LepB assay with Mycobacterial membranes did not show any inhibition compared to **MD3**, a known mycobacterial LepB inhibitor (Figure S4). Thus, binding of LepB does not seem to play a role in the mechanism of action in *Mycobacteria*.

MmpL3 is a transporter essential for Mycobacterial cell wall biosynthesis. The activity of MmpL3 can be probed by feeding mycobacterial cultures with ¹⁴C-acetic acid and monitoring its incorporation into TMM and TDM via autoradiography (Figure 2A, B). If MmpL3 is blocked, TMM levels increase while TDM levels decline. The known MmpL3 inhibitor SQ109 was included as a positive control, reducing the transporter activity to 26% at a concentration of 10 μM (Figure 2D). Importantly, the hit-compound **227** reduced MmpL3 activity to 16% at 10 μM with high accumulation of TMM, validating this transporter as an antibiotic target. Newer **227**-derivatives with improved MICs against Mtb H37Ra, **21**, and **12** inhibit MmpL3 even stronger (Figure 2D). Moreover, the previously reported MmpL3 under and over-expressing Mtb H37Rv strains¹³² were used to determine MIC shifts with the compounds (conducted by Curtis Engelhart, Dirk Schnappinger Lab). SQ109 was used as a positive control and shows the expected higher susceptibility of MmpL3 under-expressing and lower susceptibility in over-expressing strains (Figure 2C, S5B, C). Ethambutol was included as a negative control and showed no significant shifts. Interestingly, the urea analogues, including **227**, exhibited higher susceptibility only in under-expressing strains but not when MmpL3 is over-expressed, suggesting a diverging MoA compared to SQ109, which may involve additional targets.

Epoxide hydrolases, the third target class, could be linked to the MoA due to their role in mycolic acid metabolism. Although not essential to promote Mtb growth in vitro, EphD was shown to be essential for survival in macrophages and the biosynthesis of oxygenated mycolic acid species, important for maintaining the integrity of the cell envelope^{151,152}. To validate the target engagement of the urea compounds on EphD and EphF, the enzymes were cloned, expressed, and purified. Despite unsuccessful attempts to yield functional EphD, functional EphF was successfully expressed, allowing the establishment of an in vitro activity assay (Figure 2E). A new assay for Mycobacterial Ephs was devised that employs epoxystearic acid as a substrate and quantifies the enzymatic conversion from the epoxide to the diol using LC-MS. Previously, assays using radioactively labelled substrate were used to measure

II – 2. Results and Discussion

mycobacterial Eph activity. Heat controls with inactivated enzyme were included to assess background hydrolysis. **227** showed strong inhibition even at a mere 10-fold excess of compound compared to the enzyme (Figure 2E). Compound **21** also inhibits EphF, albeit to a lesser extent. As observed in the competition experiment (Figure S3F), **227** out-competes **227-p1** for both EphF and EphD. Conversely, compound **21** appears to bind EphD to a similar extent as **227** but with a significantly reduced affinity for EphF. The results from the activity assay and the competitive proteomics experiment are in line with each other. Whether this means that **21** is more effective in inhibiting EphD compared to EphF would be an interesting experiment for future studies into the role of EphD in the mechanism of action.

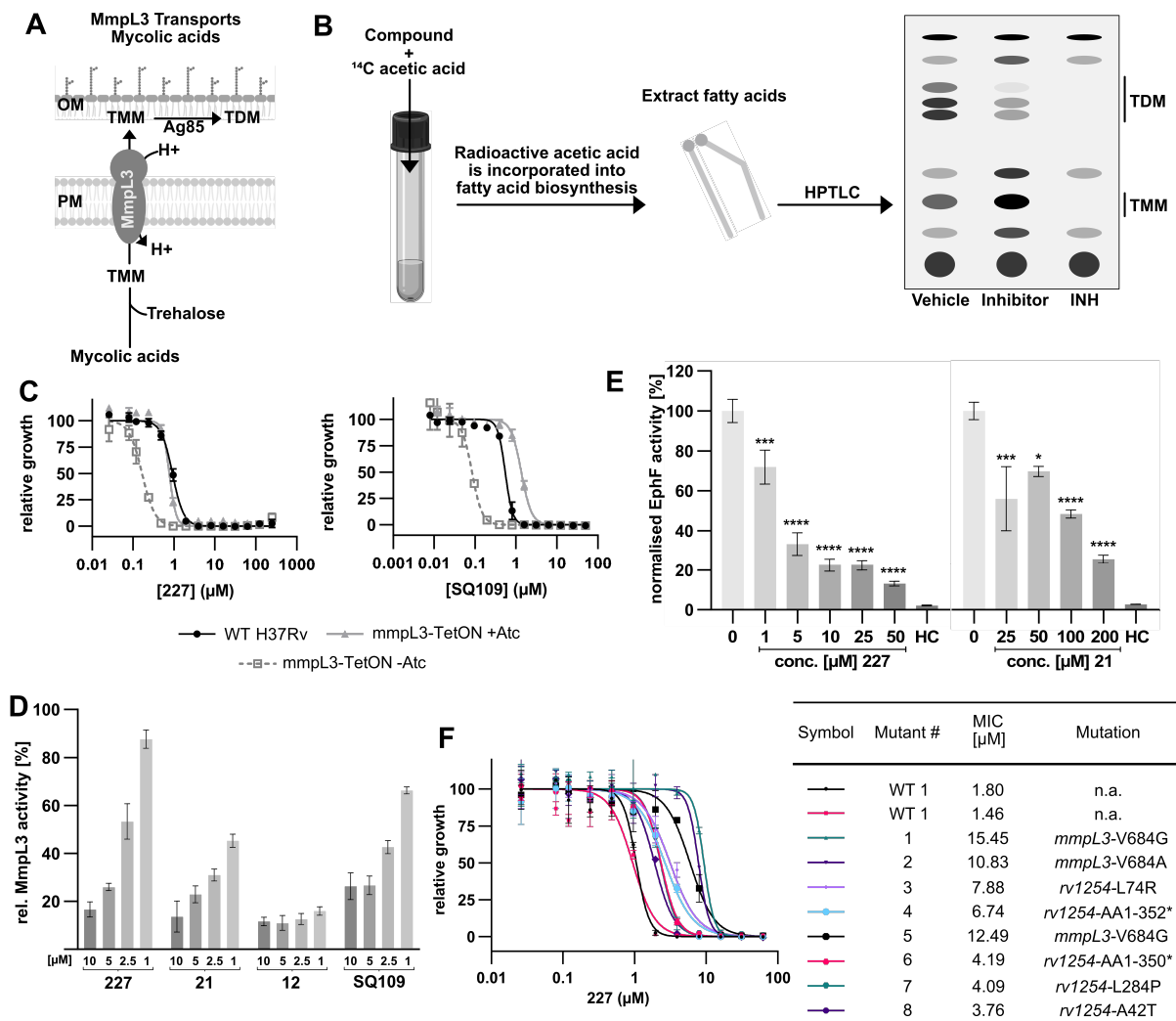


Figure 2. **227** and its derivatives inhibit MmpL3 and EphF. (A) MmpL3 is an essential mycolic acid transporter that exports trehalose monomycolate (TMM) across the mycomembrane, where it is then converted to trehalose dimycolate (TDM) by Ag85 before being incorporated into the cell wall of Mycobacteria. (B) MmpL3 activity can be measured in living cells by feeding them ¹⁴C acetic acid, which is incorporated into mycolic acids. After the extraction of fatty acids and thin layer chromatography (TLC), their relative abundance can be measured by autoradiography. As TMM is only converted to TDM after export by MmpL3, the ratio of TDM to TMM is a direct measure of MmpL3 activity. Mycolic acids can be identified by comparison to INH-treated cells, in which mycolic acid biosynthesis is completely

II – 2. Results and Discussion

inhibited. (C) Dose-response curves of Mtb H37Rv WT, MmpL3 over- (+ATc), and underexpressing (-ATc) strains dosed with **227** or SQ109. Figures each represent one of two biological replicates, each consisting of three technical replicates. (D) MmpL3 activity in Mtb H37Ra cells treated with different compound concentrations and SQ109, a known MmpL3 inhibitor. The Assay was performed in biological replicates (n=3), and the activity was calculated from the ratio of TDM to TMM and then normalised to a DMSO control. (E) EphF activity of purified EphF. Protein was pre-treated with compound or DMSO before adding 9-10-cis epoxystearic acid. After 15 minutes, the reaction was quenched with chloroform, the stearic acids were extracted, and taurocholic acid was added as an internal standard. The resulting 9,10-dihydroxystearic acid was relatively quantified by LC-MS/MS. A heat control (HC) of heat-denatured EphF was included to monitor the background hydrolysis of the epoxide. Statistical significance of inhibition (compared to DMSO) was calculated using ordinary one-way ANOVA (* = $p < 0.05$; *** = $p < 0.001$; **** = $p < 0.0001$, n=5). (F) Dose-response curves of Mtb H37Rv WT and 8 **227**-resistant mutants. The MICs and the mutations are illustrated in the table. The mutants carrying a mutation of V684 in *mmpL3* result in the biggest shift in MIC.

To further investigate additional targets of the novel urea compounds compared to SQ109, comparative whole-cell proteomic MS studies with sub-lethal doses of SQ109, **227**, and **21** in Mtb H37Ra were performed (Figure 3). SQ109 is the most advanced MmpL3 inhibitor, having reached clinical phase 2b, and was therefore chosen as the compound for the comparative analysis. There is a significant overlap of dysregulated proteins between the two urea compounds and SQ109, highlighting the fact that all three compounds target the same protein, MmpL3 (Figure 3A-D). All three compounds lead to a down-regulation of 3 subunits of the fumarate reductase complex (FrdA, FrdB, FrdD) (Figure 3E, F). Previous studies have shown that impaired succinate oxidation attenuates the activity of cell wall inhibitors, including SQ109¹⁵³. Another cluster dysregulated by all three compounds is the two carbon starvation-inducible Proteins, Rv2557 and Rv2558, whose function is still unknown but has been linked to persistence. Interestingly, some notable differences between the urea compounds and SQ109 were observed. First, the proteins belonging to the *mymA* operon and its transcription factor VirS are down-regulated (Figure 3F, G). The proteins of the *mymA* operon are required for appropriate mycolic acid composition of the cell wall and survival under acidic stress¹⁵⁴. Secondly, both **227** and **21** trigger the upregulation of the isoniazid inducible proteins IniA and IniC (Figure 3H), which provide tolerance to various cell wall biosynthesis inhibitors¹⁵⁵. Previous studies did show that SQ109 induces the *iniBAC* operon, however, these were conducted at much higher, lethal concentrations¹⁵⁶. These results indicate that in contrast to SQ109, both urea compounds target an additional step in cell wall biosynthesis. This additional step could be linked to the epoxide hydrolase targets as both **227** and **21** induce upregulation of EphF (Figure 3C), another indication that its inhibition plays a vital role in the mechanism of action of these novel compounds. Interestingly, both urea compounds induce a slight upregulation of the validated target MmpL3, while SQ109 does not (Figure 3G).

II – 2. Results and Discussion

Figure 3. Comparative Full-proteome analysis of **227**, **21**, and SQ109. (A - D) Volcano-plot of Mtb cells treated with 0.5 μ M SQ109 (A), 0.5 μ M **21** (B) or 1 μ M **227** (C, D) compared to DMSO. C and D are the same data, with differently labelled proteins. Coloured Dark blue dots indicate proteins that are significantly down-regulated by a fold-change of more than 2 ($\text{Log}_2(\text{fold change}) > 1$) in SQ109 treated cells. Maroon dots indicate proteins that are significantly up-regulated by a fold-change of more than 2 ($\text{Log}_2(\text{fold change}) > 1$) in SQ109 treated cells. Green dots indicate proteins that are significantly up-regulated by a fold-change of more than 2 ($\text{Log}_2(\text{fold change}) > 1$) in **21** treated cells. Violet dots indicate proteins that are significantly down-regulated by a fold-change of more than 2 ($\text{Log}_2(\text{fold change}) > 1$) in **21** treated cells. Light blue dot represents *IniA*, purple dot *IniC*. Light green dot is the epoxide hydrolase *EphF*, and orange dot is *MmpL3*. Pink dot is the transcriptional regulator *VirS*, responsible for activation of the *mymA* operon. Dotted lines indicate significance cut-off at $p < 0.01$ ($n=4$) and a $\text{Log}_2(\text{fold change}) > 1$. (E, F) STRING GO-term analysis of Significantly dysregulated proteins ($\text{Log}_2(\text{fold change}) > 1$ or < -1 , $p < 0.01$ of SQ109 treated cells (E) and **21** treated cells (F). For the analysis, the default STRING DB v.12.0¹⁵⁷ settings were used, and the required interaction score was set to high confidence (> 0.7). Both Compounds induce a down-regulation of the clusters CL:3015 (red) and CL:377 (dark blue), while **21** additionally induces down-regulation of the entire *mymA* operon (CL:2640, yellow) and an up-regulation of isoniazid inducible genes *iniA* and *iniC* (light blue). (G) Profile plot of the normalised abundance of *EphF*, *VirS*, and *MmpL3* across the different full proteome samples. *ephF* and *MmpL3* are slightly upregulated in **227** and **21** treated cells but not in SQ109 treated cells. *VirS* is slightly down-regulated in **21** treated cells, explaining the down-regulation of the whole *mymA* operon. (* = $p < 0.05$, ** = $p < 0.01$, **** = $p < 0.0001$ adjusted p-values, two-way ANOVA) (H) Profile plot of the mean LFQ-values of *IniA* and *IniC* across the different full proteome samples. Both proteins are concentration-dependently upregulated when cells are treated with **227** or **21**, but not induced by SQ109 (**** = $p < 0.0001$, adjusted p-values, two-way ANOVA).

To finally validate the protein targets of **227** on a genetic level, resistant mutants of Mtb H37Rv were generated at an estimated frequency of resistance of 1.5×10^{-7} at 4-fold the MIC (conducted by Curtis Engelhart, Dirk Schnappinger Lab). In total, eight resistant strains were isolated and sequenced (Figure 2F). The most substantial shift was observed for strains carrying a mutation in *mmpL3* (9.5-fold MIC), followed by strains carrying mutations in *rv1254* (4.8-fold MIC), an uncharacterised acyl transferase essential for growth. Three strains had a distinct single point mutation in *rv1254* (L74R, L284P, A42T), and another two strains had a frame-shift in *rv1254*, which resulted in a C-terminal truncation, losing the last 31 or 33 amino acids. Given the lack of direct interaction with the tailored probes, dysregulation in the full-proteome analysis, and the unknown function of *rv1254*, in-depth studies into its role in the mode of action will be subject to future work. Importantly, three strains with the most pronounced resistance each carried a single point mutation of V684 in *mmpL3*, confirming *MmpL3* as the main target of the new compound class.

2.4. Optimised 227-analogues are more potent, less hydrophobic and exhibit improved pharmacokinetic properties

Many MmpL3 inhibitors suffer from high hydrophobicity (expressed in LogP values) and, therefore, limited pharmacological properties. In fact, a CLogP of 5.2 for **227** is insufficient, and a snapshot PK experiment in mice confirmed poor bioavailability (Figure S6A). An intra-venous (i.v.) snapshot PK experiment also showed fast clearance of **227** (Figure S6B) (PK studies conducted by Matthew Zimmerman in the laboratory of Véronique Dartois). Thus, **227** needed a severe structural revision to become suitable for in vivo studies. Over 50 compounds were devised and synthesised to obtain closer insights into the structure-activity relationship (SAR) and introduce structural moieties that reduce the LogP and enhance solubility (Table 1) (synthesis conducted by Josef Braun). In the first series of **227** analogues, the substituents on the aromatic ring were varied (**1-8**, **49-51**); however, all compounds deviating from the **227**-based trifluoromethyl and chlorine substitution showed no significantly improved or, in most cases, even strongly reduced antibiotic activity. The focus was, therefore, shifted to the aliphatic side for further derivatisation. The ring size was reduced from cyclohexyl over cyclopentyl, cyclobutyl to cyclopropyl (**9-11**). While for 3 and 4-membered rings, the MIC increased to >25 μM , cyclopentyl derivative **9** remained active with a MIC of 3.2 μM . The aliphatic side was systematically varied by introducing methyl substituents, which could break planarity and influence the compound conformation. Interestingly, the incorporation of a methyl group either at 1, 2, 3, or 4 position (**12-15**) of the cyclohexyl ring significantly enhanced the antibiotic potency with the best MIC of under 0.1 μM for compound **12** bearing the methyl group at the 1-position. The two learnings were combined to minimise hydrophobicity while improving the MIC and fused the methyl group in 1-position to the cyclopentyl ring (**3**). Compound **3** indeed showed a favourable MIC of 0.4 μM compared to the non-methylated derivative **9** (3.2 μM).

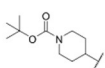
To lower the hydrophobicity further, the methyl group at the 1-position was hydroxylated (**16**, **17**) and different ligands bearing acetal groups and other hetero-atoms were introduced (**18-22**, **24-46**). Here, compound **21**, bearing a cyclobutyl acetal moiety, stood out with a MIC of 0.8 μM and an improved CLogP of 3.9. Finally, **21**, the best compound with a low CLogP, and **12**, the C1-methylated cyclohexyl derivative with the best MIC under 0.1 μM , were combined to synthesise **23**. However, this did not lead to an improved derivative as the MIC dropped to 6.25 μM , highlighting **21** as the most promising compound for in vivo studies. The mode of action of **21**, namely MmpL3- and Eph-inhibition, was confirmed to be the same as its parent **227** (Figures 2A, D, 3). Importantly, compounds **227**, **21**, and the most active compound, **12**

II – 2. Results and Discussion

showed no shift in MIC when testing against a bedaquiline-resistant clinical isolate, displaying the potential use of these compounds to treat drug-resistant TB.

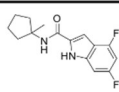
II – 2. Results and Discussion

Table 1. Overview of novel **227**-derived compounds.

									
Compound	R ¹	R ²	CLogP	MIC MTB H37Ra [μM]	Compound	R ¹	R ²	CLogP	MIC MTB H37Ra [μM]
227			5.16	1.56 - 3.125	24			3.93	50
1			5.05	3.125	25			2.68	> 50
2			4.28	> 50	26			4.68	25
3			5.12	0.39	27			3.17	> 50
4			4.75	3.125	28			3.10	> 50
5			3.38	25	29			3.69	> 50
6			3.09	> 50	30			2.76	> 50
7			3.71	25	31			3.19	> 50
8			3.82	25	32			5.57	0.39
9			4.60	3.125	33			2.61	> 50
10			4.05	25	34			2.62	> 50
11			3.71	> 50	35			5.27	25
12			5.68	< 0.1	36			4.34	> 50
13			5.68	0.39	37			4.39	> 50
14			5.68	0.39	38			3.07	> 50
15			5.68	0.39	39			4.37	12.5 - 25
16			4.53	3.125	40			3.65	>50
17			3.97	25	41			3.62	25
18			4.35	6.25	42			4.55	6.25
19			3.8	12.5	43			5.14	0.78
20			4.05	3.125	44			5.78	1.56 - 3.125
21			3.89	0.78	45			3.94	50
22			3.7	1.56-3.125	46			2.938	> 50
23			4.40	6.25 - 12.5	47			3.25	25

II – 2. Results and Discussion



Compound	R ¹	R ²	CLogP	MIC MTB H37Ra [μM]
48			2.40	> 50
49			2.88	> 50
50			2.53	> 50
51			3.35	> 50
Compound	Structure	CLogP	MIC MTB H37Ra [μM]	
52		3.87	3.125	

2.5. Compound **21** displays improved pharmacokinetic properties

As a result of the medicinal optimisation, compounds **21** and **22** were identified to have promising activity profiles to advance into in vivo studies. Of note, **21** is 2 to 4-fold antibiologically more active than the parent **227**. To select the best derivative for in vivo applications, snapshot PK studies were performed with both compounds (all PK studies conducted by Matthew Zimmerman in the laboratory of Véronique Dartois). A suitable bioavailability with both compounds was obtained exhibiting plasma concentrations above the MIC upon 25 mg/kg p.o. administration (Figure 4A, B). As **21** has a sub-micromolar MIC and displayed no pronounced cytotoxicity against human cells in a biologically relevant range ($IC_{50} = 71 \mu M$) in MTT assays (Figure S6B), it was selected for dose escalation studies (Figure 4C). The compound was well tolerated, with a dose-dependent increase in the plasma concentration. The bioavailability was slightly decreased compared to the snapshot PK analysis, probably due to a different formulation. Time over MIC was about 7 h for a 200 mg/kg dose with an AUC of $43 \mu M \cdot h$, a maximum concentration at $T_{max} = 1$ h, and a half-life of about 2.5 – 3 h, depending on the dose.

II - 2. Results and Discussion

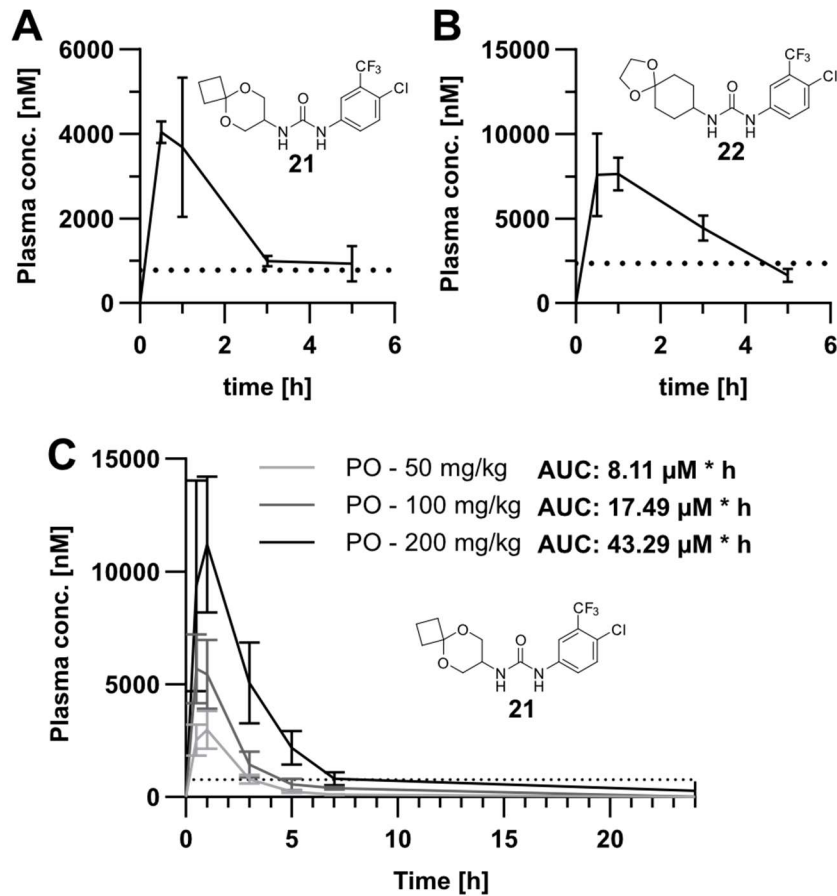


Figure 4. New **227** derivatives exhibit improved PK properties. (A, B) Snapshot PK studies of compounds **21** (A) and **22** (B). Compounds were dosed orally at 25 mg/Kg in 95% (20%) Solutol HS15, 5% DMA, and the plasma concentration was measured over time (n=2). MIC against MTB H37Ra is indicated by the dotted line. (C) Dose escalation study of compound **21**. Compounds were dosed orally in 20% Solutol HS15 on day 1 and on day 3 (n=3). The compound was well tolerated, and there was no weight loss, sickness, or necrosis.

3. Conclusion

Finding novel drugs is crucial for the continued fight against a rise in drug-resistant *Mtb*. At the same time, only two new *Mtb* drugs, bedaquiline and delamanid, against resistant strains have been approved within the past 20 years⁴⁰. In recent years, the essential mycolic acid transporter MmpL3 has been intensively studied as a promising novel drug target. Several inhibitors have been reported, and some have been validated by co-crystallisation. While there have been some reports of potential secondary targets for some of the MmpL3 inhibitors¹⁴⁵, these have not been studied in an unbiased approach. Furthermore, SAR studies and hit-to-lead developments have often only focused solely on activity (MIC) and have resulted in highly hydrophobic compounds, which suffer from poor PK properties.

In this study, an in-house library was screened and identified novel urea compounds that are active against *Mtb*. Tailored affinity-based probes were applied to identify the drug targets of the new hit compound in an unbiased manner. One of the only essential targets enriched in the affinity-based profiling experiment was the mycolic acid transporter MmpL3. Two other proteins identified as hits are the epoxide hydrolases EphF and EphD, both linked to mycolic acid metabolism¹⁵¹. MmpL3 was functionally validated as the main driver of activity by measuring its inhibition by the novel compounds and on a genomic level by generating and sequencing mutants that are resistant against **227**. The strains with the highest resistance to **227** all carried a single-point mutation of V684 in *mmpL3*. This mutation has been reported for strains resistant to indolecarboxamides^{139,158}, which indicates a similar binding mode or a conserved resistance mechanism. Some mutant strains that conferred mild resistance towards **227** had mutations in *rv1254*, an uncharacterised membrane-bound acyl transferase. As there was no direct interaction with the tailored probes nor any dysregulation in the comparative full-proteome studies, its potential role in the mode of action or metabolism of the compounds will be subject of future work. While the activity assay and sequencing of the resistant mutants validated MmpL3 as a target, overexpression of MmpL3 in *Mtb* did not result in reduced susceptibility, which is typical for MmpL3 inhibitors. This hints towards a polypharmacological mode of action. Here, we make use of the unbiased nature of affinity-based protein profiling, which identified two epoxide hydrolases as targets. Although both proteins are not essential for growth in vitro, they are essential for survival in macrophages, which could translate to improved in vivo efficacy. EphD plays a role in the biosynthesis of oxygenated mycolic acid species and in the integrity of the cell envelope. The exact role of EphF is still elusive, but due to the similar in vitro substrate specificity, a role in mycolic acid biosynthesis is also likely. While

II – 3. Conclusion

EphD could not be expressed actively, strong concentration-dependent inhibition of EphF could be shown. Comparative full proteome analysis at sub-lethal doses of **227**, **21**, and SQ109 revealed several additional dysregulated protein clusters when Mtb was treated with the novel ureas compared to SQ109. First, IniA and IniC were upregulated in the urea-treated cells. Upregulation of the Ini-operon is a well-documented tolerance mechanism against drugs that target cell wall biosynthesis. Second, the urea compounds trigger a down-regulation of the *mymA*-operon, in line with the down-regulation of its transcription factor VirS. The proteins of the *mymA* operon are required for the appropriate mycolic acid composition of the cell wall and survival under acidic stress. Lastly, both urea compounds cause an up-regulation of the target proteins MmpL3 and EphF. Taken together, these changes in the proteome of Mtb upon compound treatment and the fact that overexpression of MmpL3 does not decrease the susceptibility towards the novel compounds strongly indicate that another protein, apart from MmpL3, is targeted. The MmpL3 inhibitor AU1235 has been shown to inhibit EphD in *M. smegmatis* cells over-expressing EphD¹⁴⁶. Here, the interaction with the compounds was shown in an unbiased way. The two epoxide hydrolases EphF and EphD, were both bound by the probe **227-p1** and out-competed by **227**, EphF is inhibited by **227** in vitro, and EphF is upregulated by compound treatment. All this strongly suggests that inhibition of these epoxide hydrolases plays an important role in the mode of action of the novel urea compounds. By targeting multiple proteins in the mycolic acid biosynthesis pathway (MmpL3, EphF, EphD), two of which are essential for growth in macrophages, we have identified a promising novel hit candidate for further optimisation.

The initial hit **227** was further optimised through extensive SAR studies. The aim was to improve the activity while also focusing on lowering the hydrophobicity. It was identified that introducing acetals on the non-aromatic side of the urea compounds accomplished both goals. Compound **21** has a significantly lower cLogP (3.89) while exhibiting a sub-micromolar MIC. This lowered hydrophobicity resulted in significantly improved oral bioavailability, even with non-optimised formulations. A recent study focused on improving the solubility of AU1235-derived compounds was successful¹⁵⁹. However, the study was limited to only adamantane-containing compounds. Other, significantly more hydrophobic, MmpL3 inhibitors needed extensive formulation studies and optimisation to achieve satisfactory bioavailability¹³⁹. In future, more in-depth formulation studies could significantly improve the bioavailability of **21**, for example, by extending its half-life through sustained-release formulations¹⁶⁰. In conclusion, we were able to significantly expand the chemical space of less hydrophobic MmpL3 inhibitors beyond adamantane-containing compounds while further elucidating their polypharmacological profile beyond MmpL3 inhibition.

4. Supplementary Information

Table S1. Significant hits from volcano plot in figure 1D. *M. smegmatis* cells treated with 12.5 μ M 150-p compared to 150-pi

Uniprot ID	Gene name	Protein Description	Log ₂ fold-change	Essential ortholog in MTB? (Mycobrowser)
A0QV43	lepB	Signal peptidase I	3.23	yes
A0QT13	MSMEG_1855	Tetratricopeptide repeat protein, putative	2.72	no
A0R5I8	MSMEG_6207	Polyketide cyclase / dehydrase and lipid transport	2.59	no
A0R2U1	MSMEG_5233	RmlD substrate binding domain superfamily protein	2.45	no
A0R292	MSMEG_5030	Deazaflavin-dependent nitroreductase family protein	2.32	no
A0R5R8	MSMEG_6288	Transmembrane protein	2.19	no
A0QSW8	MSMEG_1629	Uncharacterized protein	2.17	no
A0R1J8	MSMEG_4779	Probable regulatory protein	2.13	no
A0QWJ1	yajC	Preprotein translocase, YajC subunit	1.99	no
Q3I5Q7	MSMEG_0919	HBHA-like protein, Heparin-binding hemagglutinin	1.93	no
A0R0Z5	MSMEG_4563	Puromycin N-acetyltransferase	1.72	no
A0QTV7	MSMEG_1981	Deazaflavin-dependent nitroreductase family protein	1.60	no
A0R2T3	MSMEG_5225	Lipid droplet-associated protein	1.59	no
A0R2B0	MSMEG_5048	EcsC protein family protein	1.54	no
A0QRA8	MSMEG_1049	Methyltransferase	1.53	no
A0QQB0	MSMEG_0690	Iron-sulfur cluster-binding protein	1.39	no
A0QNZ7	MSMEG_0220	Monoacylglycerol lipase	1.27	no
A0QP27	mmpL3	Trehalose monomycolate exporter MmpL3	1.18	yes
A0R5G6	MSMEG_6183	Serine protease	1.06	unclear

II – 4. Supplementary Information

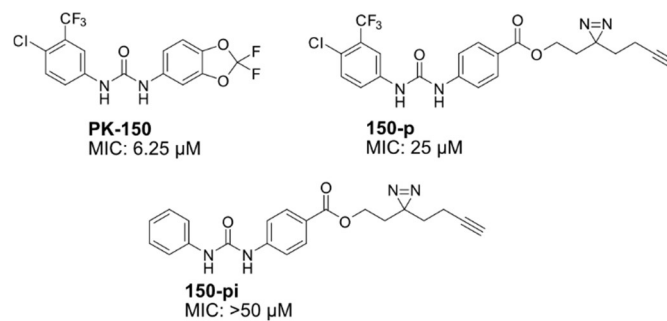


Figure S1. Structures of PK150 and the probes derived from its structure. Minimal inhibitory concentrations (MICs) in *M. tuberculosis* H37Ra show that 150-p is active, while 150-pi is inactive.

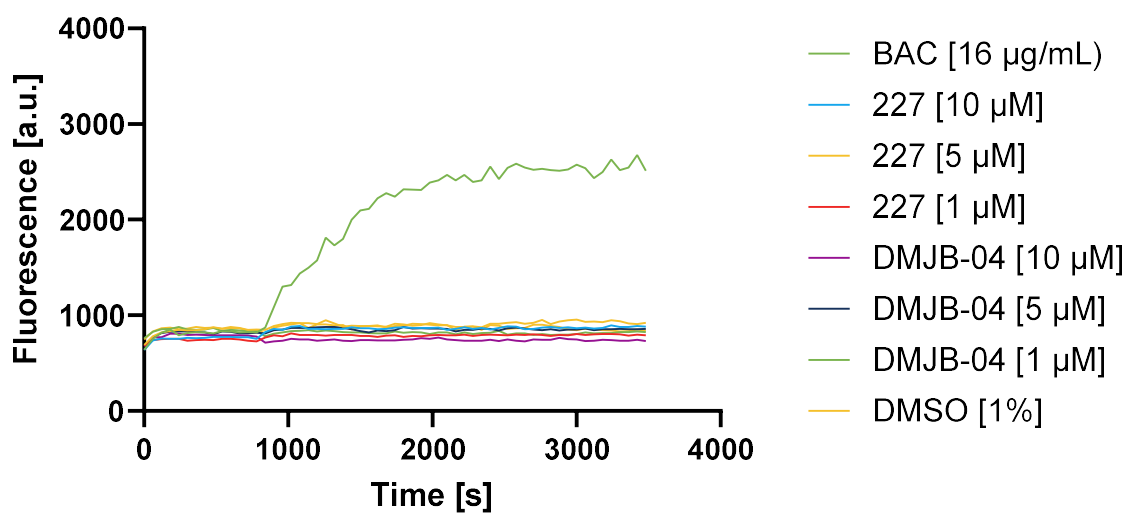


Figure S2. Membrane integrity assay. *M. tuberculosis* H37Ra cells were incubated with propidium iodide for 12 minutes before adding the indicated compounds. The Detergent benzalkonium chloride (BAC) was used as a positive control. Neither 227 nor 21 disrupt the membrane to allow propidium iodide to enter the cells. The experiment was conducted in triplicates, and the mean ($n=3$) was plotted.

II – 4. Supplementary Information

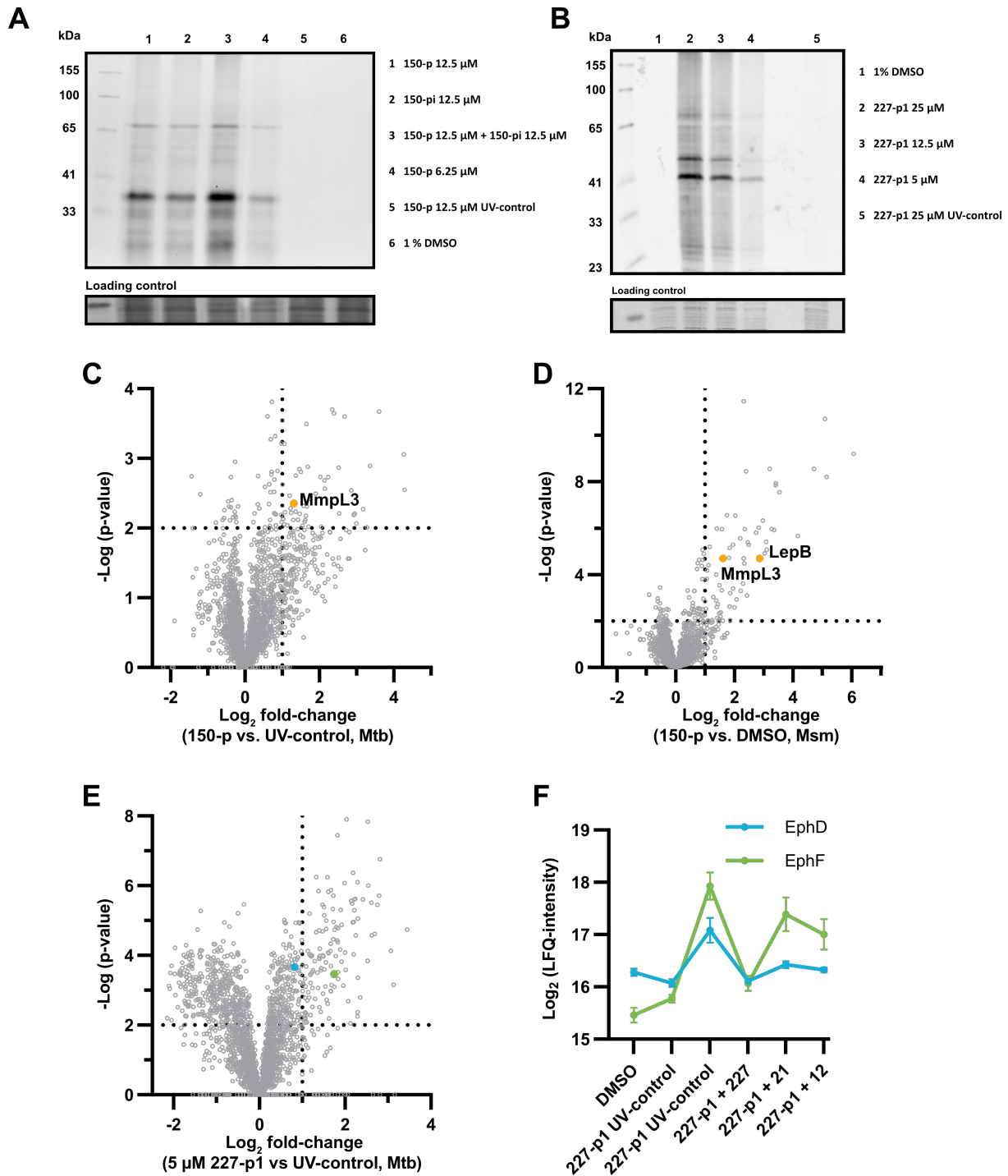


Figure S3. AfBPP to decipher protein targets. (A) Analytical labelling studies using **150-p** and **150-pi** in *M. smegmatis*. (B) Analytical labelling studies using **227-p1** in Mtb H37Ra. (C) Volcano-plot of Mtb cells treated with 12.5 μ M **150-p** compared to its UV-control. MmpL3 is also enriched in Mtb. Dotted lines indicate significance cut-off at $p < 0.01$ ($n=4$) and a $\text{Log}_2(\text{fold change}) > 1$. (D) Volcano-plot of Msm cells treated with 12.5 μ M **150-p** compared to DMSO. Both MmpL3 and LepB are significantly enriched. Dotted lines indicate significance cut-off at $p < 0.01$ ($n=7$) and a $\text{Log}_2(\text{fold change}) > 1$. (E) Volcano-plot of Mtb cells treated with 5 μ M **227-p1** compared to DMSO. Both EphD and EphF are significantly enriched. (F) Profile plot of the mean LFQ-values ($n=4$) of EphF and EphD across different proteomic samples. **227-p1** significantly enriches EphF and EphD and is strongly out-competed by **227. 21** and **12** show weaker competition in EphF binding and also slightly weaker competition in EphD binding.

II – 4. Supplementary Information

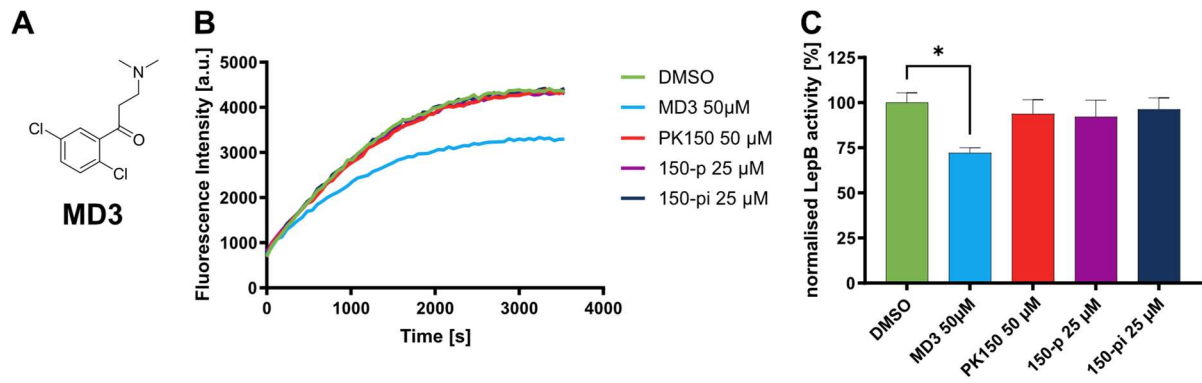


Figure S4. LepB is not a target of PK150 in Mycobacteria. (A) Structure of the known mycobacterial LepB inhibitor **MD3**. MD3 is known to strongly inhibit LepB in *Mtb* and to weakly inhibit LepB in *M. smegmatis*. (B) Cleavage of a fluorogenic LepB substrate by isolated *M. smegmatis* membranes treated with different compounds. (C) Calculated initial velocities in linear range. Neither **PK150** nor the probes derived from it modulate LepB activity. Statistical significance was determined using ordinary one-way ANOVA ($n=3$), * = $p < 0.05$.

II – 4. Supplementary Information

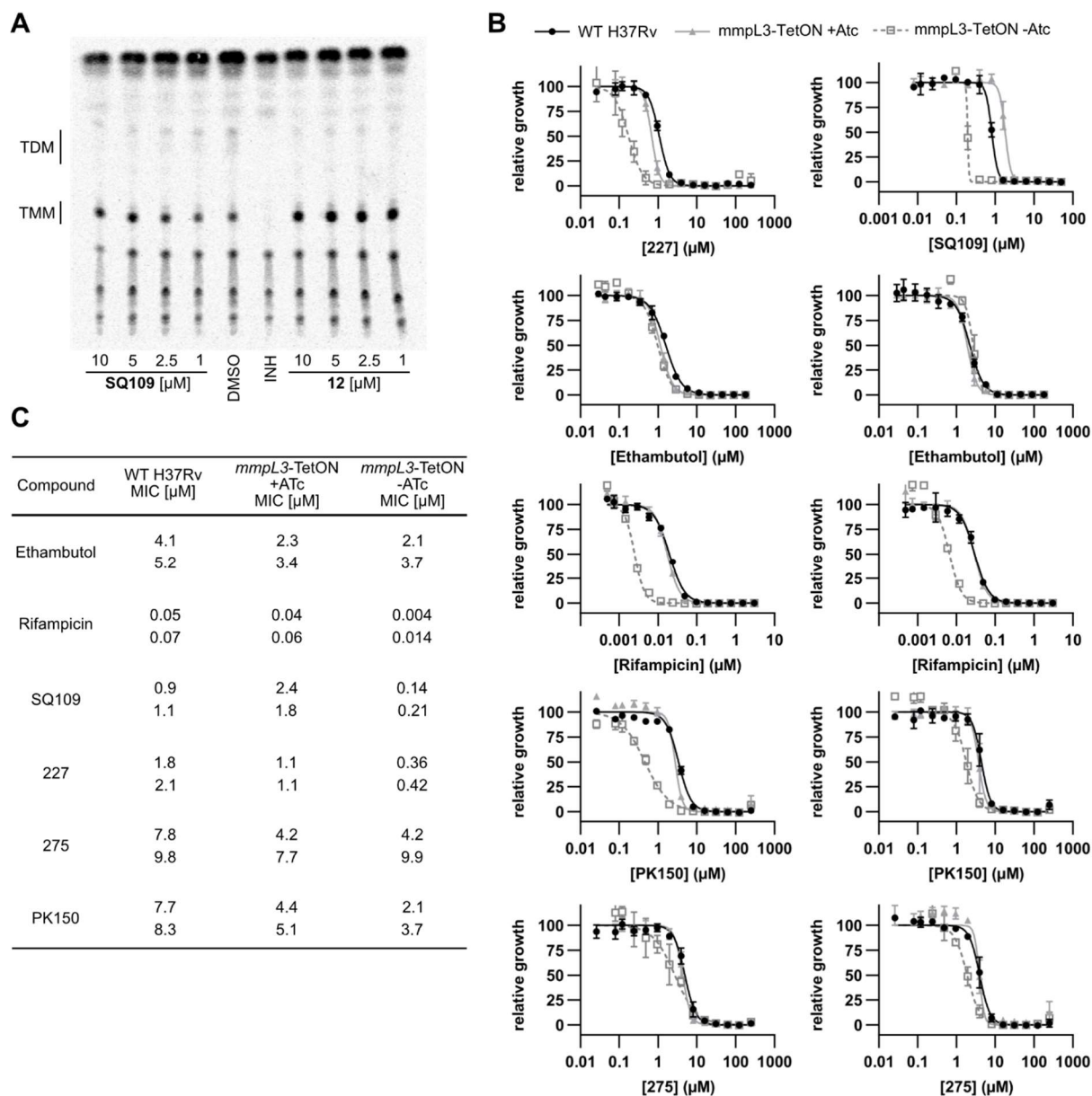


Figure S5. MmpL3 is the main target of the new compounds. (A) Example of a TLC plate quantified for the MmpL3 assay. The spots corresponding to TDM and TMM were quantified, the background was subtracted, and the ratio of TDM to TMM was calculated. (B) Dose-response curves of Mtb H37Rv WT, MmpL3 over- (+ATc), and underexpressing (-ATc) strains dosed with various compounds. Each Compound was performed in three technical triplicates and two biological replicates. Ethambutol activity is known not to be affected by MmpL3 expression levels. Rifampicin activity is known to be affected when MmpL3 is under-expressed. This is not due to direct binding. SQ109, a known MmpL3 inhibitor, exhibits distinct shifts in both directions, depending on whether MmpL3 is under- or over-expressed. (C) Table of the MICs from all under- and over-expressing experiments in Figure S5B and Figure 2D. MICs were calculated using the Gompertz model.

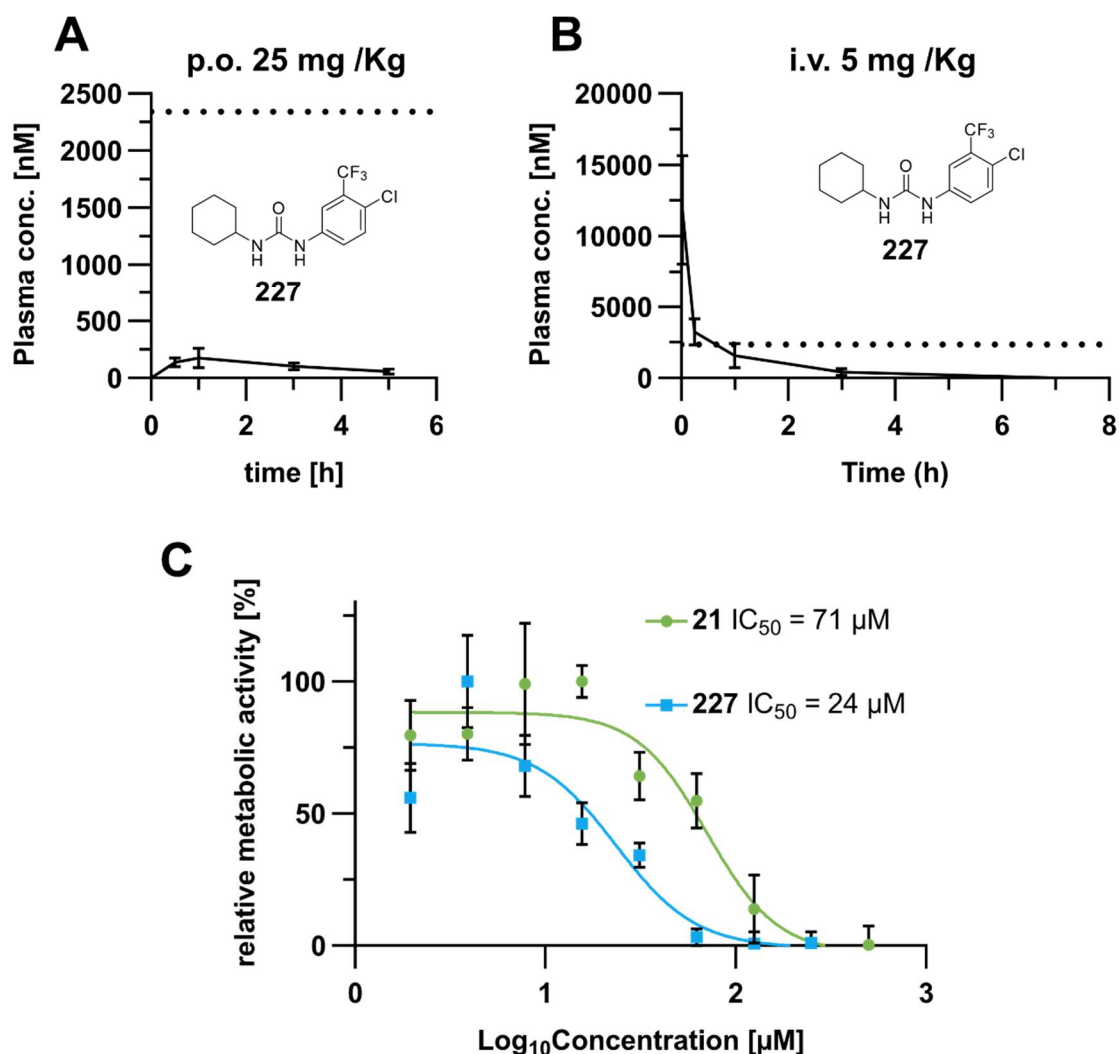


Figure S6. Initial hit **227** is not bioavailable and more toxic compared to novel compound **21**. (A) Snapshot PK study of compound **227**. Compounds were dosed orally at 25 mg/Kg in 95% (20 %) Solutol HS15, 5% DMA, and the plasma concentration was measured over time (n=2). MIC against MTB H37Ra is indicated by the dotted line. (B) Snapshot PK study of compound **227**. Compound was dosed intravenously at 5 mg/Kg in 95% PEG300, 5% DMA, and the plasma concentration was measured over time (n=4). MIC against MTB H37Ra is indicated by the dotted line. (C) MTT assay in HeLa cells of compounds **21** and **227**. 95% confidence interval (CI) of **21** (52-97 μM) and of **227** (15- 37 μM). Compound **21** displays toxicity at only very high concentrations.

5. Methods

5.1. Biochemical Methods

5.1.1. Mycobacterial culture

Unless otherwise stated, mycobacteria were cultured in 7H9+OADC+0.05% Tween-80. OADC (0.5 g/L oleic acid, 50 g/L BSA Frac V, 20 g/L Dextrose, 30 mg/L catalase) was sterile filtered and added 1:10 to autoclaved 7H9 broth (4.7 g/L 7H9 powder). The broth was stored in the fridge for no more than 4 weeks. For each culture, sterile filtered 20% Tween-80 was added freshly to a final concentration of 0.05%. *Mycobacterium tuberculosis* H37Ra was inoculated 1:100 from a glycerol Stock and grown for 10-21 days in T-175 cell culture flasks (37 °C, humidified) prior to any experiment. *M. smegmatis* was inoculated 1:1000 from a glycerol stock and grown for 3 days prior to experiments. *M. tuberculosis* was grown at 37 °C in a humidified plate incubator, while *M. smegmatis* was grown at 37 °C and 200 rpm shaking in Erlenmeyer flasks. All sample preparations for LC-MS based analysis were performed in at least four biological replicates (n=4) from four separately cultured Mycobacterial cultures.

5.1.2. Minimal inhibitory concentration measurements

To prepare the inoculum, a 10 to 14-day culture of *M. tuberculosis* H37Ra was harvested in a 50 mL falcon tube by centrifugation (7000 xg) and reconstituted in fresh 7H9+OADC+0.05% Tween-80. Five sterile glass beads were added, and the cells were vigorously vortexed to homogenise the culture. The culture was left standing for 10-20 minutes to allow the larger cell clumps to settle at the bottom. The homogenous supernatant was carefully transferred to a new sterile falcon tube, and the optical density (OD₆₀₀) was measured. The culture was adjusted to an OD₆₀₀ = 0.0063 (equivalent to 0.05 McFarland) and used as such as an inoculum for MIC measurements. For this, a serial dilution (1:1) was performed in the wells. The compounds were added from a DMSO stock to 100 µL of medium (1:50), and the serial dilution was prepared on the same plate (50 µL + 50 µL). Lastly, 50 µL of the inoculum was added to each well (accept sterile control), the plates were sealed with gas-permeable seals, and incubated for 18 days at 37 °C (humidified plate incubator).

5.1.3. Gel-based fluorescent labelling in Mycobacteria

The optical density of a late exponential to early stationary Mycobacterial culture (*M. smegmatis*: 3 days, *M. tuberculosis*: 21 days) was measured, and the cells were harvested in a 50 mL falcon tube by centrifugation (7000 xg, 10 min, 4 °C). The cell pellet was washed with

II – 5. Methods

20 mL cold PBS (7000 xg, 10 min, 4 °C) and reconstituted in PBS to a theoretical OD₆₀₀₋ value of 10. For each labelling condition, 220 µL of the cell suspension was transferred into an Eppendorf tube. 2.2 µL of the respective photo-probe was added (1 % final DMSO concentration) to the cell suspension. The cells were incubated with the photo-probes for 1 hour (37 °C, 200 rpm). After incubation, the cells were transferred to a transparent 48-well plate. While cooling, the cells were irradiated with UV light using an 18 W *Philips* TL-D BLB UV lamp ($\lambda = 310\text{-}400\text{ nm}$) to allow photo-crosslinking of the photo-reactive group. After photo-crosslinking, the cells were transferred into an Eppendorf tube and washed with 1 mL cold PBS (7000 xg, 4°C, 5 min). To lyse the cells, the pellets were reconstituted in 150 µL PBS supplemented with 0.5 % SDS and 1 % Triton X-100. The cells were sonicated (10 s, 30 % intensity, Sonopuls HD 2070 ultrasonic rod, *Bandelin electronic GmbH*) and transferred into bead-mill lysis tubes filled with 0.1 mm zirconium beads. The cells were lysed at 6500 rpm for 3x 30 s using a precllys 24 bead beater (*peq/lab*). The Lysate was centrifuged at 10.000 xg for 10 minutes, and the supernatant (120 µL) was transferred into a microcentrifuge tube and centrifuged for 10 minutes at 21.000 xg. The supernatant (100 µL) was transferred into a new centrifuge tube. The lysate was clicked to rhodamine azide by the addition of 7 µL freshly prepared click-mix (1 µL 10 mM Rhodamine-azide in DMSO, 3 µL 1.67 mM tris(benzyltriazolymethyl)amine (TBTA) in 80% tBuOH and 20% DMSO, 1 µL 50 mM CuSO₄ in water, and 2 µL 52 mM TCEP in water) and incubation for 1 h at RT. The reaction was quenched by adding 500 µL ice-cold acetone and incubating for 1 h at -20°C to precipitate all proteins. The proteins were harvested by centrifugation (20 min, 21.000 xg, 4 °C) and reconstituted in Laemmli buffer by sonication (10 s, 10% intensity). The samples were then analysed by SDS-PAGE and the fluorescence was recorded in a Fujifilm Las-4000 Luminescent Image Analyser with a Fujinon VRF43LMD3 and a 575DF20 filter.

5.1.4. Preparative labelling in *M. smegmatis* using probe 150-p for Mass spectrometry

Labelling, Lysis and Click. The *M. smegmatis* DSM43756 cells were inoculated into 5 mL 7H9 + ADC broth and incubated for 40 hours (37 °C, 200 rpm). 4 mL of the culture was then used to inoculate 60 mL 7H9 + ADC broth in 250 mL Erlenmeyer flasks with deep chicanes. The cells were grown (37 °C, 200 rpm) until they reached the stationary phase (20 – 23 hours). The OD₆₀₀₋ value was measured, and the cells were harvested in 50 mL falcon tubes by centrifugation (6000 xg, 5 min, 4 °C). The cell pellet was washed in 20 mL cold PBS (7000 xg, 5 min, 4 °C) and resuspended in PBS to a theoretical OD₆₀₀₋ value of 40. For each labelling condition, 1 mL of the cell suspension was transferred into an Eppendorf tube. 10 µL of the respective photo-probe was added (1 % final DMSO concentration) to the cell suspension. The

II – 5. Methods

cells were incubated with the photo-probes for 1 hour (37 °C, 200 rpm). After incubation, the cells were transferred to transparent 6-well plates. While cooling, the cells were irradiated with UV-light using a *Hitachi* FL8BL-B UV-lamp ($\lambda = 310\text{-}400\text{ nm}$) to allow photo-crosslinking of the diazirine group. After photo-crosslinking the cells were transferred into an Eppendorf tube and washed with 1 mL cold PBS (7000 xg, 4°C, 5 min). The cell pellet was frozen and stored at -80 °C until cell lysis. To lyse the cells, the pellets were resuspended in 1 mL PBS supplemented with 0.5 % SDS and 1 % Triton X-100. The resuspended cells were lysed by sonication (3x 15 s, 80 % intensity), cooling the samples on ice in between each sonication step. The cell debris was now removed by centrifugation (6000 xg, 5 min, 4 °C) and the supernatant was transferred into a new Eppendorf tube. The protein concentrations of the samples were determined by BCA assay (Roti Quant, Roth), and all samples were adjusted to the same protein concentration using the lysis buffer. 1 mL of each sample was transferred into a 15 mL falcon tube and clicked to biotin azide by the addition of 80 μL freshly prepared click-mix (20 μL 10 mM biotin-azide in DMSO, 30 μL 1.67 mM tris(benzyltriazolymethyl)amine (TBTA) in 80% *t*BuOH and 20% DMSO, 10 μL 50 mM CuSO_4 in water, and 20 μL 52 mM TCEP in water) and incubation for 1 h at RT. The click-reaction was quenched, and the proteins precipitated by the addition of 5 mL cold (-80 °C) Acetone (5x excess volume). The samples were incubated overnight at -20 °C.

Enrichment and Digestion. The proteins were harvested (21,000 xg, 4°C, 20 min) and washed twice with methanol. Therefore, the pellet was reconstituted in 500 μL methanol, sonicated (10 % intensity, 10 s, Sonopuls HD 2070 ultrasonic rod, *Bandelin electronic GmbH*) and harvested again via centrifugation as before. Next, the proteins were reconstituted in 500 μL 0.2% SDS in PBS by sonication (10 % intensity, 10 s) and the insoluble part was removed by centrifugation. The soluble fraction was added to 50 μL of washed (3x in 0.2% SDS in PBS) avidin-agarose beads and incubated for 1 h with continuous mixing. Afterwards, the samples were washed three times with 0.2% SDS in PBS, two times with 6 M urea and 3 times with PBS. For this the samples were centrifuged for 3 minutes at 400 xg and the supernatant was discarded each time. The beads were now resuspended in 200 μL digestion buffer 1 (3.6 M urea, 1.1 M thiourea, 5 mM TCEP in 20 mM Hepes, pH 7.5) and incubated for 30 minutes at 25 °C, 1000 rpm. The reduced bead-bound proteins were now alkylated with 5.5 mM iodoacetamide (30 min, 1000 rpm, 25 °C) and then the reaction was quenched with 10 mM DTT (30 min, 1000 rpm, 25 °C). Samples were first digested with 0.5 μg LysC (Wako) for 2 h at 25 °C before adding 600 μL 50 mM TEAB with 1.5 μg Trypsin (Promega) and a further incubation of 16 hours at 37 °C, 1000 rpm. The digest was stopped by adding 1 % FA and the peptides were desalted using 50 mg Sep-Pak C18 cartridges (Waters Corp.). Therefore, the cartridges were equilibrated with 1 mL acetonitrile, 1 mL (elution buffer (80% acetonitrile, 0.5 % FA in H_2O)) and 3 mL of wash buffer 1 (0.1 % TFA in H_2O). The samples were loaded, washed

with 3 ml wash buffer 1 and 0.5 mL of 0.5% FA in H₂O. The peptides were eluted with 2x 250 µL elution buffer and dried in a centrifugal evaporator. The peptides were reconstituted in 30 µL 1% FA and measured on an Q Exactive Plus instrument (*Thermo Fischer*).

5.1.5. LC-MS measurements on QExactive Plus.

Peptide Samples were analyzed on an UltiMate 3000 nano HPLC system (Dionex) equipped with an Acclaim C18 PepMap100 (75 µm ID × 2 cm) trap column and a 25 cm Aurora Series emitter column (25 cm × 75 µm ID, 1.6 µm FSC C18) (Ionoptics) separation column (column oven heated to 40 °C) coupled to an Q Exactive Plus Instrument (Thermo Fisher). For peptide separation, samples were loaded on the trap column and washed for 10 min with 0.1% TFA in ddH₂O at a flow rate of 5 µL/min. Subsequently, peptides were transferred to the analytical column for peptide separation and separated using the following 132 min gradient (Buffer A: H₂O + 0.1% FA; B: MeCN + 0.1% FA) with a flow rate of 300 nL/min.: in 7 min to 5% B, in 105 min from 5% to 22%, in 10 min from 22 to 35% and in another 10 min to 90% B. Separation gradient was followed by a column washing step using 90% B for 10 min and subsequent column re-equilibration with 5% B for 5 min. Peptides were ionized at a capillary temperature of 275 °C and the instrument was operated in a Top12 data dependent mode. For full scan acquisition, the orbitrap mass analyzer was set to a resolution of R = 140000, an automatic gain control (AGC) target of 3e6, and a maximal injection time of 80 ms in a scan range of 300-1500 m/z. Precursors having a charge state of >1, a minimum AGC target of 1e3 and intensities higher than 1e4 were selected for fragmentation. Peptide fragments were generated by HCD (higher-energy collisional dissociation) with a normalized collision energy of 27 % and recorded in the orbitrap at a resolution of R = 17500. Moreover, the AGC target was set to 1e5 with a maximum injection time of 100 ms scan range. Dynamic exclusion duration was set to 60 s and isolation was performed in the quadrupole using a window of 1.6 m/z.

5.1.6. Data analysis of QExactive Plus samples

MS raw data was analysed using MaxQuant¹⁶¹ software (version 2.0.3.0) and peptides were searched against the UniProt reference proteome for *M. smegmatis* mc²155 (taxon identifier: 246196, downloaded on 02.05.2022). Carbamidomethylation of cysteines was set as fixed modification, and oxidation of methionines and acetylation of N-termini were set as variable modifications. Trypsin was set as the proteolytic enzyme with a maximum of 2 missed cleavages. For the main search, precursor mass tolerance was set to 4.5 ppm and fragment mass tolerance to 0.5 Da. Label-free quantification (LFQ) mode was activated with a LFQ minimum ratio count of 2. Second peptide identification was enabled, and false discovery rate

(FDR) determination carried out by applying a decoy database and thresholds were set to 1% FDR at peptide-spectrum match and at protein levels and “match between runs” (0.7 min match and 20 min alignment time windows) option was enabled. Normalized LFQ intensities extracted from the MaxQuant result table proteinGroups.txt were further analysed with Perseus software¹⁶² (version 2.03.1). Prior to analysis, putative contaminants, reverse hits and only identified by site hits were removed. Normalized LFQ intensities were log₂ transformed and proteins with at least four valid values in at least one group were used for missing value imputation from normal distribution (width 0.3, downshift 1.8, total matrix). Two-sample Students’ t-test including permutation-based multiple testing correction (FDR = 0.05) was performed.

5.1.7. Preparative labelling in *M. tuberculosis* for Mass spectrometry

Labelling, Lysis and Click. The optical density of each biological replicate culture of the Mycobacterial culture of *M. tuberculosis* H37Ra was measured and the cells were harvested in a 50 mL falcon tube by centrifugation (7000 xg, 10 min, 4 °C). The cell pellet was washed with 20 mL cold PBS (7000 xg, 10 min, 4 °C) and reconstituted in PBS to a theoretical OD₆₀₀-value of 15. For each labelling condition, 500 µL of the cell suspension was transferred into an Eppendorf tube. 5 µL of the respective photo-probe was added (1 % final DMSO concentration) to the cell suspension. The cells were incubated with the photo-probes for 1 hour (37 °C, 200 rpm). After incubation, the cells were transferred to a transparent 48-well plate. While cooling, the cells were irradiated with UV light using an 18 W *Philips* TL-D BLB UV lamp (λ = 310- 400 nm) to allow photo-crosslinking of the photo-reactive group. After photo-crosslinking, the cells were transferred into an Eppendorf tube and washed with 1 mL cold PBS (7000 xg, 4°C, 5 min). To lyse the cells, the pellets were reconstituted in 150 µL PBS supplemented with 0.5 % SDS and 1 % Triton X-100. The cells were sonicated (10 s, 30 % intensity, Sonopuls HD 2070 ultrasonic rod, *Bandelin electronic GmbH*) and transferred into bead-mill lysis tubes filled with 0.1 mm zirconium beads. The cells were lysed at 6500 rpm for 3x 30 s using a precllys 24 bead beater (*peq/ab*). The Lysate was centrifuged at 10.000 xg for 10 minutes, and the supernatant (120 µL) was transferred into a micro-centrifuge tube and centrifuged for 10 minutes at 21.000 xg. The supernatant (100 µL) was transferred into a new centrifuge tube. The protein concentrations of the samples were determined by BCA assay (Roti Quant, Roth), and all samples were adjusted to a protein concentration of 2.23 mg/mL using the lysis buffer. 45 µL of Lysate from each sample was transferred to a 96-well plate (Polypropylene, V-bottom, *Greiner* cat. 651201), and the samples were clicked to biotin-azide. For this, 4.9 µL of click-mix (0.6 µL 20 mM biotin-azide in DMSO, 2.5 µL 1.67 mM tris(benzyltriazolymethyl)amine (TBTA) in 80% *t*BuOH and 20% DMSO, 1.2 µL 50 mM CuSO₄ in water, and 0.6 µL 100 mM

II – 5. Methods

TCEP in water) were added to each well, the plate was sealed and incubated for 90 minutes at 25 °C, 950 rpm. The reaction was quenched by the addition of 65 µL 8 M urea with 10 mM TCEP and 20 mM iodoacetamide (IAA). After 15 minutes at 25 °C, 950 rpm to allow alkylation of cysteines, the reaction was quenched by adding 2 µL 500 mM DTT per sample.

Enrichment and Digestion. All reagents used were LC-MS grade. The sample processing is based on the publication from Becker et al.¹⁰⁴ with some alterations. 10 µL of a 2-fold concentrated 1:1 mix of washed (3x H₂O) hydrophobic and hydrophilic carboxylate-coated magnetic beads (*Cytiva*) was added to each sample. To precipitate the proteins onto the beads, 175 µL ethanol were added to each sample. The plate was now placed into an automated liquid handling system (*Hamilton Microlab Prep*) for further processing. The plate was incubated for 5 minutes, 500 rpm. For each washing step, the plate was placed onto a 96-well ring magnet (*Alpaqua*, Magnum FLX) for 90 s and the supernatant was removed with a low draw speed (20 µL/s) in order to not remove any beads. The plate was then removed from the magnet and the next washing solution was added, followed by 1 minutes shaking at 800 rpm. In this way, the samples were washed 3x with 180 µL 80% ethanol and once with 180 µL acetonitrile. To elute the proteins from the carboxyl-coated beads, 75 µL 0.2% SDS in PBS was added to the samples and the plate was incubated for 5 minutes at 40°C, while shaking at 800 rpm. The plate was then placed on the magnet and the supernatant was transferred into new wells. This step was repeated and the additional 75 µL of eluted proteins was added to yield 150 µL of eluted proteins in new wells. Meanwhile, streptavidin magnet beads (*New England Biolabs*, cat# S1420S) were washed 3x with 0.2 % SDS in PBS. 50 µL of the washed streptavidin beads were added to each well containing eluted protein sample. The plate was taken out of the liquid handling system, sealed, and incubated for 1 h at 25 °C, 800 rpm in a plate shaker, with a heated lid to prevent condensation. This allowed the binding of labelled proteins to the streptavidin beads. Afterwards, the plate-seal was removed and the plate was placed back into the liquid handling system. The beads were washed 3x with 180 µL 0.1% NP-40 in PBS, 2x with 180 µL 6 M urea and 3x with 200 µL H₂O. The bead-bound proteins were digested in 100 µL 50 mM TEAB with 0.5 µg Trypsin (sequencing grade, *Promega*) overnight at 37 °C in a tightly sealed plate and with a heated lid at 800 rpm. After the tryptic digest, the peptides were eluted from the beads in the liquid handling system and subsequently desalted. For this, the samples were loaded on pre-equilibrated stage tips with two layers of SDP-RPS (*Empore*, 3M). The desalting was performed as previously described Coscia et al.¹⁶³ with some minor alterations. In short, the stage-tips were equilibrated with 150 µL wash buffer 1 (1% (vol/vol) TFA in isopropanol) before loading the samples. The samples were loaded at 500 xg for 10 minutes, followed by a wash step with 170 µL wash buffer 1 (800 xg, 10 minutes) and another washing step with 170 µL wash buffer 2 (0.2% (vol/vol) TFA in H₂O). The peptides

were eluted with 50 μ L elution buffer (1% ammonia, 80% acetonitrile) by centrifugation at 300 xg for 5 minutes, followed by 800 xg for 5 minutes. Samples were dried in a centrifugal evaporator and reconstituted in 35 μ L 1% FA for LC-MS measurements on a timsTOF Pro instrument in data-independent acquisition.

5.1.8. Full Proteome analysis in *Mtb* H37Ra

To prepare the inoculum, four 14-day cultures of *M. tuberculosis* H37Ra were harvested in 50 mL falcon tubes by centrifugation (7000 xg) and reconstituted in fresh 7H9+OADC+0.05% Tween-80. Five sterile glass beads were added, and the cells were vigorously vortexed to homogenise the culture. The culture was left standing for 10-20 minutes to allow the larger cell clumps to settle at the bottom. The homogenous supernatants were carefully transferred to a new sterile falcon tube, and the optical densities (OD₆₀₀) were measured. The cultures were adjusted to the lowest OD₆₀₀ value and used to inoculate 20 mL fresh medium (1:20) in T-25 cell culture flasks with the respective compound already added (1:1000, 0.1% DMSO). After 10 days at 37 °C (humidified), 10 mL of each culture was harvested by centrifugation (7000 xg, 4 °C), washed with cold PBS and transferred into a micro centrifuge tube. The cell pellets were reconstituted in 150 μ L PBS supplemented with 0.5 % SDS and 1 % Triton X-100. The cells were sonicated (10 s, 30 % intensity, Sonopuls HD 2070 ultrasonic rod, *Bandelin electronic GmbH*) and transferred into bead-mill lysis tubes filled with 0.1 mm zirconium beads. The cells were lysed at 6500 rpm for 3x 30 s using a precllys 24 bead beater (*peqlab*). The Lysate was centrifuged at 10.000 xg for 10 minutes, and the supernatant (120 μ L) was transferred into a micro-centrifuge tube and centrifuged for 10 minutes at 21.000 xg. The supernatant (100 μ L) was transferred into a new centrifuge tube. The protein concentrations of the samples were determined by BCA assay (Roti Quant, Roth), and all samples were adjusted to a protein concentration of 0.6 mg/mL using the lysis buffer. 25 μ L of each sample was transferred into a 96-well plate and the samples were alkylated with 10 mM TCEP and 20 mM iodoacetamide (IAA). 10 μ L of a 1:1 mix of washed (3x H₂O) hydrophobic and hydrophilic carboxylate-coated magnetic beads (*Cytiva*) was added to each sample. To precipitate the proteins onto the beads, 175 μ L ethanol were added to each sample. The plate was now placed into an automated liquid handling system (*Hamilton Microlab Prep*) for further processing. The plate was incubated for 5 minutes, 500 rpm. For each washing step, the plate was placed onto a 96-well ring magnet (*Alpaqua, Magnum FLX*) for 90 s and the supernatant was removed with a low draw speed (20 μ L/s) in order to not remove any beads. The plate was then removed from the magnet and the next washing solution was added, followed by 1 minutes shaking at 800 rpm. In this way, the samples were washed 3x with 180 μ L 80% ethanol and once with 180 μ L acetonitrile. The bead-bound proteins were digested in 100 μ L 50 mM TEAB with 0.5

µg Trypsin (sequencing grade, *Promega*) overnight at 37 °C in a tightly sealed plate and with a heated lid at 800 rpm. After the tryptic digest, the peptides were eluted from the beads in the liquid handling system, the beads were washed with 40 µL of 3.5% formic acid and the resulting 140 µL were directly transferred into MS-vials without any desalting and 2.5 µL of each sample were measured on a timsTOF Pro in data-independent acquisition mode.

5.1.9. LC-MS measurements on timsTOF Pro

Peptides were measured and online-separated using an UltiMate 3000 nano HPLC system (*Dionex*) coupled to a *Bruker* timsTOF Pro mass spectrometer via a CaptiveSpray nano-electrospray ion source and *Sonation* column oven. Peptides were first loaded on the trap column (Acclaim PepMap 100 C18, 75 µm ID x 2 cm, 3 µm particle size, *Thermo Scientific*), washed with 0.1% formic acid in water for 7 min at 5 µL/min and subsequently transferred to the separation column (*IonOpticks* Aurora C18 column, 25 cm x 75 µm, 1.7 µm) and separated over a 36 min gradient from 5% to 17% B, then to 25 % B over 18 min, then to 37% B over 6 min, followed by 10 min at 95% before re-equilibration and at a flow rate of 400 nL/min. The mobile phases A and B were 0.1 % (v/v) formic acid in water and 0.1% (v/v) formic acid in acetonitrile, respectively. The timsTOF Pro was operated in data-independent dia-PASEF mode with the dual TIMS analyser operating at equal accumulation and ramp times of 100 ms each with a set $1/K_0$ ion mobility range from 0.60 to 1.60 V × s/cm² for MS1 scans. The dia-PASEF settings for fragmentation were set to a mass range of 400 to 1201 m/z and an ion mobility range of 0.60 to 1.43 V × s × cm⁻². Two ion mobility isolation windows were performed per dia-PASEF scan with 26 m/z window widths. A total of 32 isolation windows with 1 m/z overlaps to cover the mass range were used resulting in 16 dia-PASEF scans per MS1 scan and an estimated total cycle time of 1.80 s (see Table). The collision energy was ramped linearly as a function of the mobility from 59 eV at $1/K_0 = 1.3 \text{ V} \times \text{s} \times \text{cm}^{-2}$ to 20 eV at $1/K_0 = 0.85 \text{ V} \times \text{s} \times \text{cm}^{-2}$. TIMS elution voltages were calibrated linearly to obtain the reduced ion mobility coefficients ($1/K_0$) using three Agilent ESI-L Tuning Mix ions (m/z 622, 922 and 1,222) spiked on the CaptiveSpray Source inlet filter. The timsTOF Pro was operated in data-independent dia-PASEF mode with the dual TIMS analyser operating at equal accumulation and ramp times of 100 ms each with a set $1/K_0$ ion mobility range from 0.60 to 1.60 V × s/cm² for MS1 scans. The dia-PASEF settings for fragmentation were set to a mass range of 400 to 1201 m/z and an ion mobility range of 0.60 to 1.43 V × s × cm⁻². Two ion mobility isolation windows were performed per dia-PASEF scan with 26 m/z window widths. A total of 32 isolation windows with 1 m/z overlaps to cover the mass range were used resulting in 16 dia-PASEF scans per MS1 scan and an estimated total cycle time of 1.80 s (see Table below). The collision energy was ramped linearly as a function of the mobility from 59 eV at $1/K_0 = 1.3 \text{ V} \times \text{s} \times \text{cm}^{-2}$ to 20 eV

II – 5. Methods

at $1/K_0 = 0.85 \text{ V} \times \text{s} \times \text{cm}^{-2}$. TIMS elution voltages were calibrated linearly to obtain the reduced ion mobility coefficients ($1/K_0$) using three Agilent ESI-L Tuning Mix ions (m/z 622, 922 and 1,222) spiked on the CaptiveSpray Source inlet filter.

Table of DIA-PASEF windows

MS Type	Scan	Start IM [1/K0]	End IM [1/K0]	Start Mass [m/z]	End Mass [m/z]
MS1	0	0.6	1.6	100	1700
dia-PASEF	1	0.9	1.2	800	826
dia-PASEF	1	0.6	0.9	400	426
dia-PASEF	2	0.92	1.22	825	851
dia-PASEF	2	0.62	0.92	425	451
dia-PASEF	3	0.93	1.23	850	876
dia-PASEF	3	0.63	0.93	450	476
dia-PASEF	4	0.95	1.25	875	901
dia-PASEF	4	0.65	0.95	475	501
dia-PASEF	5	0.96	1.26	900	926
dia-PASEF	5	0.66	0.96	500	526
dia-PASEF	6	0.98	1.28	925	951
dia-PASEF	6	0.68	0.98	525	551
dia-PASEF	7	0.99	1.29	950	976
dia-PASEF	7	0.69	0.99	550	576
dia-PASEF	8	1.01	1.31	975	1001
dia-PASEF	8	0.71	1.01	575	601
dia-PASEF	9	1.02	1.32	1000	1026
dia-PASEF	9	0.72	1.02	600	626
dia-PASEF	10	1.04	1.34	1025	1051
dia-PASEF	10	0.74	1.04	625	651
dia-PASEF	11	1.06	1.36	1050	1076
dia-PASEF	11	0.76	1.06	650	676

II – 5. Methods

dia-PASEF	12	1.07	1.37	1075	1101
dia-PASEF	12	0.77	1.07	675	701
dia-PASEF	13	1.09	1.39	1100	1126
dia-PASEF	13	0.79	1.09	700	726
dia-PASEF	14	1.1	1.4	1125	1151
dia-PASEF	14	0.8	1.1	725	751
dia-PASEF	15	1.12	1.42	1150	1176
dia-PASEF	15	0.82	1.12	750	776
dia-PASEF	16	1.13	1.43	1175	1201
dia-PASEF	16	0.83	1.13	775	801

5.1.10. Data analysis of timsTOF Pro measurements

MS-data were analysed using DIA-NN⁸⁷ (version 1.8.1) using the library-free mode. The library was generated using the UniProt reference proteome of *M. tuberculosis* H37Rv (taxon identifier: 83332, downloaded on 09.12.2022). For the precursor ion generation, library generation and Deep-learning based spectra, RTs and IMs prediction were enabled. Trypsin/P with maximum 2 missed cleavages; protein N-terminal M excision on; Carbamidomethyl on C as fixed modification; no variable modification; peptide length from 7 to 30; precursor charge 2–4; precursor m/z from 300 to 1800; fragment m/z from 200 to 1800 for TIMS data. Precursor FDR was set to 0.01; Mass accuracy, MS1 accuracy and Scan window were all set to 0; isotopologues, MBR and Remove likely interferences were on; Neural network classifier in single-pass mode; protein inference at gene level; heuristic protein inference was enabled (--relaxed-prot-inf); quantification strategy was set to Robust LC (high precision); Cross-run normalisation was RT-dependent; Library generation smart profiling; Speed and Ram usage was set to optimal results. LFQ quantities were extracted from the protein groups (pg) results file and were further analysed with Perseus software¹⁶² (version 2.03.1). LFQ intensities were log2 transformed and protein groups with less than four valid values in at least one group were filtered out. Two-sample Students' t-test including permutation-based multiple testing correction (FDR = 0.05) was performed for all relevant comparisons to calculate the fold-change and statistical relevance. Results table were exported and graphs prepared using *Graphpad* Prims 10.01.

5.1.11. Membrane integrity assay in *M. tuberculosis* H37Ra

To assess cell permeability upon treatment with compounds, cells were grown until they reached an OD₆₀₀ value of 0.3 - 0.7. The cells were transferred to a 50 mL falcon tube, five sterile glass beads were added, and the cells were vigorously vortexed to homogenise the culture. The culture was left standing for 10-20 minutes to allow the larger cell clumps to settle at the bottom. The homogenous supernatants were carefully transferred to a new sterile falcon tube, and the optical densities (OD₆₀₀) were measured. Cells were harvested and washed with 5 mM HEPES-NaOH buffer (pH 7.2 supplemented with 5 mM glucose) and then resuspended in the same buffer to an OD₆₀₀ of 0.4. The assay was conducted in 96-well plates (Nunc flat-bottom transparent 96-well plates: *Thermo Fischer Scientific*) with 100 μ L cell-suspension per well. As a negative control the assay was conducted in assay buffer without any cells. The assay was started by adding 1 μ L of 1 mM propidium iodide in DMF to each well (10 μ M final concentration) and incubating at 37 °C in the *TECAN* Infinite M200 Pro microplate reader to allow the propidium iodide to be integrated into the membranes. During incubation, fluorescence was measured (535 nm excitation and 617 nm emission). After 15 minutes, 1 μ L of compounds were added from DMSO-stocks with the appropriate concentrations. The fluorescence was measured for 45 minutes at 37 °C. As a positive control, 16 μ g/mL of the detergent benzalkonium chloride (BAC) were added to the cell suspension.

5.1.12. Measuring membrane bound LepB activity

Membrane preparation. A 2-day culture of *M. smegmatis* DSM43756 was inoculated (1:100) into 500 ml 7H9 + ADC broth and incubated for 40 hours (37 °C, 200 rpm). After incubation, the cells were harvested (7000 xg, 10 min, 4 °C) and washed with cold PBS (7000 xg, 10 min, 4 °C). The cells were reconstituted in 20 mL lysis buffer (50 mM TRIS/HCL pH 7.5) and lysed using a bead beater homogenizer (6 x 5500 rpm, 15 s, 2 min cooling breaks on ice after each run; Precellys Ceramic Kit CK01L, 7.0 mL tubes; Precellys 24 Homogenizer, *Bertin Technologies*). The lysate was centrifuged (12,000 x g, 4°C, 10 min) to remove intact cells and debris. Membranes were collected from the supernatant after centrifugation (39,000 x g, 4°C, 75 min) and reconstituted in cold sodium phosphate buffer (50 mM, pH 7.5). Protein concentrations were determined using Pierce BCA Protein assay kit (*Thermo Fisher Scientific, Pierce Biotechnology*).

FRET assay with membrane-bound LepB. LepB activities were measured using a Förster Resonance Energy Transfer (FRET) assay, as described by Rao et al.¹⁶⁴ with some alterations. A synthetic peptide based on the known LepB from *E. coli* based on the sequence of maltose

II – 5. Methods

binding protein, modified by 2-aminobenzoic acid (abz) and 3-nitrotyrosine (Y(NO₂)) (Y(NO₂)-FSASALAKIK(Abz), Eurogentec) was used as the substrate. Assays were performed with membrane from *M. smegmatis* DMS43756 (12.5 µg/mL total membrane protein concentration) in sodium phosphate buffer pH 7.5. Membranes containing endogenous LepB (100 µL/well final volume, sodium phosphate buffer, 50 mM, pH 7.5) were treated with the respective compound or DMSO (1:100, final assay concentration of DMSO from compound stocks 1%) at 37°C for 5 min. After addition of substrate (10 µM final substrate concentration, final dimethylformamide (DMF) concentration from substrate stock 1%) turnover was monitored by measuring fluorescence in a Tecan infinite 200Pro plate reader (340 nm excitation and 510 nm emission wavelengths, fluorescence top reading mode) at 37°C. Substrate turnover was determined and normalized to DMSO-treated samples. The Graphs were plotted using Graphpad Prism and the initial velocities were fitted in the linear range. Statistical significance was determined using ordinary one-way ANOVA (n=3).

5.1.13. MmpL3 activity assay

A stationary culture of *M. tuberculosis* H37Ra was inoculated into fresh medium (1:10) and grown to an OD₆₀₀ of 0.4. The culture was aliquoted into culture tubes (5 ml per tube) and the respective compounds were added from DMSO stocks (1:1000) and incubated for 20 minutes at 37 °C, 200 rpm. INH (20 µg/mL) was used as a control to completely inhibit mycolic acid biosynthesis. After pre-incubation with compound, 1 µL of C-14 acetic acid (1 µCi/µL in ethanol, American Radiolabeled Chemicals) was added to sample and the samples were incubated at 37 °C, 200 rpm. Cells were harvested at different time-points (1.5 mL per time-point) and harvested in micro-centrifuge tubes (7000 xg, 10 min, 4 °C). The cells were washed with cold PBS and the Pellet was reconstituted in 300 µL chloroform/methanol (2/1). The samples were vortexed and sonicated in a sonication bath (3x) before adding 100 µL HPLC-grade H₂O and centrifugation for 10 min at 17.000 xg. The organic phase was transferred into glass vials and used for HPTLC. For the HPTLCs, 20 µL of each sample was spotted and chloroform/methanol/water (30/8/1) was used to develop the plates. The HPTLC plates were incubated overnight with phosphor-imaging plates and phosphorescence was imaged using a Typhoon imager (GE Healthcare). The spots corresponding to TMMs and TDM were quantified using ImageJ and the background was subtracted before calculating the TDM/TMM ratios. The ratios were normalised to DMSO and the graphs were prepared using Graphpad Prism 10.01. The experiments were conducted in 3 independent replicates. Statistical significance was determined using an ordinary one-way ANOVA (n=3) (comparison to DMSO control).

II – 5. Methods

ACGCACGGCATAACCAGAAAGCGGACATCTGCGGGATGTTCCGGCATGATTTACCTTTCTGGGCGTTTTCCATAGTGGCGGCAATACGTGGAT
CTTTCCGCAACTCTTCTCGTAAAGACTTCAGCGCTACGGCACCCAGCGGTTTGTCTTTATTAACCGCTCCAGACCTTCATCAGTCAGCAGATA
GTTTTCGAGGAACTTTTTGCCAGCTCTTTGTTCCGACTGGCGGCGTTAATACCTGCGCTCAGCACGCCAACGAACGGTTTGGATGGTTGACC
CTTGAAGTCCGGCAGTACCGTTACACCATAATCACTTTGCTGGTGTGATGTTGGACCATGCCACGGGCCGTTGATGGTCATCGCTGTTTC
GCCTTTATTAAGGCAGCTTCTGCGATGGAGTAATCGGTGTCTGCATTATGTTTGTGTTTAAATCAGGTCAACCAGGAAGGTGACACCCGCT
TTCCGCGCCAGCGTTATCCACGCCACGTCTTAATGTCTGACTTCCGCTTTTCATACTTGAACGCATAACCCCGCTCAGCAGCAATCAGCGGC
CAGGTGAAGTACGGTCTTTCGAGGTTGAACATCAGCGCGCTTACCTTTTCGCTTTCAGTTCTTTATCCAGCGCCGGATCTCTCCAGGTT
TTTGGCGGTTCCGGCAGCAGATCTTTGTTATAAATCAGCGATAACGCTTCAACAGCGATCGGTAAGCAATCAGCTTCCGTTGTAACGTACG
GCATCCCAGGTAACGGATACAGCTTGTCTGGAACGCTTTGTCCGGGGTATTTCAGCCAACAGGCCAGATTGAGCGTAGCCACCAAAGCG
GTCGTGTGCCAGAGATAATGTACAGGCCATCGCCAGTTGCCCAACCTGTGGGAATTTCTCTCCAGTTTATCCGGATGCTCAACGGTGA
CTTAATTCGGTATCTTTCTCGAATTTCTTACCAGCTTTCAGCGAGACCGTTATAGCCTTTATCGCCGTTAATCCAGATTACCAGTTTACCTTCT
TCGATTTTCATGGGGTATGTTGATGTTGATGTTTCATGGTATATCTCCTTCTAAAGTTAAACAAAATTTTCTAGAGGGGAATTTGTTATCCG
CTCACAATTCCTTATAGTGAGTCGATTAATTTCCGCGGATCGAGATCTCGATCCTCTACGCCGACGCATCGTGGCCGGCATCACCGGCC
CCACAGGTGCGGTTGCTGGCGCTATATCGCCGACATCACCGATGGGGAAGATCGGGCTCGCCACTTCGGGCTCATGAGCGCTTGTTCGG
CGTGGGTATGGTGGCAGGCCCGTGGCCGGGGGACTGTTGGCGCCATCTCCTTGCATGCACCATTCTTTCGGCGGCGGTGCTCAACGG
CCTCAACCTACTACTGGGCTGCTTCTAATGCAGGAGTCGATAAAGGAGAGCGTCGAGATCCCGACACCATCGAATGGCGCAAAACCTTT
CGCGGTATGGCATGATAGCGCCCGGAAGAGAGTCAATTCAGGGTGGTGAATGTGAAACCAGTAACGTTATACGATGTCGACAGATATGCCGG
TGCTCTTATCAGACCGTTTCCCGCTGGTGAACCAGGCCAGCCACGTTTTCGCAAAACCGGGAAAAAGTGAAGCGGGCGATGGCGGAG
CTGAATTACATTTCCAAACCGCTGGCACAACTGGCGGGCAACAGTCGTTGCTGATTGGCGTTGCCACCTCCAGTCTGGCCCTGCACGC
GCCGTCGCAATTTGTCGCGGCGATTAATCTCGCGCCGATCAACTGGGTGCCAGCGTGGTGGTGTGATGGTGAACGAAGCGGGCTCGAA
GCCTGTAAGCGGGCGTGCACAATCTTCTCGCGCAACCGCTCAGTGGGCTGATCATAACTATCCGCTGGATGACCAGGATGCCATTGCTGT
GGAAGCTGCCTGCACTAATGTTCCGGCGTTATTTCTTGATGTCTCTGACCAGACCCCATCAACAGTATTATTTCTCCCATGAAGACGGTACG
CGACTGGGCTGGAGCATCTGGTCTGCATTGGGTACCAGCAAATCGCGCTGTTAGCGGGCCCATTAAGTTCTGTCTCGCGCGCTGTCGCTC
TGCTGGCTGGCATAAATATCTACTCGCAATCAAATTCAGCCGATAGCGGAACGGGAAGGCGACTGGAGTGCCATGTCCGGTTTTCAACAA
ACCATGCAAAATGTGAATGAGGGCATCGTTCCCACTGCGATGCTGGTTGCCAACGATCAGATGGCGCTGGGCGCAATCGCGGCCATTACCGA
GTCGGGGCTCGCGGTTGGTGGCGATATCTCGGTAGTGGGATACGACGATACCGAAGACAGCTCATGTTATATCCCGCCGTTAACCACCATCA
AACAGGATTTTCGCTGCTGGGGCAAAACCGCTGGACCGCTTCTGCAACTCTCTCAGGGCCAGGCGGTGAAGGGCAATCAGCTGTTGCC
CGTCTCACTGGTGAAGAAAAACACCCTGGCGCCAAACGCAAAACCGCCTCTCCCGCGCGTTGGCCGATTGTTAATGCAGCTGGCAC
GACAGTTTTCCCGACTGGAAGCGGGCAGTGAAGCGCAACGCAATTAATGTAAGTTAGCTCACTCATTAGGCACCCGGATCTCGACCGATGCC
CTTGAGAGCCTTCAACCCAGTCAGTCTTCCGGTGGGCGCGGGGCATGACTATGTCGCGCACTTATGACTGTCTTCTTTATCATGCAACT
CGTAGGACAGGTGCCCGCAGCGCTCTGGGTCAATTTCCGGCGAGGACCGCTTTCGCTGGAGCGCGACGATGATCGGCTGTGCTTTCGGTGA
TTCCGAATCTTGACGCCCTCGCTCAAGCCTTCGTCAGTGTCCCGCCACCAACGTTTCCGGCGAGAAGCAGGCCATTATCGCCGGCATGGC
GGCCCGACGGGTGCGCATGATGTCGCTCTGCTGTTGAGGACCCGGCTAGGCTGGCGGGGTTGCCCTACTGGTTAGCAGAATGAATCACCG
ATACGCGAGCGAACGTGAAGCGACTGTGCTGCAAAACGCTCTGCGACCTGAGCAACAACATGAATGGTCTTCGGTTTTCCGTTTTGTAAGT
CTGAAACCGGGAAGTCAGCGCCCTGCACCATTATGTTCCGGATCTGCATCGCAGGATGCTGCTGGCTACCCTGTGGAACACCTACATCTGT
ATTAACGAAGCGCTGGCATTGACCTGAGTGATTTTTCTGTTCCCGCCGATCCATACCGCCAGTTGTTTACCCTCACAACGTTCCAGTAA
CCGGGCATGTTTCATCATCAGTAACCCGATCGTGAGCATCTCTCTGTTTCATCGGTATCATTACCCCATGAACAGAAATCCCTTACACG
GAGGCATCAGTGACCAACAGGAAAAACCGCCTTAACATGGCCCGCTTATCAGAAGCCAGACATTAACGCTTCTGGAGAACTCAACGAG
CTGGACGCGGATGAACAGGCAGACATCTGTAATCGCTTACGACCACGCTGATGAGCTTACCAGCTGCTCGCGCGTTTTCCGGTATGA
CGGTGAAAACCTCTGACACATGCAGCTCCCGGAGACGGTACAGCTTGTCTGTAAGCGGATGCCGGGAGCAGACAAGCCCGTCAGGGCGCG
TCAGCGGGTGTGGCGGGTGTGGGGCGCAGCCATGACCCAGTCACGTAGCGATAGCGGAGTGTATACTGGCTTAACTATCGGCATCAGA
GCAGATTGACTGAGAGTGCACCATATGCGGTGTGAAATACCGCACAGATGCGTAAGGAGAAAAATACCGCATCAGGCGCTCTCCGCTTC
CTCGCTCACTGACTCGCTCGCTCGGTGTTCCGGCTGCGGCAGCGGTATCAGCTCACTCAAGGCGGTAATACGTTATCCACAGAATCAG
GGGATAACGCAGGAAAGAATGTGAGCAAAAGGCCAGCAAAAGGCCAGGAACCGTAAAAAGGCCGCGTTGCTGGCGTTTTCCATAGGCTC
CGCCCCCTGACGAGCATCACAATAATCGACGCTCAAGTCAGAGGTGGCGAAACCCGACAGGACTATAAAGATACCAGGCGTTTTCCCTGG
AAGCTCCCTCGTGCCTCTCCTGTTCCGACCTGCCGCTTACCGGATACCTGTCCGCTTTCTCCCTTCGGGAAGCGTGGCGCTTTCTCATA
GCTCAGCTGTAGGTATCTCAGTTCGGTGTAGGTGTTCCGCTCCAAGCTGGGCTGTGTGCACGAACCCCGTTCCAGCCGACCGCTGCGC
CTTATCCGGTAATCTGCTTTCGAGTCAACCCGTAAGACACGACTTATCGCCACTGGCAGCAGCCACTGGTAACAGGATTAGCAGAGCGA
GGTATGTAGGCGGTGCTACAGATTCTTGAAGTGGTGGCCTAACTACGGCTACACTAGAAGGACAGTATTTGGTATCTGCGCTCTGCTGAAG
CCAGTTACCTTCGAAAAAGAGTTGGTAGCTCTTATCCGGCAAAACAAACCCGCTGGTAGCGGTGGTTTTTTTTGTTTGAAGCAGCAGATT
ACGCGCAGAAAAAAGATCTCAAGAAGATCCTTTGATCTTTTCTACGGGTCTGACGCTCAGTGAACGAAAACTCAGTTAAGGGATTTTG
GTCATGAACAATAAACTGTCTGCTTACATAAACAGTAATAACAAGGGTGTATGAGCCATTTCAACGGGAAACGCTTGTCTAGGCCGCGA
TTAAATTCACATGGATGCTGATTTATATGGGTATAAATGGGCTCGGATAATGTCGGGCAATCAGGTGCGACAATCTATCGATTGATGGGA
AGCCCGATGCGCCAGAGTTGTTTCTGAAACATGGCAAGGTAGCGTTGCCAATGATGTTACAGATGAGATGGTCAAGTAACTGGCTGACG
GAATTTATGCCTTCCGACCATCAAGCATTATCCGTACTCTGATGATGCATGGTACTCACCAGTGCATCCCGGGAAAAACAGCATTCC
AGGATTAAGAAGATATCCTGATTCAGGTGAAAATATTGTTGATGCGCTGGCAGTGTCTGCGCGGTTGCAATTCGATTCTGTTGTAATTG
TCCTTTAACAGCGATCGGTATTTCTGCTCGCTCAGGCGCAATCACGAATGAATAACGGTTTTGGTTGATGCGAGTATTTGATGACGAGCG
TAATGGCTGGCCTGTTGAACAAGTCTGAAAGAAATGCATAAATTTGCCATTTCCACCGATTTCAGTGTCACTCATGGTATTTCTCACTT
GATAACCTATTTTTGACGAGGGGAAATTAATAGTTGATTTGATGTTGGACGAGTCGGAATCGCAGACCGATACCAGGATCTGCCATCTAT

II – 5. Methods

GGGATACGACGATACCGAAGACAGCTCATGTTATATCCCGCCGTTAACACCACATCAAACAGGATTTTCGCCTGCTGGGGCAAACCAGCGTGG
ACCGCTTGCTGCAACTCTCTCAGGGCCAGGCGGTGAAGGGCAATCAGCTGTTGCCCGTCTCACTGGTGAAAAGAAAAACCACCTGGCGCC
CAATACGCAAACCGCCTCTCCCCGCGCTTGGCCGATTCAATATGCAGCTGGCACGACAGGTTTCCCGACTGAAAGCGGGCAGTGAGCG
CAACGCAATTAATGTAAGTTAGCTCACTCATTAGGCACCGGGATCTCGACCGATGCCCTTGAAGCCTTCAACCCAGTCAGCTCCTCCGGT
GGCGCGGGGCATGACTATCGTCGCCGCACTTATGACTGTCTTTTATCATGCAACTCGTAGGACAGGTGCCGGCAGCGCTCTGGGTCAATTT
TCGGCGAGGACCGCTTTCGCTGGAGCGCGACGATGATCGGCCTGTGCTTGCCTTTCGGAATCTTGACACGCCCTCGCTCAAGCCTTCGT
CACTGGTCCCACCACAAACGTTTCGGCGAGAAGCAGGCCATTATCGCCGGCATGGCGGCCCCACGGGTGCGCATGATCGTGTCTCTGTGCG
TTGAGGACCCGGCTAGGCTGGCGGGGTTGCCTTACTGGTTAGCAGAATGAATCACCGATACGCGAGCGAACGTGAAGCGACTGCTGCTGCA
AAACGTCTGCGACCTGAGCAACAACATGAATGGTCTTCGGTTCCGTTTCGTAAGTCTGGAAACGCGGAAGTCAGCGCCCTGCACCATTA
TGTTCCGGATCTGCATCGCAGGATGCTGCTGGCTACCTGTGGAACACCTACATCTGTATTAACGAAGCGCTGGCATTGACCCTGAGTGATTT
TTCTCTGGTCCC GCCATCCATACCGCCAGTTGTTTACCTCACAACGTTCCAGTAACCGGGCATGTTTCATCATAGTAACCCGTATCGTGA
GCATCCTCTCTCGTTTCATCGGTATCATTACCCCCATGAACAGAAATCCCCCTTACACGGAGGCATCAGTGACCAAACAGGAAAAAACCGCCC
TTAACATGGCCCCGTTTATCAGAAGCCAGACATTAACGCTTCTGGAGAACTCAACGAGCTGGACGCGGATGAACAGGCAGACATCTGTGAAT
CGTTCACGACCAGCTGATGAGCTTACCAGCAGCTGCCTCGCGCTTTCGGTGTGACGGTGAACCTCTGACACATGCAGCTCCCGGAG
ACGGTCACAGCTTGTCTGAAGCGGATGCCGGGAGCAGACAAGCCCGTCAGGGCGCGTCAGCGGGTGTGGCGGGTGTGGGGCGCAGCC
ATGACCCAGTCACGTAGCGATAGCGGAGTGTATACTGGCTTAACTATGCGGCATCAGAGCAGATTGACTGAGAGTGCACCATATATGCGGT
GTGAAATACCGCACAGATGCGTAAGGAGAAAAATACCGCATCAGGCGCTTTCGCTTCTCGCTCACTGACTCGCTGCGCTCGGTCTCGG
CTGCGGCGAGCGGTATCAGCTCACTCAAGGGCGTAATACGGTTATCCACAGAATCAGGGGATAACGCGAGGAAAGAATGTGAGCAAAGG
CCAGCAAAAGGCCAGGAACCGTAAAAAGGCCGCTTGTGGCGTTTTTCCATAGGCTCCGCCCCCTGACGAGCATCAAAAAATCGACGCT
CAAGTCAGAGGTGGCGAAACCCGACAGGACTATAAAGATACCGGCGTTTCCCTGGAAGCTCCCTCGTGCCTCTCTGTTCGACCCCTG
CCGCTTACCGGATACCTGTCCGCTTCTCCCTTTCGGGAAGCGTGGCGTTTTTCTCATAGCTCAGCTGTAGGTATCTCAGTTCCGGTGTAGGTC
GTTTCGCTCCAAGCTGGGCTGTGTGCACGAACCCCGTTACGCCGACCGTGCCTTATCCGGTAACTATCGTCTTGTAGTCCAACCCGGT
AAGACACGACTTATCGCCACTGGCAGCAGCCACTGGTAACAGGATTAGCAGAGCGAGGTATGTAGGCGGTGTACAGAGTTCTTGAAGTGGT
GGCCTAACTACGGCTACACTAGAAGGACAGTATTTGGTATCTGCGCTCTGCTGAAGCCAGTTACCTTCGAAAAAGAGTTGGTAGCTCTTGAT
CCGGCAAACAAACCACCGCTGGTAGCGGTGGTTTTTTTGTTCGAAAGCAGCAGATTACGCGCAGAAAAAAGGATCTCAAGAAGATCCTTTGA
TCTTTTCTACGGGTCTGACGCTCAGTGAACGAAACTCACGTTAAGGGATTTTGGTTCATGAACAATAAACTGTCTGCTTACATAAACAGTA
ATACAAGGGGTGTTATGAGCCATATTAACGGGAAACGCTTGTCTAGGCGCGGATTAATTCACATGGATGCTGATTATATGGGTATAA
ATGGGCTCGCGATAATGTCCGGCAATCAGGTGCGACAATCTATCGATTGTATGGGAAGCCCGATGCGCCAGAGTTGTTTCTGAAACATGGCA
AAGGTAGCGTTGCCAATGATGTTACAGATGAGATGGTCACTAACTGGCTGACGGAATTTATGCCTTTCGACCATCAAGCATTATCCG
TACTCCTGATGATGCATGGTTACTCACCCTGCGATCCCGGGAAAAACAGCATTCCAGGTATTAGAAGAATATCCTGATTAGGTGAAATATT
GTTGATGCGCTGGCAGTGTTCCTGCGCCGTTGCATTGATTCCTGTTTGAATTGCTTTTTAACAGCGATCGCGTATTTCTGCTCGCTCAG
GCGCAATCAGGAATGAATAACGGTTTTGGTTGATGCGAGTGATTTTGTGACGAGCGTAATGGCTGGCCTGTTGAACAAGTCTGGAAAGAATG
CATAAACTTTTCCATTCTCACCAGATTGATGCTCACTCATGGTATTCTCACTTGATAACCTTATTTTACGAGGGGAAATTAATAGGTTG
TATTGATGTTGGACGAGTCGGAATCGCAGACCGATACCAGGATCTGCCATCCTATGGAACGCTCGGTGAGTTTTCTCCTCATTACAGAA
ACGGCTTTTTCAAAAATATGGTATTGATAATCCTGATATGAATAAATGCAAGTTTCATTTGATGCTCGATGAGTTTTCTAAGAATTAATCATGA
GCGGATACATATTTGAATGATTTAGAAAAATAACAAATAGGGGTTCCGCGCACATTTCCCGAAAAAGTGCCACCTGAAATTGTAACGTTAA
TATTTTGTAAATTCGCGTTAAATTTTGTAAATCAGCTCAATTTTTAACCAATAGGCGGAAATCGGCAAAATCCCTTATAAATCAAAAAGTA
GACCGAGATAGGGTTGAGTGTGTTCCAGTTTGAACAAGAGTCCACTATTAAGAACGTTGACTCCACGTCAAAGGGCGAAAAACCGTCTA
TCAGGGCGATGGCCACTACGTGAACCATCACCTAATCAAGTTTTTTGGGTCGAGGTGCCGTAAGCCTAAATCGGAACCTAAAGGGA
GCCCCGATTTAGAGCTTACGGGGAAAGCCGGCGAACGTGGCGAGAAAGGAAGGGAAGAAAGCGAAAGGAGCGGGCGCTAGGGCGCTG
GCAAGTGTAGCGGTACGCTGCGCGTAACCACCACACCCGCGCTTAAATGCGCCGCTACAGGGCGCGTCCCATTCGCCA

5.1.15. EphF activity assay

The inhibitory of compounds the epoxide hydrolase EphF from *M. tuberculosis* was assayed based on the enzymatic conversion of cis-9,10-epoxystearic acid to 9,10-dihydroxystearic acid. Therefore, 500 nM MBP-EphF in HEPES buffer (20 mM HEPES, 300 mM NaCl, 0.1 mM TCEP, pH 7.4) were combined with compounds (1:100, 1% DMSO) to a total volume of 100 µL 1.5 mL microcentrifuge tubes. The enzyme was pre-incubated with the compounds at 37°C and 300 rpm for 15 min before 500 µM cis-9,10-epoxystearic acid were added to each reaction. To assay non-enzymatic hydrolysis of the epoxide, heat controls were prepared by heat inactivating the enzyme at 98°C and 350 rpm for 15 min. After substrate addition, the reactions

II – 5. Methods

were incubated at 37°C and 300 rpm for 15 min. Then, 1 mL ice-cold chloroform was added to stop the enzymatic reaction and to precipitate the protein. The samples were subsequently vortexed and centrifuged at 12 000 x *g* and 0°C for 10 min to obtain a clear separation between the aqueous and the organic chloroform phase. 900 µL of the chloroform phase was transferred to fresh 1.5 mL low-bind microcentrifuge tubes and the liquid was evaporated at 45°C in a centrifugal vacuum concentrator. The dry residuals were reconstituted in 50 µL of 50% MS-grade ACN in ddH₂O by vortexing and placing them in an ultrasonic bath for 5 min twice. Then, samples were centrifuged at 4°C and 12 000 x *g* for 5 min and 22 µL from each sample were transferred to glass MS vials. The amount of epoxide and diol was determined by mass spectrometry. To account for deviations in LC-MS consistencies, each sample was spiked with 5 µL taurocholic acid (final concentration 45 µM) for normalization during MS analysis. Samples were analysed by LC-MS for separation of the diol and epoxide and relative quantification. LC-MS analysis was performed using an UltiMate 3000 micro HPLC system (*Dionex*) coupled to a QExactive Plus (*Thermo Fischer*) via an ESI ion source. The samples were loaded onto a equilibrated XBridge BEH300 C4 3.5 µm 2.1 x 150 mm column (*Waters*) and separated over a 15 min gradient from 26% to 90% B, followed by 5 min at 95% before re-equilibration at 26% B 7 minutes. The flow-rate was 200 µL/min. The mobile phases A and B were 0.1 % (v/v) formic acid in water and 0.1% (v/v) formic acid in acetonitrile, respectively. The QExactive plus was operated in negative mode and single ion monitoring (SIM) was performed. For the first 9 minutes of the gradient SIM was set to 499 m/z to 529 m/z to measure the eluting taurocholic acid. For the rest of the gradient, SIM window was set to 295 m/z to 317.5 m/z for monitoring of the eluting diol and any remaining epoxide. Area under the curve (AUC) was determined using XCalibur software (*Thermo Fischer Scientific*) using the GENESIS algorithm. AUCs of the diol were normalised to taurocholic acid for relative quantification. All experiments were conducted in at least 5 independent replicated with 2 technical replicates each. Values were normalised to the DMSO control and graphs were plotted using *Graphpad Prism* 10.01. Statistical significance of inhibition (compared to DMSO) was calculated using ordinary one-way ANOVA.

5.1.16. MTT Cytotoxicity Assay

HeLa cells were seeded at a density of 4000 cells per well in a transparent, flat-bottomed 96-well plate (200 µL medium per well). Cells were grown overnight in a humidified atmosphere at 37 °C and 5% CO₂ to allow the cells to adhere to the surface. Subsequently, the medium was aspirated and replaced by fresh medium supplemented with compound in concentrations ranging from 2 µM to 500 µM (DMSO content less than 1%) or 1% DMSO as a control. The cells were incubated at 37 °C, 5% CO₂ for 24 h. For the determination of metabolic activity, 20

μL 3-(4,5-dimethyl-2-thiazolyl)-2,5-diphenyl-2H-tetrazolium bromide solution (MTT, 5mg/mL in PBS) were added to each well and the cells were incubated at 37 °C, 5% CO₂ for 4 h. Thereafter, the medium was aspirated and the violet formazan crystals were dissolved in 200 μL DMSO per well under shaking (300 r.p.m., 25 min). Absorbance at 570 nm with a reference wavelength of 630 nm was recorded using an Infinite F200 pro plate reader (*Tecan*). Four biological replicates, each consisting of 3 technical replicates, were measured for each data point. Cell viability was normalized with respect to the DMSO control and fitted as log(inhibitor) vs. response variable slope (four parameters) non-linear regression using *GraphPad Prism* 10.01. Cytotoxicity is reported as the IC₅₀ value, the concentration at which 50% viability is reached.

5.1.17. Drug susceptibility testing in MmpL3 under/over-expressing *M. tuberculosis*

Drug susceptibility assays with WT *M. tuberculosis* H37Rv and the *mmpL3*-TetON strains were performed as described by Grover et al.¹³² In short, WT cells were grown in 10 mL 7H9 (10% ADNaCl, 0.2% glycerol, 0.05% tyloxapol) and mutant cells in 7H9 (+25 $\mu\text{g}/\text{mL}$ Kanamycin, +25 $\mu\text{g}/\text{mL}$ Zeocin, and +500 ng/mL anhydrotetracycline [“ATc”] for *mmpL3*-TetON) in a 25-cm² tissue culture flask with a vented cap. Medium was inoculated with 1:10 with a thawed glycerol stock, incubated for approx. 7 d at 37 °C and 5% CO₂ in a humid incubator, and grown to an OD₅₈₀ of approx. 1. The cultures were pelleted and washed with 7H9 and were diluted to OD₅₈₀ = 0.01 in 10 mL 7H9 (plus selection antibiotics but +/- ATc for *mmpL3*-TetON) and were incubated for 14 d at 37 °C and 5% CO₂ in a humid incubator, with passage to OD₅₈₀ = 0.01 in 10 mL 7H9 (same conditions) at day 7. The cultures were pelleted and washed with fresh 7H9 and were diluted to OD₅₈₀ = 0.01 in an appropriate volume of 7H9 for assay requirements (+/- ATc as appropriate). The diluted cultures were added to assay-ready 384-well plates at 50 $\mu\text{L}/\text{well}$. The flat-bottom 384-well microplates (*Greiner Bio-One*) were prepared by dispensing nanoliter volume of drugs into 2-fold dilutions with 14 doses per drug using an automated drug dispenser (D300e Digital Dispenser, *HP*). The plates were wrapped with aluminum foil in stacks of no more than six and incubated at 37 °C and 5% CO₂ in a humid incubator. The OD₅₈₀ of the plates was read on day 8 of incubation. The OD₅₈₀ values were normalized to the DMSO control (100% growth) and plotted using *Graphpad Prism* 10.01. The curves were fitted as log(inhibitor) vs. response variable slope (four parameters) non-linear regression, with bottom and top parameters constrained to 0 and 100, respectively. MIC-values were calculated using the Gompertz model¹⁶⁵.

5.1.18. Isolation of 227-resistant mutants

M. tuberculosis H37Rv was grown to an OD₅₈₀ of approx. 0.8 to get an inoculum about 10⁸ bacteria. The culture was serially diluted and lower dilutions were used to enumerate the cell titer. Dilutions with higher titer were plate on 7H10 agar plates containing various concentrations of **227**. Frequency of resistance was calculated as the number of colonies at a concentration divided by the number of cells in the inoculum. In total, Eight colonies emerged (2 at 8 µM, 6 at 4 µM), were inoculated into 7H9 (+10% ADNaCl), and grown to an OD₅₈₀ of approx. 0.8. The level of resistance was determined by susceptibility testing as described above. For whole-genome-sequencing (WGS), purified genomic DNA was isolated using Epicenter MasterPure DNA/RNA isolation kit (*Lucigen*). The sequenced genomes were then analysed for SNPs.

5.1.19. Pharmacokinetics studies

CD-1 female mice (22–25 g) were used in oral pharmacokinetic studies. All animal studies were performed in biosafety level 2 (BSL2) facilities and approved by the Institutional Animal Care and Use Committee of the New Jersey Medical School, Rutgers University, Newark, NJ.

Snapshot PK studies. Snapshot PK studies were performed as described previously¹⁶⁶. In short, uninfected CD-1 mice dosed once via 25 mg/kg (po). The po formulation was dosed as a solution consisting of 5% dimethylacetamide (DMA)/95% solutol HS15 (20% in ddH₂O). Blood was collected at 30 min, 1 h, 3 h, and 5 h after dosing. Aliquots of 50 µL of blood were taken by puncture of the lateral tail vein from each mouse (n = 2 per route and dose) and captured in CB300 blood collection tubes containing K2EDTA and stored on ice. Plasma was obtained by centrifugation for 10 min at 5000 rpm and stored at –80 °C until analysed by LC-MS.

Dose escalation study. Dose escalation study was performed as described previously¹⁶⁷. Dose escalation studies were formulated as suspensions in solutol HS15 (20% in ddH₂O). Mice were dosed with increasing doses of test compound, Sequential bleeds were collected at the appropriate time intervals (up to and including 24 h) post-dose via the tail snip method. Blood (50 µL) was collected in capillary microvette EDTA blood tubes and maintained on ice before centrifugation at 1500g for 5 min. The supernatant (plasma) was transferred into a 96-well plate and stored at -80°C. until analysed by LC-MS.

Quantitative analysis. Test compound levels in plasma were measured by LC-tandem MS (LC-MS/MS) in ESI mode on a Sciex Applied Biosystems Qtrap 6500+ triple- quadrupole mass spectrometer coupled to a Shimadzu Nexera X2 UHPLC system to quantify each drug in

II – 5. Methods

plasma. Chromatography was performed on a Waters HSS Cyano column (2.1 x 100 mm; particle size, 5 µm) using a reverse phase gradient. Milli-Q deionised H₂O with 0.1% formic acid was used for the aqueous mobile phase and 0.1% formic acid in MeCN for the organic mobile phase. Multiple-reaction monitoring of parent/daughter transitions in electrospray negative-ionization mode or electrospray positive ionisation mode was used to quantify compounds. A 1 mg/mL DMSO stock of test compound was serially diluted in 50/50 ACN/Water and subsequently diluted in blank K₂EDTA (dipotassium ethylenediaminetetraacetic acid) plasma (Bioreclamation) to create standard curves and quality control samples. Test compound was extracted by combining 20 mL of spiked plasma or study samples and 200 mL of acetonitrile/methanol (50/50) protein precipitation solvent containing 20 ng/mL verapamil internal standard (IS). Extracts were subjected to vortex mixing for 5 min and centrifuged at 4,000 rpm for 5 min. The supernatants were analysed by LC-MS. Verapamil IS was sourced from Sigma Aldrich. MRM transition values of 455.4 and 165.2 for verapamil. The sample analysis results were accepted if the concentrations of the quality control samples were within 20% of the nominal concentration.

III. Elucidating the mechanism of action of Chlorotonil

This Chapter will be part of the following publication:

Felix Deschner, **Dietrich Mostert**, Jan-Martin Daniel, Dana Schneider, Anastasia Andreas, Alexander Volz, Timo Risch, Laura Herraiz-Benitez, Andreas M. Kany, Gwenaëlle Jézéquel, Walter Hofer, Mathias Müsken, Markus Bischoff, Heike Brötz-Oesterhelt, Tanya Schneider, Stephan Sieber, Jennifer Herrmann, and Rolf Müller. Mode of action of Chlorotonil. *Manuscript in preparation, 2024*

Contributions:

FD, JH and RM conceived the Project. FD performed time-kill assays, determined initial MICs and generated the resistant mutants. DM performed all proteomic experiments. DM wrote the manuscript in this thesis, parts of which will be part of the later publication. Figures 5, 6 and 7 were initially prepared by FD and then further modified by DM.

1. Introduction

Natural products are a valuable source of novel compounds in the fight against resistant pathogenic bacteria. One such natural product is Chlorotonil A, a polyketide isolated from *Sorangium cellulosum*, a gram-negative bacterium belonging to the group of *Myxobacteria*¹⁶⁸. Chlorotonil A is highly active against Gram-positive bacteria, has moderate anti-fungal activity, and is highly potent against *Plasmodium falciparum*^{126,169}. Although Chlorotonil A is a promising antibacterial compound due to its nanomolar activity against various drug-resistant pathogens, its highly lipophilic structure limits its use as an orally available drug. To address this, the biosynthetic cluster was first identified. Here, the fact that Chlorotonil carries the dichloro-pattern suggests the involvement of a halogenating enzyme. The biosynthetic clusters were therefore screened for genes encoding for putative halogenating enzymes. A gene cluster harbouring a putative halogenase gene and a tandem-AT domain was co-localised on one scaffold. Gene knockouts confirmed this gene cluster to be responsible for the biosynthesis of Chlorotonil A and three other isomers¹⁶⁹. With this knowledge, a large-scale fermentation and purification of Chlorotonil A was established and used as a starting material for further compound optimisation¹⁷⁰. These semi-synthetic new derivatives, such as the epoxide carrying **ChB1-Epo2**, have significantly improved pharmacokinetic (PK) properties while retaining their activity and reducing the bacterial load in an *S. aureus* thigh infection model¹⁷⁰. Chlorotonil A and **ChB1-Epo2** have been shown to be effective in treating mice with established *Clostridium difficile* infections (CDIs) while having a lesser impact on the overall gut microbiota¹⁷¹. A newer derivative of Chlorotonil, termed Dehalogenil (**DHG**), retained its activity while further improving the PK properties¹⁷².

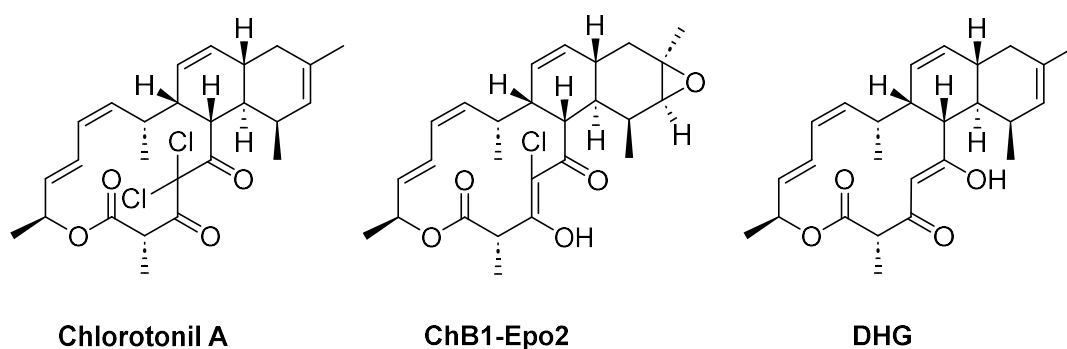


Figure 1. Structures of the natural product Chlorotonil A and its semi-synthetic derivatives ChB1-Epo2 and DHG.

The effect of Chlorotonil on *C. difficile* has been investigated on transcriptome and proteome level¹⁷¹. Chlorotonil seems to induce metabolic reprogramming while influencing metal homeostasis. So far, the mechanism of action of the Chlorotonil derivatives is still elusive. In this study, variety of proteomic and biochemical methods was applied to elucidate the mechanism of action of Chlorotonil.

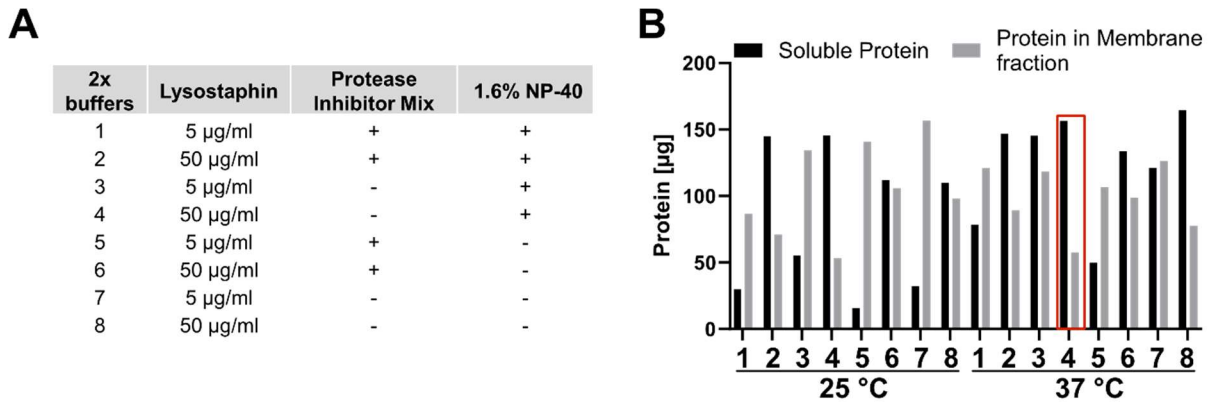
2. Results and Discussion

2.1. Thermal Proteome Profiling in *S. aureus*

Thermal proteome profiling (TPP) has extensively been shown to be a valuable method for target elucidation in human cells^{173–175}. So far, only one study has shown that TPP can also be used for probing drug-target interactions in living bacteria¹⁷⁶. This previous study performed experiments only in non-pathogenic *E. coli* K12. Our goal was to extend this method to more relevant, pathogenic bacteria. Here, the focus was set on methicillin-resistant *Staphylococcus aureus* (MRSA). One of the most critical steps when performing TPP in living cells is the lysis after compound and temperature treatment. Most lysis protocols, especially for bacteria, include several steps that can re-solubilise crashed-out proteins. While this is preferential for most applications, TPP only works when the denatured and precipitated proteins are not re-solubilised. This excludes the use of most commonly used detergents and mechanical cell-disruption techniques such as sonication and bead-beating. Gram-positive bacteria, like *S. aureus*, are especially hard to lyse and, therefore, require harsh lysis conditions. One way around this is the use of enzymes that are able to degrade the cell wall. The most well-known enzyme used for this is Lysozyme, a glycoside hydrolase (muramidase) that catalyses the hydrolysis of specific linkages in peptidoglycans that make up the cell wall of Gram-positive bacteria. Lysozyme can also be used to lyse Gram-negative bacteria when combined with outer-membrane permeabilisers such as EDTA¹⁷⁷. However, Lysozyme is not effective against *S. aureus* due to a genus-specific o-acetylation at C6-OH of muramic acid catalysed by OatA¹⁷⁸. The Enzyme Lysostaphin, first isolated in 1961¹⁷⁹, is a glycyglycine endopeptidase which specifically cleaves the cross-linking pentaglycine bridges in staphylococcal cell walls¹⁸⁰. This enzyme is active at relatively low amounts and is, therefore, ideally suited for the preparation of proteomic samples. To identify optimal conditions for the lysis of *S. aureus* TPP samples, eight different buffers were tested at two different incubation temperatures. The variables in the buffers were two different concentrations of Lysostaphin, a protease inhibitor mix, and the addition of the detergent NP-40. NP-40 was shown to not re-solubilise precipitated proteins up to a concentration of 1%¹⁷⁶. All buffers contained DNase due to the lack of any mechanical lysis that would shear the genomic DNA. The buffers were prepared as 2-fold concentrates and added to the same volume of *S. aureus* USA300 cells in PBS (Figure 2A). The cells were incubated for 30 minutes at the respective temperatures and then lysed by a freeze-thaw cycle of liquid nitrogen and 25 °C, repeated three times. The cell debris was removed, and the soluble protein and membrane-bound protein fraction were separated by centrifugation. Afterwards, the membrane fraction was re-solubilised in PBS with 0.2% SDS

III – 2. Results and Discussion

and sonication. The total protein concentrations of all samples were measured and compared (Figure 2B). The best lysis condition was identified to be buffer 4 and incubation at 37°C. This condition yielded the highest ratio of soluble to insoluble protein.



Final Lysis Conditions: 25 µg/mL Lysostaphin, 0.8% NP-40, 15 µg/mL DNase I in PBS pH 7.4

Figure 2. Determining the ideal lysis conditions for in situ thermal proteome profiling in *S. aureus*. (A) Overview of different buffers tested. All buffers are based on PBS pH 7.4 with 30 µg/mL DNase I. (B) Protein concentrations of soluble and insoluble fractions after cell lysis with different buffers and at two different concentrations. Buffer 4 at 37 °C had the highest ratio of soluble/insoluble protein and one of the highest overall concentrations of soluble protein and was therefore used for further experiments.

Thermal proteome profiling using these lysis conditions was performed in *S. aureus* USA300 to identify potential protein targets of the Chlorotonil-derivative **ChB1-Epo2**. The MIC of this compound in this strain was 0.08 µg/mL. However, in order to see a significant thermal shift of a direct compound target, the target protein should be fully engaged with the compound. For this reason, a high compound concentration of 4 µg/mL (50x MIC) was used as a single-dose experiment. The cells were treated for 45 minutes at 37 °C, exposed to a thermal gradient and lysed according to the new protocol. After several washing steps, the proteins were digested and TMT-labelled to allow pooling of all temperature points of one experiment. The complex mixtures were fractionated offline and measured on an Orbitrap Fusion MS instrument. The samples were measured in an MS3-based TMT method for more accurate quantification of peptides using the TMT reporter ions. The resulting melting curves were fitted, and the thermal shifts in both biological replicates were calculated (Figure 3, Table 1).

III – 2. Results and Discussion

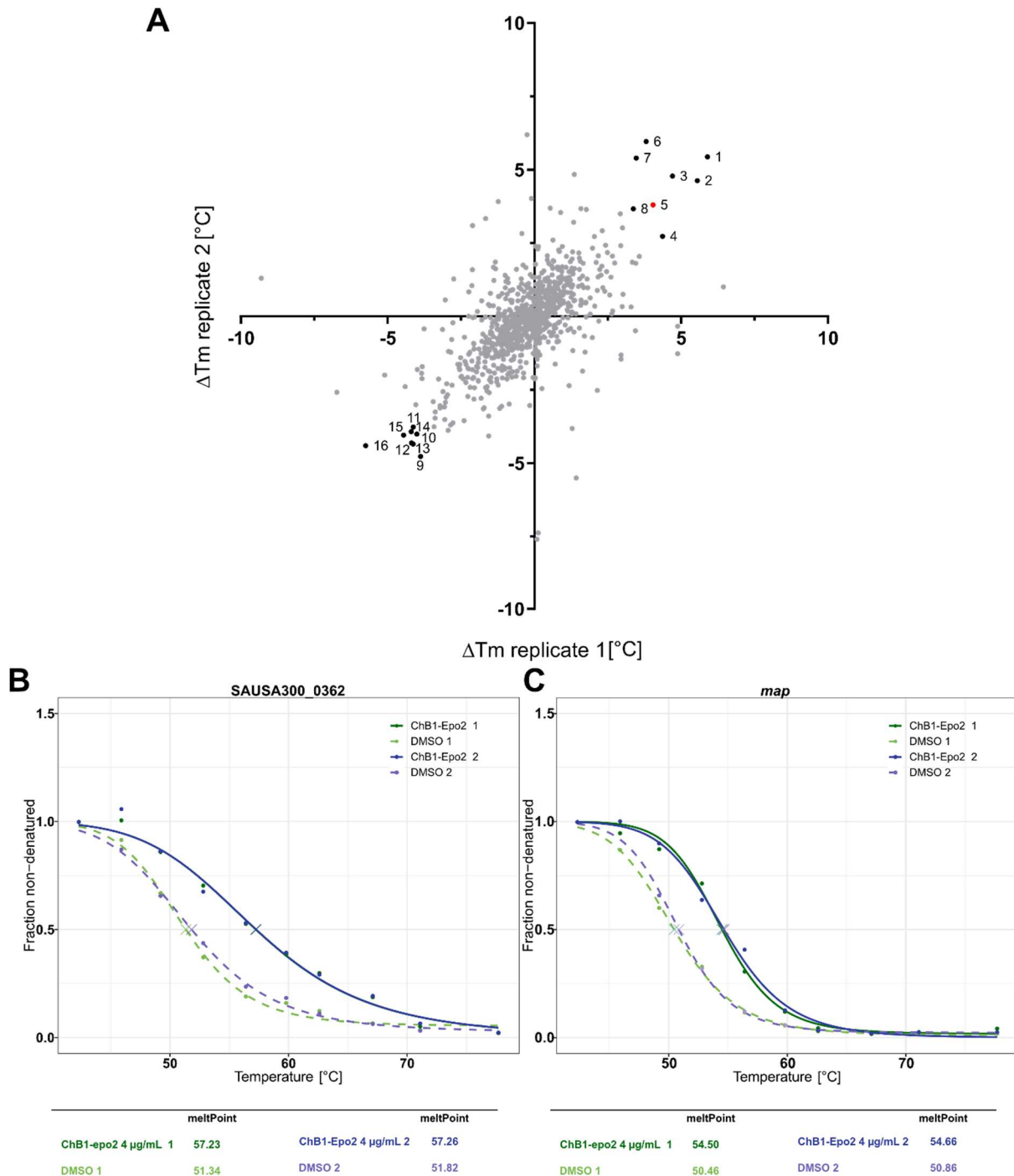


Figure 3. Thermal protein profiling in living *S. aureus* USA 300 treated with 4 µg/mL **ChB1-Epo2**. (A) Thermal shifts (ΔT_m) between Treated and untreated cells in both biological replicates were calculated using the TPP R-package (see methods for details). All proteins that passed all significance criteria are numbered (See Table 1 for details). (B) Melting curves of the most stabilised protein SAUSA300_0362 (1). (C) Melting curves of the only stabilised protein essential for growth, MetAP (red dot, 5).

In total, eight proteins were stabilised and passed all significance tests (see methods for details), while eight proteins were significantly destabilised. Among the significantly destabilised proteins are three ribosomal proteins (*rplB*, *rplC*, *rplF*). In fact, 8 out of 15 proteins that are destabilised by more than 3°C are ribosomal proteins (Table S1). While this could be

III – 2. Results and Discussion

an indication of a potential ribosomal target protein, a down-shift of the melting temperature of ribosomal proteins is often caused by changes in metal-ion concentrations¹⁷⁶.

Table 1. List of all significant protein hits from the TPP experiment. Numbers are in accordance with Figure 2A.

#	Gene name	Protein Name	$\Delta T_m 1$	$\Delta T_m 2$
Stabilised				
1	SAUSA300_0362	Mechanosensitive ion channel family protein	5.9	5.4
2	SAUSA300_2234	Inosine-uridine preferring nucleoside hydrolase	5.5	4.6
3	SAUSA300_1448	Transcriptional regulator, Fur family	4.7	4.8
4	SAUSA300_1654	Uncharacterized peptidase	4.4	2.7
5	<i>map</i>	Methionine aminopeptidase	4.0	3.8
6	<i>nrn</i>	Ribonuclease R	3.8	6.0
7	SAUSA300_1349	Glycosyl transferase, group 1 family protein	3.5	5.4
8	<i>aldA2</i>	Aldehyde dehydrogenase	3.4	3.7
Destabilised				
9	<i>rplC</i>	Large ribosomal subunit protein uL3	-3.9	-4.8
10	SAUSA300_0538	Uncharacterized epimerase/dehydratase	-4.0	-4.0
11	<i>ddl</i>	D-alanine--D-alanine ligase	-4.1	-3.8
12	<i>rplF</i>	Large ribosomal subunit protein uL6	-4.1	-4.3
13	<i>thrB</i>	Homoserine kinase	-4.2	-4.3
14	<i>glk</i>	Glucokinase	-4.2	-3.9
15	<i>rplB</i>	Large ribosomal subunit protein uL2	-4.5	-4.0
16	SAUSA300_0373	Uncharacterized protein	-5.8	-4.4

The most stabilised protein is an uncharacterised ion channel (SAUSA300_0362) with an 80% sequence identity with the Potassium efflux system KefA from *S. saccharolyticus*. The methionine aminopeptidase (*map*, MetAP) is the only stabilised protein that is essential for growth. For all other stabilised proteins, deletion mutants from the Nebraska Transposon Mutant Library (NTML) were tested for potential shifts in MIC. None of these mutants had a shift in MIC compared to the wild-type strain (data not shown). To further investigate the potential role of the most stabilised protein SAUSA300_0362, a probable potassium channel, the MIC in the presence of elevated KCl concentrations was determined. Interestingly, when the medium is supplemented with 500 mM KCl, the susceptibility of the cells is vastly reduced (Table 2, Table S2).

III – 2. Results and Discussion

Table 2. MICs of **DHG**, **ChB1-Epo2** and control compound PK150 against *S. aureus* USA 300 JE2 WT and Transposon mutants. NE323 is the transposon mutant of SAUSA300_0362, and NE572 is a randomly chosen transposon mutant of a gene not involved in metal homeostasis.

MICs [μ M]	Dehalogenil			ChB1-Epo2			PK150		
Strain	WT	NE323	NE572	WT	NE323	NE572	WT	NE323	NE572
MH2	0.04	<0.02	0.04	0.04	<0.02	<0.02	0.625	0.3125	0.3125
+ 500 mM KCl	10	10	10	1.25	0.625	1.25	0.625	0.3125	0.3125
+ 500 mM NaCl	<0.02	0.04	0.04	<0.02	0.04	<0.02	0.625	0.625	0.625

For **ChB1-Epo2**, the MIC in WT *S. aureus* USA300 shifts by over 30-fold, while the shift for the newer Chlorotonil-derivative, **Dehalogenil**, has an even more pronounced shift of 250-fold compared to the MIC in normal growth medium. This effect is only observable for KCl and not for NaCl. In fact, the WT strain seems to be slightly more susceptible to both derivatives when NaCl was added to the medium. For the transposon mutant of SAUSA300_0362 (NE323), there is no shift towards more susceptibility when adding NaCl. However, the lower susceptibility towards both compounds when adding KCl is the same for the transposon mutant of SAUSA300_0362 (NE323) or another randomly chosen transposon mutant. The urea compound PK150 was used as a control compound to control for compound-unspecific MIC shifts. These results are a strong indication that the mode of action of the Chlorotonil derivatives is linked to potassium homeostasis. The supplemented concentration of 500 mM KCl is in the range of normal intracellular concentrations in bacteria¹⁸¹. If the mechanisms that control the potassium gradient from high intracellular to low extracellular concentrations are disrupted by Chlorotonil, this could lead to an influx of water due to the osmotic pressure or efflux of potassium. When the extracellular concentration of potassium is supplemented to be in the same concentration range as the natural intracellular concentration, no flux of ions or water across the membrane will take place. The fact that the shift is the same for the WT strain and the transposon mutant of the hit Protein SAUSA300_0362, a potassium efflux pump, suggests that binding of the Chlorotonil directly to this protein is not responsible for the effect on potassium homeostasis. The observed thermal stabilisation is most likely a secondary effect caused by the disruption of potassium homeostasis in another way. While the MIC of **ChB1-Epo2** shifted significantly when supplementing the medium with KCl, the resulting MIC of 1.25 μ M is still relatively potent, hinting towards a polypharmacological mechanism of action.

The only significantly stabilised protein that is essential for bacterial growth was the methionine aminopeptidase (MetAP). MetAPs are metallopeptidases that are conserved across all organisms, from bacteria to eukaryotes¹⁸². They remove the N-terminal methionine from nascent polypeptides, a crucial step for protein maturation¹⁸³. While most MetAPs are active

with various bound divalent cations, in bacteria, cobalt generally leads to the highest *in vitro* activity^{183–185}. To investigate the potential impact of the Chlorotonil derivatives on MetAP activity, the *map* gene from *S. aureus* USA300 was cloned into a pETG41K vector. The expressed SaMetAP is N-terminally maltose binding protein (MBP) –tagged, as untagged protein was expressed insolubly. The N-terminally MBP-tagged protein was expressed and purified. The fusion protein was used for initial activity studies. After confirming that the purified protein was indeed active, the MBP-tag was cleaved by adding TEV-protease. The cleaved SaMetAP was purified and used for activity assays. First, the optimal protein-to-metal concentration was determined to be a 3 to 6-fold molar excess of CoCl₂. Using these optimised conditions, the protein was pre-incubated with CoCl₂, followed by incubating with the Chlorotonil derivatives for 30 minutes before the addition of the methionine-p-nitroanilide (MetpNA) substrate. The release of cleaved para-nitroanilide was measured, the linear range was fitted by a linear regression fit, and the slopes were calculated (Figure 4).

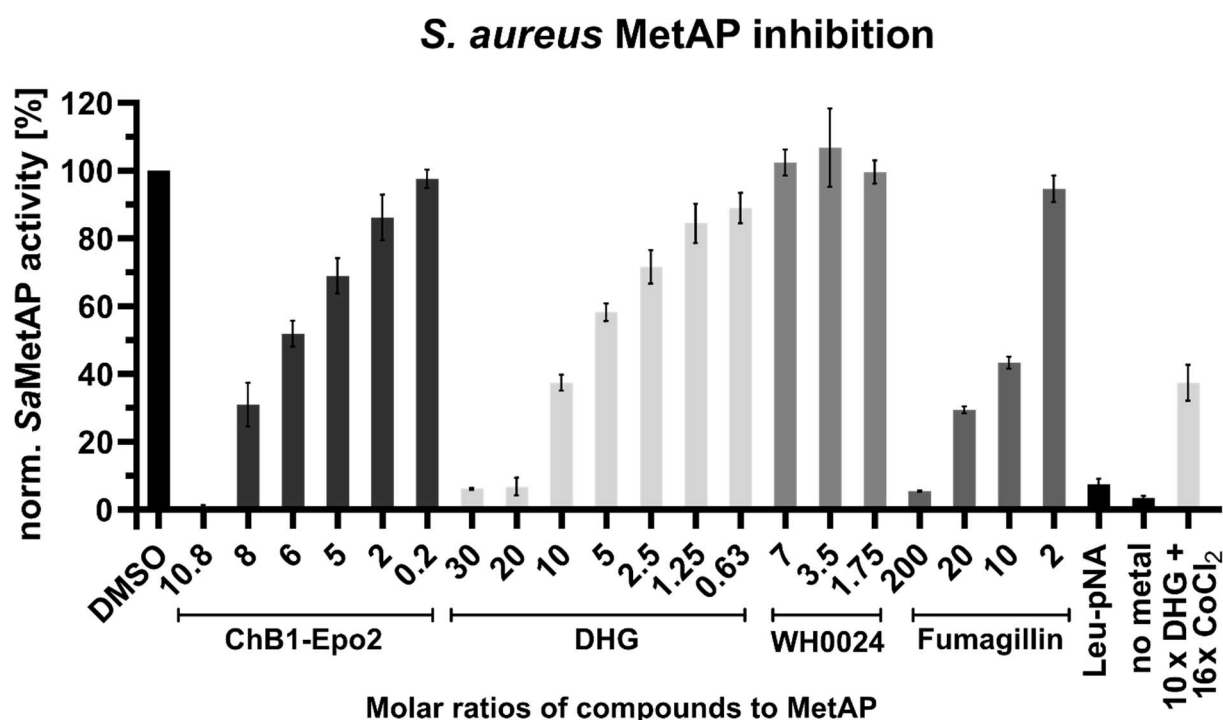


Figure 4. SaMetAP activity assay using recombinantly expressed and purified SaMetAP. Slopes of the linear fits are normalised to their respective DMSO control. **ChB1-Epo2** and **DHG** inhibit SaMetAP in a concentration-dependent manner. The inactive Chlorotonil derivative WH0024 does not show any inhibition. Fumagillin, a known human MetAP-2 inhibitor, also inhibits SaMetAP. The enzyme is inactive without addition of CoCl₂ and it specifically cleaves only Met-pNA and not the leucine derivative Leu-pNA. The assay was performed in at least 2 independent replicates consisting of 3 technical triplicates.

Both active Chlorotonil derivatives **ChB1-Epo2** and **DHG** inhibit the SaMetAP in a dose-dependent manner with a molar excess of about 6-fold, leading to about 50% inhibition. Interestingly, an inactive Chlorotonil derivative WH0024, which lacks the crucial Diketo moiety, did not inhibit SaMetAP, while Fumagillin, a human MetAP-2 inhibitor, also showed

concentration-dependent inhibition of SaMetAP. These activity assays were conducted using a 3-fold molar excess of CoCl₂. To test whether the observed inhibition is merely due to a complexation of Co²⁺, rather than direct inhibition of the protein, a 10-fold molar excess of **DHG** with a 16-fold molar excess of CoCl₂ was measured, which resulted in the same inhibition as before, pointing to an inhibition of the enzyme and not just a complexation of the metal cofactor. Of note, SaMetAP is slightly inhibited by higher concentrations of CoCl₂, so a DMSO control with the higher CoCl₂ concentration was also included and used for normalisation. The in vitro assay confirms that the Chlorotonil derivatives inhibit SaMetAP.

While this is an interesting finding, a time-kill assay of **DHG** in *S. aureus* (conducted by Felix Deschner, HIPS) showed that at concentrations above the MIC, **DHG** acts rapidly bactericidal (data not shown). At 2x and 10x MIC, cells are eradicated after only 20 minutes. This clearly indicates a main mechanism of action independent of the SaMetAP inhibition, as this would be a slower acting mechanism, as it only affects newly synthesised proteins. At sub-MIC concentrations, growth is strongly delayed, and at 0.5x MIC, cell count is significantly reduced before achieving full growth after 24 h. Importantly, this was not due to the development of spontaneous resistance, as isolated clones showed no change in susceptibility.

2.2. Full proteome analysis of *S. aureus* treated with DHG

To investigate the changes in protein expression in response to **DHG** treatment, *S. aureus* cells were treated with 0.2x MIC and grown until stationary. Samples from each culture were analysed after 30 minutes, in the exponential phase, and in the early stationary phase. Overall, the proteomic changes were very similar across the different growth stages. Here, the focus is put on the samples from the exponential phase (Figure 5). In total, 16 and 27 proteins were significantly up- and downregulated by a fold-change of more than Log₂(1.5), respectively (Figure 5A). Due to a lack of detailed protein annotation in *S. aureus*, pathway analysis is not fully reliable. However, pathway analysis using *STRING DB* (version 12)¹⁵⁷ resulted in two protein clusters among the upregulated proteins (Figure 5B). All proteins of the main potassium uptake system KdpABC (cluster strength: 2.13), as well as some secreted bacterial haemolysins (cluster strength: 1.19), showed significant functional enrichment. This full-proteome analysis confirms the previous findings that the Chlorotonil derivatives dysregulate the potassium ion homeostasis. The fact that the potassium uptake system (KdpABC) is upregulated suggests an uncontrolled release of potassium ions upon treatment, which the cell compensates through upregulation of KdpABC. Interestingly, two of the most strongly down-regulated proteins in are BetA and GbsA, both involved in the biosynthesis of the most important prokaryotic osmoprotectant, glycine betaine (*N,N,N*-trimethyl glycine, GB). GB is

III – 2. Results and Discussion

produced when organisms are exposed to a high osmotic environment. Along with other solutes, it is accumulated to maintain a higher osmolarity in the cytoplasm compared to the environment and thus provide turgor pressure¹⁸⁶. For its biosynthesis, choline is first taken up into the cell by specific uptake proteins. Then, choline is oxidised to betaine aldehyde by the choline dehydrogenase BetA. A second oxidation step is then catalysed by the glycine betaine aldehyde dehydrogenase (GbsA, BetB) to yield GB^{187,188}. Up-regulating GB biosynthesis is normally a response to high osmolarity. Down-regulation could, therefore, be a response to a perceived low osmolarity. This would also explain the reduced susceptibility under higher potassium concentrations. K⁺ is the most important solute under normal osmolar conditions. An induced efflux of K⁺-ions would signal a low-osmolarity environment and could, therefore, trigger a down-regulation of GB biosynthesis. A Chlorotoni-induced potassium efflux could be triggered by the most stabilised protein from the TPP experiment SAUSA300_0362, a mechanosensitive potassium efflux pump. So far, the results do not indicate a direct binding to this potassium channel as the transposon mutant is still susceptible to the Chlorotoni derivatives. A non-proteinogenic target in the membrane could also lead to a potassium efflux. Studies into membrane-lipid binding of **DHG** are currently being conducted and are the subject of a later publication.

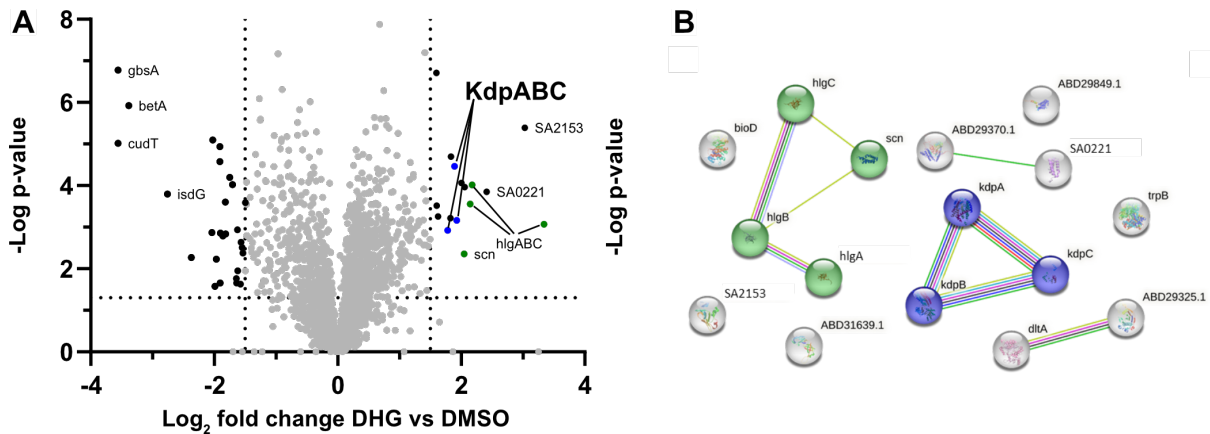


Figure 5. Full proteome analysis of *S. aureus* treated with a sub-MIC concentration of **DHG**. (A) Volcano plot of *S. aureus* ATCC29213 treated with 0.2x MIC **DHG** compared to the vehicle control (DMSO). The subunits of the main K⁺-importer KdpABC is upregulated while the glycine betaine (GB) biosynthesis proteins (BetA, GbsA) are downregulated. All MS experiments were conducted in 4 biological replicates and significance of fold-changes was calculated using a two-tailed students t-test and permutation based FDR (<0.05). (B) GO-term analysis of significantly upregulated protein in *S. aureus* shows upregulation of potassium uptake (blue) and secreted toxins (green). GO-term analysis was performed using STRING-DB (v.12)¹⁵⁷.

2.3. Full proteome analysis of Chlorotonil-resistant *S. aureus*

Resistant *S. aureus* ATCC29213 mutants were generated by long-term exposure and adaptation (LEA) (performed by Felix Deschner, HIPS). After one week of daily passaging in a medium with sub-MIC concentrations of Chlorotonil A and **DHG**, resistant mutants with more than a 64-fold shift in susceptibility could be isolated and were analysed for single nucleotide polymorphisms (SNPs) and other genetic phenotypes by whole genome sequencing (WGS). Four mutants were selected for full-proteome analysis compared to the WT strain (Table 3). All four mutants carry at least one mutation in *farR*. Mutants with high-level resistance carry an additional mutation in *farR* or, in the case of Sa_D3, an SNP upstream of *farE*. FarR is the negative transcription regulator of the fatty acid efflux pump FarE¹⁸⁹.

Table 3. List of Chlorotonil-resistant mutants of *S. aureus* ATCC29213 used for comparative proteomics. Mutants are cross-resistant to Rhodomyrtone (ROM) and carry mutations in *farR*.

Fold-change		ChA	DHG	ROM	<i>farR</i>	<i>farE</i>
Sa_WT	Sa_WT	1 (0.025)	1 (0.0625)	1 (0.5)		
Sa1_TSB_D3	Sa_D3	>64	>64	>64	Val115Ile	-52A > T
Sa2_TSB_D3	Sa_D6	8	32	4-8	Val115Ile	
Sa1_MHB_D3	Sa_D11	>64	>64	>64	Val115Ile	Glu151Lys
Sa2_MHB_A8	Sa_A11	>64	>64	>64	Arg96Ile	Cys116Arg

^a -52A > T exchange of A to T 52 bp upstream of the coding region

The resistant mutants and the WT were grown, and their proteome was analysed and compared to the WT (Figure 6). Here, both FarR and FarE were found to be strongly upregulated. The mutations seem to lead to an inactivation of the negative regulator FarR, as FarE is strongly upregulated. The level of upregulation of FarR/E seems to correlate with the level of resistance as the less resistant mutant Sa_D6 has a fold-change of 32 compared to a 128-fold change in the high-resistance strains (Figure 7A). In literature, *farR* mutations are reported to convey resistance to Rhodomyrtone (ROM), a membrane-active antibiotic inducing cell lysis¹⁹⁰. Therefore, the Chlorotonil-resistant *S. aureus* strains were tested for cross-resistance to ROM (conducted by Felix Deschner, HIPS). Indeed, the mutants were also resistant to ROM to the same extent (Table 3), suggesting the same lipid-mediated resistance mechanism via FarE overexpression. The exported fatty acids interact with Chlorotonil, causing neutralisation of Chlorotonil. Lower susceptibility towards Chlorotonil when adding lysyl-phosphatidylglycerol (lysyl-PG) to the medium (performed by Felix Deschner, data not shown) corroborates this mechanism of resistance.

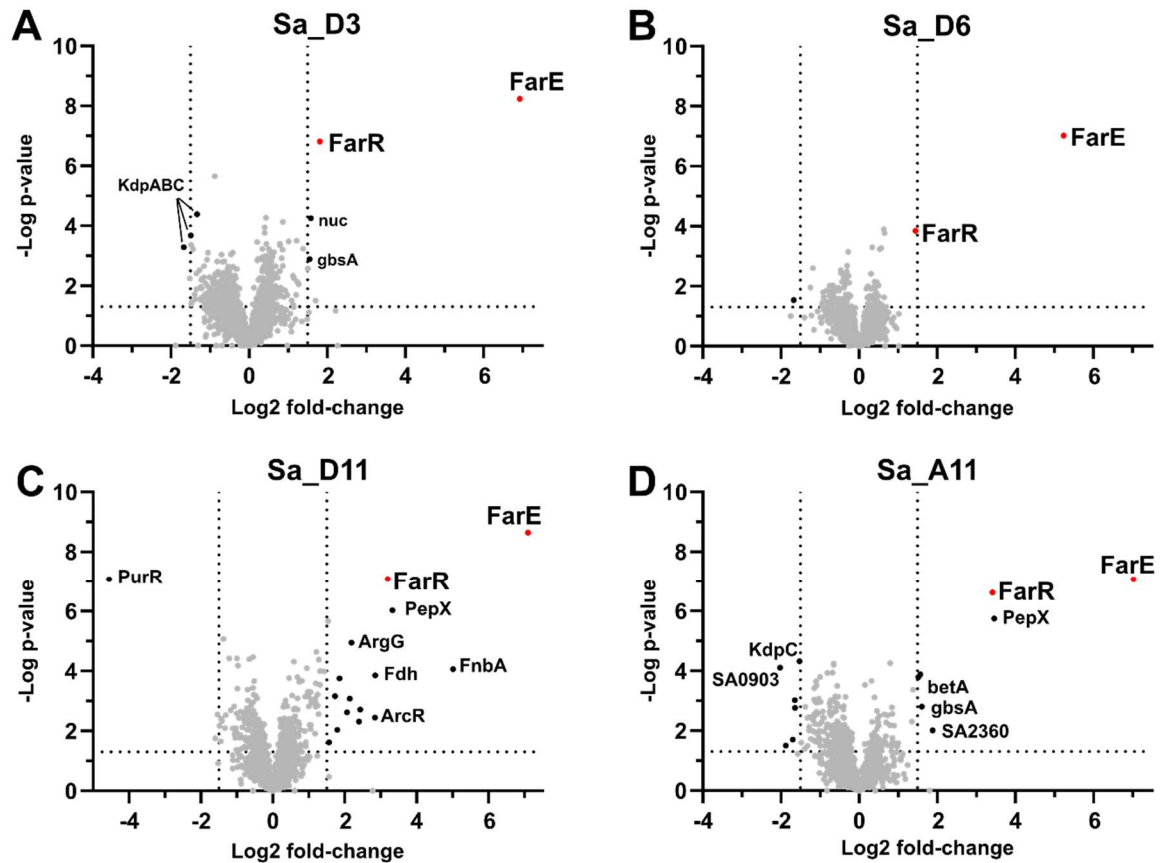


Figure 6. Full-proteome analysis of Chlorotoniil-resistant *S. aureus* mutants compared to the WT. All mutants overexpress FarR and FarE. The high-level resistant mutants have additional dysregulated proteins. All MS experiments were conducted in 4 biological replicates and significance of fold-changes was calculated using a two-tailed students t-test and permutation-based FDR (<0.05).

Interestingly, the high-level-resistant mutants, Sa_D3, Sa_D11 and SA_A11, show the exact reverse of what was seen when treating WT *S. aureus* with sub-MIC levels of **DHG**. While treatment of the WT induced a down-regulation of BetA and GbsA and an upregulation of KdpABC, these two show the exact opposite (Figure 7B). This trend was also not reversed when treating the mutants with **DHG** (Figure 7C). The reversal of the KdpABC and BetA, GbsA expression compared to treatment of the WT do, however, also indicate a mechanism of action in which the Chlorotoniil-derivatives influence potassium homeostasis. How this reversal is linked to resistance and the *farR/E* mutations needs to be investigated further. The less resistant clone does not exhibit the reversal of the expression levels, indicating that the higher resistance could also be linked to the changes in the expression levels of these proteins in addition to FarE overexpression. Further studies into potential non-proteinogenic targets of Chlorotoniil, such as lipids, are ongoing and might elucidate this further.

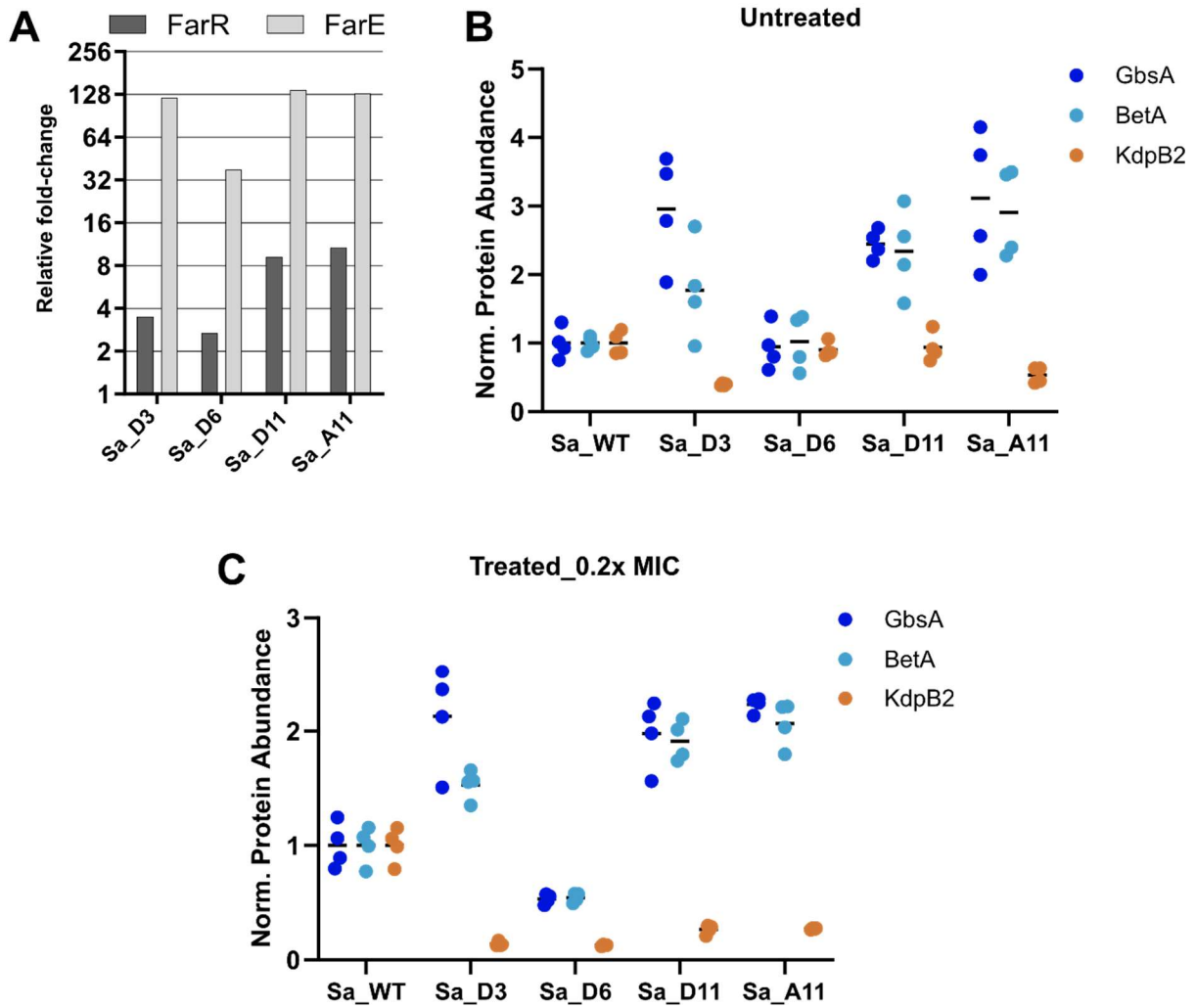


Figure 7. *S. aureus* mutants exhibit strong upregulation of FarE and dysregulation of proteins responsible for potassium homeostasis. (A) FarR and FarE fold changes compared to WT. FarR and FarE are strongly upregulated in *S. aureus* mutants. The high-level resistant mutants have a 128-fold increase in FarE levels, while the less resistant strain (Sa_D6) exhibits a 32-fold increase. (B) Normalised protein abundance of selected proteins from the full proteome analysis of the *S. aureus* mutants compared to the WT. The high-level resistant mutants show an upregulation of GbsA and BetA, which the low-level resistant mutant Sa_D6 does not. Sa_D3 and Sa_A11 also down-regulate the potassium importer Kdp (KdpB2 is exemplary for this). (C) Normalised protein abundance of selected proteins from *S. aureus* mutants treated with 0.2x MIC of **DHG** compared to WT treated with 0.2x MIC. The upregulation of GbsA and BetA in the high-resistant mutants is still evident. Interestingly, all mutants show a down-regulation of the potassium import system compared to the treated WT. Low-level resistant mutant Sa_D6 also exhibits a downregulation of GbsA and BetA.

3. Conclusion

Due to the growing problem of antimicrobial resistance, there is an urgent need to find novel antibiotics. Natural products (NPs) have proven to be an essential source of antibiotic compounds in the past¹⁹¹. One promising NP with nanomolar activity against various pathogenic bacteria is Chlorotonil. Recently, extensive structure-activity relationship (SAR) studies have resulted in novel, highly active derivatives with improved pharmacokinetic (PK) properties¹⁷⁰. The exact mechanism of action of Chlorotonil and its derivatives is still elusive. In this study, known TPP protocols were adapted to be used in *S. aureus*, a widespread Gram-positive pathogen. Using TPP in living *S. aureus* cells, several significantly stabilised and destabilised proteins were identified. The only significantly stabilised protein essential for growth was the methionine aminopeptidase. This protein was cloned, expressed and purified to be used in an in vitro assay. The MetAP is inhibited by **ChB1-Epo2** and **DHG** in a concentration-dependent manner. An attempt to generate co-crystal structures of MetAP with bound compound was unsuccessful. While crystal structures of MetAP with bound cobalt were obtained, the limited solubility of the Chlorotonil derivatives hindered the formation of co-crystals. A time-kill assay performed by Felix Deschner (HIPS), showed a very fast mode of action in which cells were killed within 20 minutes of compound treatment. Such a fast mechanism of action makes it unlikely that MetAP inhibition is the primary mode of action. It can be therefore concluded that this is merely a secondary target of Chlorotonil.

The most strongly stabilised protein in the TPP experiment was a potassium transporter (SAUSA300_0362). The effect on potassium homeostasis was further investigated by measuring drug susceptibility in the presence of high concentrations of potassium and sodium. Indeed, supplementing the growth medium with high concentrations of potassium vastly reduces the susceptibility of *S. aureus* against two Chlorotonil derivatives. Moreover, treating wild-type *S. aureus* strains with a sub-lethal dose of **DHG** leads to an upregulation of the main potassium importer KdpABC and a down-regulation of BetA and BetB, the proteins responsible for the biosynthesis of glycine betaine, an important osmoprotectant. These findings point towards a perceived low-osmolarity environment induced by **DHG**. This could be caused by a **DHG**-induced potassium efflux. However, direct involvement of the most stabilised protein, the potassium efflux pump SAUSA300_0362, could not be shown using the transposon mutant NE323. Furthermore, whole-proteome analysis of Chlorotonil-resistant *S. aureus* mutants identified an interesting resistance mechanism. Mutations in *farR* lead to a strong upregulation of the fatty acid exporter FarE. This resistance mechanism was previously shown for the antibiotic Rhodomyrtone (ROM). Indeed, Chlorotonil resistant mutants are cross-resistant to ROM, confirming that the resistance mechanism is the same as for ROM. Here, the

III – 3. Conclusion

upregulation of FarE increases the efflux of certain fatty acids, which bind to Chlorotoniil, neutralising its activity.

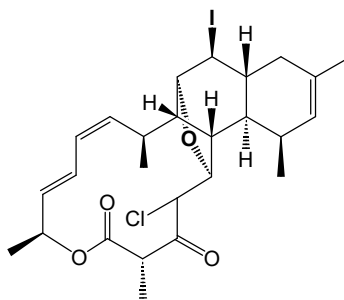
Interestingly, the dysregulation of KdpABC, BetA and BetB (GbsA) is reversed in the high-level resistance mutants. While the exact reason for this still has to be investigated, this also points towards a mechanism of action on potassium homeostasis. Of note, transcriptome analysis of Rhodomyltone-resistant clones and of Rhodomyltone treated WT *S. aureus* did not reveal any dysregulation of *betA*, *gbsA*, or *kdpABC*¹⁹⁰. This indicates that dysregulation of these proteins is a direct response to the mechanism of action of Chlorotoniil and is not merely linked to FarR/E dysregulation. The effect of Chlorotoniil on various lipids is currently being investigated. These findings will be published together with the findings shown in this study. In conclusion, the use of TPP and comparative full-proteome analysis have been vital in the effort to further understand the mechanism of action of Chlorotoniil and are helping to piece together results from different experiments. Furthermore, resistance generation with subsequent proteomic investigation has identified the primary resistance mechanism in *S. aureus* against Chlorotoniil.

4. Supplementary Information

Table S1. List of all proteins with a thermal shift > 3°C from the TPP experiment.

Gene name	Protein Name	$\Delta T_m 1$	$\Delta T_m 2$
Stabilised			
<i>SAUSA300_0362</i>	Mechanosensitive ion channel family protein	5.9	5.4
<i>SAUSA300_2234</i>	Inosine-uridine preferring nucleoside hydrolase	5.5	4.6
<i>SAUSA300_1448</i>	Transcriptional regulator, Fur family	4.7	4.8
<i>map</i>	Methionine aminopeptidase	4.0	3.8
<i>mnr</i>	Ribonuclease R	3.8	6.0
<i>SAUSA300_1349</i>	Glycosyl transferase, group 1 family protein	3.5	5.4
<i>aldA2</i>	Aldehyde dehydrogenase	3.4	3.7
<i>SAUSA300_0834</i>	D-isomer specific 2-hydroxyacid dehydrogenase	3.0	3.0
Destabilised			
<i>glk</i>	Glucokinase	-4.2	-3.9
<i>srtA</i>	Sortase	-3.1	-3.5
<i>rplR</i>	50S ribosomal protein L18	-3.1	-3.1
<i>metK</i>	S-adenosylmethionine synthase	-3.2	-3.0
<i>rplV</i>	50S ribosomal protein L22	-3.2	-3.1
<i>SAUSA300_2076</i>	Putative aldehyde dehydrogenase	-3.4	-3.3
<i>rplU</i>	50S ribosomal protein L21	-3.4	-3.5
<i>rpmC</i>	50S ribosomal protein L29	-3.4	-3.8
<i>rplC</i>	50S ribosomal protein L3	-3.9	-4.8
<i>SAUSA300_0538</i>	Uncharacterized epimerase/dehydratase	-4.0	-4.0
<i>rpsD</i>	30S ribosomal protein S4	-4.0	-3.0
<i>ddl</i>	D-alanine--D-alanine ligase	-4.1	-3.8
<i>rplF</i>	50S ribosomal protein L6	-4.1	-4.3
<i>thrB</i>	Homoserine kinase	-4.2	-4.3
<i>rplB</i>	50S ribosomal protein L2	-4.5	-4.0

III – 4. Supplementary Information



WH0024

Figure S1. Structure of the inactive Chlorotoniol derivative WH0024.

5. Methods

5.1. Biochemical Methods

5.1.1. Bacterial strains and culture

All *S. aureus* strains were cultured in Mueller Hinton Broth 2 (MHB) unless otherwise stated. *E. faecium* ATCC51559 was cultivated in TSB (17.5 g/L casein tryptone, 3 g/L Soja peptone, 2.5 g/L glucose, 5 g/L NaCl, 2.5 g/L potassium dihydrogen phosphate). All cultures were inoculated from Agar plates or glycerol stocks and incubated at 37 °C, 200 rpm.

5.1.2. Thermal Proteome Profiling in *S. aureus* USA300

S. aureus USA300 was inoculated into 2 separate culture tubes with B-Medium (LB-medium, Roth, 1 g/L potassium dihydrogen phosphate) and grown overnight at 37°C, 200 rpm. All steps were performed in biological duplicates. The overnight cultures were inoculated into 20 ml B-medium and grown until stationary. The cells were harvested in falcon tubes and washed with cold PBS (6000 xg, 4°C, 5 min). The cells were now reconstituted in PBS to a theoretical OD₆₀₀ of 20/ml. Per replicate, 1.2 mL of the culture was transferred into two new microcentrifuge tubes and **ChB1-Epo2** or DMSO were added (1:100, 1% DMSO final). The cells were incubated for 45 minutes at 37 °C, 200 rpm and then the each of the 4 samples was split into 10x 100 µL in 200 µL PCR tubes. The samples were placed into a preheated thermal cycler at the positions corresponding to the following temperatures.

Sample	1	2	3	4	5	6	7	8	9	10
T [°C]	42.3	45.9	49.2	52.8	56.4	59.8	62.6	67.1	71.1	77.7

The samples were heated for 3 minutes, followed by an incubation at RT for another 3 minutes. Next, 100 µL of 2x Lysis buffer (PBS pH 7.4, 50 µg/mL Lysostaphin, 1.6% NP-40, 30 µg/mL DNase I) and the cells were incubated at 37 °C for 30 minutes. The samples were snap-frozen in liquid nitrogen and thawed at 25 °C. This was repeated 4 times in total. 180 µL of each sample was transferred into a new Protein LoBind microcentrifuge tube and centrifuged (6000 xg, 4°C, 10 minutes) to remove cell debris. 160 µL of the supernatant were transferred into an ultracentrifuge tube (*Beckman Coulter*) and subjected to ultra-centrifugation (20 minutes, 100.000 xg, 4 °C) to remove the aggregated proteins. The protein concentration of the supernatant of the first 2 temperature points was determined using the Roti®-Quant universal kit (Carl Roth) for BCA assay. All samples were adjusted to a total protein concentration of 65 µg in 100 µL based on the average of the first 2 temperature points, and the proteins were

III – 5. Methods

precipitated by adding a 5-fold excess of ice-cold LC-MS grade acetone and incubating overnight at -20 °C. The following day the precipitated proteins were pelleted (21.000 xg, 20 min, 4 °C) and the supernatant was aspirated. To remove residual impurities, the pellet was reconstituted in 500 µL ice cold methanol by sonication (10 s, 10 % intensity, Sonopuls HD 2070 ultrasonic rod, BANDELIN electronic GmbH & Co. KG) and pelleted again. The methanol was aspirated and the protein pellet was reconstituted in 200 µL X-buffer (7 M urea, 2 M thiourea in 20 mM HEPES buffer pH 7.5) and the proteins were reduced by the addition of 1 mM DTT (from 1 M stock in H₂O) and incubating under gentle mixing (25 °C, 950 rpm, 45 minutes). To alkylate the reduced cysteines of the proteins, 5.5 mM iodoacetamide was added (550 mM stock in 50 mM in H₂O) and incubated for 30 minutes (25 °C, 950 rpm). The alkylation reaction was quenched by adding 4 mM DTT (from 1 M stock in H₂O) and incubating for 30 minutes (25 °C, 950 rpm). The proteins were pre-digested by adding LysC (2.5 µg/mL, 0.5 mg/mL stock, FUJIFILM Wako Chemical Corporation) and incubating for 3 hours (25 °C, 950 rpm, 45 minutes). After pre-digest, 600 µL 50 mM triethylammonium bicarbonate (TEAB) was added to each sample, followed by the addition of 1.3 µL of Trypsin (0.5 mg/ml stock, sequencing grade, modified; Promega) for overnight digest (37 °C, 950 rpm). The following morning, the digest was quenched by adding 8 µL of formic acid (FA) and the peptides were desalted using Sep-Pak C18 1 cc Vac cartridges (Waters) using the following procedure: Using gravity flow, the cartridges were first washed with 2 ml elution buffer (80 % MeCN, 0.5 % FA) followed by washing 3x with 1 ml 0.1 % TFA. The samples were now loaded and then washed 3x with 0.1 % TFA and 1x with 0.5 ml 0.5 % FA. The peptides were eluted from the cartridges with 2 x 250 µL elution buffer under gravity flow and once with 250 µL elution buffer under vacuum. The peptides were dried using a centrifugal vacuum concentrator and subsequently reconstituted in 7.5 µL TMT-labelling buffer (50 mM HEPES, 20 % MeCN, pH 8.5) through repeated vortexing, sonication (bath) and centrifugation. For TMT-labelling, 5 µL of previously prepared TMT isobaric labels (TMT10plex™ isobaric Labels Reagent set 1x 0.8 mg, Thermo Fischer Scientific) were added (10 µg/µL stock concentration in anhydrous MeCN), vortexed, centrifuged and incubated for 1 h (450 rpm, 25 °C). The labelling reaction was quenched by the addition of hydroxylamine to a final concentration of 0.4 %. To test whether the TMT labelling was successful, 187.5 µL of 0.1 % FA were added to each sample, and 2 µL of each temperature point within a condition were combined, dried in a centrifugal vacuum concentrator, reconstituted in 1 % FA, and the samples were measured using LC-MS/MS. After confirming complete TMT labelling, all temperature points within a condition were pooled (25 µg of protein based on initial protein concentration) and dried in a centrifugal vacuum concentrator. The combined samples were now fractionated. For this, the labelled peptides were now reconstituted in 105 µL HILIC buffer A (95 % MeCN, 0.1 % TFA) by sonication and transferred to a LC-MS vial. The peptide fractionation was carried out using an UltiMate 3000

HPLC system (Dionex) equipped with an YMC-Pack PVA-Sil column (5 μm , 150 x 2.1 mm, 120 \AA , YMC Europe GmbH). Gradient elution was carried out with 95 % MeCN, 5 % H₂O, 0.1 % TFA (A) and 95 % H₂O, 5 % MeCN, 0.1 % TFA (B). 100 μL of the sample was injected and separated using a 62.5 min gradient (7.5 min 0% B, 50 min to 30 % B, 3.5 min to 50 % B, 2.5 min to 100 % B) at a flow rate of 0.2 mL/min, followed by a washing and equilibration step. During equilibration, an on-line UV detector at 215 nm was used to monitor peptide elution. Fractions were collected into a 96-well plate and then pooled into 5 greater fractions, which were dried in a centrifugal vacuum concentrator and subsequently reconstituted in 100 μL 1 % FA by placing the tubes in a sonication bath for 10 min. The peptides were then filtered using freshly equilibrated (300 μL , 1 % FA) 0.22 μM Ultrafree-MC® centrifugal filters (Merck, UFC30GVNB). The filtered samples were transferred into LC-MS vials. The experiment was conducted in duplicate.

5.1.3. Mass spectrometry for thermal proteome profiling

TMT-labelled peptide samples were analyzed on an UltiMate 3000 nano HPLC system (Dionex) equipped with an Acclaim C18 PepMap100 (75 μm ID x 2 cm) trap column and a 25 cm Aurora Series emitter column (25 cm x 75 μm ID, 1.6 μm FSC C18) (Ionoptics) separation column (column oven heated to 40 °C) coupled to an Orbitrap Fusion (Thermo Fisher) in NSI-spray setting. For peptide separation, samples were loaded on the trap column and washed for 10 min with 0.1% TFA in ddH₂O at a flow rate of 5 $\mu\text{L}/\text{min}$. Subsequently, peptides were transferred to the analytical column for peptide separation and separated using the following 120min gradient (Buffer A: H₂O + 0.1% FA; B: MeCN + 0.1% FA) with a flow rate of 300 nL/min.: in 10 min to 5% B, in 50 min from 5% to 22% and in 60 min from 22% to 35%. The separation gradient was followed by a column washing step using 90% B for 10 min and subsequent column re-equilibration with 5% B for 5 min. MS full scans were recorded at a resolution of 120.000 with the following parameters: Ion transfer tube temperature 275 °C, RF lens amplitude 60 %, 375-1500 m/z scan range, automatic gain control (AGC) target of 2.0×10^5 , 3 s cycle time and 20 ms maximal injection time. Peptides with a higher intensity than 5.0×10^3 and charge states between 2 and 7 were selected for fragmentation in the collisional-induced dissociation (CID) cell at 35 % collision energy and analysed in the ion trap using rapid scan rate. In the ion trap, the isolation window was set to 1.6 m/z, an AGC target of 1.0×10^4 and a maximal injection time of 100 ms. For MS3-based reporter ion quantification, the number of synchronous precursor selections (SPS) was set to 10 with an isolation window of 2.5 m/z. The selected precursors were fragmented using the higher-energy collisional dissociation (HCD) cell at 55 % collision energy and analysed in the orbitrap at a resolution of 60.000 with the AGC target set to 2×10^5 and a maximal injection time of 118 ms.

5.1.4. Data analysis of thermal proteome profiling experiments

MS raw data was analysed using MaxQuant¹⁶¹ software (version 1.6.17.0), and peptides were searched against Uniprot database for *S. aureus* USA300 (taxon identifier: 367830, downloaded on 13.11.2020, canonical). Carbamidomethylation of cysteines was set as fixed modification, and oxidation of methionines and acetylation of N-termini were set as variable modifications. Trypsin was set as a proteolytic enzyme with a maximum of 2 missed cleavages. For the main search, precursor mass tolerance was set to 4.5 ppm and fragment mass tolerance to 0.5 Da. Fractions were assigned for each experiment. Group-specific parameters were set to “Reporter ion MS3” with 10plex TMT isobaric labels for N-terminal and lysine modification selected. The isotope correction factor was set for each TMT channel according to the data sheet of the TMT labels. Carbamidomethylation of cysteines was set as fixed modification, and oxidation of methionines and acetylation of N-termini were set as variable modifications. Trypsin was set as proteolytic enzyme with a maximum of 2 missed cleavages. For main search, precursor mass tolerance was set to 4.5 ppm and fragment mass tolerance to 0.5 Da. Second peptide identification was enabled, and false discovery rate (FDR) determination was carried out by applying a decoy database and thresholds were set to 1% FDR at peptide-spectrum match and at protein levels. The remaining parameters were used as default settings. Calculated corrected reporter ion intensities were normalized to the channel corresponding to the lowest temperature and were used to determine the melting curves of the proteins and the resulting thermal shifts (T_m). These were calculated using R (version 4.1.1) and the TPP package¹¹³ (version 3.20.1) using the “analyzeTPPTR” function. Proteins that fulfilled all requirements¹⁹² were considered to have a significant thermal shift. For visualization of the TPP output files, the data was filtered as follows: $R^2 > 0.8$ for all fitted curves, plateaus < 0.3 for DMSO curves, steepest slopes of melting curves < -0.06 , difference in T_m between both DMSO replicates < 1.5 °C. The resulting T_m shifts were visualized using GraphPad Prism 10.

5.1.5. Full Proteome analysis

S. aureus ATCC29213 and the Chlorotoni resistant mutants were inoculated from glycerol stocks into MHB2 and grown overnight. The following day the overnight culture was inoculated into fresh medium with DMSO (0.1%) or compound added (depending on the experiment) to an OD_{600} of 0.5. Cells were grown at 37 °C, 200 rpm and the optical density was measured regularly. For samples of the exponential phase, samples were harvested after about 2.5 hours ($OD_{600} \sim 2$). For samples of the stationary phase, samples were harvested after about 9 hours

III – 5. Methods

(OD₆₀₀ ~7). The samples were harvested and washed with cold PBS (6000 xg, 4°C, 5 minutes) and reconstituted in 200 µL lysis buffer (PBS pH 7.4, 0.4% SDS, 1 % Triton X-100). The cells were sonicated (10 s, 30 % intensity, Sonopuls HD 2070 ultrasonic rod, *Bandelin electronic GmbH*) and transferred into bead-mill lysis tubes filled with 0.1 mm zirconium beads. The cells were lysed at 6500 rpm for 3x 30 s using a precellys 24 bead beater (*peq/lab*). The Lysate was centrifuged at 10.000 xg for 10 minutes, and the supernatant (180µL) was transferred into a micro-centrifuge tube and centrifuged for 10 minutes at 21.000 xg. The supernatant (150 µL) was transferred into a new centrifuge tube. The protein concentrations of the samples were determined by BCA assay (Roti Quant, Roth), and all samples were adjusted to the same protein concentration using the lysis buffer. 80 µL of each sample was transferred into a 96-well PCR plate and the samples were alkylated with 10 mM TCEP and 20 mM iodoacetamide (IAA). 10 µL of a 1:1 mix of washed (3x H₂O) hydrophobic and hydrophilic carboxylate-coated magnetic beads (*Cytiva*) was added to each sample. To precipitate the proteins onto the beads, 135 µL ethanol were added to each sample. The plate was incubated for 10 minutes, 500 rpm. For each washing step, the plate was placed onto a 96-well magnet (*Dynamag, Invitrogen*) for 90 s and the supernatant was carefully removed. The plate was then removed from the magnet and the next washing solution was added, followed by 1 minutes shaking at 800 rpm. In this way, the samples were washed 3x with 180 µL 80% ethanol and once with 180 µL acetonitrile. The bead-bound proteins were digested in 50 µL 50 mM TEAB with 0.5 µg Trypsin (sequencing grade, *Promega*) overnight at 37 °C in a tightly sealed plate and with a heated lid at 800 rpm. After the tryptic digest, the peptides were eluted from the beads, and the beads were washed with 50 µL of 1% formic acid and the resulting 100 µL were directly transferred into MS-vials without any desalting and 2.5 µL (250 ng) of each sample were measured on a timsTOF Pro in data-independent acquisition mode.

5.1.6. Mass spectrometry for full proteome analysis

Peptides were measured and online-separated using an UltiMate 3000 nano HPLC system (*Dionex*) coupled to a *Bruker* timsTOF Pro mass spectrometer via a CaptiveSpray nano-electrospray ion source and *Sonation* column oven. The method was the same as described in chapter II – 5.1.10.

5.1.7. Data analysis of timsTOF Pro measurements

MS-data were analysed using DIA-NN⁸⁷ (version 1.8.1) using the library-free mode. The library was generated using the UniProt proteome for *S. aureus* USA300 (taxon identifier: 367830, downloaded on 07.06.2022, canonical). For the precursor ion generation, library generation

and Deep-learning based spectra, RTs and IMs prediction were enabled. Trypsin/P with maximum 2 missed cleavages; protein N-terminal M excision on; Carbamidomethyl on C as fixed modification; no variable modification; peptide length from 7 to 30; precursor charge 2–4; precursor m/z from 300 to 1800; fragment m/z from 200 to 1800 for TIMS data. Precursor FDR was set to 0.01; Mass accuracy, MS1 accuracy and Scan window were all set to 0; isotopologues, MBR and Remove likely interferences were on; Neural network classifier in single-pass mode; protein inference at gene level; heuristic protein inference was enabled (--relaxed-prot-inf); quantification strategy was set to Robust LC (high precision); Cross-run normalisation was RT-dependent; Library generation smart profiling; Speed and Ram usage was set to optimal results. LFQ quantities were extracted from the protein groups (pg) results file and were further analysed with Perseus software¹⁶² (version 2.03.1). LFQ intensities were log₂ transformed and protein groups with less than four valid values in at least one group were filtered out. Two-sample Students' t-test including permutation-based multiple testing correction (FDR = 0.05) was performed for all relevant comparisons to calculate the fold-change and statistical relevance. Results table were exported and graphs prepared using *Graphpad Prims* 10.01.

5.1.8. Cloning and Expression of *S. aureus* MetAP

The *map* gene was amplified from the extracted genomic DNA of *S. aureus* USA300 using PCR and the primers in the following table:

Primer 1	ggggacaagttgtacaaaaagcaggcttgagaatcttattttcagggcATGATTGTAAAAACAGAAGA AGAATTACAAG
Primer 2	ggggaccactttgtacaagaagctgggtgCTATTCTTCTTCAATCTTTGTCGTTAAAATC

The resulting PCR fragment was purified using a preparative agarose gel and subsequent DNA gel extraction. The cleaned PCR fragment was then cloned into pETG41K (via pDONR207) using the Gateway BP and LR Clonase (*Invitrogen*) according to the standard manufacturer protocol. The plasmid was transformed into BL21 DE3 cells and grown on LB-kanamycin plates. Two colonies were picked, grown in LB-Kan and the plasmid extracted using a miniprep kit (*Machery Nagel*). The plasmid was sequenced and a colony with the correct sequence was used for protein Expression purification. The MBP-TEV-SaMetAP fusion protein was expressed solubly at 18°C overnight. 2 L of LB-Kan were inoculated (1:100) with BL21 DE3 pETG41K_SaMetAP and grown to OD₆₀₀ = 0.5. Protein expression was induced by adding IPTG to a final concentration of 0.5 mM. The next day, cells were harvested and washed with cold PBS. Cell pellets were reconstituted in lysis buffer (50 mM Hepes pH 7.5, 150 mM NaCl, 1 mM TCEP, 5% glycerol, 1 mM PMSF, small amount of DNASE) and lysed by sonication (7

min at 30%, 3 min at 60%, 7 min at 30% intensity, Sonopuls HD 2070 ultrasonic rod, *Bandelin electronic GmbH*). The lysate was cleared at 38.000 xg for 45 min and the supernatant was filtered through a 0.45 µm filter prior to purification using an Äkta Pure Protein Purification System (*Cytiva*). Due to the low binding capacity of the MBPTrap the purification was split into 14 runs (from 2 L harvested cells). Each time, 5 mL Lysate was loaded onto an equilibrated 5 mL MBPTrap column (*Cytiva*) at a flow-rate of 2 mL/min. The column was washed with 6 column-volumes (CV) buffer A (50 mM Hepes pH 7.4, 150 mM NaCl, 1 mM TCEP, 5% glycerol, 5 mM EDTA) at a flow-rate of 5 mL/min and eluted over 3 CVs with 100% buffer B (50 mM Hepes pH 7.4, 150 mM NaCl, 1 mM TCEP, 5 mM EDTA, 5% glycerol, 10 mM Maltose). The elution fractions were pooled (not concentrated) and the MBP-tag was removed by TEV cleavage using TEV-protease at a ratio of 1:20 at 4°C overnight (stirring). The following morning, the TEV-digest was monitored by IP-MS. Precipitated protein was removed by centrifugation. The supernatant was desalted using 2 combined 5 mL HiTrap Desalting column (*Cytiva*) into buffer C (50 mM Hepes pH 7.4, 150 mM NaCl, 1 mM TCEP, 5% glycerol) to remove EDTA. The His-MBP tag and uncleaved fusion protein was removed by loading the sample onto two connected 5 mL HisTrapHP columns (*Cytiva*) at a flow-rate of 5 mL/min. Cleaved SaMetAP was eluted using 7.5% buffer D (50 mM Hepes pH 7.4, 150 mM NaCl, 1 mM TCEP, 5% glycerol, 500 mM imidazole). The bound HisMBP tag and fusion protein eluted only at 100% buffer D. The presence of cleaved SaMetAP was confirmed by IP-MS and SDS-PAGE and the fractions were pooled and concentrated. The protein was then further purified by size-exclusion chromatography in buffer A using a Superdex 75pg (*Cytiva*) and eluted fractions corresponding to SaMetAP were concentrated up to 10 mg/mL, snap-frozen in liquid nitrogen and stored at -80 °C.

5.1.9. SaMetAP activity assay

To measure the activity of SaMetAP the protein was thawed on ice and diluted into assay buffer (50 mM Hepes, 150 mM NaCl, 0.1 mM TCEP) to a final concentration of 5 µM. The ideal Metal concentration was determined to be a 3 to 5-fold excess of CoCl₂. The metal was added from a 100x stock and the protein was incubated for 15 minutes at room temperature. Meanwhile, compounds or DMSO were added to a plate from 100-fold stocks. 100 µL of pre-incubated cobalt-bound enzyme was added to each well. The plate was incubated at 35 °C for 15 minutes while measuring the absorption at 405 nM in a plate reader (*Tecan F200 pro*). The substrate was added using a Multipette® (*Eppendorf*). Here, 1 µL of 100 mM methionine-p-nitroanilide (MetpNA) was added for a final concentration of 1 mM. The absorbance was measured every minute for 3 hours. The release of cleaved para-nitroanilide was measured

III – 5. Methods

(405 nm) and the linear range was fitted by a linear regression fit and the slopes calculated using *GraphPad Prism* 10.01.

IV. Pronucleotide probes reveal a diverging specificity for AMPylation vs UMPylation of human and bacterial nucleotide transferases

This Chapter is based on the following publication:

Dietrich Mostert, Wilhelm Andrei Bubeneck, Theresa Rauh, Pavel Kielkowski, Aymelt Itzen, Kirsten Jung and Stephan A. Sieber, Pronucleotide probes reveal a diverging specificity for AMPylation vs UMPylation of human and bacterial nucleotide transferases. *Biochemistry*, **2024**, <https://pubs.acs.org/doi/full/10.1021/acs.biochem.3c00568>

Some results of this chapter are part of the Master thesis of WAB:

Wilhelm Andrei Bubeneck, A Pronucleotide Probe Allows the *In Situ* Investigation of UMPylation in Human Cells Using MS-based Proteomics. Master Thesis, **2021**¹⁹³

Contributions:

DM, WAB, and SAS planned the project and all Experiments. WAB synthesised the UMP pronucleotide probe and performed initial gel-based labelling. DM Performed all proteomic and validation experiments included in this work. DM and SAS prepared the manuscript for publication and parts of figure 1 were initially prepared by WAB and then adapted for this dissertation by DM.

1. Introduction

Post-translational modifications (PTMs) largely enhance the functional scope of proteins beyond the structural diversity of the 20 natural amino acids. These modifications play crucial roles in, e.g., cellular signalling, enzyme catalysis, and the structural integrity of proteins^{60,194–196}. However, PTMs are not limited to enhancing the functions of proteins within a cell but can also be involved in the onset of numerous diseases^{197–200}. These include aberrant PTMs in signalling cascades leading to uncontrolled cellular growth of cancer cells^{201–205} as well as in the warfare of pathogens that dysregulate the host cell physiology²⁰⁶. For example, bacteria have evolved numerous ways to interfere with human signalling, silencing the immune response and promoting infection^{207,208}. This interkingdom warfare is mediated by bacterial effector proteins, often transferred into human cells via type III secretion systems²⁰⁹. Once inside the cell, these effectors mediate various PTMs, including phosphorylation, acetylation, proteolysis, and the transfer of larger molecules such as adenosine diphosphate (ADP)-ribose or adenosine monophosphate (AMP). Many effectors have common targets, such as membrane-bound guanosine triphosphatases (GTPases) from the Rho family involved in signal transduction that regulates the actin cytoskeleton and diverse immune processes, mitogen-activated protein kinases (MAPKs) and nuclear factor kappa B (NF- κ B) which are both part of signalling pathways responsible for immune response regulation^{49,206,210–212}.

AMPylation (also termed adenylylation) was first discovered in *Escherichia coli* as a regulatory mechanism for glutamine synthetase²¹³. In addition, several other AMPylators were discovered in bacteria. These enzymes, including VopS from *Vibrio parahaemolyticus* and IbpA from *Histophilus somni*, are secreted into host cells where they AMPylate GTPases of the Rho family, leading to a disruption of the actin cytoskeleton and a characteristic rounded cell phenotype²¹⁰. The catalytic regions of both enzymes share a conserved filamentation induced by cyclic AMP (Fic) domain mediating the covalent attachment of an AMP moiety to a Ser, Thr, or Tyr protein side chain^{211,214}. A single Fic-domain-containing enzyme, termed FICD (HYPE), was also discovered in eukaryotic cells. It AMPylates the chaperone BiP (HSPA5) in the endoplasmic reticulum, which regulates the unfolded-protein response (UPR)^{196,215–217}. Moreover, the recent discovery of the pseudokinase SelO as an AMPylator in human cells highlights that Fic-independent enzymes can also catalyse this PTM²¹⁸.

Since the discovery of AMPylation, methods to decipher the cellular substrates have been developed utilising a diverse set of chemical probes bearing radioactive, fluorescent, or affinity reporter tags^{210,219}. Here, recent advancements in the profiling of AMPylation targets within cell lysates using ATP analogues functionalised with alkyne tags for protein enrichment via click chemistry to biotin azide, subsequent avidin enrichment, and mass spectrometric (MS)

analysis revealed new potential substrates of Fic-enzymes VopS and FICD^{220,221}. A cell-permeable AMP pronucleotide probe (**pro-N6pA**) for the identification of AMPylated proteins in intact human cells was recently introduced^{222,223}. In addition, this method was used to identify targets of VopS in *V. parahaemolyticus* infected human cells²²⁴.

While these previous efforts largely focused on the identification of AMPylation protein substrates, the transfer of alternative nucleotides, such as UMP, via these enzymes is rather underexploited. In vitro studies with several Fic-enzymes, including VopS and FICD, demonstrated a relaxed substrate specificity for VopS, transferring AMP, GMP, CMP, and UMP, while FICD showed efficient transfer for solely AMP²¹¹. However, how these in vitro results translate into cellular nucleotide specificities, i.e., considering the large amount of cellular ATP as a competitor, remains elusive. Of note, studies into nucleotide specificity have focused only on the bifunctional wild-type FICD, which typically shows low AMPylation and, hence, likely low general NMPylation activity²¹¹. Interestingly, a recent study with YdiU, a bacterial homolog of the human pseudokinase SelO, demonstrated the inactivation of chaperones via UMPylation, suggesting that other nucleotides could play a role in these processes²²⁵.

To analyse the *in situ* specificity for AMPylation vs UMPylation, a cell-permeable pronucleotide UMPylation probe (**pro-N3pU**) was designed and synthesised and applied together with the **pro-N6pA** probe in cellular labelling studies. The aim was to investigate the nucleotide selectivity of human AMPylators and of the bacterial effector protein VopS during infection.

2. Results and Discussion

2.1. Design of a UMPylation pronucleotide

To study cellular UMPylation, a tailored probe bearing an alkyne handle for target protein enrichment and a masked pronucleotide moiety for cellular uptake was designed. The latter was already successfully applied in the first AMPylation probe generation^{222,224}. Once inside the cell, the pronucleotide is cleaved by hydrolases, and the AMP probe is subsequently converted into the triphosphate by a kinase²²⁶ (Figure 1A). The probe design contains two main features: the terminal alkyne handle on the heterocyclic N³ and the phosphoramidate prodrug moiety (Figure 1B). First, the alkyne handle is necessary for chemical proteomics in-gel and MS-based analysis. The position on the heterocyclic N³ possesses two advantages: synthetic feasibility and that it likely decreases its incorporation into nucleic acids due to the hindrance of the Watson-Crick-Franklin base pairing. Second, the phosphoramidate moiety has been shown to yield the desired modified nucleoside triphosphates on many ‘highly challenging’ nucleotide analogues^{226,227}. The UMP/CMP kinase structure responsible for phosphorylation of CMP and UMP analogues to the corresponding NDPs and NTPs has an induced-fit active site enabling the accommodation of various substrates.²²⁸

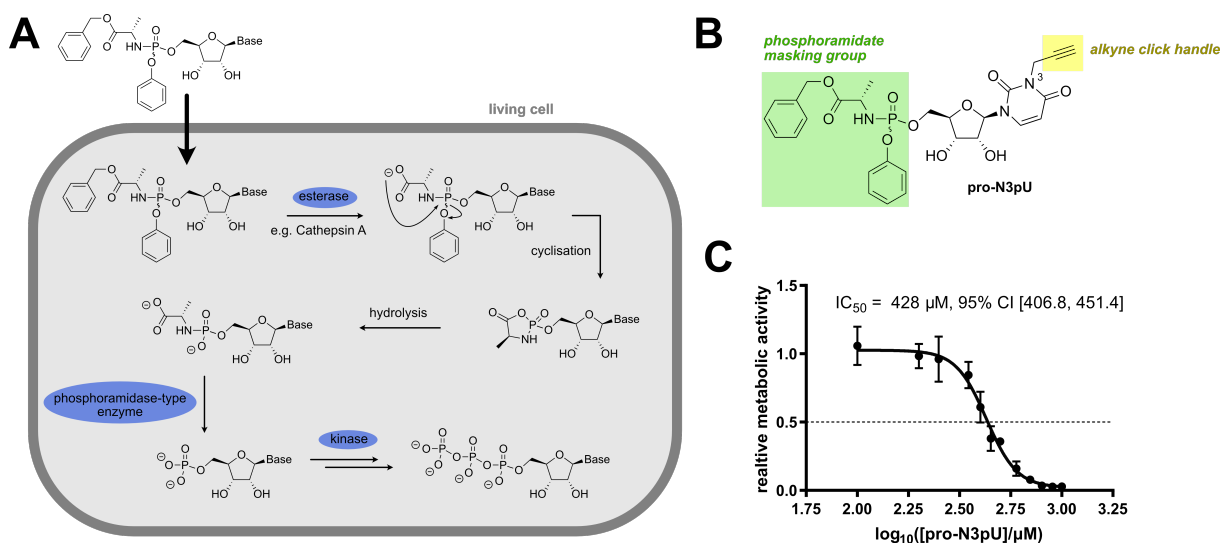


Figure 1. Phosphoramidate pronucleotide probes are cell-permeable and well-tolerated. (A) Postulated mechanism for the metabolic activation of phosphoramidate pro-nucleotides in living cells²²⁶. (B) Structure of the phosphoramidate UMPylation probe **pro-N3pU**. (C) MTT assay of **pro-N3pU** in HeLa cells (n=3). This figure was adapted from: W. A. Bubeneck¹⁹³.

The synthesis followed published procedures²²², starting with the alkylation of the N3-position of commercially available uridine with propargyl bromide (synthesis was conducted by W. A.

Bubeneck). The final compound was isolated as a 1/1 mixture of diastereomers due to unselective substitution at the phosphorus (V) and was used as such in proteomic experiments due to the fact that the R-P and S-P isomers usually exhibit similar rates of metabolism and are difficult to separate by chromatography²²⁶.

2.2. Labelling in human cells reveals promiscuity of nucleotide transfer

Prior to pro-N3pU labelling in human cells, the viability of HeLa cells in the presence of the probe was tested. Satisfyingly, toxicity was only observed at high concentrations with an IC50 value > 400 μ M in MTT assays (Figure 1C) (MTT assay was conducted by W. A. Bubeneck). The probe was subsequently incubated with intact HeLa cells for 4, 8, and 16 h at various concentrations (Figure S1A). Cell lysis followed by click chemistry to rhodamine azide and fluorescent SDS-PAGE of the labelled proteome revealed an optimal concentration of 150 μ M and 16 h incubation time for clearly visible protein signals. Interestingly, a direct comparison with the pro-N6pA AMPylation probe resulted in an overall comparable labelling pattern (Figure S1B). In order to decipher the targets of pro-N3pU, HeLa cells were labelled under the optimised conditions, followed by cell lysis and click of the treated proteome with biotin azide to facilitate the enrichment of probe-modified proteins on avidin beads (Figure 2A). Tryptic digest and LC-MS/MS analysis via label-free quantification (LFQ) enables the ranking of protein hits in volcano plots compared to a DMSO control sample. Of note, both probes seem to only slightly enrich the well-known AMPylation target HSPA5 (Log₂ fold-change of ~0.5). The high endogenous levels of HSPA5 combined with a high background binding to agarose-avidin beads could make it challenging to achieve higher enrichment values for HSPA5 with this experimental setup.

Interestingly, a side-by-side comparison of significantly (p -value > 0.01) enriched proteins by either pro-N3pU or pro-N6pA probes revealed a largely comparable profile of targets (Figure 2B). In fact, 37 out of 41 proteins that were enriched by pro-N3pU with a log₂-fold enrichment > 2 are also enriched by pro-N6pA with a log₂-fold enrichment > 1 among both datasets including proteins such as CTSA and CTSB, previously identified as major AMPylation targets. The overlap is still evident when comparing hits enriched by both probes by a fold-change > 2 (Figure S2A). As these comparisons can be somewhat misleading depending on the fold-change cut-off used, the best way to visualize the similarities is to plot the fold-changes of both probes against each other directly and calculate the correlation. Given the vast correlation of targets by either probe (Pearson correlation $r = 0.86$) and the correlation of the fold-changes overall (Pearson correlation $r = 0.89$) (Figure 2C), it can be concluded that human nucleotide transferases are rather promiscuous in the substrate selection. Considering the high

IV – 2. Results and Discussion

concentration of ATP in the cell, it is remarkable that 150 μM of probe concentration was sufficient to compete for binding. Of note, this method does not distinguish between different types of AMPylating enzymes, and it is possible that more enzymes are involved in this process.

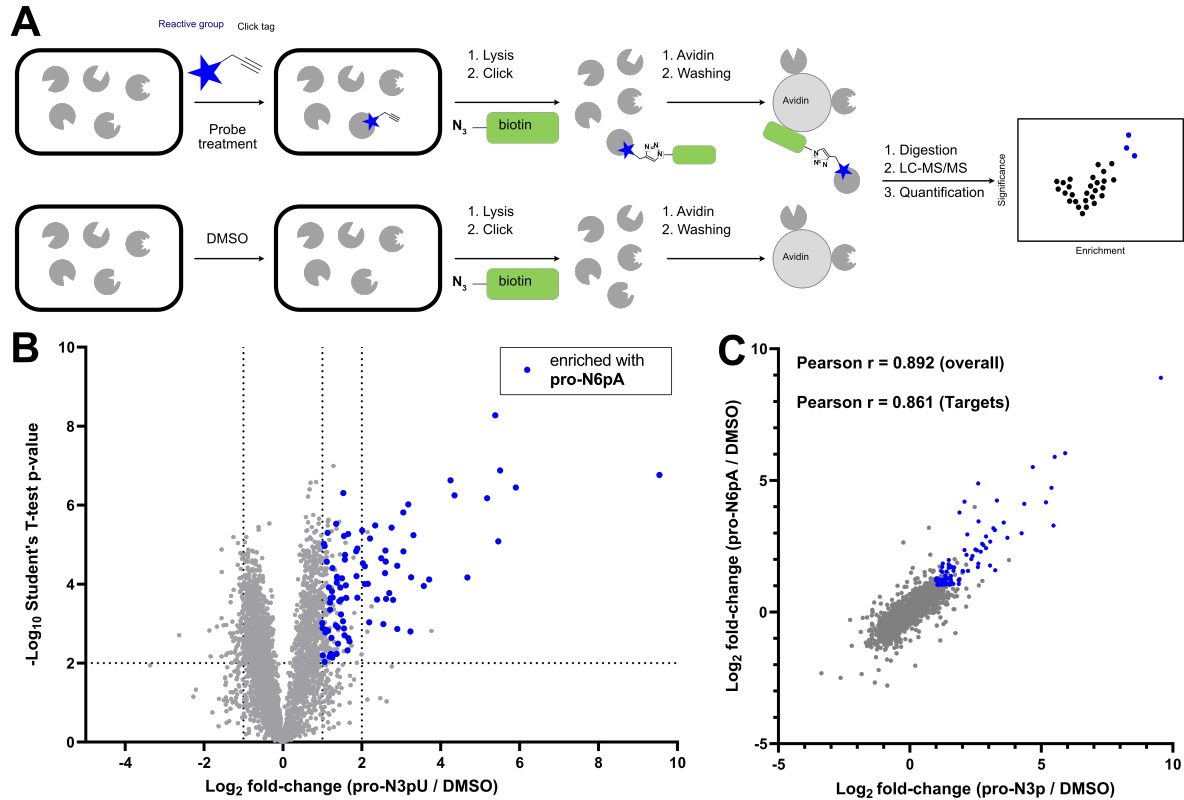


Figure 2. Metabolic labelling in living cells suggests a degree of promiscuity between AMPylation and UMPylation. (A) Schematic overview of the workflow for metabolic labelling using activity-based probes. (B) Volcano-plot of HeLa cells treated with 150 μM pro-N3pU for 16 hours compared to DMSO control. Proteins that are also enriched by the AMPylation probe pro-N6pA ($p < 0.01$ and a $\text{Log}_2(\text{fold change}) > 1$) are marked in blue. Dotted lines indicate cut-off at $p < 0.01$ ($n=4$) and a $\text{Log}_2(\text{fold change}) > 1$ and $\text{Log}_2(\text{fold change}) > 2$. (C) Scatter plot plotting $\text{Log}_2(\text{fold changes})$ of all significant ($p < 0.01$) proteins from the pro-N3pU enrichment experiment against the $\text{Log}_2(\text{fold changes})$ of all significant proteins from the pro-N6pA enrichment experiment. The overlapping protein targets from (B) are marked in blue, and the respective Pearson correlation of all proteins and of all Targets $\text{Log}_2(\text{fold change}) > 1$ was calculated using prism 10.01. Figure 2A was adapted from W. A. Bubeneck¹⁹³.

2.3. *V. parahaemolyticus* effector protein VopS solely AMPylates human proteins

Intrigued by the relaxed substrate tolerance of human AMPylators, the attention was turned to the class of protein nucleotide transferases in bacteria. VopS of *V. parahaemolyticus* was previously shown to address a specific set of rho GTPases in human cells via the pro-N6pA

IV – 2. Results and Discussion

probe²²⁴. To investigate if the reported *in vitro* substrate tolerance of VopS towards different nucleotide substrates²¹¹ also holds true for its action in living cells during infection, the novel pro-N3pU probe was applied in HeLa cells infected with *V. parahaemolyticus*. Cells were infected with bacteria in a multiplicity of infection (MOI) of 1:10, resulting in characteristic round-shaped cells after 90 min (Figure 3A). Accordingly, a strain carrying the corresponding VopS active site H348A mutation did not affect HeLa cell morphology.

With these established conditions, HeLa cells were treated individually with both pro-N6pA and pro-N3pU cells prior to the infection with bacteria. Cells were prepared as described above, and LC-MS/MS-based proteome analysis revealed a comparable pro-N6pA enrichment of target proteins as observed before²²⁴ that was absent in the mutant control (Figure 3B). Strikingly, no significant protein enrichment was observed with pro-N3pU, highlighting that VopS performs AMPylation but no UMPylation of human protein targets (Figure 3C, S3A). Both probes exhibit the same enrichment pattern of endogenously enriched samples in the infection assay, but while pro-N6pA additionally enriches the known VopS substrates (Figure S3B), the UMPylation probe pro-N3pU only enriches the endogenously AMP/UMPylation targets and not any of the VopS targets (Figure S3C), highlighting the diverging specificity of VopS and the human AMPylators. To rule out that the diverging nucleotide promiscuity of human AMPylators and VopS is only due to the shorter time span (16 h vs 90 min), HeLa cells were labelled with both probes for only 90 minutes (Figure S2B, C). As expected, the overall enrichment is significantly lower for both probes. However, both probes lead to similar labelling patterns, also after only 90 minutes. This confirms that the human AMPylators are indeed more promiscuous than the bacterial VopS, even when given the same amount of time for labelling. To finally validate this substrate specificity, an *in vitro* experiment was performed with recombinant VopS and Cdc42 as a cognate substrate. Enzymes were incubated with 100 μ M ATP and 100 μ M UTP for 90 min at 30 °C before being analysed by intact protein mass spectrometry (IP-MS) (Figure 3D, E). For this experiment, it can be assumed that the ionization potential of Cdc42-AMP and Cdc42-UMP are the same. In intact protein MS, the ionization potential is mainly driven by the amino acid sequence. Both AMP and UMP differ only slightly in size but introduce the same charge to the protein and, therefore, should not differ in their effect on the ionization potential. When VopS and Cdc42 are incubated with an equimolar amount of ATP and UTP, the preferred substrate is clearly ATP. While both Cdc42 adducts (+AMP, +UMP) are detected, the signal for Cdc42-AMP is far greater than the signal for Cdc42-UMP (Figure 3E). When taking into account the higher intracellular concentration of ATP (3152 μ M) compared to UTP (576 μ M)²²⁹, this *in vitro* preference for AMPylation translates to a negligible rate of UMPylation *in vivo*, as seen in the metabolic labelling experiments using the pronucleotide probes.

IV – 2. Results and Discussion

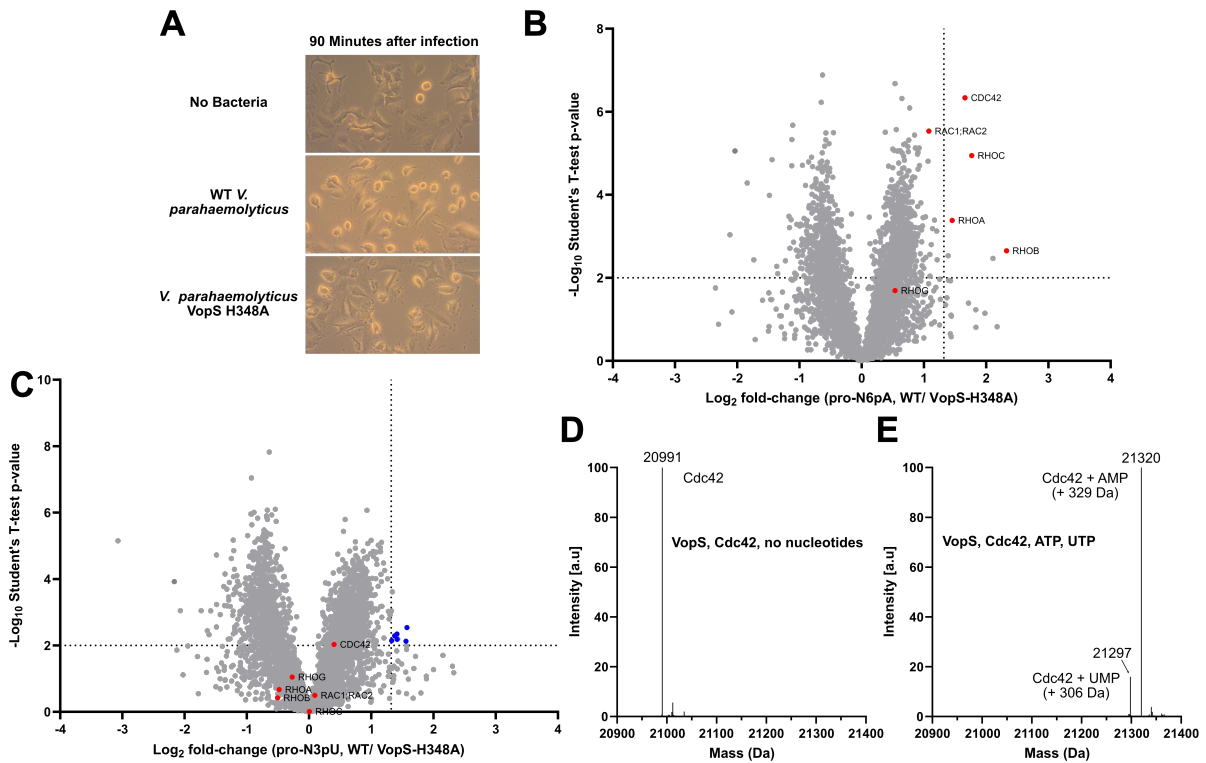


Figure 3. The bacterial AMPylator VopS does not UMPylate in an in situ infection assay. (A) Differences in phenotypic appearance when infecting HeLa cells with *V. parahaemolyticus* wild type or VopS mutant H348A for 90 minutes (MOI = 10). (B) Volcano plot of HeLa cells (treated with 100 μ M pro-N6pA) infected with *V. parahaemolyticus* WT compared to VopS H348 mutant infection. Dotted lines indicate cut-off at $p < 0.01$ ($n=4$) and a fold change > 2.5 ($\text{Log}_2 > 1.322$). Known VopS AMPylation targets are highlighted in red. (C) Volcano plot of HeLa cells (treated with 150 μ M pro-N3pU) infected with *V. parahaemolyticus* WT compared to VopS H348 mutant infection. Dotted lines indicate cut-off at $p < 0.01$ ($n=4$) and a fold change > 2.5 ($\text{Log}_2 > 1.322$). Known VopS AMPylation targets are highlighted in red. False positive hits are marked in blue and their respective profile plots are shown in Figure S3D. (D) No nucleotide control of in vitro assay of VopS and the substrate Cdc42. Intact protein mass of Cdc42 (monoisotopic) without any modification. Figure is representative of 3 independent replicates. (E) In vitro assay of VopS and the substrate Cdc42 with 100 μ M ATP and UTP (equimolar). Intact protein mass of Cdc42 (monoisotopic) modified with AMP and, to a far lesser extent, UMP. Figure is representative of 3 independent replicates.

3. Conclusion

The pronucleotide probes were showcased to be useful to decipher the substrate and target scope of human and bacterial nucleotide transferases and demonstrate the need for complementary approaches in the study of enzymes under *in vitro* and *in situ* conditions. While assays with the recombinant VopS enzyme indicated a relatively relaxed specificity for several nucleotides²¹¹, the *in situ* labelling suggests at least no tolerance for UTP as an alternative substrate to ATP. On the other hand, human nucleotide transferases exhibited a rather relaxed substrate tolerance with the probes, which was unexpected given the previously obtained specificity of FICD solely for ATP *in vitro*²¹¹. However, it cannot be excluded that other nucleotide transferases, such as SelO, modify protein targets more promiscuously. Future studies into the distinct targets of different human AMPylators and their potential difference in nucleotide promiscuity could give further insights into the role of different NMPylations in human cells. For example, AMPylation was shown to play an important role during neuronal development and degeneration²³⁰. Understanding how this substrate promiscuity might translate into different phenotypes under varying cellular conditions could give further insights into the role of these PTMs during these processes. The pronucleotide probes represent an ideal tool for gaining further insight into the substrate promiscuity of different human NMPylators. The probes could be used in various knock-down cells to identify the substrate scope and the nucleotide specificity of different known and putative NMPylators. Acquiring such a detailed understanding of different NMPylators would be the foundation for targeting this enzyme class for clinical use.

4. Supplementary Figures

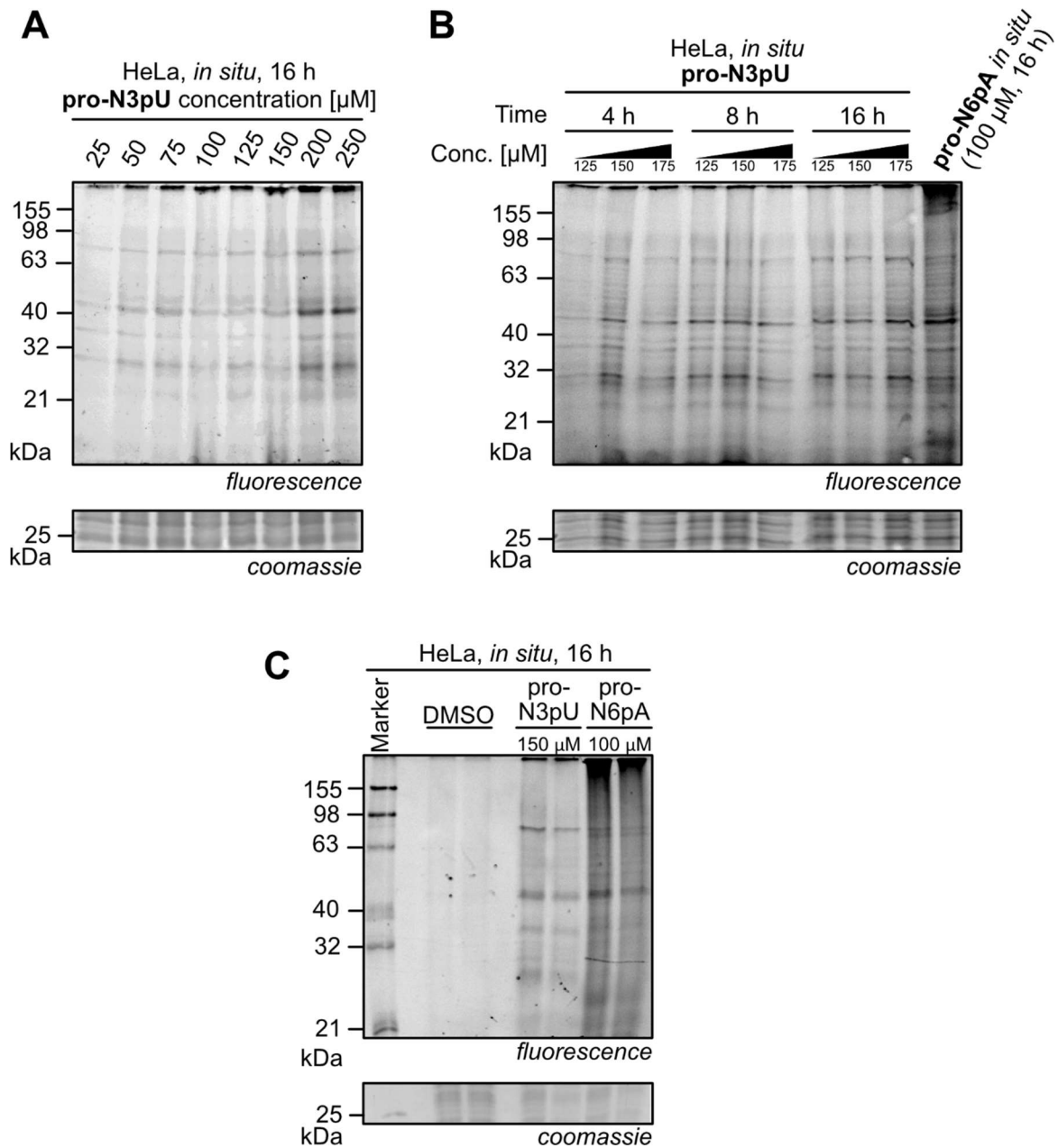


Figure S1. Initial analytical labelling using pro-N3pU to determine ideal conditions visualized by in-gel fluorescence after clicking treated samples with rhodamine azide. (A) Concentration-dependent labelling (B) Concentration- and time-dependent labeling, including a direct comparison with AMPylation probe pro-N6pA. (C) Analytical labelling in human cells, including a DMSO control to exclude unspecific fluorescence (Duplicates).

IV – 4. Supplementary Figures

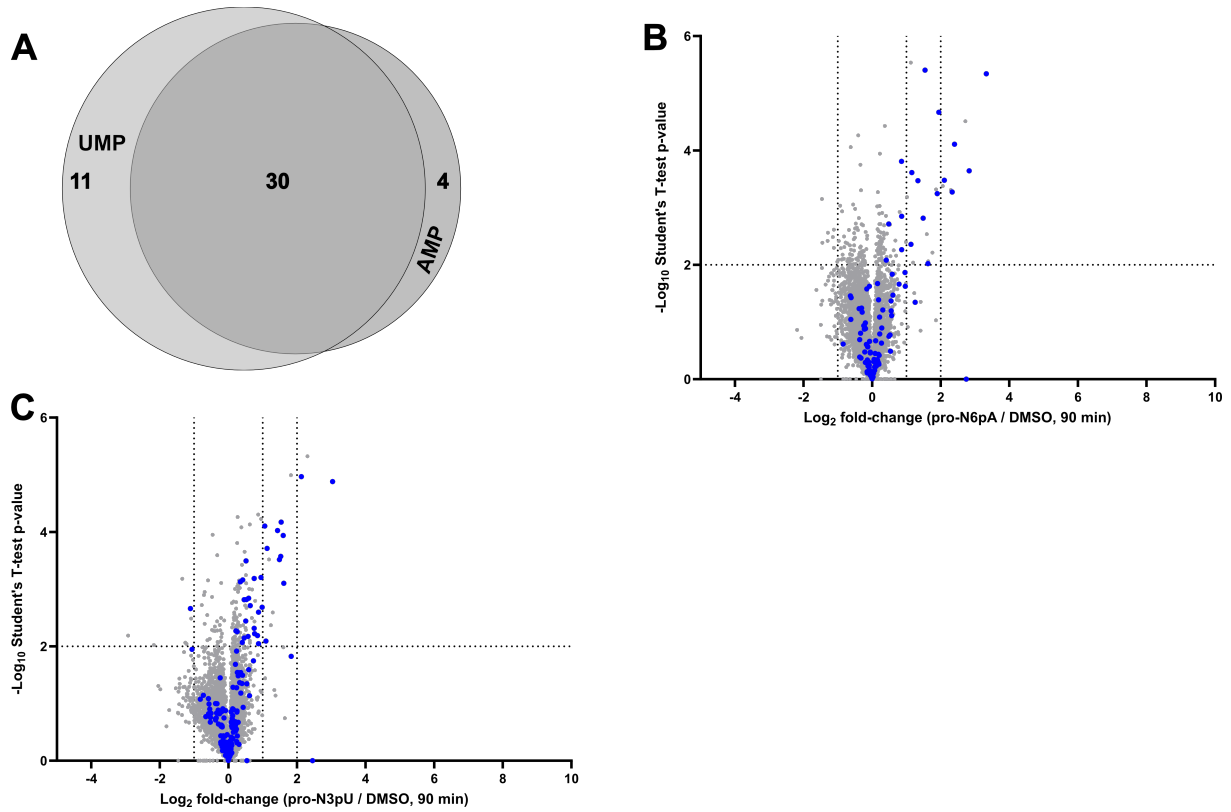


Figure S2. (A) Venn-Diagram of all proteins enriched by the pro-N3pU and pro-N6pA probes by a fold-change of more than 2. There is a significant overlap of both probes. Of note, some of the proteins that do not overlap are still enriched by both probes, just not to the same extent. (B, C) Volcano-plot of HeLa cells treated with 150 μ M pro-N6pA (B) or 100 μ M pro-N3pU (C) for 90 minutes compared to DMSO control. Proteins that are also enriched by the respective probe after 16h h incubation ($p < 0.01$ and a $\text{Log}_2(\text{fold change}) > 1$) are marked in blue. Dotted lines indicate cut-off at $p < 0.01$ ($n=4$) and a $\text{Log}_2(\text{fold change}) > 1$ and $\text{Log}_2(\text{fold change}) > 2$. Both probes enrich many of the same proteins as after 16 h incubation, albeit to a lesser extent.

IV – 4. Supplementary Figures

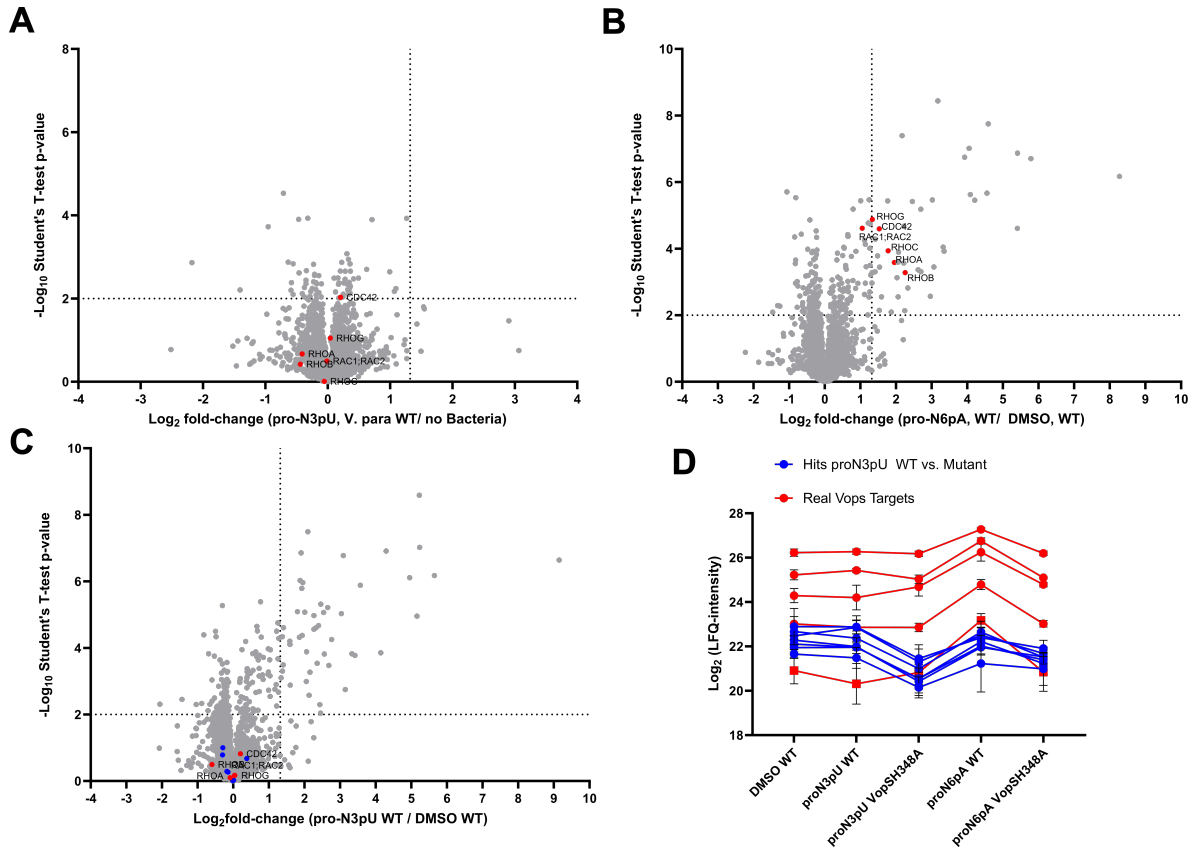


Figure S3. (A) Volcano plot of HeLa cells (treated with 150 μ M pro-N3pU) infected with *V. parahaemolyticus* WT compared to no bacterial infection; (B) HeLa cells (treated with 100 μ M pro-N6pA) infected with *V. parahaemolyticus* WT compared to HeLa cells (treated with DMSO) infected with *V. parahaemolyticus* WT; (C) HeLa cells (treated with 150 μ M pro-N3pU) infected with *V. parahaemolyticus* WT compared to HeLa cells (treated with DMSO) infected with *V. parahaemolyticus* WT. Dotted lines indicate cut-off at $p < 0.01$ ($n=4$) and a fold change > 2.5 ($\log_2 > 1.322$). Known VopS AMPylation targets are highlighted in red. False positive hits from Figure 3C are marked in blue and their respective profile plots are shown in Figure S3D. (D) Profile plots of the VopS targets and apparently enriched proteins from Figure 3C. False hits (blue) are not enriched by the probe but are merely less abundant in the mutant-treated cells due to missing value imputation.

5. Methods

5.1. Biochemical Methods

5.1.1. Cell Culture

Human epitheloid cervix carcinoma cells (HeLa) purchased from Sigma Aldrich (93021013) were cultivated with high glucose Dulbecco's Modified Eagle's Medium (DMEM) supplemented with 10 % fetal bovine serum (FBS) (Sigma-Aldrich) and 2 mM L-glutamine (Sigma-Aldrich) in T-175 culture flask (Sarstedt). Cells were maintained at 37 °C in a humidified 5% CO₂ atmosphere.

5.1.2. Bacterial Strains and Media

Vibrio parahaemolyticus strain RIMD 2210633 was received from Dr. Tetsuya Ida and Dr. Takeshi Honda from the Research Institute for Microbial Diseases, Osaka University. The bacteria were cultured in lysogeny broth (LB) medium (10 g/L casein peptone, 5 g/L NaCl, 5 g/L yeast extract, pH = 7.5) supplemented with NaCl for a total content of 3% at 30 °C, 200 r.p.m. *Vibrio parahaemolyticus* (strain RIMD 2210633) mutant VopS- H348A and the VopS deletion mutant (Δ VopS) were obtained by double homologous recombination using a suicide plasmid as described in a previous study²²⁴.

5.1.3. MTT Cytotoxicity Assay

HeLa cells were seeded at a density of 4000 cells per well in a transparent, flat-bottomed 96-well plate (200 μ L medium per well). Cells were grown overnight in a humidified atmosphere at 37 °C and 5% CO₂ to allow the cells to adhere to the surface. Subsequently, the medium was aspirated and replaced by fresh medium supplemented with pro-N3pU in concentrations ranging from 100 μ M to 1mM (DMSO content less than 1%) or 1% DMSO as a control. The cells were incubated at 37 °C, 5% CO₂ for 24 h. For the determination of metabolic activity, 20 μ L 3-(4,5-dimethyl-2-thiazolyl)-2,5-diphenyl-2H-tetrazolium bromide solution (MTT, 5mg/mL in PBS) were added to each well and the cells were incubated at 37 °C, 5% CO₂ for 4 h. Thereafter, the medium was aspirated and the violet formazan crystals were dissolved in 200 μ L DMSO per well under shaking (300 r.p.m., 10min). Absorbance at 570 nm with a reference wavelength of 630 nm was recorded using an Infinite F200 pro plate reader (Tecan). Three biological replicates were measured for each data point. Cell viability was normalized with respect to the DMSO control (highest absorbance) and fitted by least-squares regression with

variable-slope logistic function using Prism (GraphPad). Cytotoxicity is reported as the IC50 value, the concentration at which 50% viability is reached.

5.1.4. Analytical *in Situ* Labeling

HeLa cells were seeded into 6-well plates and treated with various concentrations of **pro-N3pU** for three different time periods. The previously described labelling using **pro-N6pA** at 100 μ M for 16 hours was included as a control. After probe treatment, the cells were harvested by carefully scraping them off and transferring them into micro-centrifuge tubes. The cells were then washed with 1 ml of cold PBS. The cell pellets were reconstituted in 100 μ L lysis buffer (1% NP-40, 1% sodium deoxycholate, 1 tablet protease inhibitor (cOmplete, Mini, EDTA-free protease inhibitor cocktail, Roche, 1 tablet in 15 mL). The samples were incubated for 15 minutes on ice and inverted twice. The lysed cells were centrifuged (21,000 xg, 5 min, 4 °C) and the soluble supernatant was transferred into a new tube. The protein concentrations of the samples were determined by BCA assay (Roti Quant, Roth) and all samples were adjusted to the same protein concentration using the lysis buffer. The samples were clicked to Rhodamine-azide by copper-catalyzed azide-alkyne cycloaddition (CuAAC) with 0.2 mM Rhodamine.azide, 0.1 mM TBTA ligand (1.67 mM stock in 80% *t*-BuOH, 20 % DMSO, TCI), 1 mM TCEP (52 mM stock in H₂O) and 1 mM CuSO₄ (50 mM stock in H₂O). The reaction was quenched by the addition of 100 μ L 2x l  mml buffer and samples were analyzed via SDS-PAGE with fluorescent imaging.

5.1.5. Preparative *in Situ* Labeling

All proteomics experiments were conducted in 4 independent biological replicates. HeLa cells were seeded into 10 cm petri dishes and grown until 90 % confluence. Cells were treated with 150 μ M of **pro-N3pU** or 100 μ M **pro-N6pA** for 16 hours (37°C, 5% CO₂). After probe treatment, the cells were harvested by carefully scraping them off and transferring them into falcon tubes. The cells were then washed with 1 ml of cold PBS and transferred into micro-centrifuge tubes. The cell pellets were reconstituted in 230 μ L lysis buffer (1% NP-40, 1% sodium deoxycholate, 1 tablet protease inhibitor (cOmplete, Mini, EDTA-free protease inhibitor cocktail, Roche, 1 tablet in 15 mL). The samples were incubated for 15 minutes on ice and inverted twice. The lysed cells were centrifuged (21,000 xg, 5 min, 4 °C) and the soluble supernatant (200 μ L) was transferred into a new tube. The protein concentrations of the samples were determined by BCA assay (Roti Quant, Roth) and all samples were adjusted to the same protein concentration using the lysis buffer. The samples were clicked to biotin-azide as described in the analytical labeling protocol. The reaction was quenched and the proteins precipitated by the addition of

5-fold excess ice cold acetone and incubated overnight at -20 °C. The proteins were harvested (21,000 xg, 4°C, 20 min) and washed twice with methanol. Therefore, the pellet was reconstituted in 500 µL methanol, sonicated (10 % intensity, 10 s, Sonopuls HD 2070 ultrasonic rod, Bandelin electronic GmbH) and harvested again via centrifugation as before. Next, the proteins were reconstituted in 500 µL 0.2% SDS in PBS by sonication (10 % intensity, 10 s) and the insoluble part was removed by centrifugation. The soluble fraction was added to 50 µL of washed (3x in 0.2% SDS in PBS) avidin-agarose beads and incubated for 1 h with continuous mixing. Afterwards, the samples were washed three times with 0.2% SDS in PBS, two times with 6 M urea and 3 times with PBS. For this the samples were centrifuged for 3 minutes at 400 xg and the supernatant was discarded each time. The beads were now resuspended in 200 µL digestion buffer 1 (3.6 M urea, 1.1 M thiourea, 5 mM TCEP in 20 mM HEPES, pH 7.5) and incubated for 30 minutes at 25 °C, 1000 rpm. The reduced bead-bound proteins were now alkylated with 5.5 mM iodoacetamide (30 min, 1000 rpm, 25 °C) and then the reaction was quenched with 10 mM DTT (30 min, 1000 rpm, 25 °C). Samples were first digested with 0.5 µg LysC (Wako) for 2 h at 25 °C before adding 600 µL 50 mM TEAB with 1.5 µg Trypsin (Promega) and a further incubation of 16 hours at 37 °C, 1000 rpm. The digest was stopped by adding 1 % FA and the peptides were desalted using 50 mg Sep-Pak C18 cartridges (Waters Corp.). Therefore, the cartridges were equilibrated with 1 mL acetonitrile, 1 mL (elution buffer (80% acetonitrile, 0.5 % FA in H₂O)) and 3 ml of wash buffer 1 (0.1 % TFA in H₂O). The samples were loaded, washed with 3 ml wash buffer 1 and 0.5 mL of 0.5% FA in H₂O. The peptides were eluted with 2x 250 µL elution buffer and dried in a centrifugal evaporator. The peptides were reconstituted in 30 µL 1% FA and measured on an Q Exactive Plus instrument.

5.1.6. Preparative *in Situ* labeling with infection

HeLa cells were seeded and labelled in the same way as the non-infection samples. Two additional plates were seeded which were later used to count the amount of cells per dish. In parallel, cultures of the desired *Vibrio parahaemolyticus* strains were inoculated from cryostocks and grown overnight. The overnight cultures were inoculated 1:100 into fresh medium and grown for 2.5 h. The OD₆₀₀ of the bacterial cultures were measured and the CFUs per µL were calculated. After counting the amount of HeLa cells on the two additional plates, the needed amount of bacteria for a MOI of 10 were harvested and then taken up in DMEM with 2 mM L-glutamine and 15 µM **pro-N3pU** or 10 µM **pro-N6pA**. The HeLa cells were washed with PBS and the respective bacteria-compound mix in DMEM was added to the plates. The cells were now incubated for 90 min at 37 °C, 5% CO₂. The cells were harvested and further processed as described in the *in situ* labelling without infection.

5.1.7. *In Vitro* UMPylation/AMPylation assay

The *in vitro* UMPylation/AMPylation assay with recombinant VopS was performed as described previously²²⁴ with some minor changes. Purified VopS (AA 31-378, 1 μ M) was incubated with a mix of 100 μ M ATP and 100 μ M UTP and the known AMPylation target Cdc42 (AA 1-188, 25 μ M) in assay buffer (20 mM Hepes, pH 7.5, 100 mM NaCl, 5 mM MgCl₂, 0.1 mg/mL BSA, 1 mM DTT) for 90 min at 30 °C. The samples were analyzed by intact protein MS (IPMS) as described previously²²⁴.

5.1.8. Mass Spectrometry Analysis of Proteomics Samples

Peptide Samples were analyzed on an UltiMate 3000 nano HPLC system (Dionex) equipped with an Acclaim C18 PepMap100 (75 μ m ID \times 2 cm) trap column and a 25 cm Aurora Series emitter column (25 cm \times 75 μ m ID, 1.6 μ m FSC C18) (Ionoptics) separation column (column oven heated to 40 °C) coupled to an Q Exactive Plus Instrument (Thermo Fisher). For peptide separation, samples were loaded on the trap column and washed for 10 min with 0.1% TFA in ddH₂O at a flow rate of 5 μ L/min. Subsequently, peptides were transferred to the analytical column for peptide separation and separated using the following 132 min gradient (Buffer A: H₂O + 0.1% FA; B: MeCN + 0.1% FA) with a flow rate of 300 nL/min.: in 7 min to 5% B, in 105 min from 5% to 22%, in 10 min from 22 to 35% and in another 10 min to 90% B. Separation gradient was followed by a column washing step using 90% B for 10 min and subsequent column re-equilibration with 5% B for 5 min. Peptides were ionized at a capillary temperature of 275 °C and the instrument was operated in a Top12 data dependent mode. For full scan acquisition, the orbitrap mass analyzer was set to a resolution of R = 140000, an automatic gain control (AGC) target of 3e6, and a maximal injection time of 80 ms in a scan range of 300-1500 m/z. Precursors having a charge state of >1, a minimum AGC target of 1e3 and intensities higher than 1e4 were selected for fragmentation. Peptide fragments were generated by HCD (higher-energy collisional dissociation) with a normalized collision energy of 27 % and recorded in the orbitrap at a resolution of R = 17500. Moreover, the AGC target was set to 1e5 with a maximum injection time of 100 ms scan range. Dynamic exclusion duration was set to 60 s and isolation was performed in the quadrupole using a window of 1.6 m/z.

5.1.9. Data analysis

MS raw data was analyzed using MaxQuant¹⁶¹ software (version 2.0.3.0) and peptides were searched against Uniprot database for Homo sapiens (taxon identifier: 9606, downloaded on 14.03.2022, canonical, reviewed). For infection assays, all proteins in the UniProt database of

the *Vibrio parahaemolyticus* serotype O3:K6, strain RIMD 2210633, taxon identifier: 223926, canonical version, reviewed and unreviewed proteomes were added to the MaxQuant contaminants file. Carbamidomethylation of cysteines was set as fixed modification and oxidation of methionines and acetylation of N-termini were set as variable modifications. Trypsin was set as proteolytic enzyme with a maximum of 2 missed cleavages. For main search, precursor mass tolerance was set to 4.5 ppm and fragment mass tolerance to 0.5 Da. Label free quantification (LFQ) mode was activated with a LFQ minimum ratio count of 1. Second peptide identification was enabled, and false discovery rate (FDR) determination carried out by applying a decoy database and thresholds were set to 1% FDR at peptide-spectrum match and at protein levels and “match between runs” (0.7 min match and 20 min alignment time windows) option was enabled. Normalized LFQ intensities extracted from the MaxQuant result table proteinGroups.txt were further analyzed with Perseus¹⁶² software (version 2.03.1). Prior to analysis, putative contaminants, reverse hits and only identified by site hits were removed. Normalized LFQ intensities were log₂ transformed and proteins with at least four valid values in at least one group were used for missing value imputation from normal distribution (width 0.3, downshift 1.8, total matrix). Two-sample Students’ t-test including Benjamini-Hochberg multiple testing correction (FDR = 0.05) was performed. The protein hits in the different various comparisons are listed in the supplementary Excel File.

V. References

- (1) World Health Organisation. *AMR Priority List*. <https://www.who.int/news-room/fact-sheets/detail/antimicrobial-resistance> (accessed 2023-12-18).
- (2) Murray, C. J.; Ikuta, K. S.; Sharara, F.; Swetschinski, L.; Robles Aguilar, G.; Gray, A.; Han, C.; Bisignano, C.; Rao, P.; Wool, E.; Johnson, S. C.; Browne, A. J.; Chipeta, M. G.; Fell, F.; Hackett, S.; Haines-Woodhouse, G.; Kashef Hamadani, B. H.; Kumaran, E. A. P.; McManigal, B.; Agarwal, R.; Akech, S.; Albertson, S.; Amuasi, J.; Andrews, J.; Aravkin, A.; Ashley, E.; Bailey, F.; Baker, S.; Basnyat, B.; Bekker, A.; Bender, R.; Bethou, A.; Bielicki, J.; Boonkasidecha, S.; Bukosia, J.; Carvalheiro, C.; Castañeda-Orjuela, C.; Chansamouth, V.; Chaurasia, S.; Chiurchiù, S.; Chowdhury, F.; Cook, A. J.; Cooper, B.; Cressey, T. R.; Criollo-Mora, E.; Cunningham, M.; Darboe, S.; Day, N. P. J.; De Luca, M.; Dokova, K.; Dramowski, A.; Dunachie, S. J.; Eckmanns, T.; Eibach, D.; Emami, A.; Feasey, N.; Fisher-Pearson, N.; Forrest, K.; Garrett, D.; Gastmeier, P.; Giref, A. Z.; Greer, R. C.; Gupta, V.; Haller, S.; Haselbeck, A.; Hay, S. I.; Holm, M.; Hopkins, S.; Iregbu, K. C.; Jacobs, J.; Jarovsky, D.; Javanmardi, F.; Khorana, M.; Kissoon, N.; Kobeissi, E.; Kostyanov, T.; Krapp, F.; Krumkamp, R.; Kumar, A.; Kyu, H. H.; Lim, C.; Limmathurotsakul, D.; Loftus, M. J.; Lunn, M.; Ma, J.; Mturi, N.; Munera-Huertas, T.; Musicha, P.; Mussi-Pinhata, M. M.; Nakamura, T.; Nanavati, R.; Nangia, S.; Newton, P.; Ngoun, C.; Novotney, A.; Nwakanma, D.; Obiero, C. W.; Olivás-Martínez, A.; Olliaro, P.; Ooko, E.; Ortiz-Brizuela, E.; Peleg, A. Y.; Perrone, C.; Plakkal, N.; Ponce-de-Leon, A.; Raad, M.; Ramdin, T.; Riddell, A.; Roberts, T.; Robotham, J. V.; Roca, A.; Rudd, K. E.; Russell, N.; Schnall, J.; Scott, J. A. G.; Shivamallappa, M.; Sifuentes-Osornio, J.; Steenkeste, N.; Stewardson, A. J.; Stoeva, T.; Tasak, N.; Thaiprakong, A.; Thwaites, G.; Turner, C.; Turner, P.; van Doorn, H. R.; Velaphi, S.; Vongpradith, A.; Vu, H.; Walsh, T.; Waner, S.; Wangrangsimakul, T.; Wozniak, T.; Zheng, P.; Sartorius, B.; Lopez, A. D.; Stergachis, A.; Moore, C.; Dolecek, C.; Naghavi, M. Global Burden of Bacterial Antimicrobial Resistance in 2019: A Systematic Analysis. *Lancet* **2022**, 399 (10325), 629–655. [https://doi.org/10.1016/S0140-6736\(21\)02724-0](https://doi.org/10.1016/S0140-6736(21)02724-0).
- (3) O’Neill, J. Tackling Drug-Resistance Infections Globally: Final Report and Recommendations. The Review on Antimicrobial Resistance Chaired by Jim O’Neill. [Online **2016**, No. May, 1–84.
- (4) O’Neill, J. Antimicrobial Resistance: Tackling a Crisis for the Health and Wealth of Nations. *Rev. Antimicrob. Resist.* **2016**, No. December, 1–16.

V – References

- (5) Center for Disease Control. *2019 Antibiotic Resistance Threats Report* | CDC. <https://www.cdc.gov/drugresistance/biggest-threats.html> (accessed 2023-12-18).
- (6) World Health Organisation. *WHO publishes list of bacteria for which new antibiotics are urgently needed*. <https://www.who.int/news/item/27-02-2017-who-publishes-list-of-bacteria-for-which-new-antibiotics-are-urgently-needed> (accessed 2023-12-18).
- (7) Fleming, A. On the Antibacterial Action of Cultures of a Penicillium, with Special Reference to Their Use in the Isolation of B. Influenzæ. *Br. J. Exp. Pathol.* **1929**, *10* (3), 226–236.
- (8) Neu, H. C.; Gootz, T. D. Antimicrobial Chemotherapy. *Med. Microbiol.* **1996**.
- (9) Ur Rahman, S.; Ali, T.; Ali, I.; Khan, N. A.; Han, B.; Gao, J. The Growing Genetic and Functional Diversity of Extended Spectrum Beta-Lactamases. *Biomed Res. Int.* **2018**, *2018*. <https://doi.org/10.1155/2018/9519718>.
- (10) Jerala, R. Synthetic Lipopeptides: A Novel Class of Anti-Infectives. *Expert Opin. Investig. Drugs* **2007**, *16* (8), 1159–1169. <https://doi.org/10.1517/13543784.16.8.1159>.
- (11) Barros, E. M.; Martin, M. J.; Selleck, E. M.; Lebreton, F.; Sampaio, J. L. M.; Gilmore, M. S. Daptomycin Resistance and Tolerance Due to Loss of Function in Staphylococcus Aureus Dsp1 and Asp23. *Antimicrob. Agents Chemother.* **2019**, *63* (1). <https://doi.org/10.1128/AAC.01542-18/ASSET/B37B40F9-D222-4D28-BDA6-788C253C49F6/ASSETS/GRAPHIC/AAC.01542-18-F0006.JPEG>.
- (12) Sköld, O. Sulfonamide Resistance: Mechanisms and Trends. *Drug Resist. Updat.* **2000**, *3* (3), 155–160. <https://doi.org/10.1054/DRUP.2000.0146>.
- (13) Correia, S.; Poeta, P.; Hébraud, M.; Capelo, J. L.; Igrejas, G. Mechanisms of Quinolone Action and Resistance: Where Do We Stand? *J. Med. Microbiol.* **2017**, *66* (5), 551–559. <https://doi.org/10.1099/JMM.0.000475/CITE/REFWORKS>.
- (14) Bordeleau, E.; Stogios, P. J.; Evdokimova, E.; Koteva, K.; Savchenko, A.; Wright, G. D. ApmA Is a Unique Aminoglycoside Antibiotic Acetyltransferase That Inactivates Apramycin. *MBio* **2021**, *12* (1), 1–11. https://doi.org/10.1128/MBIO.02705-20/SUPPL_FILE/MBIO.02705-20-SF008.PDF.
- (15) Darby, E. M.; Trampari, E.; Siasat, P.; Gaya, M. S.; Alav, I.; Webber, M. A.; Blair, J. M. A. Molecular Mechanisms of Antibiotic Resistance Revisited. *Nat. Rev. Microbiol.* **2022**, *21* (5), 280–295. <https://doi.org/10.1038/s41579-022-00820-y>.
- (16) Lee Ventola, C. The Antibiotic Resistance Crisis Part 1: Causes and Threats. **2015**, *40* (4).

V – References

- (17) Bartlett, J. G.; Gilbert, D. N.; Spellberg, B. Seven Ways to Preserve the Miracle of Antibiotics. **2013**. <https://doi.org/10.1093/cid/cit070>.
- (18) The Antibiotic Alarm. *Nature*. Nature Publishing Group March 12, 2013, p 141. <https://doi.org/10.1038/495141a>.
- (19) *EUR-Lex - 32023H0622(01) - EN - EUR-Lex*. [https://eur-lex.europa.eu/legal-content/EN/TXT/?uri=CELEX:32023H0622\(01\)](https://eur-lex.europa.eu/legal-content/EN/TXT/?uri=CELEX:32023H0622(01)) (accessed 2023-12-19).
- (20) Klein, E. Y.; Van Boeckel, T. P.; Martinez, E. M.; Pant, S.; Gandra, S.; Levin, S. A.; Goossens, H.; Laxminarayan, R. Global Increase and Geographic Convergence in Antibiotic Consumption between 2000 and 2015. *Proc. Natl. Acad. Sci. U. S. A.* **2018**, *115* (15), E3463–E3470. https://doi.org/10.1073/PNAS.1717295115/SUPPL_FILE/PNAS.1717295115.SAPP.PDF.
- (21) Sharland, M.; Pulcini, C.; Harbarth, S.; Zeng, M.; Gandra, S.; Mathur, S.; Magrini, N. Classifying Antibiotics in the WHO Essential Medicines List for Optimal Use—Be AWaRe. *Lancet Infect. Dis.* **2018**, *18* (1), 18–20. [https://doi.org/10.1016/S1473-3099\(17\)30724-7](https://doi.org/10.1016/S1473-3099(17)30724-7).
- (22) Cook, M. A.; Wright, G. D. The Past , Present , and Future of Antibiotics. **2022**, 7793 (August).
- (23) Mullard, A. Achaogen Bankruptcy Highlights Antibacterial Development Woes. *Nat. Rev. Drug Discov.* **2019**, *18* (6), 411. <https://doi.org/10.1038/D41573-019-00085-W>.
- (24) Glover, R. E.; Singer, A. C.; Roberts, A. P.; Kirchhelle, C. The Antibiotic Subscription Model: Fostering Innovation or Repackaging Old Drugs? *The Lancet Microbe* **2023**, *4* (1), e2–e3. [https://doi.org/10.1016/S2666-5247\(22\)00235-X](https://doi.org/10.1016/S2666-5247(22)00235-X).
- (25) Mishra, A.; Surolia, A. Mycobacterium Tuberculosis: Surviving and Indulging in an Unwelcoming Host. *IUBMB Life*. Blackwell Publishing Ltd September 20, 2018, pp 917–925. <https://doi.org/10.1002/iub.1882>.
- (26) Cohen, A.; Dahl Mathiasen, V.; Schön, T.; Wejse, C. The Global Prevalence of Latent Tuberculosis: A Systematic Review and Meta-Analysis. <https://doi.org/10.1183/13993003.00655-2019>.
- (27) Bagcchi, S. WHO’s Global Tuberculosis Report 2022. *The Lancet Microbe* **2023**, *4* (1), e20. [https://doi.org/10.1016/s2666-5247\(22\)00359-7](https://doi.org/10.1016/s2666-5247(22)00359-7).
- (28) Craggs, P. D.; Pedro, L.; De Carvalho, S.; Rogers, D.; Lee, R. E. Bottlenecks and Opportunities in Antibiotic Discovery against Mycobacterium Tuberculosis. **2022**.

V – References

- <https://doi.org/10.1016/j.mib.2022.102191>.
- (29) Fernandes, G. F. S.; Thompson, A. M.; Castagnolo, D.; Denny, W. A.; Dos Santos, J. L. Tuberculosis Drug Discovery: Challenges and New Horizons. *J. Med. Chem.* **2022**, *65* (11), 7489–7531. https://doi.org/10.1021/ACS.JMEDCHEM.2C00227/ASSET/IMAGES/LARGE/JM2C00227_0016.JPEG.
- (30) Dulberger, C. L.; Rubin, E. J.; Boutte, C. C. The Mycobacterial Cell Envelope — a Moving Target. *Nat. Rev. Microbiol.* **2020**, *18* (1), 47–59. <https://doi.org/10.1038/S41579-019-0273-7>.
- (31) Liu, J.; Barry, C. E.; Besra, G. S.; Nikaido, H. Mycolic Acid Structure Determines the Fluidity of the Mycobacterial Cell Wall. *J. Biol. Chem.* **1996**, *271* (47), 29545–29551. <https://doi.org/10.1074/JBC.271.47.29545>.
- (32) Karakousis, P. C.; Bishai, W. R.; Dorman, S. E. Mycobacterium Tuberculosis Cell Envelope Lipids and the Host Immune Response. *Cell. Microbiol.* **2004**, *6* (2), 105–116. <https://doi.org/10.1046/j.1462-5822.2003.00351.x>.
- (33) Joyce, G.; Williams, K. J.; Robb, M.; Noens, E.; Tizzano, B.; Shahrezaei, V.; Robertson, B. D. Cell Division Site Placement and Asymmetric Growth in Mycobacteria. *PLoS One* **2012**, *7* (9), e44582. <https://doi.org/10.1371/JOURNAL.PONE.0044582>.
- (34) Hett, E. C.; Rubin, E. J. Bacterial Growth and Cell Division: A Mycobacterial Perspective. *Microbiol. Mol. Biol. Rev.* **2008**, *72* (1), 126–156. <https://doi.org/10.1128/MMBR.00028-07/ASSET/16F75C19-D1BA-4EAA-B38C-07C6160F1053/ASSETS/GRAPHIC/ZMR0010821750005.JPEG>.
- (35) Lendeckel, U.; Venz, S.; Wolke, C. Macrophages: Shapes and Functions. *Chemtexts* **2022**, *8* (2), 12. <https://doi.org/10.1007/S40828-022-00163-4>.
- (36) Awuh, J. A.; Trude, •; Flo, H. Molecular Basis of Mycobacterial Survival in Macrophages. <https://doi.org/10.1007/s00018-016-2422-8>.
- (37) de Chastellier, C.; Forquet, F.; Gordon, A.; Thilo, L. Mycobacterium Requires an All-around Closely Apposing Phagosome Membrane to Maintain the Maturation Block and This Apposition Is Re-Established When It Rescues Itself from Phagolysosomes. *Cell. Microbiol.* **2009**, *11* (8), 1190–1207. <https://doi.org/10.1111/J.1462-5822.2009.01324.X>.
- (38) Madacki, J.; Laval, F.; Grzegorzewicz, A.; Lemassu, A.; Záhorszská, M.; Arand, M.; Mcneil, M.; Daffé, M.; Jackson, M.; Lanéelle, M.-A.; Korduláková, J. Impact of the Epoxide Hydrolase EphD on the Metabolism of Mycolic Acids in Mycobacteria. *J. Biol.*

V – References

- Chem.* **2018**, 293, 5172–5184. <https://doi.org/10.1074/jbc.RA117.000246>.
- (39) World Health Organisation. WHO Consolidated Guidelines on Tuberculosis Module 4: Treatment Drug-Resistant Tuberculosis Treatment. **2020**.
- (40) Dhameliya, T. M.; Vekariya, D. D.; Patel, H. Y.; Patel, J. T. Comprehensive Coverage on Anti-Mycobacterial Endeavour Reported during 2022. *Eur. J. Med. Chem.* **2023**, 255 (April), 115409. <https://doi.org/10.1016/j.ejmech.2023.115409>.
- (41) Dahl, V. N.; Tiberi, S.; Goletti, D.; Wejse, C. Armed Conflict and Human Displacement May Lead to an Increase in the Burden of Tuberculosis in Europe. *Int. J. Infect. Dis.* **2022**, 124, S104–S106. <https://doi.org/10.1016/j.ijid.2022.03.040>.
- (42) Ponomarenko, E. A.; Poverennaya, E. V.; Ilgisonis, E. V.; Pyatnitskiy, M. A.; Kopylov, A. T.; Zgoda, V. G.; Lisitsa, A. V.; Archakov, A. I. The Size of the Human Proteome: The Width and Depth. *Int. J. Anal. Chem.* **2016**, 2016. <https://doi.org/10.1155/2016/7436849>.
- (43) Prabakaran, S.; Lippens, G.; Steen, H.; Gunawardena, J. Post-Translational Modification: Nature's Escape from Genetic Imprisonment and the Basis for Dynamic Information Encoding. *Wiley Interdiscip. Rev. Syst. Biol. Med.* **2012**, 4 (6), 565–583. <https://doi.org/10.1002/WSBM.1185>.
- (44) Walsh, C. T.; Garneau-Tsodikova, S.; Gatto, G. J. Protein Posttranslational Modifications: The Chemistry of Proteome Diversifications. *Angewandte Chemie - International Edition*. John Wiley & Sons, Ltd November 18, 2005, pp 7342–7372. <https://doi.org/10.1002/anie.200501023>.
- (45) Walsh, C. Posttranslational Modification of Proteins : Expanding Nature's Inventory. **2006**, 490.
- (46) Duong-Ly, K. C.; Peterson, J. R. The Human Kinome and Kinase Inhibition. *Curr. Protoc. Pharmacol.* **2013**, 60 (1), 2.9.1-2.9.14. <https://doi.org/10.1002/0471141755.PH0209S60>.
- (47) Oppermann, F. S.; Gnad, F.; Olsen, J. V.; Hornberger, R.; Greff, Z.; Kéri, G.; Mann, M.; Daub, H. Large-Scale Proteomics Analysis of the Human Kinome. *Mol. Cell. Proteomics* **2009**, 8 (7), 1751–1764. <https://doi.org/10.1074/mcp.M800588-MCP200>.
- (48) Eglen, R. M.; Reisine, T. The Current Status of Drug Discovery Against the Human Kinome. <https://home.liebertpub.com/adt> **2009**, 7 (1), 22–43. <https://doi.org/10.1089/ADT.2008.164>.
- (49) Ribet, D.; Cossart, P. Post-translational Modifications in Host Cells during Bacterial

V – References

- Infection. *FEBS Lett.* **2010**, *584* (13), 2748–2758. <https://doi.org/10.1016/j.febslet.2010.05.012>.
- (50) Ribet, D.; Cossart, P. Pathogen-Mediated Posttranslational Modifications: A Re-Emerging Field. *Cell.* 2010, pp 694–702. <https://doi.org/10.1016/j.cell.2010.11.019>.
- (51) Collier, R. J.; Cole, H. A. Diphtheria Toxin Submit Active in Vitro. *Science (80-.)*. **1969**, *164* (3884), 1179–1182. <https://doi.org/10.1126/SCIENCE.164.3884.1179>.
- (52) Chambers, K. A.; Scheck, R. A. Bacterial Virulence Mediated by Orthogonal Post-Translational Modification. *Nat. Chem. Biol.* **2020**, *16* (10), 1043–1051. <https://doi.org/10.1038/S41589-020-0638-2>.
- (53) Buchrieser, C.; Glaser, P.; Rusniok, C.; Nedjari, H.; D’Hauteville, H.; Kunst, F.; Sansonetti, P.; Parsot, C. The Virulence Plasmid PWR100 and the Repertoire of Proteins Secreted by the Type III Secretion Apparatus of Shigella Flexneri. *Mol. Microbiol.* **2000**, *38* (4), 760–771. <https://doi.org/10.1046/J.1365-2958.2000.02179.X>.
- (54) Hubber, A.; Roy, C. R. Modulation of Host Cell Function by Legionella Pneumophila Type IV Effectors. <https://doi.org/10.1146/annurev-cellbio-100109-104034> **2010**, *26*, 261–283. <https://doi.org/10.1146/ANNUREV-CELLBIO-100109-104034>.
- (55) Mukherjee, S.; Keitany, G.; Li, Y.; Wang, Y.; Ball, H. L.; Goldsmith, E. J.; Orth, K. Yersinia YopJ Acetylates and Inhibits Kinase Activation by Blocking Phosphorylation. *Science* **2006**, *312* (5777), 1211–1214. <https://doi.org/10.1126/SCIENCE.1126867>.
- (56) Mittal, R.; Peak-Chew, S. Y.; McMahon, H. T. Acetylation of MEK2 and I Kappa B Kinase (IKK) Activation Loop Residues by YopJ Inhibits Signaling. *Proc. Natl. Acad. Sci. U. S. A.* **2006**, *103* (49), 18574–18579. <https://doi.org/10.1073/PNAS.0608995103>.
- (57) Wang, J.; Li, B. X.; Ge, P. P.; Li, J.; Wang, Q.; Gao, G. F.; Qiu, X. B.; Liu, C. H. Mycobacterium Tuberculosis Suppresses Innate Immunity by Coopting the Host Ubiquitin System. *Nat. Immunol.* **2015**, *16* (3), 237–245. <https://doi.org/10.1038/NI.3096>.
- (58) Wang, J.; Ge, P.; Qiang, L.; Tian, F.; Zhao, D.; Chai, Q.; Zhu, M.; Zhou, R.; Meng, G.; Iwakura, Y.; Gao, G. F.; Liu, C. H. The Mycobacterial Phosphatase PtpA Regulates the Expression of Host Genes and Promotes Cell Proliferation. *Nat. Commun.* **2017**, *8* (1), 1–16. <https://doi.org/10.1038/s41467-017-00279-z>.
- (59) Qiang, L.; Zhang, Y.; Liu, C. H. Mycobacterium Tuberculosis Effector Proteins: Functional Multiplicity and Regulatory Diversity. *Cell. Mol. Immunol.* **2021**, *18* (5), 1343–1344. <https://doi.org/10.1038/s41423-021-00676-x>.

V – References

- (60) Aebersold, R.; Agar, J. N.; Amster, I. J.; Baker, M. S.; Bertozzi, C. R.; Boja, E. S.; Costello, C. E.; Cravatt, B. F.; Fenselau, C.; Garcia, B. A.; Ge, Y.; Gunawardena, J.; Hendrickson, R. C.; Hergenrother, P. J.; Huber, C. G.; Ivanov, A. R.; Jensen, O. N.; Jewett, M. C.; Kelleher, N. L.; Kiessling, L. L.; Krogan, N. J.; Larsen, M. R.; Loo, J. A.; Ogorzalek Loo, R. R.; Lundberg, E.; Maccoss, M. J.; Mallick, P.; Mootha, V. K.; Mrksich, M.; Muir, T. W.; Patrie, S. M.; Pesavento, J. J.; Pitteri, S. J.; Rodriguez, H.; Saghatelian, A.; Sandoval, W.; Schlüter, H.; Sechi, S.; Slavoff, S. A.; Smith, L. M.; Snyder, M. P.; Thomas, P. M.; Uhlén, M.; Van Eyk, J. E.; Vidal, M.; Walt, D. R.; White, F. M.; Williams, E. R.; Wohlschläger, T.; Wysocki, V. H.; Yates, N. A.; Young, N. L.; Zhang, B. How Many Human Proteoforms Are There? *Nat. Chem. Biol.* **2018**, *14* (3), 206–214. <https://doi.org/10.1038/nchembio.2576>.
- (61) Aken, B. L.; Achuthan, P.; Akanni, W.; Amode, M. R.; Bernsdorff, F.; Bhai, J.; Billis, K.; Carvalho-Silva, D.; Cummins, C.; Clapham, P.; Gil, L.; Girón, C. G.; Gordon, L.; Hourlier, T.; Hunt, S. E.; Janacek, S. H.; Juettemann, T.; Keenan, S.; Laird, M. R.; Lavidas, I.; Maurel, T.; McLaren, W.; Moore, B.; Murphy, D. N.; Nag, R.; Newman, V.; Nuhn, M.; Ong, C. K.; Parker, A.; Patricio, M.; Riat, H. S.; Sheppard, D.; Sparrow, H.; Taylor, K.; Thormann, A.; Vullo, A.; Walts, B.; Wilder, S. P.; Zadissa, A.; Kostadima, M.; Martin, F. J.; Muffato, M.; Perry, E.; Ruffier, M.; Staines, D. M.; Trevanion, S. J.; Cunningham, F.; Yates, A.; Zerbino, D. R.; Flicek, P. Ensembl 2017. *Nucleic Acids Res.* **2017**, *45* (D1), D635–D642. <https://doi.org/10.1093/NAR/GKW1104>.
- (62) Overington, J. P.; Al-Lazikani, B.; Hopkins, A. L. How Many Drug Targets Are There? *Nat. Rev. Drug Discov.* **2006**, *5* (12), 993–996. <https://doi.org/10.1038/nrd2199>.
- (63) Meissner, F.; Geddes-McAlister, J.; Mann, M.; Bantscheff, M. The Emerging Role of Mass Spectrometry-Based Proteomics in Drug Discovery. *Nat. Rev. Drug Discov.* **2022**, *21* (9), 637–654. <https://doi.org/10.1038/s41573-022-00409-3>.
- (64) Abele, M.; Doll, E.; Bayer, F. P.; Meng, C.; Lomp, N.; Neuhaus, K.; Scherer, S.; Kuster, B.; Ludwig, C. Unified Workflow for the Rapid and In-Depth Characterization of Bacterial Proteomes. *Mol. Cell. Proteomics* **2023**, *22* (8), 100612. <https://doi.org/10.1016/j.mcpro.2023.100612>.
- (65) Dupree, E. J.; Jayathirtha, M.; Yorkey, H.; Mihasan, M.; Petre, B. A.; Darie, C. C. A Critical Review of Bottom-Up Proteomics: The Good, the Bad, and the Future of This Field. *Proteomes* **2020**, *Vol. 8, Page 14* **2020**, *8* (3), 14. <https://doi.org/10.3390/PROTEOMES8030014>.
- (66) Le, P.; Kunold, E.; Macsics, R.; Rox, K.; Jennings, M. C.; Ugur, I.; Reinecke, M.; Chaves-

V – References

- Moreno, D.; Hackl, M. W.; Fetzer, C.; Mandl, F. A. M.; Lehmann, J.; Korotkov, V. S.; Hacker, S. M.; Kuster, B.; Antes, I.; Pieper, D. H.; Rohde, M.; Wuest, W. M.; Medina, E.; Sieber, S. A. Repurposing Human Kinase Inhibitors to Create an Antibiotic Active against Drug-Resistant *Staphylococcus Aureus*, Persisters and Biofilms. *Nat. Chem.* **2020**, *12* (2), 145–158. <https://doi.org/10.1038/s41557-019-0378-7>.
- (67) Doellinger, J.; Schneider, A.; Hoeller, M.; Lasch, P. Sample Preparation by Easy Extraction and Digestion (SPEED) - A Universal, Rapid, and Detergent-Free Protocol for Proteomics Based on Acid Extraction. *Mol. Cell. Proteomics* **2020**, *19* (1), 209–222. <https://doi.org/10.1074/mcp.TIR119.001616>.
- (68) Wiśniewski, J. R.; Zougman, A.; Nagaraj, N.; Mann, M. Universal Sample Preparation Method for Proteome Analysis. *Nat. Methods* **2009**, *6* (5), 359–362. <https://doi.org/10.1038/nmeth.1322>.
- (69) Kulak, N. A.; Pichler, G.; Paron, I.; Nagaraj, N.; Mann, M. Minimal, Encapsulated Proteomic-Sample Processing Applied to Copy-Number Estimation in Eukaryotic Cells. *Nat. Methods* **2014**, *11* (3), 319–324. <https://doi.org/10.1038/nmeth.2834>.
- (70) Moggridge, S.; Sorensen, P. H.; Morin, G. B.; Hughes, C. S. Extending the Compatibility of the SP3 Paramagnetic Bead Processing Approach for Proteomics. *J. Proteome Res.* **2018**, *17* (4), 1730–1740. <https://doi.org/10.1021/acs.jproteome.7b00913>.
- (71) Hughes, C. S.; Moggridge, S.; Müller, T.; Sorensen, P. H.; Morin, G. B.; Krijgsveld, J. Single-Pot, Solid-Phase-Enhanced Sample Preparation for Proteomics Experiments. *Nat. Protoc.* **2019**, *14* (1), 68–85. <https://doi.org/10.1038/s41596-018-0082-x>.
- (72) Sielaff, M.; Kuharev, J.; Bohn, T.; Hahlbrock, J.; Bopp, T.; Tenzer, S.; Distler, U. Evaluation of FASP, SP3, and IST Protocols for Proteomic Sample Preparation in the Low Microgram Range. *J. Proteome Res.* **2017**, *16* (11), 4060–4072. <https://doi.org/10.1021/acs.jproteome.7b00433>.
- (73) Müller, T.; Kalxdorf, M.; Longuespée, R.; Kazdal, D. N.; Stenzinger, A.; Krijgsveld, J. Automated Sample Preparation with SP 3 for Low-input Clinical Proteomics. *Mol. Syst. Biol.* **2020**, *16* (1), 9111. https://doi.org/10.15252/MSB.20199111/SUPPL_FILE/MSB199111-SUP-0007-SDATATABLES1-2.ZIP.
- (74) Link, A. J.; Eng, J.; Schieltz, D. M.; Carmack, E.; Mize, G. J.; Morris, D. R.; Garvik, B. M.; Yates, J. R. Direct Analysis of Protein Complexes Using Mass Spectrometry. *Nat. Biotechnol.* **1999**, *17* (7), 676–682. <https://doi.org/10.1038/10890>.

V – References

- (75) El-Faramawy, A.; Siu, K. W. M.; Thomson, B. A. Efficiency of Nano-Electrospray Ionization. *J. Am. Soc. Mass Spectrom.* **2005**, *16* (10), 1702–1707. <https://doi.org/10.1016/J.JASMS.2005.06.011/METRICS>.
- (76) Juraschek, R.; Dülcks, T.; Karas, M. Nanoelectrospray - More than Just a Minimized-Flow Electrospray Ionization Source. *J. Am. Soc. Mass Spectrom.* **1999**, *10* (4), 300–308. [https://doi.org/10.1016/S1044-0305\(98\)00157-3/METRICS](https://doi.org/10.1016/S1044-0305(98)00157-3/METRICS).
- (77) Bian, Y.; Zheng, R.; Bayer, F. P.; Wong, C.; Chang, Y. C.; Meng, C.; Zolg, D. P.; Reinecke, M.; Zecha, J.; Wiechmann, S.; Heinzlmeir, S.; Scherr, J.; Hemmer, B.; Baynham, M.; Gingras, A. C.; Boychenko, O.; Kuster, B. Robust, Reproducible and Quantitative Analysis of Thousands of Proteomes by Micro-Flow LC–MS/MS. *Nat. Commun.* **2020**, *11* (1), 1–12. <https://doi.org/10.1038/s41467-019-13973-x>.
- (78) Makarov, A. Electrostatic Axially Harmonic Orbital Trapping: A High-Performance Technique of Mass Analysis. *Anal. Chem.* **2000**, *72* (6), 1156–1162. <https://doi.org/10.1021/AC991131P>.
- (79) Scigelova, M.; Makarov, A. Orbitrap Mass Analyzer – Overview and Applications in Proteomics. *Proteomics* **2006**, *6* (S2), 16–21. <https://doi.org/10.1002/PMIC.200600528>.
- (80) Michalski, A.; Damoc, E.; Hauschild, J. P.; Lange, O.; Wieghaus, A.; Makarov, A.; Nagaraj, N.; Cox, J.; Mann, M.; Horning, S. Mass Spectrometry-Based Proteomics Using Q Exactive, a High-Performance Benchtop Quadrupole Orbitrap Mass Spectrometer. *Mol. Cell. Proteomics* **2011**, *10* (9), M111.011015. <https://doi.org/10.1074/mcp.M111.011015>.
- (81) Senko, M. W.; Remes, P. M.; Canterbury, J. D.; Mathur, R.; Song, Q.; Eliuk, S. M.; Mullen, C.; Earley, L.; Hardman, M.; Blethrow, J. D.; Bui, H.; Specht, A.; Lange, O.; Denisov, E.; Makarov, A.; Horning, S.; Zabrouskov, V. Novel Parallelized Quadrupole/Linear Ion Trap/Orbitrap Tribid Mass Spectrometer Improving Proteome Coverage and Peptide Identification Rates. *Anal. Chem.* **2013**, *85* (24), 11710–11714. <https://doi.org/10.1021/ac403115c>.
- (82) Heil, L. R.; Damoc, E.; Arrey, T. N.; Pashkova, A.; Denisov, E.; Petzoldt, J.; Peterson, A. C.; Hsu, C.; Searle, B. C.; Shulman, N.; Riffle, M.; Connolly, B.; Maclean, B. X.; Remes, P. M.; Senko, M. W.; Stewart, H. I.; Hock, C.; Makarov, A. A.; Hermanson, D.; Zabrouskov, V.; Wu, C. C.; Maccoss, M. J. Evaluating the Performance of the Astral Mass Analyzer for Quantitative Proteomics Using Data-Independent Acquisition. **2023**. <https://doi.org/10.1021/acs.jproteome.3c00357>.
- (83) Meier, F.; Beck, S.; Grassl, N.; Lubeck, M.; Park, M. A.; Raether, O.; Mann, M. Parallel

V – References

- Accumulation-Serial Fragmentation (PASEF): Multiplying Sequencing Speed and Sensitivity by Synchronized Scans in a Trapped Ion Mobility Device. *J. Proteome Res.* **2015**, *14* (12), 5378–5387. https://doi.org/10.1021/ACS.JPROTEOME.5B00932/ASSET/IMAGES/LARGE/PR-2015-00932K_0003.JPEG.
- (84) Vasilopoulou, C. G.; Sulek, K.; Brunner, A. D.; Meitei, N. S.; Schweiger-Hufnagel, U.; Meyer, S. W.; Barsch, A.; Mann, M.; Meier, F. Trapped Ion Mobility Spectrometry and PASEF Enable In-Depth Lipidomics from Minimal Sample Amounts. *Nat. Commun.* **2020**, *11* (1), 1–11. <https://doi.org/10.1038/s41467-019-14044-x>.
- (85) Krasny, L.; Huang, P. H. Data-Independent Acquisition Mass Spectrometry (DIA-MS) for Proteomic Applications in Oncology. *Mol. Omi.* **2021**, *17* (1), 29–42. <https://doi.org/10.1039/d0mo00072h>.
- (86) Ludwig, C.; Gillet, L.; Rosenberger, G.; Amon, S.; Collins, B. C.; Aebersold, R. Data-independent Acquisition-based SWATH - MS for Quantitative Proteomics: A Tutorial. *Mol. Syst. Biol.* **2018**, *14* (8), 1–23. <https://doi.org/10.15252/msb.20178126>.
- (87) Demichev, V.; Messner, C. B.; Vernardis, S. I.; Lilley, K. S.; Ralser, M. DIA-NN: Neural Networks and Interference Correction Enable Deep Proteome Coverage in High Throughput. *Nat. Methods* **2020**, *17* (1), 41–44. <https://doi.org/10.1038/s41592-019-0638-x>.
- (88) Gessulat, S.; Schmidt, T.; Zolg, D. P.; Samaras, P.; Schnatbaum, K.; Zerweck, J.; Knaute, T.; Rechenberger, J.; Delanghe, B.; Huhmer, A.; Reimer, U.; Ehrlich, H. C.; Aiche, S.; Kuster, B.; Wilhelm, M. Prosit: Proteome-Wide Prediction of Peptide Tandem Mass Spectra by Deep Learning. *Nat. Methods* **2019**, *16* (6), 509–518. <https://doi.org/10.1038/s41592-019-0426-7>.
- (89) Ong, S. E.; Blagoev, B.; Kratchmarova, I.; Kristensen, D. B.; Steen, H.; Pandey, A.; Mann, M. Stable Isotope Labeling by Amino Acids in Cell Culture, SILAC, as a Simple and Accurate Approach to Expression Proteomics. *Mol. Cell. Proteomics* **2002**, *1* (5), 376–386. <https://doi.org/10.1074/MCP.M200025-MCP200>.
- (90) Bantscheff, M.; Schirle, M.; Sweetman, G.; Rick, J.; Kuster, B. Quantitative Mass Spectrometry in Proteomics: A Critical Review. *Anal. Bioanal. Chem.* **2007**, *389* (4), 1017–1031. <https://doi.org/10.1007/S00216-007-1486-6>.
- (91) Rauniyar, N.; Yates, J. R. Isobaric Labeling-Based Relative Quantification in Shotgun Proteomics. *J. Proteome Res.* **2014**, *13* (12), 5293–5309. <https://doi.org/10.1021/PR500880B/ASSET/IMAGES/LARGE/PR-2014->

V – References

00880B_0008.JPEG.

- (92) Dayon, L.; Sonderegger, B.; Kussmann, M. Combination of Gas-Phase Fractionation and MS3 Acquisition Modes for Relative Protein Quantification with Isobaric Tagging. *J. Proteome Res.* **2012**, *11* (10), 5081–5089. https://doi.org/10.1021/PR300519C/SUPPL_FILE/PR300519C_SI_001.PDF.
- (93) Li, J.; Van Vranken, J. G.; Pontano Vaites, L.; Schweppe, D. K.; Huttlin, E. L.; Etienne, C.; Nandhikonda, P.; Viner, R.; Robitaille, A. M.; Thompson, A. H.; Kuhn, K.; Pike, I.; Bomgardner, R. D.; Rogers, J. C.; Gygi, S. P.; Paulo, J. A. TMTpro Reagents: A Set of Isobaric Labeling Mass Tags Enables Simultaneous Proteome-Wide Measurements across 16 Samples. *Nat. Methods* **2020**, *17* (4), 399–404. <https://doi.org/10.1038/s41592-020-0781-4>.
- (94) Cox, J.; Hein, M. Y.; Lubner, C. A.; Paron, I.; Nagaraj, N.; Mann, M. Accurate Proteome-Wide Label-Free Quantification by Delayed Normalization and Maximal Peptide Ratio Extraction, Termed MaxLFQ. *Mol. Cell. Proteomics* **2014**, *13* (9), 2513–2526. <https://doi.org/10.1074/mcp.M113.031591>.
- (95) Bader, J. M.; Albrecht, V.; Mann, M. MS-Based Proteomics of Body Fluids: The End of the Beginning. *Mol. Cell. Proteomics* **2023**, *22* (7), 100577. <https://doi.org/10.1016/J.MCPRO.2023.100577>.
- (96) Kitata, R. B.; Yang, J. C.; Chen, Y. J. Advances in Data-Independent Acquisition Mass Spectrometry towards Comprehensive Digital Proteome Landscape. *Mass Spectrom. Rev.* **2023**, *42* (6), 2324–2348. <https://doi.org/10.1002/MAS.21781>.
- (97) Li, M.; Patel, H. V.; Cognetta, A. B.; Smith, T. C.; Mallick, I.; Cavalier, J.-F.; Previti, M. L.; Canaan, S.; Aldridge, B. B.; Cravatt, B. F.; Seeliger, J. C. Identification of Cell Wall Synthesis Inhibitors Active against Mycobacterium Tuberculosis by Competitive Activity-Based Protein Profiling. *Cell Chem. Biol.* **2021**, 1–14. <https://doi.org/10.1016/j.chembiol.2021.09.002>.
- (98) Moffat, J. G.; Vincent, F.; Lee, J. A.; Eder, J.; Prunotto, M. Opportunities and Challenges in Phenotypic Drug Discovery: An Industry Perspective. *Nat. Rev. Drug Discov.* **2017**, *16* (8), 531–543. <https://doi.org/10.1038/nrd.2017.111>.
- (99) Kubota, K.; Funabashi, M.; Ogura, Y. Target Deconvolution from Phenotype-Based Drug Discovery by Using Chemical Proteomics Approaches. *Biochim. Biophys. Acta - Proteins Proteomics* **2019**, *1867* (1), 22–27. <https://doi.org/10.1016/j.bbapap.2018.08.002>.

V – References

- (100) Evans, M. J.; Cravatt, B. F. Mechanism-Based Profiling of Enzyme Families. *Chemical Reviews*. American Chemical Society August 2006, pp 3279–3301. <https://doi.org/10.1021/cr050288g>.
- (101) Fonović, M.; Bogyo, M. Activity-Based Probes as a Tool for Functional Proteomic Analysis of Proteases. *Expert Rev. Proteomics* **2008**, 5 (5), 721–730. <https://doi.org/10.1586/14789450.5.5.721>.
- (102) Barglow, K. T.; Cravatt, B. F. Activity-Based Protein Profiling for the Functional Annotation of Enzymes. *Nat. Methods* **2007**, 4 (10), 822–827. <https://doi.org/10.1038/nmeth1092>.
- (103) Wu, P.; Bertozzi, C. R.; Meldal, M.; Barry, K. The Nobel Prize in Chemistry 2022: Fulfilling Demanding Applications with Simple Reactions. *Cite This ACS Chem. Biol* **2022**, 2022. <https://doi.org/10.1021/acscchembio.2c00788>.
- (104) Becker, T.; Wiest, A.; Telek, A.; Bejko, D.; Hoffmann-Röder, A.; Kielkowski, P. Transforming Chemical Proteomics Enrichment into a High-Throughput Method Using an SP2E Workflow. *JACS Au* **2022**, 2 (7), 1712–1723. <https://doi.org/10.1021/jacsau.2c00284>.
- (105) Pan, S.; Zhang, H.; Wang, C.; Yao, S. C. L.; Yao, S. Q. Target Identification of Natural Products and Bioactive Compounds Using Affinity-Based Probes. *Nat. Prod. Rep.* **2016**, 33 (5), 612–620. <https://doi.org/10.1039/C5NP00101C>.
- (106) Geurink, P. P.; Prely, L. M.; Van Der Marel, G. A.; Bischoff, R.; Overkleeft, H. S. Photoaffinity Labeling in Activity-Based Protein Profiling. *Top. Curr. Chem.* **2012**, 324, 85–113. https://doi.org/10.1007/128_2011_286/COVER.
- (107) Dubinsky, L.; Krom, B. P.; Meijler, M. M. Diazirine Based Photoaffinity Labeling. *Bioorg. Med. Chem.* **2012**, 20 (2), 554–570. <https://doi.org/10.1016/J.BMC.2011.06.066>.
- (108) Hill, J. R.; Robertson, A. A. B. Fishing for Drug Targets: A Focus on Diazirine Photoaffinity Probe Synthesis. *J. Med. Chem.* **2018**, 61 (16), 6945–6963. https://doi.org/10.1021/ACS.JMEDCHEM.7B01561/ASSET/IMAGES/LARGE/JM-2017-01561D_0008.JPEG.
- (109) Conway, L. P.; Jadhav, A. M.; Homan, R. A.; Li, W.; Rubiano, J. S.; Hawkins, R.; Lawrence, R. M.; Parker, C. G. Evaluation of Fully-Functionalized Diazirine Tags for Chemical Proteomic Applications. *Chem. Sci.* **2021**, 12 (22), 7839–7847. <https://doi.org/10.1039/D1SC01360B>.
- (110) Huynh, K.; Partch, C. L. Analysis of Protein Stability and Ligand Interactions by Thermal

V – References

- Shift Assay. *Curr. Protoc. Protein Sci.* **2015**, 79 (1), 28.9.1-28.9.14. <https://doi.org/10.1002/0471140864.PS2809S79>.
- (111) Jafari, R.; Almqvist, H.; Axelsson, H.; Ignatushchenko, M.; Lundb, T.; Martinez Molina, D. The Cellular Thermal Shift Assay for Evaluating Drug Target Interactions in Cells. *Nat. Protoc.* **2014**. <https://doi.org/10.1038/nprot.2014.138>.
- (112) Savitski, M. M.; Reinhard, F. B. M.; Franken, H.; Werner, T.; Savitski, M. F.; Eberhard, D.; Molina, D. M.; Jafari, R.; Dovega, R. B.; Klaeger, S.; Kuster, B.; Nordlund, P.; Bantscheff, M.; Drewes, G. Tracking Cancer Drugs in Living Cells by Thermal Profiling of the Proteome. *Science* (80-.). **2014**, 346 (6205), 1255784. <https://doi.org/10.1126/science.1255784>.
- (113) Franken, H.; Mathieson, T.; Childs, D.; Sweetman, G. M. A.; Werner, T.; Tögel, I.; Doce, C.; Gade, S.; Bantscheff, M.; Drewes, G.; Reinhard, F. B. M.; Huber, W.; Savitski, M. M. Thermal Proteome Profiling for Unbiased Identification of Direct and Indirect Drug Targets Using Multiplexed Quantitative Mass Spectrometry. *Nat. Protoc.* **2015**, 10 (10), 1567–1593. <https://doi.org/10.1038/nprot.2015.101>.
- (114) Ball, K. A.; Webb, K. J.; Coleman, S. J.; Cozzolino, K. A.; Jacobsen, J.; Jones, K. R.; Stowell, M. H. B.; Old, W. M. An Isothermal Shift Assay for Proteome Scale Drug-Target Identification. *Commun. Biol.* **2020**, 3 (1), 1–10. <https://doi.org/10.1038/s42003-020-0795-6>.
- (115) Kirsch, V. C.; Orgler, C.; Braig, S.; Jeremias, I.; Auerbach, D.; Müller, R.; Vollmar, A. M.; Sieber, S. A. The Cytotoxic Natural Product Vioprolide A Targets Nucleolar Protein 14, Which Is Essential for Ribosome Biogenesis. *Angew. Chemie Int. Ed.* **2020**, 59 (4), 1595–1600. <https://doi.org/10.1002/anie.201911158>.
- (116) Carnero Corrales, M. A.; Zinken, S.; Konstantinidis, G.; Rafehi, M.; Abdelrahman, A.; Wu, Y.-W.; Janning, P.; Müller, C. E.; Laraia, L.; Waldmann, H. Thermal Proteome Profiling Identifies the Membrane-Bound Purinergic Receptor P2X4 as a Target of the Autophagy Inhibitor Indophagolin. *Cell Chem. Biol.* **2021**, 1–8. <https://doi.org/10.1016/j.chembiol.2021.02.017>.
- (117) Mateus, A.; Kurzawa, N.; Becher, I.; Sridharan, S.; Helm, D.; Stein, F.; Typas, A.; Savitski, M. M. Thermal Proteome Profiling for Interrogating Protein Interactions. *Mol. Syst. Biol.* **2020**, 16 (3), 1–11. <https://doi.org/10.15252/msb.20199232>.
- (118) Mateus, A.; Määttä, T. A.; Savitski, M. M. Thermal Proteome Profiling: Unbiased Assessment of Protein State through Heat-Induced Stability Changes. *Proteome Sci.* **2016**, 15 (1), 13. <https://doi.org/10.1186/s12953-017-0122-4>.

V – References

- (119) Sridharan, S.; Kurzawa, N.; Werner, T.; Günthner, I.; Helm, D.; Huber, W.; Bantscheff, M.; Savitski, M. M. Proteome-Wide Solubility and Thermal Stability Profiling Reveals Distinct Regulatory Roles for ATP. *Nat. Commun.* **2019**, *10* (1), 1–13. <https://doi.org/10.1038/s41467-019-09107-y>.
- (120) Jarzab, A.; Kurzawa, N.; Hopf, T.; Moerch, M.; Zecha, J.; Leijten, N.; Bian, Y.; Musiol, E.; Maschberger, M.; Stoehr, G.; Becher, I.; Daly, C.; Samaras, P.; Mergner, J.; Spanier, B.; Angelov, A.; Werner, T.; Bantscheff, M.; Wilhelm, M.; Klingenspor, M.; Lemeer, S.; Liebl, W.; Hahne, H.; Savitski, M. M.; Kuster, B. Meltome Atlas—Thermal Proteome Stability across the Tree of Life. *Nat. Methods* **2020**, *17* (5), 495–503. <https://doi.org/10.1038/s41592-020-0801-4>.
- (121) Gaetani, M.; Sabatier, P.; Saei, A. A.; Beusch, C. M.; Yang, Z.; Lundström, S. L.; Zubarev, R. A. Proteome Integral Solubility Alteration: A High-Throughput Proteomics Assay for Target Deconvolution. *J. Proteome Res.* **2019**, *18* (11), 4027–4037. <https://doi.org/10.1021/acs.jproteome.9b00500>.
- (122) Cassini, A.; Högberg, L. D.; Plachouras, D.; Quattrocchi, A.; Hoxha, A.; Simonsen, G. S.; Colomb-Cotinat, M.; Kretzschmar, M. E.; Devleeschauwer, B.; Cecchini, M.; Ouakrim, D. A.; Oliveira, T. C.; Struelens, M. J.; Suetens, C.; Monnet, D. L.; Strauss, R.; Mertens, K.; Struyf, T.; Catry, B.; Latour, K.; Ivanov, I. N.; Dobрева, E. G.; Tambic Andrašević, A.; Soprek, S.; Budimir, A.; Paphitou, N.; Žemlicková, H.; Schytte Olsen, S.; Wolff Sönksen, U.; Märtin, P.; Ivanova, M.; Lyytikäinen, O.; Jalava, J.; Coignard, B.; Eckmanns, T.; Abu Sin, M.; Haller, S.; Daikos, G. L.; Gikas, A.; Tsiodras, S.; Kontopidou, F.; Tóth, Á.; Hajdu, Á.; Guólaugsson, Ó.; Kristinsson, K. G.; Murchan, S.; Burns, K.; Pezzotti, P.; Gagliotti, C.; Dumpis, U.; Liuimiene, A.; Perrin, M.; Borg, M. A.; de Greeff, S. C.; Monen, J. C.; Koek, M. B.; Elstrøm, P.; Zabicka, D.; Deptula, A.; Hryniewicz, W.; Caniça, M.; Nogueira, P. J.; Fernandes, P. A.; Manageiro, V.; Popescu, G. A.; Serban, R. I.; Schréterová, E.; Litvová, S.; Štefkovicová, M.; Kolman, J.; Klavs, I.; Korošec, A.; Aracil, B.; Asensio, A.; Pérez-Vázquez, M.; Billström, H.; Larsson, S.; Reilly, J. S.; Johnson, A.; Hopkins, S. Attributable Deaths and Disability-Adjusted Life-Years Caused by Infections with Antibiotic-Resistant Bacteria in the EU and the European Economic Area in 2015: A Population-Level Modelling Analysis. *Lancet. Infect. Dis.* **2019**, *19* (1), 56–66. [https://doi.org/10.1016/S1473-3099\(18\)30605-4](https://doi.org/10.1016/S1473-3099(18)30605-4).
- (123) CDC. Antibiotic Resistance Threats in The United States 2019. *Cdc* **2019**, *10* (1). <https://doi.org/10.1186/s13756-020-00872-w>.
- (124) Timmins, G. S.; Deretic, V. Mechanisms of Action of Isoniazid. *Mol. Microbiol.* **2006**, *62* (5), 1220–1227. <https://doi.org/10.1111/J.1365-2958.2006.05467.X>.

V – References

- (125) Shetye, G. S.; Franzblau, S. G.; Cho, S. New Tuberculosis Drug Targets, Their Inhibitors, and Potential Therapeutic Impact. *Transl. Res.* **2020**, *220*, 68–97. <https://doi.org/10.1016/j.trsl.2020.03.007>.
- (126) Aggarwal, A.; Parai, M. K.; Shetty, N.; Wallis, D.; Woolhiser, L.; Hastings, C.; Dutta, N. K.; Galaviz, S.; Dhakal, R. C.; Shrestha, R.; Wakabayashi, S.; Walpole, C.; Matthews, D.; Floyd, D.; Scullion, P.; Riley, J.; Epemolu, O.; Norval, S.; Snavey, T.; Robertson, G. T.; Rubin, E. J.; Ioerger, T. R.; Sirgel, F. A.; van der Merwe, R.; van Helden, P. D.; Keller, P.; Böttger, E. C.; Karakousis, P. C.; Lenaerts, A. J.; Sacchettini, J. C. Development of a Novel Lead That Targets M. Tuberculosis Polyketide Synthase 13. *Cell* **2017**, *170* (2), 249-259.e25. <https://doi.org/10.1016/j.cell.2017.06.025>.
- (127) Shao, M.; Mcneil, M.; Cook, G. M.; Lu, X. European Journal of Medicinal Chemistry MmpL3 Inhibitors as Antituberculosis Drugs. *Eur. J. Med. Chem.* **2020**, *200*, 112390. <https://doi.org/10.1016/j.ejmech.2020.112390>.
- (128) Umare, M. D.; Khedekar, P. B.; Chikhale, R. V. Mycobacterial Membrane Protein Large 3 (MmpL3) Inhibitors : A Promising Approach to Combat Tuberculosis. **2021**, *3*, 1–14. <https://doi.org/10.1002/cmdc.202100359>.
- (129) Williams, J. T.; Abramovitch, R. B. Molecular Mechanisms of MmpL3 Function and Inhibition. **2023**, *29* (5), 190–212. <https://doi.org/10.1089/mdr.2021.0424>.
- (130) Grzegorzewicz, A. E.; Pham, H.; Gundi, V. A. K. B.; Scherman, M. S.; North, E. J.; Hess, T.; Jones, V.; Gruppo, V.; Born, S. E. M.; Korduláková, J.; Chavadi, S. S.; Morisseau, C.; Lenaerts, A. J.; Lee, R. E.; McNeil, M. R.; Jackson, M. Inhibition of Mycolic Acid Transport across the Mycobacterium Tuberculosis Plasma Membrane. *Nat. Chem. Biol.* **2012**, *8* (4), 334–341. <https://doi.org/10.1038/nchembio.794>.
- (131) Tahlan, K.; Wilson, R.; Kastrinsky, D. B.; Arora, K.; Nair, V.; Fischer, E.; Barnes, S. W.; Walker, J. R.; Alland, D.; Barry, C. E.; Boshoff, H. I. SQ109 Targets MmpL3, a Membrane Transporter of Trehalose Monomycolate Involved in Mycolic Acid Donation to the Cell Wall Core of Mycobacterium Tuberculosis. *Antimicrob. Agents Chemother.* **2012**, *56* (4), 1797–1809. <https://doi.org/10.1128/AAC.05708-11>.
- (132) Grover, S.; Engelhart, C. A.; Pérez-Herrán, E.; Li, W.; Abrahams, K. A.; Papavinasundaram, K.; Bean, J. M.; Sassetti, C. M.; Mendoza-Losana, A.; Besra, G. S.; Jackson, M.; Schnappinger, D. Two-Way Regulation of MmpL3 Expression Identifies and Validates Inhibitors of MmpL3 Function in Mycobacterium Tuberculosis. *ACS Infect. Dis.* **2021**. <https://doi.org/10.1021/acsinfecdis.0c00675>.
- (133) Pandya, A. N.; Prathipati, P. K.; Hegde, P.; Li, W.; Graham, K. F.; Mandal, S.; Drescher,

V – References

- K. M.; Destache, C. J.; Ordway, D.; Jackson, M.; Northa, E. J. Indole-2-Carboxamides Are Active against Mycobacterium Abscessus in a Mouse Model of Acute Infection. *Antimicrob. Agents Chemother.* **2019**, *63* (3), 14–18. <https://doi.org/10.1128/AAC.02245-18>.
- (134) Kozikowski, A. P.; Onajole, O. K.; Stec, J.; Dupont, C.; Viljoen, A.; Richard, M.; Chaira, T.; Lun, S.; Bishai, W.; Raj, V. S.; Ordway, D.; Kremer, L. Targeting Mycolic Acid Transport by Indole-2-Carboxamides for the Treatment of Mycobacterium Abscessus Infections. *J. Med. Chem.* **2017**, *60* (13), 5876–5888. <https://doi.org/10.1021/acs.jmedchem.7b00582>.
- (135) Hu, T.; Yang, X.; Liu, F.; Sun, S.; Xiong, Z.; Liang, J.; Yang, X.; Wang, H.; Yang, X.; Guddat, L. W.; Yang, H.; Rao, Z.; Zhang, B. Structure-Based Design of Anti-Mycobacterial Drug Leads That Target the Mycolic Acid Transporter MmpL3. *Structure* **2022**, *30* (10), 1395-1402.e4. <https://doi.org/10.1016/j.str.2022.07.009>.
- (136) Xu, Z.; Meshcheryakov, V. A.; Poce, G.; Chng, S. S. MmpL3 Is the Flippase for Mycolic Acids in Mycobacteria. *Proc. Natl. Acad. Sci. U. S. A.* **2017**. <https://doi.org/10.1073/pnas.1700062114>.
- (137) Li, W.; Upadhyay, A.; Fontes, F. L.; North, E. J.; Wang, Y.; Crans, D. C.; Grzegorzewicz, A. E.; Jones, V.; Franzblau, S. G.; Lee, R. E.; Crick, D. C.; Jackson, M. Novel Insights into the Mechanism of Inhibition of MmpL3, a Target of Multiple Pharmacophores in Mycobacterium Tuberculosis. *Antimicrob. Agents Chemother.* **2014**, *58* (11), 6413–6423. <https://doi.org/10.1128/AAC.03229-14>.
- (138) Imran, M.; Arora, M. K.; Chaudhary, A.; Khan, S. A.; Kamal, M.; Alshammari, M. M.; Alharbi, R. M.; Althomali, N. A.; Alzimam, I. M.; Alshammari, A. A.; Alharbi, B. H.; Alshengeti, A.; Alsaleh, A. A.; Alqahtani, S. A.; Rabaan, A. A. MmpL3 Inhibition as a Promising Approach to Develop Novel Therapies against Tuberculosis: A Spotlight on SQ109, Clinical Studies, and Patents Literature. *Biomedicines* **2022**, *10* (11). <https://doi.org/10.3390/biomedicines10112793>.
- (139) Rao, S. P. S.; Lakshminarayana, S. B.; Kondreddi, R. R.; Herve, M.; Camacho, L. R.; Bifani, P.; Kalapala, S. K.; Jiricek, J.; Ma, N. L.; Tan, B. H.; Ng, S. H.; Nanjundappa, M.; Ravindran, S.; Seah, P. G.; Thayalan, P.; Lim, S. H.; Lee, B. H.; Goh, A.; Barnes, W. S.; Chen, Z.; Gagaring, K.; Chatterjee, A. K.; Pethe, K.; Kuhen, K.; Walker, J.; Feng, G.; Babu, S.; Zhang, L.; Blasco, F.; Beer, D.; Weaver, M.; Dartois, V.; Glynn, R.; Dick, T.; Smith, P. W.; Diagana, T. T.; Manjunatha, U. H. Indolcarboxamide Is a Preclinical Candidate for Treating Multidrug-Resistant Tuberculosis. *Sci. Transl. Med.* **2013**. <https://doi.org/10.1126/scitranslmed.3007355>.

V – References

- (140) Graham, J.; Wong, C. E.; Day, J.; Mcfaddin, E.; Ochsner, U.; Hoang, T.; Young, C. L.; Ribble, W.; Degroote, M. A.; Jarvis, T.; Sun, X. Discovery of Benzothiazole Amides as Potent Antimycobacterial Agents. **2018**. <https://doi.org/10.1016/j.bmcl.2018.08.026>.
- (141) Raynaud, C.; Daher, W.; Johansen, M. D.; Roquet-Banères, F.; Blaise, M.; Onajole, O. K.; Kozikowski, A. P.; Herrmann, J. L.; Dziadek, J.; Gobis, K.; Kremer, L. Active Benzimidazole Derivatives Targeting the MmpL3 Transporter in Mycobacterium Abscessus. *ACS Infect. Dis.* **2020**. <https://doi.org/10.1021/acsinfecdis.9b00389>.
- (142) La Rosa, V.; Poce, G.; Canseco, J. O.; Buroni, S.; Pasca, M. R.; Biava, M.; Raju, R. M.; Porretta, G. C.; Alfonso, S.; Battilocchio, C.; Javid, B.; Sorrentino, F.; Ioerger, T. R.; Sacchetti, J. C.; Manetti, F.; Botta, M.; De Logu, A.; Rubin, E. J.; De Rossi, E. MmpL3 Is the Cellular Target of the Antitubercular Pyrrole Derivative BM212. *Antimicrob. Agents Chemother.* **2012**, *56* (1), 324–331. <https://doi.org/10.1128/AAC.05270-11>.
- (143) Zhang, B.; Li, J.; Yang, X.; Wu, L.; Zhang, J.; Yang, Y.; Zhao, Y.; Zhang, L.; Yang, X.; Yang, X.; Cheng, X.; Liu, Z.; Jiang, B.; Jiang, H.; Guddat, L. W.; Yang, H.; Rao, Z. Crystal Structures of Membrane Transporter MmpL3, an Anti-TB Drug Target. *Cell* **2019**, *176* (3), 636-648.e13. <https://doi.org/10.1016/j.cell.2019.01.003>.
- (144) Li, W.; Stevens, C. M.; Pandya, A. N.; Darzynkiewicz, Z.; Bhattarai, P.; Tong, W.; Gonzalez-Juarrero, M.; North, E. J.; Zgurskaya, H. I.; Jackson, M. Direct Inhibition of MmpL3 by Novel Antitubercular Compounds. *ACS Infect. Dis.* **2019**, *5* (6). <https://doi.org/10.1021/acsinfecdis.9b00048>.
- (145) Li, K.; Schurig-Briccio, L. A.; Feng, X.; Upadhyay, A.; Pujari, V.; Lechartier, B.; Fontes, F. L.; Yang, H.; Rao, G.; Zhu, W.; Gulati, A.; No, J. H.; Cintra, G.; Bogue, S.; Liu, Y. L.; Molohon, K.; Orlean, P.; Mitchell, D. A.; Freitas-Junior, L.; Ren, F.; Sun, H.; Jiang, T.; Li, Y.; Guo, R. T.; Cole, S. T.; Gennis, R. B.; Crick, D. C.; Oldfield, E. Multitarget Drug Discovery for Tuberculosis and Other Infectious Diseases. *J. Med. Chem.* **2014**, *57* (7), 3126–3129. https://doi.org/10.1021/JM500131S/SUPPL_FILE/JM500131S_SI_001.PDF.
- (146) Madacki, J.; Kopál, M.; Jackson, M.; Korduláková, J. Mycobacterial Epoxide Hydrolase EphD Is Inhibited by Urea and Thiourea Derivatives. *Int. J. Mol. Sci.* **2021**, *22* (6), 2884. <https://doi.org/10.3390/ijms22062884>.
- (147) Shao, M.; Mcneil, M.; Cook, G. M.; Lu, X. MmpL3 Inhibitors as Antituberculosis Drugs. *Eur. J. Med. Chem.* **2020**, 112390. <https://doi.org/10.1016/j.ejmech.2020.112390>.
- (148) Rostovtsev, V. V.; Green, L. G.; Fokin, V. V.; Sharpless, K. B. A Stepwise Huisgen Cycloaddition Process: Copper(I)-Catalyzed Regioselective “Ligation” of Azides and

V – References

- Terminal Alkynes. *Angew. Chemie Int. Ed.* **2002**, *41* (14), 2596–2599. [https://doi.org/10.1002/1521-3773\(20020715\)41:14<2596::AID-ANIE2596>3.0.CO;2-4](https://doi.org/10.1002/1521-3773(20020715)41:14<2596::AID-ANIE2596>3.0.CO;2-4).
- (149) Tornøe, C. W.; Christensen, C.; Meldal, M. Peptidotriazoles on Solid Phase: [1,2,3]-Triazoles by Regiospecific Copper(I)-Catalyzed 1,3-Dipolar Cycloadditions of Terminal Alkynes to Azides. *J. Org. Chem.* **2002**, *67* (9), 3057–3064. https://doi.org/10.1021/JO011148J/SUPPL_FILE/JO011148J_S.PDF.
- (150) Kapopoulou, A.; Lew, J. M.; Cole, S. T. The MycoBrowser Portal: A Comprehensive and Manually Annotated Resource for Mycobacterial Genomes. *Tuberculosis* **2011**, *91* (1), 8–13. <https://doi.org/10.1016/J.TUBE.2010.09.006>.
- (151) Madacki, J.; Laval, F.; Grzegorzewicz, A.; Lemassu, A.; Záhorszka, M.; Arand, M.; Mcneil, M.; Daffé, M.; Jackson, M.; Lanéelle, M.; Korduláková, J. Impact of the Epoxide Hydrolase EphD on the Metabolism of Mycolic Acids in Mycobacteria. **2018**, *293*, 5172–5184. <https://doi.org/10.1074/jbc.RA117.000246>.
- (152) Rengarajan, J.; Bloom, B. R.; Rubin, E. J. Genome-Wide Requirements for Mycobacterium Tuberculosis Adaptation and Survival in Macrophages. *Proc. Natl. Acad. Sci. U. S. A.* **2005**, *102* (23), 8327–8332. <https://doi.org/10.1073/PNAS.0503272102>.
- (153) Adolph, C.; McNeil, M. B.; Cook, G. M. Impaired Succinate Oxidation Prevents Growth and Influences Drug Susceptibility in Mycobacterium Tuberculosis. *MBio* **2022**, *13* (4). <https://doi.org/10.1128/mbio.01672-22>.
- (154) Singh, A.; Gupta, R.; Vishwakarma, R. A.; Narayanan, P. R.; Paramasivan, C. N.; Ramanathan, V. D.; Tyagi, A. K. Erratum: Requirement of the MymA Operon for Appropriate Cell Wall Ultrastructure and Persistence of Mycobacterium Tuberculosis in the Spleens of Guinea Pigs (Journal of Bacteriology (2022) DOI: 10.1128/JB.00094-21). *J. Bacteriol.* **2022**, *204* (1), 4173–4186. <https://doi.org/10.1128/JB.00520-21>.
- (155) Alland, D.; Steyn, A. J.; Weisbrod, T.; Aldrich, K.; Jacobs, W. R. Characterization of the Mycobacterium Tuberculosis IniBAC Promoter, a Promoter That Responds to Cell Wall Biosynthesis Inhibition. *J. Bacteriol.* **2000**, *182* (7), 1802–1811. <https://doi.org/10.1128/JB.182.7.1802-1811.2000>.
- (156) Lee, R. E.; Protopopova, M.; Crooks, E.; Slayden, R. A.; Terrot, M.; Barry, C. E. Combinatorial Lead Optimization of [1,2]-Diamines Based on Ethambutol as Potential Antituberculosis Preclinical Candidates. *J. Comb. Chem.* **2003**, *5* (2), 172–187. <https://doi.org/10.1021/cc020071p>.

V – References

- (157) Szklarczyk, D.; Kirsch, R.; Koutrouli, M.; Nastou, K.; Mehryary, F.; Hachilif, R.; Gable, A. L.; Fang, T.; Doncheva, N. T.; Pyysalo, S.; Bork, P.; Jensen, L. J.; Von Mering, C. The STRING Database in 2023: Protein-Protein Association Networks and Functional Enrichment Analyses for Any Sequenced Genome of Interest. *Nucleic Acids Res.* **2023**, *51* (D1), D638–D646. <https://doi.org/10.1093/NAR/GKAC1000>.
- (158) Stanley, S. A.; Grant, S. S.; Kawate, T.; Iwase, N.; Shimizu, M.; Wivagg, C.; Silvis, M.; Kazyanskaya, E.; Aquadro, J.; Golas, A.; Fitzgerald, M.; Dai, H.; Zhang, L.; Hung, D. T. Identification of Novel Inhibitors of M. Tuberculosis Growth Using Whole Cell Based High-Throughput Screening. *ACS Chem. Biol.* **2012**, *7* (8), 1377–1384. <https://doi.org/10.1021/cb300151m>.
- (159) Alsayed, S. S. R.; Lun, S.; Payne, A.; Bishai, W. R.; Gunosewoyo, H. Design, Synthesis and Antimycobacterial Evaluation of Novel Adamantane and Adamantanol Analogues Effective against Drug-Resistant Tuberculosis. *Bioorg. Chem.* **2021**, *106* (October 2020), 104486. <https://doi.org/10.1016/j.bioorg.2020.104486>.
- (160) Gao, P.; Nie, X.; Zou, M.; Shi, Y.; Cheng, G. Recent Advances in Materials for Extended-Release Antibiotic Delivery System. *J. Antibiot. (Tokyo)*. **2011**, *64* (9), 625–634. <https://doi.org/10.1038/ja.2011.58>.
- (161) Cox, J.; Mann, M. MaxQuant Enables High Peptide Identification Rates, Individualized p.p.b.-Range Mass Accuracies and Proteome-Wide Protein Quantification. *Nat. Biotechnol.* **2008**, *26* (12), 1367–1372. <https://doi.org/10.1038/nbt.1511>.
- (162) Tyanova, S.; Temu, T.; Sinitcyn, P.; Carlson, A.; Hein, M. Y.; Geiger, T.; Mann, M.; Cox, J. The Perseus Computational Platform for Comprehensive Analysis of (Prote)Omics Data. *Nat. Methods* **2016**, *13* (9), 731–740. <https://doi.org/10.1038/nmeth.3901>.
- (163) Coscia, F.; Doll, S.; Bech, J. M.; Schweizer, L.; Mund, A.; Lengyel, E.; Lindebjerg, J.; Madsen, G. I.; Moreira, J. M.; Mann, M. A Streamlined Mass Spectrometry–Based Proteomics Workflow for Large-scale FFPE Tissue Analysis. *J. Pathol.* **2020**, *251* (1), 100–112. <https://doi.org/10.1002/path.5420>.
- (164) Rao, S.; Bockstael, K.; Nath, S.; Engelborghs, Y.; Anné, J.; Geukens, N. Enzymatic Investigation of the Staphylococcus Aureus Type i Signal Peptidase SpsB - Implications for the Search for Novel Antibiotics. *FEBS J.* **2009**, *276* (12), 3222–3234. <https://doi.org/10.1111/j.1742-4658.2009.07037.x>.
- (165) Lambert, R. J. W.; Pearson, J. Susceptibility Testing: Accurate and Reproducible Minimum Inhibitory Concentration (MIC) and Non-Inhibitory Concentration (NIC) Values. *J. Appl. Microbiol.* **2000**, *88* (5), 784–790. <https://doi.org/10.1046/J.1365->

V – References

2672.2000.01017.X.

- (166) Hegde, P. V.; Howe, M. D.; Zimmerman, M. D.; Boshoff, H. I. M.; Sharma, S.; Remache, B.; Jia, Z.; Pan, Y.; Baughn, A. D.; Dartois, V.; Aldrich, C. C. Synthesis and Biological Evaluation of Orally Active Prodrugs and Analogs of Para-Aminosalicylic Acid (PAS). **2022**. <https://doi.org/10.1016/j.ejmech.2022.114201>.
- (167) Inoyama, D.; Awasthi, D.; Capodagli, G. C.; Neiditch, M. B.; Kumar, P.; Freundlich, J. S.; Tsotetsi, K.; Sukheja, P.; Zimmerman, M.; Li, S.-G.; Jadhav, R.; Russo, R.; Wang, X.; Grady, C.; Richmann, T.; Shrestha, R.; Li, L.; Ahn, Y.-M.; Pin, H.; Liang, H.; Mina, M.; Park, S.; Perlin, D. S.; Connell, N.; Ronique Dartois, V.; Alland, D. A Preclinical Candidate Targeting Mycobacterium Tuberculosis KasA In Brief A Preclinical Candidate Targeting Mycobacterium Tuberculosis KasA. *Cell Chem. Biol.* **2020**, *27*, 560–570. <https://doi.org/10.1016/j.chembiol.2020.02.007>.
- (168) Gerth, K.; Steinmetz, H.; Höfle, G.; Jansen, R. Chlorotonil A, Ein Macrolid Mit Einzigartigem-Dichlor-1,3-Dionfunktion Aus *Sorangium Cellulosum*, So Ce1525. *Angew. Chemie* **2008**, *120* (3), 610–613. <https://doi.org/10.1002/ange.200703993>.
- (169) Jungmann, K.; Jansen, R.; Gerth, K.; Huch, V.; Krug, D.; Fenical, W.; Müller, R. Two of a Kind-The Biosynthetic Pathways of Chlorotonil and Anthracimycin. *ACS Chem. Biol.* **2015**, *10* (11), 2480–2490. <https://doi.org/10.1021/acschembio.5b00523>.
- (170) Hofer, W.; Oueis, E.; Fayad, A. A.; Deschner, F.; Andreas, A.; de Carvalho, L. P.; Hüttel, S.; Bernecker, S.; Pätzold, L.; Morgenstern, B.; Zaburanyi, N.; Bischoff, M.; Stadler, M.; Held, J.; Herrmann, J.; Müller, R. Regio- and Stereoselective Epoxidation and Acidic Epoxide Opening of Antibacterial and Antiplasmodial Chlorotonils Yield Highly Potent Derivatives. *Angew. Chemie Int. Ed.* **2022**, *61* (30). <https://doi.org/10.1002/anie.202202816>.
- (171) Bublitz, A.; Brauer, M.; Wagner, S.; Hofer, W.; Müsken, M.; Deschner, F.; Lesker, T. R.; Neumann-Schaal, M.; Paul, L.-S.; Nübel, U.; Bartel, J.; Kany, A. M.; Zühlke, D.; Bernecker, S.; Jansen, R.; Sievers, S.; Riedel, K.; Herrmann, J.; Müller, R.; Fuchs, T. M.; Strowig, T. The Natural Product Chlorotonil A Preserves Colonization Resistance and Prevents Relapsing *Clostridioides Difficile* Infection. *Cell Host Microbe* **2023**, *31* (5), 734-750.e8. <https://doi.org/10.1016/j.chom.2023.04.003>.
- (172) Hofer, W.; Deschner, F.; Jézéquel, G.; Pessanha de Carvalho, L.; Abdel-Wadood, N.; Pätzold, L.; Bernecker, S.; Morgenstern, B.; Kany, A. M.; Große, M.; Stadler, M.; Bischoff, M.; Hirsch, A. K. H.; Held, J.; Herrmann, J.; Müller, R. Functionalization of Chlorotonils: Dehalogenil as Promising Lead Compound for In Vivo Application. *Angew.*

- Chemie Int. Ed.* **2024**, e202319765. <https://doi.org/10.1002/ANIE.202319765>.
- (173) Savitski, M. M.; Reinhard, F. B. M.; Franken, H.; Werner, T.; Savitski, M. F.; Eberhard, D.; Molina, D. M.; Jafari, R.; Dovega, R. B.; Klaeger, S.; Kuster, B.; Nordlund, P.; Bantscheff, M.; Drewes, G. Tracking Cancer Drugs in Living Cells by Thermal Profiling of the Proteome. *Science* (80-). **2014**, 346 (6205). https://doi.org/10.1126/SCIENCE.1255784/SUPPL_FILE/TABLE_S9_THERMAL_PROFILING_DASATINIB_INTACT_CELLS.XLSX.
- (174) Becher, I.; Werner, T.; Doce, C.; Zaal, E. A.; Tögel, I.; Khan, C. A.; Rueger, A.; Muelbaier, M.; Salzer, E.; Berkers, C. R.; Fitzpatrick, P. F.; Bantscheff, M.; Savitski, M. M. Thermal Profiling Reveals Phenylalanine Hydroxylase as an Off-Target of Panobinostat. *Nat. Chem. Biol.* **2016**, 12 (11), 908–910. <https://doi.org/10.1038/nchembio.2185>.
- (175) Kirsch, V. C.; Orgler, C.; Braig, S.; Jeremias, I.; Auerbach, D.; Müller, R.; Vollmar, A. M.; Sieber, S. A. The Cytotoxic Natural Product Vioprolide A Targets Nucleolar Protein 14 Essential for Ribosome Biogenesis. *Angew. Chem. Int. Ed. Engl.* **2019**, 1–7. <https://doi.org/10.1002/anie.201911158>.
- (176) Mateus, A.; Bobonis, J.; Kurzawa, N.; Stein, F.; Helm, D.; Hevler, J.; Typas, A.; Savitski, M. M. Thermal Proteome Profiling in Bacteria: Probing Protein State in Vivo. *Mol. Syst. Biol.* **2018**, 14 (7), 1–15. <https://doi.org/10.15252/msb.20188242>.
- (177) Pellegrini, A.; Thomas, U.; von Fellenberg, R.; Wild, P. Bactericidal Activities of Lysozyme and Aprotinin against Gram-negative and Gram-positive Bacteria Related to Their Basic Character. *J. Appl. Bacteriol.* **1992**, 72 (3), 180–187. <https://doi.org/10.1111/J.1365-2672.1992.TB01821.X>.
- (178) Bera, A.; Herbert, S.; Jakob, A.; Vollmer, W.; Götz, F. Why Are Pathogenic Staphylococci so Lysozyme Resistant? The Peptidoglycan O-Acetyltransferase OatA Is the Major Determinant for Lysozyme Resistance of Staphylococcus Aureus. *Mol. Microbiol.* **2005**, 55 (3), 778–787. <https://doi.org/10.1111/J.1365-2958.2004.04446.X>.
- (179) A Schindler, B. C.; Schuhardt, V. T. Formulae and Methods of the Marine Biological Laboratory. *Biocheem. Biophys. Res. Commun* **1961**, 25, 260.
- (180) Kokai-Kun, J. F.; Walsh, S. M.; Chanturiya, T.; Mond, J. J. Lysostaphin Cream Eradicates Staphylococcus Aureus Nasal Colonization in a Cotton Rat Model. *Antimicrob. Agents Chemother.* **2003**, 47 (5), 1589–1597. <https://doi.org/10.1128/AAC.47.5.1589-1597.2003/ASSET/D2ACF12C-BEAC-4686-97A6-57B9D6333C18/ASSETS/GRAPHIC/AC0531005001.JPEG>.

V – References

- (181) Szatmári, D.; Sárkány, P.; Kocsis, B.; Nagy, T.; Miseta, A.; Barkó, S.; Longauer, B.; Robinson, R. C.; Nyitrai, M. Intracellular Ion Concentrations and Cation-Dependent Remodelling of Bacterial MreB Assemblies. *Sci. Reports* 2020 101 **2020**, 10 (1), 1–13. <https://doi.org/10.1038/s41598-020-68960-w>.
- (182) Datta, B. MAPs and POEP of the Roads from Prokaryotic to Eukaryotic Kingdoms. *Biochimie* **2000**, 82 (2), 95–107. [https://doi.org/10.1016/S0300-9084\(00\)00383-7](https://doi.org/10.1016/S0300-9084(00)00383-7).
- (183) Lowther, W. T.; Matthews, B. W. Structure and Function of the Methionine Aminopeptidases. *Biochim. Biophys. Acta - Protein Struct. Mol. Enzymol.* **2000**, 1477 (1–2), 157–167. [https://doi.org/10.1016/S0167-4838\(99\)00271-X](https://doi.org/10.1016/S0167-4838(99)00271-X).
- (184) Oefner, C.; Douangamath, A.; D’Arcy, A.; Häfeli, S.; Mareque, D.; Sweeney, A. Mac; Padilla, J.; Pierau, S.; Schulz, H.; Thormann, M.; Wadman, S.; Dale, G. E. The 1.15 Å Crystal Structure of the Staphylococcus Aureus Methionyl-Aminopeptidase and Complexes with Triazole Based Inhibitors. *J. Mol. Biol.* **2003**, 332 (1), 13–21. [https://doi.org/10.1016/S0022-2836\(03\)00862-3](https://doi.org/10.1016/S0022-2836(03)00862-3).
- (185) Kishor, C.; Gumpena, R.; Reddi, R.; Addlagatta, A. Structural Studies of Enterococcus Faecalis Methionine Aminopeptidase and Design of Microbe Specific 2,2'-Bipyridine Based Inhibitors. *Medchemcomm* **2012**, 3 (11), 1406. <https://doi.org/10.1039/c2md20096a>.
- (186) Csonka, L. N. Physiological and Genetic Responses of Bacteria to Osmotic Stress. *Microbiol. Rev.* **1989**, 53 (1), 121–147. <https://doi.org/10.1128/membr.53.1.121-147.1989>.
- (187) Wargo, M. J. Homeostasis and Catabolism of Choline and Glycine Betaine: Lessons from Pseudomonas Aeruginosa. *Appl. Environ. Microbiol.* **2013**, 79 (7), 2112–2120. <https://doi.org/10.1128/AEM.03565-12>.
- (188) Sleator, R. D.; Hill, C. Bacterial Osmoadaptation: The Role of Osmolytes in Bacterial Stress and Virulence. *FEMS Microbiol. Rev.* **2002**, 26 (1), 49–71. [https://doi.org/10.1016/S0168-6445\(01\)00071-7](https://doi.org/10.1016/S0168-6445(01)00071-7).
- (189) Alnaseri, H.; Kuiack, R. C.; Ferguson, K. A.; Schneider, J. E. T.; Heinrichs, D. E.; McGavin, M. J. DNA Binding and Sensor Specificity of FarR, a Novel Tetr Family Regulator Required for Induction of the Fatty Acid Efflux Pump FarE in Staphylococcus Aureus. *J. Bacteriol.* **2019**, 201 (3). <https://doi.org/10.1128/JB.00602-18>.
- (190) Nguyen, M.-T.; Saising, J.; Tribelli, P. M.; Nega, M.; Diene, S. M.; François, P.; Schrenzel, J.; Spröer, C.; Bunk, B.; Ebner, P.; Hertlein, T.; Kumari, N.; Härtner, T.;

V – References

- Wistuba, D.; Voravuthikunchai, S. P.; Mäder, U.; Ohlsen, K.; Götz, F. Inactivation of FarR Causes High Rhodomyrtone Resistance and Increased Pathogenicity in *Staphylococcus Aureus*. *Front. Microbiol.* **2019**, *10* (MAY), 1–14. <https://doi.org/10.3389/fmicb.2019.01157>.
- (191) Wright, G. D. Opportunities for Natural Products in 21st Century Antibiotic Discovery. *Nat. Prod. Rep.* **2017**, *34* (7), 694–701. <https://doi.org/10.1039/C7NP00019G>.
- (192) Franken, H.; Mathieson, T.; Childs, D.; Sweetman, G. M. A.; Werner, T.; Tögel, I.; Doce, C.; Gade, S.; Bantscheff, M.; Drewes, G.; Reinhard, F. B. M.; Huber, W.; Savitski, M. M. Thermal Proteome Profiling for Unbiased Identification of Direct and Indirect Drug Targets Using Multiplexed Quantitative Mass Spectrometry. *Nat. Protoc.* **2015**, *10* (10), 1567–1593. <https://doi.org/10.1038/nprot.2015.101>.
- (193) Bubeneck, W. A. A Pronucleotide Probe Allows the In Situ Investigation of UMPylation in Human Cells Using, 2021.
- (194) Walsh, C. T.; Garneau-Tsodikova, S.; Gatto, G. J. Protein Posttranslational Modifications: The Chemistry of Proteome Diversifications. *Angewandte Chemie - International Edition*. December 1, 2005, pp 7342–7372. <https://doi.org/10.1002/anie.200501023>.
- (195) Casey, A. K.; Orth, K. Enzymes Involved in AMPylation and DeAMPylation. *Chem. Rev.* **2018**, *118* (3), 1199–1215. <https://doi.org/10.1021/ACS.CHEMREV.7B00145>.
- (196) Ham, H.; Woolery, A. R.; Tracy, C.; Stenesen, D.; Krämer, H.; Orth, K. Unfolded Protein Response-Regulated *Drosophila* Fic (DFic) Protein Reversibly AMPylates BiP Chaperone during Endoplasmic Reticulum Homeostasis. *J. Biol. Chem.* **2014**, *289* (52), 36059–36069. <https://doi.org/10.1074/jbc.M114.612515>.
- (197) Vogl, A. M.; Brockmann, M. M.; Giusti, S. A.; Maccarrone, G.; Vercelli, C. A.; Bauder, C. A.; Richter, J. S.; Roselli, F.; Hafner, A.-S.; Dedic, N.; Wotjak, C. T.; Vogt-Weisenhorn, D. M.; Choquet, D.; Turck, C. W.; Stein, V.; Deussing, J. M.; Refojo, D. Neddylation Inhibition Impairs Spine Development, Destabilizes Synapses and Deteriorates Cognition. *Nat. Neurosci.* **2015**, *18* (2). <https://doi.org/10.1038/nn.3912>.
- (198) Song, Y.; Brady, S. T. Post-Translational Modifications of Tubulin: Pathways to Functional Diversity of Microtubules. *Trends Cell Biol.* **2015**, *25* (3), 125–136. <https://doi.org/10.1016/J.TCB.2014.10.004>.
- (199) Magiera, M. M.; Singh, P.; Gadadhar, S.; Janke, C. Tubulin Posttranslational Modifications and Emerging Links to Human Disease. *Cell* **2018**, *173* (6), 1323–1327.

V – References

- <https://doi.org/10.1016/j.cell.2018.05.018>.
- (200) Rebelo, A. P.; Ruiz, A.; Dohrn, M. F.; Wayand, M.; Farooq, A.; Danzi, M. C.; Beijer, D.; Aaron, B.; Vandrovцова, J.; Houlden, H.; Matalonga, L.; Abreu, L.; Rouleau, G.; Estiar, M. A.; Van de Vondel, L.; Gan-Or, Z.; Baets, J.; Schüle, R.; Zuchner, S. BiP Inactivation Due to Loss of the DeAMPylation Function of FICD Causes a Motor Neuron Disease. *Genet. Med.* **2022**, *24* (12), 2487–2500. <https://doi.org/10.1016/J.GIM.2022.08.019>.
- (201) Anbalagan, M.; Huderson, B.; Murphy, L.; Rowan, B. G. Post-Translational Modifications of Nuclear Receptors and Human Disease. *Nucl. Recept. Signal.* **2012**, *10* (Figure 1). <https://doi.org/10.1621/nrs.10001>.
- (202) Narayan, S.; Bader, G. D.; Reimand, J. Frequent Mutations in Acetylation and Ubiquitination Sites Suggest Novel Driver Mechanisms of Cancer. *Genome Med.* **2016**, *8* (1), 1–13. <https://doi.org/10.1186/s13073-016-0311-2>.
- (203) Wang, Y.; Zhang, J.; Li, B.; He, Q. Y. Advances of Proteomics in Novel PTM Discovery: Applications in Cancer Therapy. *Small Methods.* 2019. <https://doi.org/10.1002/smt.201900041>.
- (204) Holstein, E.; Dittmann, A.; Kääriäinen, A.; Pesola, V.; Koivunen, J.; Pihlajaniemi, T.; Naba, A.; Izzi, V. The Burden of Post-translational Modification (Ptm)— Disrupting Mutations in the Tumor Matrisome. *Cancers (Basel).* **2021**, *13* (5), 1–18. <https://doi.org/10.3390/cancers13051081>.
- (205) Tikhonov, D.; Kulikova, L.; Kopylov, A. T.; Rudnev, V.; Stepanov, A.; Malsagova, K.; Izotov, A.; Kulikov, D.; Zulkarnaev, A.; Enikeev, D.; Potoldykova, N.; Kaysheva, A. L. Proteomic and Molecular Dynamic Investigations of PTM-Induced Structural Fluctuations in Breast and Ovarian Cancer. *Sci. Rep.* **2021**, *11* (1), 19318. <https://doi.org/10.1038/s41598-021-98201-7>.
- (206) Ham, H.; Sreelatha, A.; Orth, K. Manipulation of Host Membranes by Bacterial Effectors. *Nat. Publ. Gr.* **2011**. <https://doi.org/10.1038/nrmicro2602>.
- (207) Li, H.; Xu, H.; Zhou, Y.; Zhang, J.; Long, C.; Li, S.; Chen, S.; Zhou, J. M.; Shao, F. The Phosphothreonine Lyase Activity of a Bacterial Type III Effector Family. *Science (80-)*. **2007**, *315* (5814), 1000–1003. https://doi.org/10.1126/SCIENCE.1138960/SUPPL_FILE/LI.SOM.PDF.
- (208) Arbibe, L.; Kim, D. W.; Batsche, E.; Pedron, T.; Mateescu, B.; Muchardt, C.; Parsot, C.; Sansonetti, P. J. An Injected Bacterial Effector Targets Chromatin Access for Transcription Factor NF- κ B to Alter Transcription of Host Genes Involved in Immune

V – References

- Responses. **2007**. <https://doi.org/10.1038/ni1423>.
- (209) Hauser, A. R. The Type III Secretion System of *Pseudomonas Aeruginosa*: Infection by Injection. *Nature Reviews Microbiology*. 2009, pp 654–665. <https://doi.org/10.1038/nrmicro2199>.
- (210) Yarbrough, M. L.; Li, Y.; Kinch, L. N.; Grishin, N. V; Ball, H. L.; Orth, K. AMPylation of Rho GTPases by *Vibrio* VopS Disrupts Effector Binding and Downstream Signaling. *Science (80-)*. **2009**, 323 (5911), 269–272. <https://doi.org/10.1126/science.1166382>.
- (211) Mattoo, S.; Durrant, E.; Chen, M. J.; Xiao, J.; Lazar, C. S.; Manning, G.; Dixon, J. E.; Worby, C. A. Comparative Analysis of *Histophilus Somni* Immunoglobulin-Binding Protein A (IbpA) with Other Fic Domain-Containing Enzymes Reveals Differences in Substrate and Nucleotide Specificities. *J. Biol. Chem.* **2011**, 286 (37), 32834–32842. <https://doi.org/10.1074/jbc.M111.227603>.
- (212) Müller, M. P.; Peters, H.; Blümer, J.; Blankenfeldt, W.; Goody, R. S.; Itzen, A. The *Legionella* Effector Protein DrrA AMPylates the Membrane Traffic Regulator Rab1b. *Science (80-)*. **2010**, 329 (5994), 946–949. <https://doi.org/10.1126/science.1192276>.
- (213) Jiang, P.; Peliska, J. A.; Ninfa, A. J. The Regulation of *Escherichia Coli* Glutamine Synthetase Revisited: Role of 2-Ketoglutarate in the Regulation of Glutamine Synthetase Adenylylation State. *Biochemistry* **1998**, 37 (37), 12802–12810. <https://doi.org/10.1021/BI980666U/ASSET/IMAGES/LARGE/BI980666UF00007.JPEG>.
- (214) Engel, P.; Goepfert, A.; Stanger, F. V; Harms, A.; Schmidt, A.; Schirmer, T.; Dehio, C. Adenylylation Control by Intra- or Intermolecular Active-Site Obstruction in Fic Proteins. *Nature* **2012**. <https://doi.org/10.1038/nature10729>.
- (215) Sanyal, A.; Chen, A. J.; Nakayasu, E. S.; Lazar, C. S.; Zbornik, E. A.; Worby, C. A.; Koller, A.; Mattoo, S. A Novel Link between Fic (Filamentation Induced by CAMP)-Mediated Adenylylation/AMPylation and the Unfolded Protein Response *. **2015**. <https://doi.org/10.1074/jbc.M114.618348>.
- (216) Preissler, S.; Rato, C.; Chen, R.; Antrobus, R.; Ding, S.; Fearnley, I. M.; Ron, D. AMPylation Matches BiP Activity to Client Protein Load in the Endoplasmic Reticulum. *Elife* **2015**, 4 (DECEMBER2015), 1–33. <https://doi.org/10.7554/eLife.12621>.
- (217) Preissler, S.; Rato, C.; Perera, L. A.; Saudek, V.; Ron, D. FICD Acts Bifunctionally to AMPylate and De-AMPylation the Endoplasmic Reticulum Chaperone BiP. *Nat. Publ. Gr.* **2016**. <https://doi.org/10.1038/nsmb.3337>.

V – References

- (218) Sreelatha, A.; Yee, S. S.; Lopez, V. A.; Park, B. C.; Kinch, L. N.; Pilch, S.; Servage, K. A.; Zhang, J.; Jiou, J.; Karasiewicz-Urbańska, M.; Łobočka, M.; Grishin, N. V.; Orth, K.; Kucharczyk, R.; Pawłowski, K.; Tomchick, D. R.; Tagliabracci, V. S. Protein AMPylation by an Evolutionarily Conserved Pseudokinase. *Cell* **2018**, *175* (3), 809-821.e19. <https://doi.org/10.1016/j.cell.2018.08.046>.
- (219) Hao, Y. H.; Chuang, T.; Ball, H. L.; Luong, P.; Li, Y.; Flores-Saaib, R. D.; Orth, K. Characterization of a Rabbit Polyclonal Antibody against Threonine-AMPylation. *J. Biotechnol.* **2011**, *151* (3), 251–254. <https://doi.org/10.1016/J.JBIOTEC.2010.12.013>.
- (220) Grammel, M.; Luong, P.; Orth, K.; Hang, H. C. A Chemical Reporter for Protein AMPylation. *J. Am. Chem. Soc.* **2011**, *133* (43), 17103–17105. <https://doi.org/10.1021/ja205137d>.
- (221) Gulen, B.; Rosselin, M.; Fauser, J.; Albers, M. F.; Pett, C.; Krisp, C.; Pogenberg, V.; Schlüter, H.; Hedberg, C.; Itzen, A. Identification of Targets of AMPylating Fic Enzymes by Co-Substrate-Mediated Covalent Capture. *Nat. Chem.* **2020**, *12* (8), 732–739. <https://doi.org/10.1038/s41557-020-0484-6>.
- (222) Kielkowski, P.; Buchsbaum, I. Y.; Kirsch, V. C.; Bach, N. C.; Drukker, M.; Cappello, S.; Sieber, S. A. FICD Activity and AMPylation Remodelling Modulate Human Neurogenesis. *Nat. Commun.* **2020**, *11* (1), 1–13. <https://doi.org/10.1038/s41467-019-14235-6>.
- (223) Kielkowski, P.; Buchsbaum, I. Y.; Becker, T.; Bach, K.; Cappello, S.; Sieber, S. A. A Pronucleotide Probe for Live-Cell Imaging of Protein AMPylation. *ChemBioChem* **2020**, *21* (9), 1285–1287. <https://doi.org/10.1002/cbic.201900716>.
- (224) Rauh, T.; Brameyer, S.; Kielkowski, P.; Jung, K.; Sieber, S. A. MS-Based in Situ Proteomics Reveals AMPylation of Host Proteins during Bacterial Infection. *ACS Infect. Dis.* **2020**, *6* (12), 3277–3289. <https://doi.org/10.1021/acsinfecdis.0c00740>.
- (225) Yang, Y.; Yue, Y.; Song, N.; Li, C.; Yuan, Z.; Wang, Y.; Ma, Y.; Li, H.; Zhang, F.; Wang, W.; Jia, H.; Li, P.; Li, X.; Wang, Q.; Ding, Z.; Dong, H.; Gu, L.; Li, B. The YdiU Domain Modulates Bacterial Stress Signaling through Mn²⁺-Dependent UMPylation. *Cell Rep.* **2020**, *32* (12), 108161. <https://doi.org/10.1016/j.celrep.2020.108161>.
- (226) Mehellou, Y.; Rattan, H. S.; Balzarini, J. The ProTide Prodrug Technology: From the Concept to the Clinic. *J. Med. Chem.* **2018**, *61* (6), 2211–2226. <https://doi.org/10.1021/acs.jmedchem.7b00734>.
- (227) Pradere, U.; Garnier-Amblard, E. C.; Coats, S. J.; Amblard, F.; Schinazi, R. F. Synthesis

V – References

- of Nucleoside Phosphate and Phosphonate Prodrugs. *Chem. Rev.* **2014**, *114* (18), 9154–9218. <https://doi.org/10.1021/CR5002035>.
- (228) Segura-Peñ, D.; Sekulic, N.; Ort, S.; Konrad, M.; Lavie, A. Substrate-Induced Conformational Changes in Human UMP/CMP Kinase* □ S. **2004**. <https://doi.org/10.1074/jbc.M401989200>.
- (229) Traut, T. W. Physiological Concentrations of Purines and Pyrimidines. *Mol. Cell. Biochem.* **1994**, *140* (1), 1–22. <https://doi.org/10.1007/BF00928361>.
- (230) Sieber, S. A.; Cappello, S.; Kielkowski, P. From Young to Old: AMPylation Hits the Brain. *Cell Chem. Biol.* **2020**, *27* (7), 773–779. <https://doi.org/10.1016/j.chembiol.2020.05.009>.

